THE UNIVERSITY OF QUEENSLAND

AUSTRALIA

Functional investigation of neural circuits in larval zebrafish

Andrew Wayne Thompson

BSc (Hons Class I in Neuroscience)

A thesis submitted for the degree of Doctor of Philosophy at

The University of Queensland in 2015

School of Biomedical Sciences

Abstract

A fundamental goal of modern neuroscience is to understand the principles by which neural circuits within the brain lead to cognition and behaviour. Technological advances in the fields of microscopy and optogenetics have very recently allowed for the activity of all cells within a functional circuit to be observed and recorded, meaning that this goal is now within reach. Due to the physical and optical properties of neural tissue, these technologies remain most useful for the analysis of circuits that span very small volumes, meaning that small animal model organisms, with brains less than approximately 1 mm across, are most amenable to these types of analyses. The larval zebrafish model has emerged as an optimal balance between small size and the high complexity of a vertebrate brain. This thesis describes the development and application of several of these technological advances to examine neural circuits underlying perception and behaviour in the larval zebrafish.

Due to the relative recency of zebrafish as a model for functional neuroscience, the genetic and experimental tools required for in depth circuit analysis have not been widely available. Thirteen transgenic zebrafish lines have been developed during this thesis for expressing optogenetic proteins throughout the brain, such as GCaMP5G for imaging neuronal calcium dynamics, and ChR2(ET/TC) and eNpHR3.0 for activating and silencing neuronal activity, respectively. These biological tools were developed in combination with optical techniques for probing neural circuits. This thesis describes the design and construction of a custom selective plane illumination microscope for the rapid imaging of neuronal activity across large areas of the zebrafish brain. The use of a spatial light modulator is also described for the targeted stimulation of ChR2(ET/TC) in the cerebellum of larval zebrafish. This experiment provided preliminary data for the functional investigation of connections between cerebellar cells and the optic tectum, as well as confirming the validity of this technique for analysis of other neuronal circuits *in vivo*.

Since learning is one of the most interesting yet ill-defined processes controlled by the brain, this thesis aimed to use the tools developed above to examine the changes across neuronal circuit activity responsible for learning in larval zebrafish, specifically those in the cerebellum responsible for motor learning. A classical

conditioning assay was administered to 7-day-old zebrafish by pairing a non-startling tone with an aversive tail shock stimulus. This paradigm has been extensively used in other model organisms, however failed to produce a significant learning behaviour in the experiments performed for this thesis. More recent evidence suggests that zebrafish only begin to show learning from approximately one month of age. However, the data presented here indicate that zebrafish up to six weeks of age were still unable to undergo classical conditioning to pairings of auditory and electric stimuli. A number of issues potentially explain this result, such as the slow development of the auditory system and lower importance of auditory stimuli for juvenile animals, or the possible conflicting effects of prepulse inhibition versus potentiation of startle responses in these animals. Given these results, there was no opportunity to investigate the changes in cerebellar activity accompanying learning in this assay.

Despite the negative results in the classical conditioning assay, the tools developed during this thesis have been used for the investigation of other important circuits in larval zebrafish, specifically those in the optic tectum. In its mammalian homolog, the superior colliculus, this area of the brain is known to have a function in selecting appropriate motor behaviours by integrating multiple sources of sensory information. While the tectum has been widely studied for its role in visual behaviours, it remains unknown if this multisensory function is conserved in larval zebrafish. This thesis therefore aimed to address this question by examining the activity of cells in the zebrafish optic tectum in response to visual, auditory, and water flow stimuli using the transgenic lines and microscopy techniques outlined above. Functional clusters of tectal neurons were found that were responsive to each of these stimuli, with different clusters having distinct response profiles corresponding to particular stimulus features. Though cells were often found to be responsive to more than one feature, very few cells were shared between different sensory modalities. Cells responding to specific stimulus features were found to vary significantly between repeated presentations, but clusters generally contained core populations of consistently responsive cells.

Overall this thesis has developed a number of tools for the examination of neural circuits in larval zebrafish and further examined the properties of one important

region, the optic tectum. It has shown that tone-and-shock pairings are not a viable method for classical conditioning in larval or juvenile zebrafish. It has also demonstrated that the tectum, like its mammalian counterpart, can process information from multiple sensory modalities and does so using clusters of similarly responsive neurons. In particular, it is shown that the tectum receives strong visual and water flow information. Future investigations will examine integration of multiple sensory modalities in tectal circuits during simultaneously presented stimuli, and the specific effects of cerebellar activity on the modification of these circuits during normal sensory stimulation. This thesis provides a valuable contribution of knowledge to the burgeoning field of the zebrafish tectum, and lays a solid platform for further investigations of the functional circuits underlying behaviours.

Declaration by author

This thesis is composed of my original work, and contains no material previously published or written by another person except where due reference has been made in the text. I have clearly stated the contribution by others to jointly-authored works that I have included in my thesis.

I have clearly stated the contribution of others to my thesis as a whole, including statistical assistance, survey design, data analysis, significant technical procedures, professional editorial advice, and any other original research work used or reported in my thesis. The content of my thesis is the result of work I have carried out since the commencement of my research higher degree candidature and does not include a substantial part of work that has been submitted to qualify for the award of any other degree or diploma in any university or other tertiary institution. I have clearly stated which parts of my thesis, if any, have been submitted to qualify for another award.

I acknowledge that an electronic copy of my thesis must be lodged with the University Library and, subject to the policy and procedures of The University of Queensland, the thesis be made available for research and study in accordance with the Copyright Act 1968 unless a period of embargo has been approved by the Dean of the Graduate School.

I acknowledge that copyright of all material contained in my thesis resides with the copyright holder(s) of that material. Where appropriate I have obtained copyright permission from the copyright holder to reproduce material in this thesis.

Publications during candidature

Conference presentations:

Thompson, A.W. & Scott, E.K. (2012), Tools for analysing the cerebellar circuits involved in zebrafish motor learning, Presented at QBI Brain Plasticity Symposium, Brisbane, Australia.

Thompson, A.W. & Scott, E.K. (2012), Analysis of the cerebellar circuits involved in motor learning, Presented at SBMS Postgraduate Conference, Brisbane, Australia.

Thompson, A.W., Staykov, E. & Scott, E.K. (2013), Optogenetic analysis of the cerebellar circuits involved in zebrafish motor learning, Presented at Australian Neuroscience Society Meeting, Melbourne, Australia. (Istvan Törk Prize Winner)

Thompson, A.W. & Scott, E.K. (2013), Analysis of cerebellar neural activity during associative learning in Zebrafish, Presented at SBMS Postgraduate Conference, Brisbane, Australia.

Thompson, A.W., Heap, L.A. & Scott, E.K. (2014) Decoding zebrafish neural circuits using Selective Plane Illumination Microscopy (SPIM), Presented at Microscopy @ UQ Conference, Brisbane, Australia.

Thompson, A.W., Heap, L.A., Favre-Bulle, I., Rubinsztein-Dunlop, H., Scott, E.K. (2014), Decoding zebrafish neural circuits using optogenetics and patterned excitation, Presented at SBMS Postgraduate Conference, Brisbane, Australia.

Thompson, A.W., Heap, L.A., Favre-Bulle, I., Rubinsztein-Dunlop, H., Scott, E.K. (2014), Optogenetics and holography to assess the role of cerebellar input on tectal processing, Presented at Society for Neuroscience Conference, Washington, United States of America.

Thompson, A.W., Heap, L.A., Favre-Bulle, I., Rubinsztein-Dunlop, H., Scott, E.K. (2015), Optogenetics and holography to assess the role of cerebellar input on tectal processing, Presented at Australia and New Zealand Zebrafish Meeting, Gold Coast, Australia.

Publications included in this thesis

No publications included.

Contributions by others to the thesis

R. Dunning (Scott Laboratory, The University of Queensland) performed the addition of multiple restriction sites to the pME-MCS plasmid described in Chapter 2. D. Preece (School of Mathematics and Physics, The University of Queensland) and L. Heap (Scott Laboratory, The University of Queensland) assisted in the design and construction of the selective plane illumination microscope described in Chapter 2. I. Favre-Bulle (School of Mathematics and Physics, The University of Queensland) designed and added the SLM light path to the microscope described in Chapter 2. G. Vanwalleghem (Scott Laboratory, The University of Queensland) analysed the neuropil data using Thunder in Figure 4.7A. L. Heap (Scott Laboratory, The University of Queensland) acquired confocal images of retinal ganglion cell axons shown in Figure 4.7A. R. Faville (Queensland Brain Institute, The University of Queensland) assisted in the initial development of MATLAB code for analysing the data. E. Scott, L. Heap and G. Vanwalleghem (Scott Laboratory, The University of Queensland) made comments and suggestions on the analysis of the data and writing presented in this thesis.

Statement of parts of the thesis submitted to qualify for the award of another degree

None.

Acknowledgements

I would first like to thank my supervisor, Ethan Scott, for taking me on as a PhD student. You have always been very supportive of my goals and the way in which I have tried to achieve them. You have allowed me the freedom to develop the tools and techniques which excite me and created a shift in the lab from looking at behaviours and anatomy to focusing on the function of the underlying circuitry. You have pushed me when I needed pushing but also allowed me the space to carry out my research independently. Thank you.

I would like to thank all of the members of the Scott lab for creating a helpful and supportive environment for the past four years. In particular I want to thank the circuits crew for comments and suggestions for during the preparation of this thesis. I want to thank Lucy Heap for always being there and suffering by my side through this PhD process over the last couple years. Your friendship and encouragement has meant a lot to me. Gilles Vanwalleghem, even though you have only been in the lab a relatively short time I immediately thought of you as both a friend and mentor. I admire your commitment to your work and your family and hope to have many more fun and exciting board game nights with you in the future.

I want to thank Rebecca Dunning for your help getting me set up in the lab and for your help in the molecular biology and transgenesis during my PhD. I would like to thank Daryl Preece, who taught all of the biologists in the lab how a lens worked. Your help and insights were crucial during the design and construction of the SPIM. I would like to thank Itia Favre-Bulle for all of your hard work implementing the SLM on our microscope, and for helping with all the more recent additions and modifications to the rig. Thanks also to Richard Faville, who helped me in the initial stages of code development.

I would like to give my most heartfelt thank you to Victoria McGuire. After a rough couple of years you came into my life when I needed you the most. You have given me unconditional love and support and made this whole thing worthwhile. It has been fun and challenging, but I couldn't imagine finishing this PhD without you by my side. No matter what the future brings, I love you, and I am very lucky to have known you. Thank you.

A big thank you goes to Justin Christoforou for being my best friend for the last four years, and for the decade before that. You've been a true friend and you deserve so much credit. My biggest thank you goes to my parents, Debra and David. You have always put your children first and I can never truly convey my gratitude for all of the hard work and sacrifices you have made for me. You have supported me emotionally and financially throughout the PhD process and I want you to know how proud I am to be your son. This thesis dedicated to you.

I would like to extend my thanks to Geoff Goodhill and Zac Pujic for being excellent mentors and friends during my time before beginning this PhD and fostering my desire to continue a career in research. I would also like to thank Geoff and the other members of my advisory committee, Pankaj Sah and Bruno van Swinderen, who pushed me to delve deeper into my data and look for the interesting findings that would be waiting within. Thank you also to Annabel McGuire for your comments on structuring this thesis during the drafting process.

Thank you to the School of Biomedical Sciences and The University of Queensland, you have been my second home for the past eleven years and I have really enjoyed my time here. I would like to thank the university and the Australian Government for the living allowance provided by Australian Postgraduate Award, and for the funding for this project coming from an NHMRC Project Grant (APP1066887), an ARC Future Fellowship (FT110100887), and ARC Discovery Project Grants (DP140102036 and DP110103612) awarded to Ethan Scott.

Keywords

zebrafish, neuroscience, tectum, optogenetics, learning, microscopy, circuits, coding

Australian and New Zealand Standard Research Classifications (ANZSRC)

ANZSRC code: 060603, Animal Physiology - Systems, 50%

ANZSRC code: 110999, Neurosciences not elsewhere classified, 40%

ANZSRC code: 060199, Biochemistry and Cell Biology not elsewhere classified, 10%

Fields of Research (FoR) Classification

FoR code: 0606, Physiology, 50%

FoR code: 1109, Neurosciences, 40%

FoR code: 0601, Biochemistry and Cell Biology, 10%

Table of Contents

List of Figures

List of Tables

List of Abbreviations

3D	three-dimensional
ANCOVA	analysis of covariance
Arch	archaerhodopsin-3
ChR2	channelrhodopsin-2
CRISPR	clustered regularly interspaced short palindromic repeat
CS	conditioning stimulus
DCN	deep cerebellar nuclei
DNA	deoxyribonucleic acid
dpf	days post fertilisation
EC	eurydendroid cell
eNpHR	enhanced halorhodopsin
FWHM	full width at half maximum
GCL	granule cell layer
GFP	green fluorescent protein
MI	matching index
NA	numerical aperture
nMLF	nucleus of the medial longitudinal fasciculus
NpHR	halorhodopsin
OGB-1	Oregon Green-488–1,2-bis(o-aminophenoxy)ethane-N,N,N',N'-tetraacetic acid–1-acetoxymethyl-1
OKR	optokinetic response
OMR	optomotor response
PATagRFP	photoactivatable mutant of red fluorescent protein
PCA	principal components analysis
PVIN	periventricular interneuron
PVL	periventricular layer
PVN	periventricular neuron
PVPN	periventricular projection neuron
RGC	retinal ganglion cell
RNA	ribonucleic acid
ROI	region of interest
SAC	stratum album centrale

SFGS	stratum fibrosum et griseum
SGC	stratum griseum centrale
SIN	superficial interneuron
SLM	spatial light modulator
SO	stratum opticum
SPIM	selective plane illumination microscopy
SPV	stratum periventriculare
TALEN	transcription activator-like effector nuclease
TLN	Tupfel long fin *nacre*
UAS	upstream activating sequence
US	unconditioned stimulus
VSFP	voltage-sensitive fluorescent protein
YFP	yellow fluorescent protein

Chapter 1

Introduction

1.1 Preamble

The human brain is an enormously complex organ responsible for interpreting all of the sensations and producing all of the thoughts, emotions and interactions that we have with the world around us. One of the fundamental mysteries remaining to be explained in modern neuroscience is how networks of cells in the brain communicate with one another to encode perceptions of the external world and generate appropriate behaviours in response. This question requires an understanding of how populations of neurons in the brain form functional circuits and how changes in activity among these pathways result in behaviours. Due to the complexity of this challenge, it has been addressed from a range of different perspectives, each with particular advantages and disadvantages.

First described by Julius Bernstein and Emil du Bois-Reymond in the nineteenth century (Schuetze, 1983), the action potential forms the basis of communication between neurons in the brain. This action potential is an electrical event in the cells whereby the resting membrane potential is depolarised, opening voltage-gated sodium channels in the membrane that propagate this wave of depolarization along the axon of a neuron away from the cell body. This is a transient depolarization that is rapidly repolarized by voltage-gated potassium channels. Once at the axon terminal, the wave of depolarization causes calcium entry into the cell through voltage-gated calcium channels, triggering release of neurotransmitters such as gamma-aminobutyric acid (GABA), glutamate or dopamine from synapses. These neurotransmitters diffuse across the synapse and are bound by specific receptors on the dendrites of post-synaptic cells, causing either a rise (excitation) or fall (inhibition) in the membrane potential of that cell depending on the neurotransmitter received. The dendrites of post-synaptic neurons are typically long and extensively branched, such that they are able to receive and summate excitatory and inhibitory signals from hundreds or even thousands of different pre-synaptic cells. If this cell is excited beyond a critical threshold, it too will initiate action potential firing and carry signals forward through the networks of cells in the brain to process information. While a great amount is known about the physiology action potential firing, it is unclear how information is encoded by the rate, frequency and relative timing of action potentials within networks of neurons in the brain.

Not only does the probability and frequency of this process vary depending on the different morphology and physiology of the cells involved, the strength of the connections at the synapse can change over time depending on previous experience. This change in synaptic strength, or synaptic plasticity, is critical to the processes of learning and memory (Bailey et al., 2015; Martin et al., 2000; Siegelbaum & Kandel, 1991). These synapses do not operate in isolation however, and the brain relies on distributed networks of neurons for receiving and processing information and generating behaviours. This creates a challenge with respect to examining neuronal circuits from individual synapses, to local circuits, and the whole brain level (Figure 1.1). A comprehensive understanding of functional connectivity of neuronal networks across these vastly different scales will have wide-ranging benefits from understanding the basis of cognition, neuropsychiatric disorders and the general human condition. Until recently however, technical limitations have prevented an accurate analysis of how individual cells act together as a population in functional networks (Lewis et al., 2015).

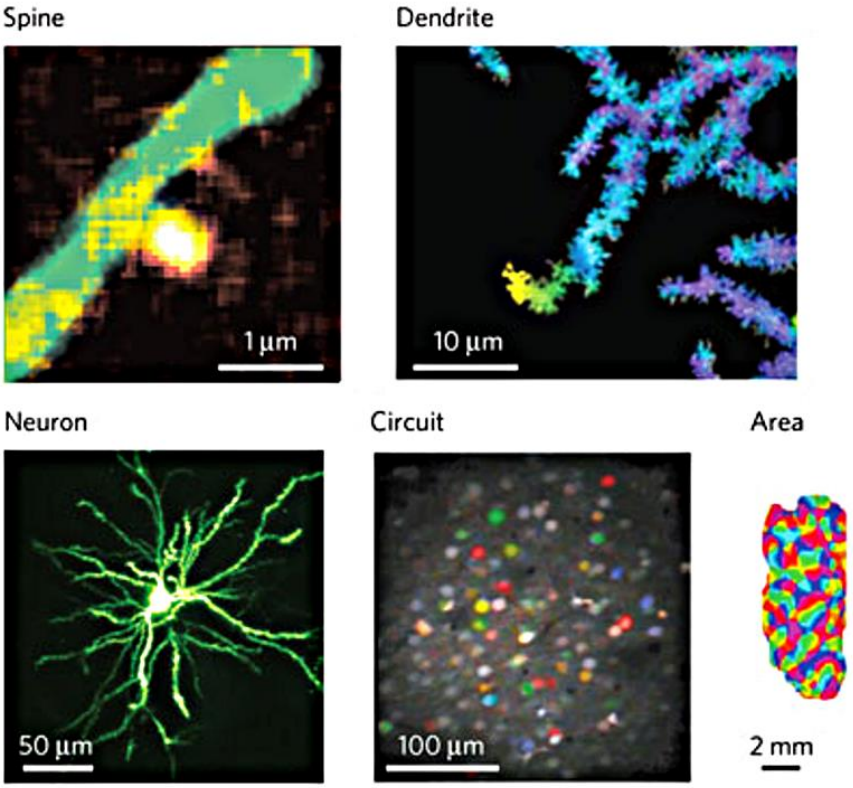

Figure 1.1. Investigating neuronal function across different spatial scales. Representative examples show activity visualised using a variety of optical indicators and microscopy techniques to investigate the function of neuronal structures and circuits. Example images are of a single synaptic spine in the mouse hippocampus, the dendritic tree of a cerebellar Purkinje cell, a layer-2/3 pyramidal neuron in the mouse visual cortex, a local circuit of cells with different orientation preferences in the rat visual cortex, and the orientation preferences across a large area of the cat visual cortex. Image adapted from Scanziani & Häusser (2009).

1.2 Experimental approaches for studying neuronal function

1.2.1 Electrophysiology

Since the first studies recording electrical activity from the cortex of the cat (Li & Jasper, 1953), the electrode has been the foremost tool for examining neuronal cell activity. Electrophysiology detects changes in electrical activity along the cell membrane with excellent temporal and voltage sensitivity. As such, electrophysiology has been used to great effect in the study of the biophysical and biochemical properties of individual neurons. For example, using microelectrodes that form a seal with the cell membrane (patch clamp), current or voltage changes can be recorded to examine the functional signalling from excitatory and inhibitory circuits on the firing of action potentials within a given cell. Depending on the size of the electrode, this can be restricted even to the fine dendritic processes of neurons to examine individual synaptic inputs (Davie et al., 2006). These electrodes can also provide direct delivery of current or membrane potential changes to cells to manipulate neuronal firing as desired and further examine neuronal function.

While electrophysiology remains unparalleled in terms of signal-to-noise sensitivity and temporal resolution, there are still a number of limitations to this technique. For instance, *in vivo* studies are invasive and usually require the animal to be immobilised and sedated, which can have significant impacts on neural function (Greenberg et al., 2008; Momosaki et al., 2004; Movshon et al., 2003; Pack et al., 2001; Rinberg et al., 2006; Scheibler et al., 1999). As such, electrophysiology is often performed *ex vivo* in slice cultures, which eliminates countless *in vivo* circuit interactions and makes it impossible to investigate long-range functional connections. In addition, recordings are usually restricted to only one or a few cells at a time, making it quite difficult to establish the functional role of these cells in distributed neural networks. The introduction of multi-electrode arrays has begun to address this limitation, however these are still deficient in their ability to observe multiple cells across different brain regions as they interact within a circuit (Obein et al., 2015; Spira & Hai, 2013).

Multi-electrode arrays are often designed to examine cells in superficial layers of the cortex, making it challenging to assess the function of neuronal circuits in deeper brain regions, or indeed across a variety of depths. The extracellular nature of

multiunit recording also makes it impossible to detect subthreshold activity, and creates challenges such as spike sorting to differentiate signals from individual neurons, and their specific locations (Delgado Ruz & Schultz, 2014). Additionally, electrophysiology generally records from quite a sparse sample of neurons in the targeted region. This is important if there is bias towards neurons with inherently higher firing rates dominating activity traces. For this reason electrophysiology has so far been unable to fully characterise how populations of cells in a neuronal circuit produce patterns of activity relevant to behaviours.

1.2.2 Measurements of whole-brain activity

At the opposing end of the scale, activity across multiple connected regions of the brain can be detected simultaneously using a number of non-invasive techniques that can be applied in either animal or human studies. For example, electroencephalography (EEG) measures the local field potentials of cells underneath the scalp as they undergo firing activity. This is useful for looking at the activity of the average population response of different regions with high temporal resolution and identifying local brain states. It is also useful for examining synchrony across different areas, but lacks the sensitivity of more invasive electrical recording techniques such as electrocorticogram, where subdural electrodes are places on the cortical surface (Buzsáki et al., 2012). Functional magnetic resonance imaging (fMRI) measures changes in blood flow and oxygenation levels across the brain as a proxy for neuronal activity within areas perfused by that blood (Heeger et al., 2000; Heeger & Ress, 2002). As with EEG, this technique is useful for exploring the general brain regions that are linked to certain behaviours, and uncovering potential correlations between connected areas. However, this method of analysis is also dependent on the average activity of the population of cells within a given region. While the spatial resolution of fMRI is generally greater than EEG, neither technique allows activity to be resolved at the single cell level, nor how these cells may communicate with one another to encode information. In order to more thoroughly address the question of how circuits act together to process information and generate behaviours, a technique is required that allows for the simultaneous recording of neural activity across large numbers of neurons *in vivo* with a high spatial and temporal resolution.

Many of the above limitations can be overcome with the use of optics to image fluorescent indicators of neuronal activity, a technique known as optical physiology, or optophysiology. As light can theoretically achieve spatial and temporal resolution equivalent to electrophysiology, this can provide an optimal balance allowing activity across large populations of neurons to be imaged simultaneously at a resolution great enough to identify firing events in individual cells. In reality however, electrophysiology currently offers faster sampling rates, deeper recording depths and greater signal-to-noise ratios than traditional optical methods. While new advances are regularly being developed in this field (Papagiakoumou, 2013; Vaziri & Emiliani, 2012), electrophysiology remains the preferred method for in-depth analyses of single cell properties, while optical recording techniques have become the dominant means to analyse larger neural circuits *in vivo* (see Figure 1.2). The main advantages and disadvantages of different methods for recording of neuronal activity are summarised in Table 1.1, clearly suggesting that optical imaging techniques are optimally-suited for the analysis of patterns of activity across neuronal networks underlying behaviour in this thesis.

	Electrophysiology	Electroencephalography (EEG)	Functional Magnetic Resonance Imaging (fMRI)	Optical Physiology
Spatial resolution	High (subcellular)	Very low	Low	High (subcellular, with high magnification imaging)
Temporal resolution	High	High	Low	Moderate
Coverage	Low (even with multielectrode arrays)	High	High	Moderate
Sensitivity (SNR)	High	Moderate	Moderate	Moderate
Activity manipulation	Yes (directly via electrode)	No	No	Yes (through expression of optogenetic proteins)
Depth penetration	High (low if cells are visually-targeted)	Low	High	Moderate
Invasiveness	High	Low	Low	Low
Ideal applications	Synaptic integration, membrane conductance, ion channel properties	Non-invasive studies of human cortical activity	Non-invasive regional connectivity studies	Network & circuit analyses in small animal models

Table 1.1. Advantages and disadvantages of various methods for examining neuronal activity. While methodologies exist within each group that have specific properties optimized for different conditions, the general trends for each category are listed. Sources: (Buzsáki et al., 2012; Heeger & Ress, 2002; Scanziani & Häusser, 2009; Sejnowski et al., 2014).

Originally, the first viable method for optically recording neural activity was through the use of chemical dyes (Cohen et al., 1978). Fluorescent dyes that directly report on changes in membrane voltage were originally developed in the 1970s (Cohen et al., 1974) and have continued to progress in their development since (Hill et al., 2014; Tsytsarev et al., 2014). Recent generations of voltage dye, such as JPW-4090 (di-2-ANBDQPQ), have responses rate in the microsecond range and achieve a peak change in fluorescence of around 10-13% (Zhou et al., 2007). This dye has recently been used for optical mapping of cortical slices to examine circuits in mouse barrel cortex (Lo et al., 2015). While the significant temporal kinetics of these dyes allow separation of individual action potentials, their low signal-to-noise ratios makes it difficult to measure minor voltage changes, especially when sampling from a large population of densely packed neurons (Hill et al., 2014).

Intracellular calcium plays a role in many different processes involved in neuronal communication, including as a second-messenger from glutamate receptor activation, triggering neurotransmitter release at the synaptic cleft, as well as a significant role in regulating gene transcription associated with learning and memory (Grienberger & Konnerth, 2012; Ross, 1989; Simms & Zamponi, 2014). Indeed action potentials have been associated with a rise in internal calcium concentrations of up to 1000% (Berridge et al., 2000). As such fluorescent dyes have been developed to detect changes in intracellular calcium as a means for examining neural activity (Tsein, 1980). Calcium dyes have many advantages over voltage indicators (Grewe & Helmchen, 2009), including a greater signal-to-noise ratio and less invasive loading methods through the use of cell permeable acetoxymethyl (AM) esters (Tsein et al., 1982). Modern calcium dyes such as Oregon Green-488–1,2-bis(o-aminophenoxy)ethane-N,N,N',N'-tetraacetic acid–1-acetoxymethyl-1 (OGB-1), have been used extensively the analysis of neural circuits in rodent cerebellum (Flusberg et al., 2008; Ozden et al., 2008), frontal cortex (Komiyama et al., 2010), somatosensory cortex (Kerr et al., 2007; Winship & Murphy, 2008) and visual cortex (Greenberg et al., 2008; Rochefort et al., 2009).

These dyes do however have disadvantages relative to voltage indicators or electrophysiology. While calcium imaging can be used to detect small, subthreshold changes in activity in the dendrites of cells sparsely-labelled with OGB-1 *in vivo*,

these are often undetected when imaging the cell body (Jia et al., 2010). When analysing large networks of tightly apposed neuronal cells *in vivo* using calcium indicators, signals are therefore usually biased towards the action potential responses from individual cells, rather than the subthreshold communication between them (Peterka et al., 2011). Furthermore, although negative fluorescence changes have been observed to olfactory cues using calcium-green in insects (Sachse & Galizia, 2002), it is rare for calcium dyes to be used to detect responses from inhibitory transmission in the literature. Finally, although the use of dyes for optical recording of neuronal activity has made valuable contributions to the literature, dye loading by AM esters or bulk electroporation can often lack reproducibility and the means to target specific cell types or circuits within the brain. In order to achieve this, fluorescent reporter proteins have been developed that can be encoded by specific genetic sequences and incorporated into the genome of animals to be endogenously transcribed and expressed within particular cells (Tantama et al., 2012).

1.2.3 Optogenetic indicators

Optogenetics describes the use of genetically-encoded proteins to either observe or manipulate the activity of a cell when exposed to a specific wavelength of light. A growing variety of indicators are now available for imaging neuronal dynamics, including genetically-encoded indicators for voltage (Knöpfel et al., 2015), calcium (Tian et al., 2012), glutamate (Hires et al., 2008), chloride (Markova et al., 2008) and pH (Sankaranarayanan et al., 2000). While the latter two have specific roles in the analysis of inhibitory circuits, voltage sensors remain the fastest and most direct measure of neuronal activity (Knöpfel et al., 2015). Voltage sensors are either based on a voltage-sensing domain, such as VSFP (Sakai et al., 2001), VSFP2.1 (Lundby et al., 2010) and VSFP-Butterfly 1.2 (Akemann et al., 2012), or on opsins, such as Arch(D95N) (Kralj et al., 2012) and QuasAr1 and 2 (Hochbaum et al., 2014). Similarly to voltage dyes however, genetically-encoded voltage indicators usually combine very fast response rates with relatively low signal-to-noise ratios. As a result, strong light intensities are required to image these proteins at frame rates high enough to detect reliable signals, leading to increased photodamage. Therefore, in order to optically record activity from large, distributed networks in the brain,

indicators of second-messengers with slower kinetics, such as calcium, are comparatively more useful.

Similar to voltage indicators, multiple variants of protein calcium sensors have been used to measure neuronal activity such as aequorin (Baker et al., 1971) and Yellow Cameleon-2.1 (Tsuchiya et al., 2002), however it is the use of the GCaMP family of reporters that has become most prominent. GCaMP is a fusion protein based on a circularly permutated green fluorescent protein (GFP) and the calcium-binding protein, calmodulin (Nakai et al., 2001). Upon the binding of calcium by calmodulin, a conformational change causes an increase in GFP fluorescence, which can be correlated to the number of action potential spikes (Yaksi & Friedrich 2006). Variations of this protein have been optimised for increased speed and sensitivity over several generations including GCaMP3 (Tian et al., 2009), and more recent versions such as GCaMP5G (Akerboom et al., 2012) and GCaMP6s, m, and f (Chen et al., 2013). Due to their favourable properties such as increased brightness, dynamic range and temporal kinetics, these tools have been used to examine murine neural circuits responsible for vision (Cruz-Martin et al., 2014), taste (Barretto et al., 2015), audition (Schneider et al., 2014), learning (Lovett-Barron et al., 2014) and plasticity (Kuhlman et al., 2013). Given their numerous advantages, these tools are often used in combination with optogenetic manipulators of activity for comprehensive investigation of neural circuit function. The main advantages and disadvantages of different tools for optical reporting of neuronal activity are summarised in Table 1.2, clearly suggesting that genetically-encoded calcium sensors are the tool best suited for imaging neuronal activity across broad circuits in this thesis.

.

	Voltage dyes (JPW4090, VF2.4.Cl, di-4-ANEPPS, RH 795)	Calcium dyes (OGB-1, Fura-2, Fluo-4)	FRET-based voltage sensors (VSFP2.3, VSFP-Butterfly 1.2)	Opsin-based voltage sensors (Arch(D95N), QuasAr1)	GECIs (aequorin, Cameleon-2.1, GCaMP5G)
Temporal resolution	High	Moderate	High	High	Moderate
Sensitivity (∆F/F)	Low	High	Low	Low	High
Labelling coverage	Moderate	Moderate	High	High	High
Quantum Yield	Moderate	High	Moderate	Low	Moderate
Photobleaching	Moderate	Moderate	Low	Low	Low
Ideal applications	Synaptic properties of small networks *in vitro*	Firing within small networks *in vivo*	Synaptic properties of small networks *in vivo*	Synaptic properties of small networks *in vivo*	Firing within large networks *in vivo*

Table 1.2 Advantages and disadvantages of various optical probes of neuronal activity. While variants exist with improved properties optimized for various conditions, the general trends for each category are listed. Common examples of probes in each category are listed in brackets below category labels. Sources: (Akemann et al., 2012; Akerboom et al., 2012; Baker et al., 1971; Hill et al., 2014; Hochbaum et al., 2014; Knöpfel et al., 2006; Knöpfel et al., 2015; Kralj et al., 2012; Lundby et al., 2010; Miller et al., 2012; Tsuchiya et al., 2002; Tsytsarev et al., 2014).

1.2.4 Optogenetic modulators

As with indicators of neural activity, genetically-encoded proteins that can either increase or decrease neural activity also exist in many forms. For instance, action potentials can be inhibited by hyperpolarising neurons expressing light-gated chloride channels such as enhanced halorhodopsin (eNpHR) (Gradinaru et al., 2008) or proton pumps such as archaerhodopsin-3 (Arch) (Chow et al., 2010). Optimised versions of these proteins have been developed for increased efficiency (Gradinaru et al., 2010; Han et al., 2011), and new tools have been created from different rhodopsins for other beneficial properties such as peak excitation wavelengths (Chuong et al., 2014). These tools have been used to investigate neural circuits in the mouse modulated by acetylcholine (Witten et al., 2010), as well as those involved in anxiety (Tye et al., 2011), fear (Do-Monte et al., 2015), vision (Olsen et al., 2012) and social behaviours (Lee et al., 2014; Yizhar et al., 2011b).

Genetically-encoded proteins capable of stimulating neuronal activity are almost exclusively based on bacterial opsins, such as channelrhodopsin-2 (ChR2) (Boyden et al., 2005; Nagel et al., 2003). ChR2 is a cation channel that changes conformation to open upon stimulation with blue light, at wavelengths around 488 nm. When opened, positively-charged ions such as sodium and hydrogen rapidly travel from extracellular sources into the cell down the high concentration gradient. This depolarises the cell from its resting membrane potential and increases the probability of action potential firing. Similar proteins have also been utilised for triggering neural activity such as VChR1, a rhodopsin derived from *Volvox carteri* with red-shifted excitation wavelengths (Zhang et al., 2008), as well as numerous other engineered ChR2 variants with improved properties and kinetics (Berndt et al., 2011; Klapoetke et al., 2014; Kleinlogel et al., 2011; Lin et al., 2009; Yizhar et al., 2011b). Many of these tools have been used in isolation to examine functional connectivity in the mouse brain (Wang et al., 2007), as well as in combination with optogenetic inhibitors to investigate circuits involved in vison (Adesnik et al., 2012; Olsen et al., 2012), fear (Jennings et al., 2013), anxiety (Tye et al., 2011) and social behaviours (Lee et al., 2014), as well as learning and memory (Huff et al., 2013; Johansen et al., 2014).

The expression of optogenetic proteins can be genetically targeted to restricted populations of cells, thereby improving the precision with which selected brain networks can be examined (Bozza et al., 2004; Branda & Dymecki, 2004; Diez-Garcia et al., 2007; Jefferis & Livet, 2012). In mammalian systems, optogenetic proteins are typically expressed transiently from viral vectors injected directly into the brain regions of interest (Britt et al., 2012; Zhang et al., 2012). This carries with it difficulties associated with specific targeting, efficiency, viral load and damage at the injection site (Packer et al., 2013), and as such, stable expression from transgenic animals is the preferred method in small model systems.

In order to investigate neuronal circuits in awake, behaving animals, optogenetic stimulation in rodents and other higher order vertebrates is also often carried out using light delivered by fibre-optic cannulas (Britt et al., 2012; Zhang et al., 2012). Not only does this procedure require invasive surgery, but excitation of optogenetic manipulators is significantly attenuated at increasing distances from the light source due to the absorbance and scattering of light in the tissue (Al-Juboori et al., 2013; Favre-Bulle et al., 2015; Yizhar et al., 2011a). This same fact also makes it extremely difficult to optically record from neural activity indicators at any significant depth within the brain of these animals. These issues can be mitigated somewhat by the use of 2-photon imaging and stimulation (Denk et al., 1990; Mostany et al., 2015; Packer et al., 2012; Prakash et al., 2012), but can also be minimized by the use of small animal models such as the larval zebrafish, in which light does not need to penetrate the same volume of tissue as rodent models.

1.2.5 Microscopy

The optical imaging of neuronal activity reporters, and often the stimulation of optogenetic proteins, requires the use of microscopy to achieve resolution at the level of individual cells. As such, there is a strong need for interdisciplinary approaches when developing experimental approaches targeted towards optogenetic investigations of neural circuits. Traditional raster scanning techniques such as confocal microscopy (Wilson & Sheppard, 1984) and 2-photon microscopy (Denk et al., 1990) offer sufficient optical clarity but have low temporal resolution relative to the patterns of activity of broad neuronal networks. Consequently, several microscopy techniques have been recently developed for imaging large brain

volumes at high spatial and temporal resolution. Light sheet microscopy (Vladimirov et al., 2014), light field microscopy (Prevedel et al., 2014), SCAPE microscopy (Bouchard et al., 2015), and 3D projection-based microscopy using a spatial light modulator (Quirin et al., 2014) have all been used recently with sufficient spatial and temporal resolution to map correlated responses across neuronal networks *in vivo*. While each of these different techniques have significant advantages and disadvantages (discussed in detail in Chapter 2.2), selective plane illumination microscopy (Huisken et al., 2004) offered a means for simple, fast, and cost-effective imaging of neuronal populations and was chosen for the imaging of neuronal activity in this thesis.

In addition to imaging neuronal activity, advances microscopy techniques have allowed more precise and targeted optogenetic activation of cells within a circuit. A spatial light modulator has recently been shown to sculpt light in three-dimensions to optically drive activity from specific cells in the mouse cortex *in vitro* (Packer et al., 2012) and *in vivo* (Packer et al., 2015). This method stimulating optogenetic tools can theoretically be combined with light sheet to imaging to examine neural circuits without any impediments. As such, Chapter 2.4 of this thesis aimed to examine the utility of spatial light modulator-driven activation of cells in one brain region while simultaneously recording neuronal activity in another region using light sheet microscopy. While limitations and changes are described that can improve this technique, activity from the genetically-encoded calcium indicator, GCaMP5G (Akerboom et al., 2012), was observed in response to stimulation of the channelrhodopsin variant ChR2(ET/TC) (Berndt et al., 2011) *in vivo*. Overall, the use of genetically-encoded calcium indicators and opsin-based activity manipulators, combined with refined optical imaging and stimulating techniques provide outstanding opportunities to probe the neural mechanisms underlying behaviour (Figure 1.2).

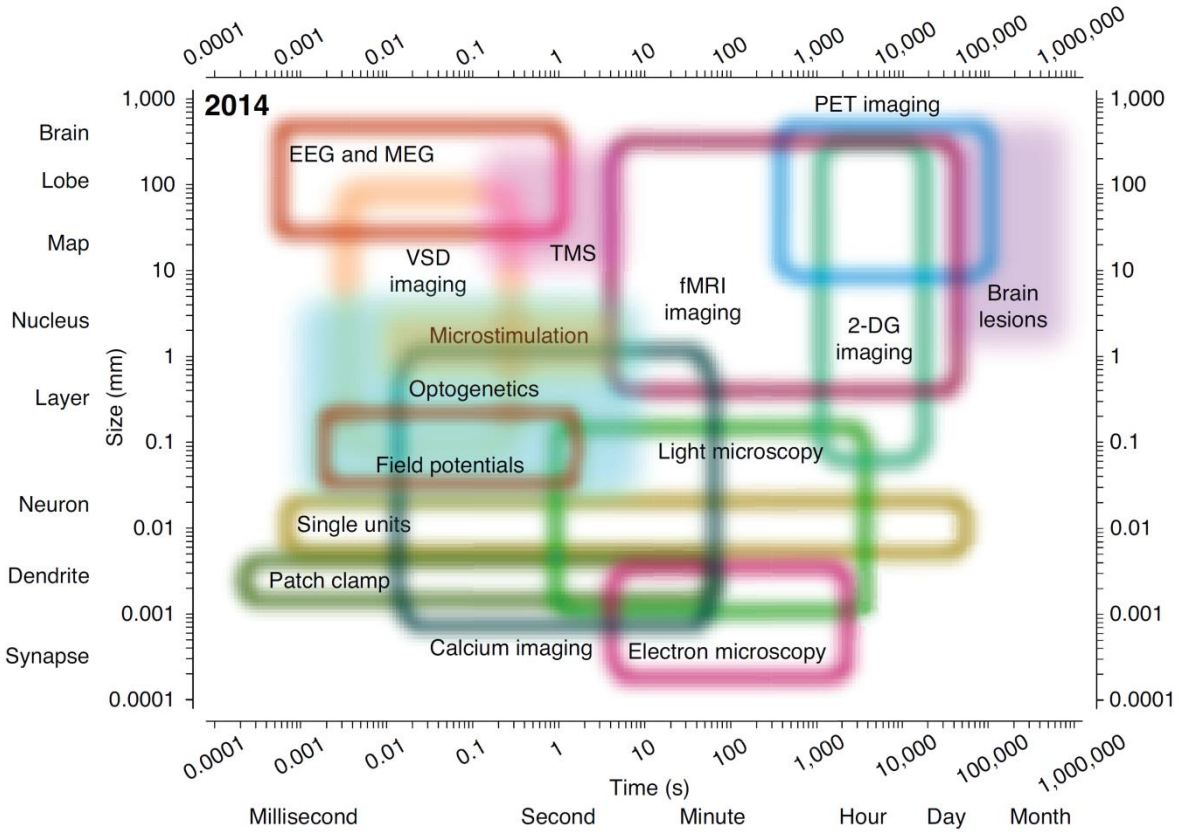

Figure 1.2. Methods for the investigation of neuronal circuits span several orders of magnitude in both spatial and temporal resolution, adapted from Sejnowski et al. (2014). Open regions represent methods for measuring activity while filled areas represent methods for perturbing normal activity. New developments in calcium imaging, optogenetics and light microscopy have further improved these techniques, offering relatively high resolution in both the spatial and temporal domains.

1.3 Zebrafish as a model organism for functional neuroscience

Due to the many technical constrains outlined above, and the enormous complexity of the human brain, we currently lack a deep understanding of how functional networks in the brain allow us to consciously perceive and interact with the world around us. Small animal models offer both reduced complexity of the neural circuits underlying behaviours, and provide fewer technical and ethical limitations to the observation and manipulation of these circuits in live subjects. In taking this approach, a balance is required between organisms that may be too simple to share common functional circuits with humans, such as *Caenorhabditis elegans* (de Bono & Maricq, 2005) and *Drosophila melanogaster* (Owald et al., 2015), and mammalian models with more complex circuits that remain difficult to study *in vivo*. In evolutionary terms, fish provide a suitable compromise by retaining many basic brain structures seen in other vertebrates, albeit with reduced circuit complexity. While the mouse brain contains roughly 70 million (Herculano-Houzel et al., 2006) to 75 million (Williams, 2000) neurons, the larval zebrafish (*Danio rerio*) only contains around 78 thousand neurons at 7 days post fertilization (dpf) (Hill et al., 2003). As such, the zebrafish has become a favoured model organism for many labs investigating neuronal circuits underlying basic behaviours.

The relatively small brain volumes of larval zebrafish make them extremely valuable for optically imaging activity across large neuronal populations *in vivo*. Importantly for this, mutant strains of zebrafish have been isolated that lack pigmentation and remain optically transparent during larval stages (Lister et al., 1999). During this time, most brain regions develop and possess homologous areas to those in higher-order vertebrates such as the spinal cord, cerebellum and olfactory bulb (Mueller & Wullimann, 2005). However, the range of questions able to be addressed using this model is limited due to the lack of a cerebral cortex and only ambiguous homology to telencephalic structures such as the hippocampus or amygdala (Mueller et al., 2011). Furthermore, complex behaviours such as aggression (Oliveira et al., 2011), courtship (Darrow & Harris, 2004) and other social interactions (Al-Imari & Gerlai, 2008; Miller & Gerlai, 2012) are not present in larval zebrafish, making studies during their transparent ages restricted to simple behaviours derived from more primitive brain structures.

1.3.1 Behavioural repertoire of zebrafish larvae

Despite their comparatively simple neuronal circuitry, larval zebrafish still have a vast behavioural repertoire (Fero et al., 2011). From an early age, larval zebrafish naturally perform a variety of swimming behaviours (Budick & O'Malley, 2000), as well as distinctive startle responses when presented with different aversive stimuli (Burgess & Granato, 2007). As they develop, larvae also gain the ability to orient themselves in response to water flow stimuli (Suli et al., 2012), as well as the ability to track and capture prey items (Borla et al., 2002; McElligott & O'Malley, 2005). A number of other visually-driven behaviours have also be examined in larval zebrafish, including phototaxis (Burgess et al., 2010), optomotor and optokinetic responses (Roeser & Baier, 2003), as well as escape from looming stimuli (Temizer et al., 2015). While the tectum has been examined in relation to all of these behaviours, its role in zebrafish to non-visual sensory modalities has not been examined. In Chapter 4 of this thesis, the responses of tectal neurons to auditory and water flow stimuli are compared with visually-driven responses in an attempt to decipher how tectal circuits filter and integrate sensory information and generate behaviours.

Several studies have also examined the capacity for learning in larval zebrafish (reviewed by Roberts et al., 2013). In particular, there is evidence that larval (Aizenberg & Schuman, 2011) and juvenile (Lee et al., 2010; Valente et al., 2012) zebrafish are capable of learning conditioned behaviours. While the cerebellum is known to be important in these behaviours (Freeman & Steinmetz, 2011; Strick et al., 2009), the precise activity within neural circuits that lead to such behaviours remains unclear. Chapter 3 of this thesis describes attempts to develop an assay in which the cerebellar circuits underlying learning can be addressed in larval zebrafish using optogenetics.

1.3.2 Optogenetic dissection of zebrafish neural circuits

Given the relative optical clarity of the larval zebrafish, neuronal activity has been monitored using fluorescent indicators of activity. In particular, calcium dyes have been used for the investigation of circuits responsible for visual behaviours in the hindbrain (Orger et al., 2008), tectal circuits involved in vision (Niell & Smith, 2005; Ramdya & Engert, 2008; Sumbre et al., 2008) and cerebellar circuits active during

learning (Aizenberg & Schuman, 2011). Due to the simple and efficient transgenesis techniques available for zebrafish however, genetically-encoded calcium indicators have also been extensively used for the investigation of visual processing in the tectum (Bianco & Engert, 2015; Hunter et al., 2013; Nikolaou et al., 2012; Romano et al., 2015). This is in addition to circuits in the spinal cord (de Vico Fallani et al., 2015; Warp et al., 2012), cerebellum (Matsui et al., 2014) and nucleus of the medial longitudinal fasciculus (nMLF) (Thiele et al., 2014).

Using 2-photon microscopy, genetically-encoded calcium indicators have been imaged in response to optokinetic (Portugues et al., 2014) and motor adaptation tasks (Ahrens et al., 2012) in larval zebrafish. With the aid of anatomical registration, volumetric data from these experiments have been combined to analyse circuits involved in these behaviours across the whole brain. While these studies allowed the comparison of averaged responses between regions through registration, more recent advances in microscopy techniques have effectively allowed the entire 70-80 thousand neurons of the larval zebrafish brain to be imaged in three dimensions several times per second at a single cell resolution (Prevedel et al., 2014; Vladimirov et al., 2014). Using these techniques, neuronal activity has been correlated in circuits distributed across the brain in response to olfactory stimuli within a single trial (Prevedel et al., 2014).

The same properties that allow neural circuits to be imaged in larval zebrafish so effectively also make them ideally suited for optogenetic manipulations. Optogenetic activation of cells in the zebrafish was first carried out using an activator that is not based on an opsin, the light gated glutamate receptor (LiGluR) (Szobota, et al., 2007). Here, whole animal illumination was used to reversibly block an escape response to a tactile stimulus, which was attributed to activation of Rohon-Beard cells in the spinal cord. However, despite using the fish with the same expression pattern, Douglass et al. (2008) observed stimulation of Rohon-Beard cells using ChR2 was able to initiate rather than prevent escape response. These conflicting results may be due the fact that illumination of ChR2 in the latter study was targeted to individual cells as opposed to wide-field illumination which is likely to have activated several other cells and circuits that may regulate escape responses. This highlights the need for either tight genetic or optical restriction when attempting to

examine neuronal circuits responsible for particular behaviours. As such, optogenetic tools such as ChR2 and eNpHR have been used to examine the function of many circuits including those in the hindbrain (Arrenberg et al., 2009) and spinal cord (Ljunggren et al., 2014; Warp et al., 2012) that regulate locomotion, as well as the role of nMLF cells in controlling posture and tail orientation (Thiele et al., 2014).

Optogenetics have also been extensively employed to examine behaviours related to the visual system. Cells in the zebrafish hindbrain that integrate oculomotor information and stabilize eye positions have been analysed optogenetically using both NpHR (Miri et al., 2011) and ChR2 (Gonçalves et al., 2014). Circuits in the hindbrain responsible for the generation of saccades during optokinetic responses have also been identified by targeted loss-of-function and gain-of-function using NpHR and ChR2, respectively (Schoonheim et al., 2010). ChR2 has also been used to isolate circuits in the anterior-ventral optic tectum and pretectum that are responsible for the initiation of J-turns, behaviour specific to prey capture in larvae (Fajardo et al., 2013). Given the expansion in optogenetic analyses of neural circuits using larval zebrafish, a number of recent reviews have examined this topic (Baier & Scott, 2009; Del Bene & Wyart, 2012; Portugues et al., 2013; Wyart & Del Bene, 2011). Chapter 4 of this thesis adds to the current growth of literature in this area and uses optogenetic indicators of activity to investigate circuits responsible for processing sensory information in the larval zebrafish tectum.

1.4 Summary

In order to decipher the neural codes and mechanisms by which cognition and behaviour are controlled by the brain, the activity of all cells throughout these networks must be examined *in vivo*. Until recently however, this goal has remained beyond our reach. New developments in optogenetics and microscopy have fundamentally improved our ability to observe and modify the responses of individual cells within neural circuits, making it possible to record activity from multiple different brain regions and link patterns of activity to given behaviours. Particularly amenable to these types of studies, the larval zebrafish model system has gained swift popularity for examining the neural mechanisms by which information is filtered, processed and integrated in the brain. Through the use of genetically-encoded calcium indicators and volumetric imaging techniques, the responses of cells in

distributed brain networks have been recorded at single cell resolution in zebrafish responding to olfactory (Prevedel et al., 2014) and visual (Vladimirov et al., 2014) cues. Building on this work, this thesis has aimed to utilize these techniques in order to examine the neural circuits responsible for learning and sensory perception in larval zebrafish. While limitations still remain, especially with genetic targeting of proteins for optogenetic manipulations, future developments will continue to allow more precise studies that will significantly improve our understanding of the fundamental processes by which the brain operates.

Chapter 2

Technical approaches for investigating functional neural circuits

2.1 Introduction

Larval zebrafish offer a number of beneficial attributes that combine to allow researchers to observe and manipulate activity in the nervous system of a live, behaving animal. In this chapter, I describe a number of experimental techniques that I have implemented that make use of the advantages of the zebrafish model and support studies investigating the function of neuronal circuits. I first outline the design and operation of a selective-plane illumination microscope for the rapid acquisition of data across large populations of active neurons in the larval zebrafish. Secondly, I utilise the transgenic capacity of these animals by creating several lines of fish expressing proteins for both detecting and manipulating neural activity. Both of these methods have been integrated and used for the experiments described in Chapter 4, and form the basis for a number of ongoing experiments within the lab.

2.2 Imaging of neuronal activity

2.2.1 Microscopy techniques

As discussed in Chapter 1.2, multi-electrode recordings are able to provide outstanding temporal resolution but do not presently have the ability to detect neural activity from all cells in a network with single-cell resolution. The use of optogenetic proteins to optically observe and manipulate activity provides the ability to simultaneously examine entire neural circuits, however if expression of fluorescent activity indicators is not spatially restricted by genetic techniques, broad epifluorescent illumination of the brain can lead to emission of light from its entire three-dimensional volume. Lenses can be used to magnify the image of a particular focal plane onto a camera in order to measure various different properties indicated by these proteins, however scattered light from unfocused axial positions will also be imaged. Therefore, epifluorescence microscopy lacks the ability to optically section tissue, and is an unfavourable option for optogenetics in neural circuits.

These problems can be circumvented by a number of techniques that, in most cases, aim to restrict illumination of the sample to a particular focal plane and eliminate out-of-focus light. Highly utilised for decades, confocal microscopy operates by scanning a diffraction-limited spot across the focal plane of a sample to restrict illumination and collect emitted light through a pinhole in the confocal plane to

eliminate out-of-focus light in both the lateral and axial dimensions (Wilson & Sheppard, 1984). This can be improved further by using light with roughly twice the normal excitation wavelength of the fluorescent indicator, or 2-photon microscopy (Denk et al., 1990). In this method, the simultaneous absorption and summation of two low energy photons to induce excitation of the fluorophore occurs at very low rates, dramatically reducing the axial scatter of the point-spread-function. The use of infrared wavelengths in this technique also allows scanning at increased depths with reduced photodamage of the sample. However, the downside of both of these raster scanning techniques remains in the temporal dynamics. Given the millisecond timescale of neuronal activity across circuits in the brain, it is beneficial capture an image of the entire network simultaneously without the delays associated with laser scanning.

Several recent advances in microscopy have allowed for vast brain circuits to be imaged simultaneously at a single cell resolution. For example, light field microscopy, developed by Levoy and colleagues (2006), has recently been applied to the task of imaging whole-brain neural activity at up to tens of volumes per second (Prevedel et al., 2014). The axial point spread function of a 0.5 µm bead in this setup has half maximal intensity up to 5.6 µm from the source in either direction, meaning that despite using 3D deconvolution methods, separation of individual cells is ambiguous across this dimension in animals expressing fluorescent indicators densely throughout the brain. 3D microscopy of neurons has also been achieved using a spatial light modulator and wavefront coding to selectively illuminate selected areas across extended depth-of-field in a 3-dimensional volume (Quirin et al., 2014). In this case, separation of adjacent signals in the axial dimension is yet again difficult, and becomes significantly more so with increased depth in the sample. Such techniques have no moving parts and are able to achieve imaging rates of 30-50 volumes per second, however can be understandably susceptible to minor movements in the sample. Fortunately, techniques exist that balance restricted optical sectioning while allowing for rapid scanning of the sample.

Such imaging can be achieved using selective plane illumination microscopy (SPIM), (Huisken et al., 2004). SPIM acts to eliminate out-of-focus light by creating a thin sheet of light at the focal plane of the imaging objective that enters the sample from

the side. This restricts illumination to a single plane at any given point in time that can be imaged simultaneously without point or line-scanning of the sample. The plane is produced either by focusing light through a cylindrical lens (Huisken et al., 2004), or by rapidly scanning a beam of light across a single plane to illuminate a single plane (Keller et al., 2008). The sample can either be moved through the light sheet, or the plane can then be moved through the sample while simultaneously moving the imaging objective to keep the light sheet in the focal plane. This technique has recently been applied to the functional imaging of neuronal activity in larval zebrafish (Ahrens et al., 2013; Panier et al., 2013), achieving up to 3 volumes per second in some instances (Vladimirov et al., 2014), well within the decay time of the latest generation of GCaMP5 or GCaMP6 calcium sensors (Chen et al., 2013).

Although a commercially available light sheet microscope has been developed by Zeiss (Lightsheet Z.1), recent studies have exclusively used custom microscopes designed and built by individual research labs (Ahrens et al., 2013; Keller et al., 2008; Panier et al., 2013; Vladimirov et al., 2014). Since advances to light sheet imaging methods are being regularly developed, and different experimental questions require the flexibility to probe the specimen with drug treatments, sensory stimuli or optogenetic perturbations, the trend for custom-built light sheet microscopes is ideally suited for this research. As such, I report here the design and construction of a selective plane illumination microscope for the study of functional neuronal circuits in larval zebrafish.

2.2.2 Design and construction of a Selective Plane Illumination Microscope

A custom selective-plane illumination microscope was built based on the design presented at openspim.org (Pitrone et al., 2013), adapted with the aid of D. Preece (School of Mathematics and Physics, The University of Queensland) and L. Heap (Scott Laboratory, The University of Queensland). The configuration presented here relied on a fixed illumination and imaging plane through which an immobilized zebrafish larva was moved (Figure 2.1; Table 2.1). In the standard configuration of the microscope design, light from a 488 nm laser was directed into a tube by a fibre optic cable, collimated at both ends, to maintain a single line beam. In the illumination tube, the beam was first expanded through a series of lenses to increase its diameter. An F = -50 mm concave lens was paired with an F = +200 mm convex

lens 150 mm apart to achieve a 4 x beam expansion. Following this, the beam then passed through a horizontal slit with manually-adjustable width, set to approximately 1 mm wide. The horizontal slit of light then passed through an F = +75 mm plano-convex cylindrical lens to compress it into a thin vertical line that was imaged onto the back focal plane of a long working distance 10 x objective. This vertical line is then transformed by the illumination objective to produce a very thin horizontal line at the focal plane of the illumination objective.

As light focuses to this horizontal line in reality, the wave properties of the Gaussian beam cause it to converge not to a 1-dimensional line, but rather to a 2-dimensional sheet of light. This is the principal by which SPIM operates, creating a plane of light over which illumination is relatively restricted and constant. The thickness of the light sheet at its focal point, and hence resolution of optical sectioning, is determined by the diffraction limits of the illumination objective, which is set by its numerical aperture (Siegman, 1986). In light sheet microscopy, the range over which the illumination is restricted is calculated by the Rayleigh range (Siegman, 1986), with illumination increasing significantly on either side of the focal point. In the design presented here, the 0.25NA objective produced a theoretical limit of approximately 1 µm for light sheet thickness at the beam waist centre, with a range of approximately 13 µm over which the sheet is restricted. Outside of this range, the light diverges more rapidly and prevents clear optical sectioning due to out-of-focus illumination of the sample.

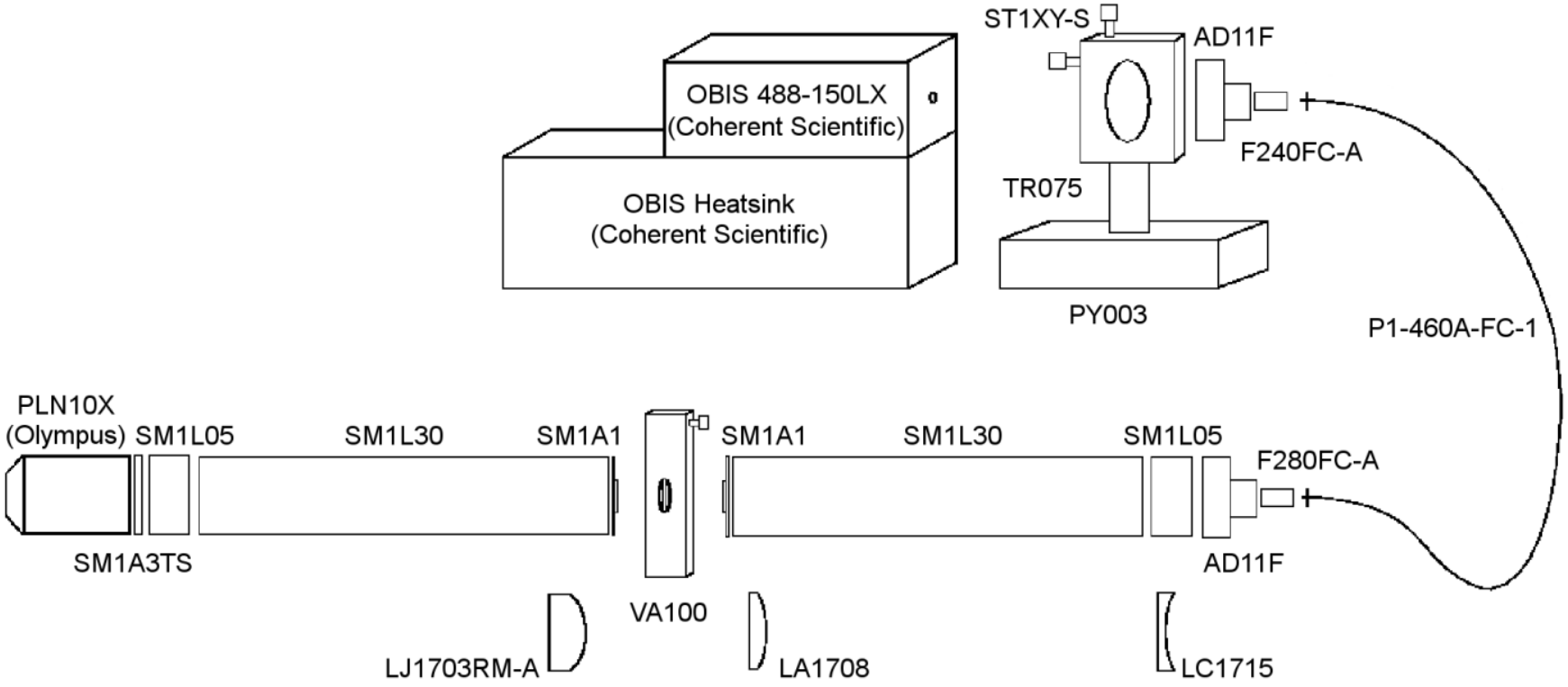
ST1XY-S
AD11F
OBIS 488-150LX
(Coherent Scientific)
F240FC-A
OBIS Heatsink
(Coherent Scientific)
TR075
PY003
P1-460A-FC-1
PLN10X
(Olympus)
SM1L05
SM1L30
SM1A1
SM1A1
SM1L30
SM1L05
F280FC-A
SM1A3TS
AD11F
VA100
LJ1703RM-A
LA1708
LC1715

Figure 2.1 (previous page). Diagrammatic representation of the light sheet illumination system of the SPIM outlined in this chapter. All components are Thorlabs part numbers unless otherwise specified.

Table 2.1: List of components required for the custom Selective Plane Illumination Microscope outlined above.

Module	**Component**	**Product**	**Manufacturer**
Illumination Source	DPSS Laser	OBIS 488-150 LX	Coherent
Illumination Path	Laser-to-fibre launcher	ST1XYS XY Translator	Thorlabs
		PY003 Pitch & Yaw Stage	
		AD11F Collimator Mount	
	Fibre Collimator	F240FC-A NA=0.51	
	Fibre Optic Patch Cable	P1-460A-FC-1 Single Mode Fibre	
	Fibre Collimator	F280FC-A NA=0.15	
	Vertical Translation Stage	MVS005	
	Beam Expander	LC1715 f=-50mm Concave Lens	
		LA1708 f=200mm Convex Lens	
	Adjustable Slit	VA100	
	Cylindrical Lens	LJ1703RM-A f=75mm Convex Cylindrical Lens	
	Illumination Objective	PLN 10X 0.25NA	Olympus
Detection Path	Detection Objective	XLUMPFLN 20XW 1.0NA	
	Microscope Body	SliceScope	Scientifica
	Camera	PCO-Edge 5.5	PCO
Specimen Positioning System	X-Y axis Translation & Rotation Stage	XYR1	Thorlabs
	Piezo Z-axis Stage	Nano-Z450 (Custom built)	Mad City Labs
Control Software	Image Acquisition & Stimulus Delivery	Micro-Manager	Vale Lab, UCSF

In actual experimental conditions, the back aperture of the illumination objective was not completely filled by the light beam, creating a slightly thicker light sheet that was sufficiently uniform across a wider lateral range. However, the position of the light sheet relative to both the sample and the detection objective were crucial for clear imaging. During experiments, the light sheet was independently aligned with the imaging objective by a manually-adjustable x/y-axis stage, and an additional manually-adjustable z-axis stage. To align the sheet, a fluorescent sample was mounted in an imaging chamber and moved through the light sheet until a strong fluorescent signal was observed. The focus of the imaging objective was then adjusted until the sharpest image was achieved and the x-, y-, and z-positions of the light sheet were moved. This process continued iteratively until a sharper image could no longer be achieved.

As described above, this microscope design relied on the light sheet and imaging objectives remaining stable while the sample was moved in the z-axis to achieve 3-dimensional scans. To be able to resolve neuronal activity, this movement needed to occur rapidly over the depth of the zebrafish brain, and with enough precision to register individual cells in different slices across time. For this purpose, I commissioned the development of a custom-made piezo-driven z-axis stage that was designed and built by Mad City Labs (Z450, Mad City Labs) (Figure 2.2). This stage was designed with 450 microns of travel at 1 nm resolution, and the ability to trave the full range at 250 Hz. Detailed, whole-brain scans with a high temporal resolution are therefore only limited by the fluorophore brightness and detector sensitivity under these conditions. Using a light sheet with 8 mW intensity at the sample (measured by Digitech Luxmeter, Electus Distribution, Australia) to image a 7 dpf larva with pan-neuronal GCaMP5G (Chapter 2.3.1), the entire tectum could be sampled at approximately 1 Hz with this stage (Movie 1). While moving the sample was technically simpler than synchronously moving the plane of both the light sheet and the imaging objective, it could induce responses to the acceleration that would confound detection of unrelated neuronal activity. While these artefacts were usually found to disappear within the first five seconds of volumetric imaging (data not shown), single-plane imaging was chosen as the preferred method for the data acquired in further chapters.

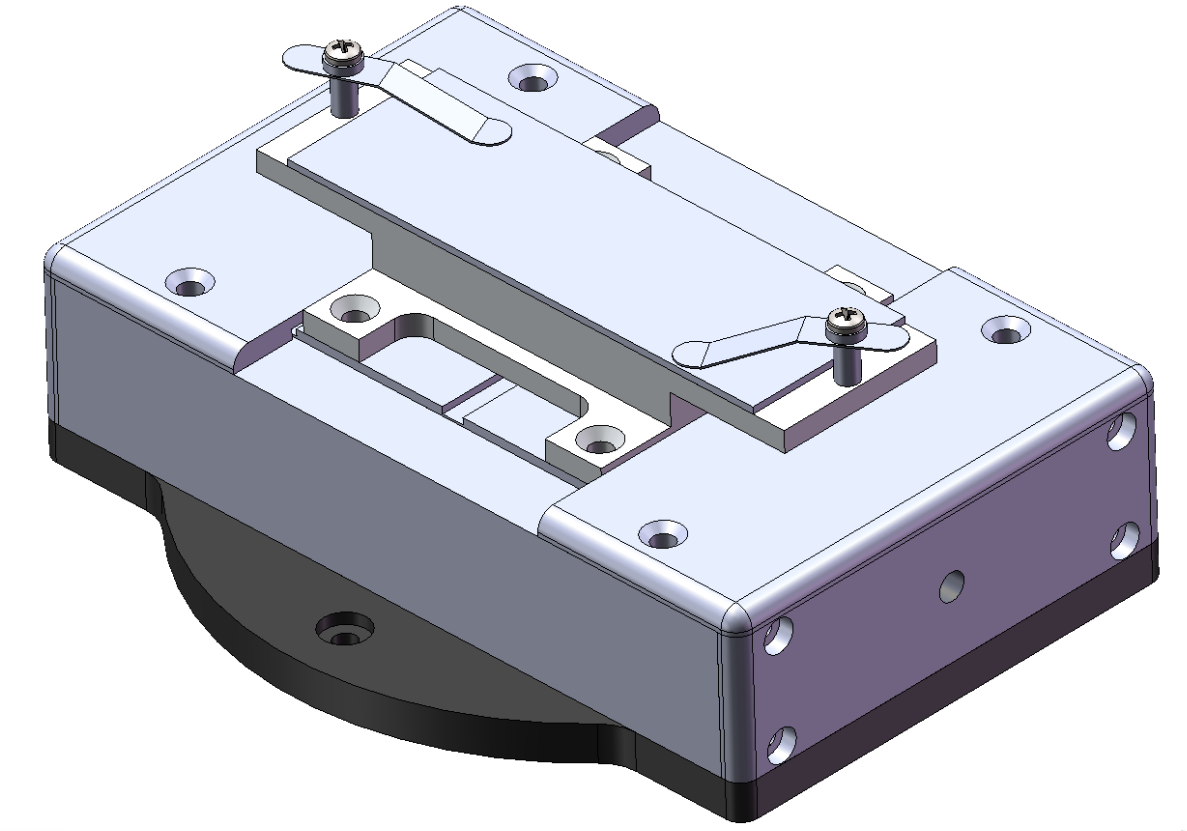

Figure 2.2. Custom Z450 piezo stage from Mad City Labs, capable of 450 µm travel at 250 Hz. SolidWorks eDrawing file produced by Mad City Labs.

Using this configuration and the sample chamber described in Chapter 2.3.3, the point spread function of the custom-built SPIM was empirically measured. Qdot® 525 streptavidin-conjugated nanocrystals (Q10143MP, Thermo Fisher Scientific, Australia) were suspended in 1.5% low-melting point agarose (Progen Biosciences, Australia), and illuminated with a light sheet produced from an OBIS 488 nm laser (OBIS 488-150 LX, Coherent Scientific) at approximately 15 mW at the sample. This is the wavelength primarily used during single-photon excitation of GCaMP5G for observation of neuronal activity (Akerboom et al., 2012) and hence is the . These nanocrystals are approximately 15 nm across, well below the diffractive limit of the imaging objective (XLUMPFLN 20XW, Olympus), and thus light from these Qdots was imaged as a point-source. Light emitted from the quantum dots was imaged on an sCMOS camera (PCO.Edge 5.5; PCO, Germany) through a 495 nm dichroic (FF495-DI03-25x36, Semrock) and 534 nm emission filter (FF02-535/30-25, Semrock).

Three individual dots were imaged at 300 nm intervals spanning 10 µm below to 10 µm above the nanocrystal. The theoretical FWHM of the nanocrystal image in a non-scattering medium using the XLUMPFLN 20XW objective lens (Olympus) in a confocal system at 488 nm is approximately 250 nm in the lateral axis and 950 nm in the z-axis (Cole et al., 2011). However, due to the significant amount of light scattering in the agarose prior to entering the objective, as well as slight imprecisions in the imaging light path, the average point spread function of these quantum dots, shown in Figure 2.3A-B, is significantly larger. Gaussian curves were fitted to the lateral and axial intensity profiles of the nanocrystals, revealing a full width at half maximum (FWHM) of approximately 1.75 µm in the lateral axis and 6.31 µm in the z-axis (Figure 2.3C). By comparison, this is significantly lower than the axial FWHM of 11.3 µm for light-field microscopy with a 20X 0.5NA objective (Prevedel et al., 2014), but slightly greater than the approximately 4.4 µm achieved by Kaufmann and colleagues (2012) using a 20X 0.5NA objective and multidirectional SPIM (Huisken & Stainier, 2007).

Neuronal cell bodies in the zebrafish brain are tightly packed, and as light passes through these cells there is an increased scattering of photons the further through the animal the light penetrates (Favre-Bulle et al., 2015). As such, when a light sheet

is projected through the zebrafish brain the proximal side of the beam waist centre is illuminated with a more focused light than the distal side. As the light sheet already diverges significantly beyond the Rayleigh range, this can cause issues when imaging large samples and trying to maintain the ability to resolve individual cells. Therefore, in some experiments when whole-brain imaging was desired, the fibre optic cable between the laser and illumination path was split by a 50:50 cable (FC488-50B-FC; Thorlabs). In this configuration, two identical illumination paths were used to produce two equivalent light sheets that simultaneously illuminated both hemispheres of the brain. Each light sheet was separately aligned to the detection objective and the opposite light sheet prior to imaging.

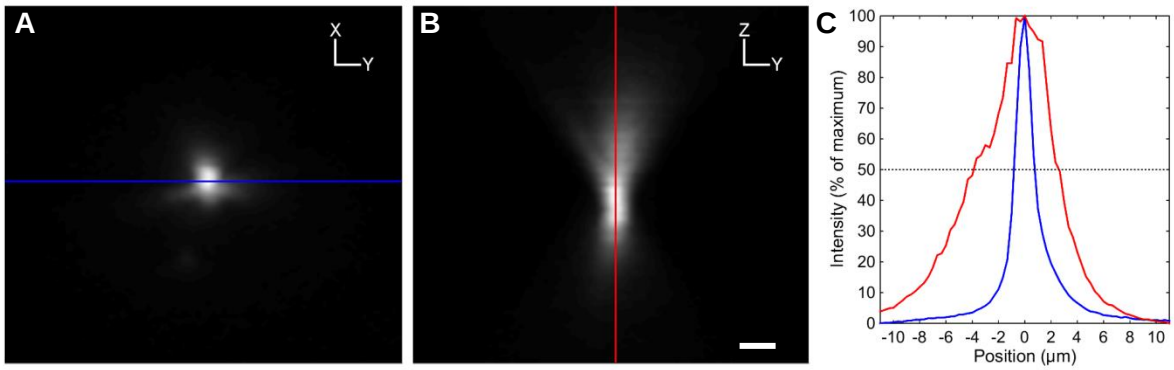

Figure 2.3. Point spread function of custom-built selective-plane illumination microscope. (A-B) Lateral (A) and axial (B) view of the point spread function, measured as the average emission of three quantum dot nanocrystals at 525 nm. Scale bar = 2 µm. (C) Intensity profiles of the point spread function in the lateral (blue) and axial (red) dimensions. Full width at half maximum (dotted line) is approximately 1.75 µm in the lateral axis and 6.31 µm in the z-axis.

2.2.3 Imaging chamber design

For the functional imaging of neuronal circuits using SPIM, larval zebrafish are most often immobilized in low melt agarose for imaging. Since illumination is targeted from the side, the amount of agarose surrounding the animal must be minimized to prevent unwanted scattering of the light. This has previously been achieved by embedding larvae in agarose within a thin capillary tube and extruding them for imaging (Ahrens et al., 2013; Panier et al., 2013). While this strategy allows for the animal to be rotated within the light sheet, it does not offer flexibility in the types of manipulations that can be made to the sample post-embedding. Taking this into account, imaging chambers roughly 5 mm wide were designed and created that allow sample access and prevent imaging aberrations from the chamber walls (Figure 2.4).

Repeatable, cost-effective chambers were constructed by mounting glass coverslips against the two open edges of a long U-shaped well using 1.5% low-melting point agarose. These wells were formed by isolating ten staples from a standard strip of 26/6 steel staples (EXP6, Corporate Express, Australia) (Figure 2.4B). For the sharpest imaging conditions, the coverslip walls of each chamber must be oriented perpendicular to the light sheet. However, since chambers were constructed by hand on the morning of each imaging experiment, minor levels of variance were introduced between the light paths for different larvae. Any deviations in the angle of the coverslip away from perpendicular cause the sheet to refract and pass through the sample at an angle, resulting in less of the animal being illuminated within the focal plane of the imaging objective. Again, due to light scattering through agarose and the thin width of the imaging chamber, the specimen was also required to be positioned within 2 mm of the dorsal surface of the chamber.

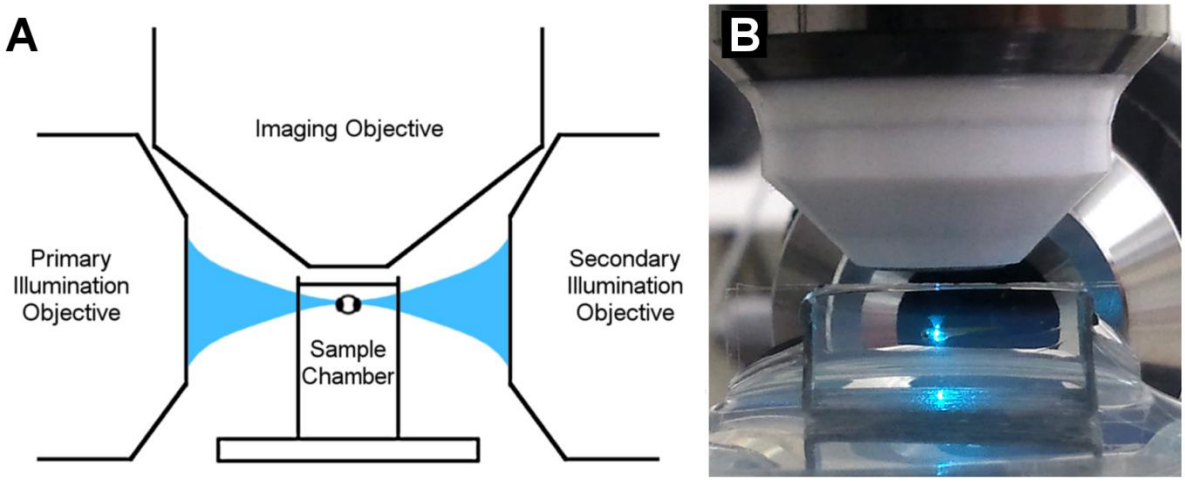

Figure 2.4. Sample positioning in the imaging chamber relative to the illumination and imaging objectives of the selective plane illumination microscope. (A-B) The 8 mm wide chamber is positioned between either one or two illumination objectives with 10.5 mm focal length each. The light sheet is projected into the sample (zebrafish larva) from both sides (blue regions, panel A), creating a thin plane of illumination and eliminating out-of-focus light in the imaging plane. The larva is positioned dorsal side up, with its rostro-caudal axis perpendicular to the direction of illumination from the two planes. The working distance of the imaging objective, and therefore maximum depth able to be observed within the chamber, is 2 mm. Each larva is therefore embedded less than 2 mm from the chamber surface for imaging of neuronal activity.

2.3 Transgenesis of zebrafish for studying neuronal function

2.3.1 Genetic control of protein expression

A number of tools have been described in the literature to allow for modification of gene expression in the zebrafish model organism. For example, chemical mutagenesis can be employed on a mass scale to identify genes and circuits responsible for specific behaviours (Baraban et al., 2007; de Bruijn et al., 2009). While forward genetic approaches like this are a useful means to identify novel genes implicated in the function of various circuits, they do not allow for the specific manipulation of circuits under the control of target genes. For this purpose, precise techniques have been developed that take advantage of clustered regularly interspaced short palindromic repeats (CRISPRs) (Ablain et al., 2015; Hwang et al., 2013) and transcription activator-like effector nucleases (TALENs) (Bedell et al., 2012). These two systems have been used to great effect in the targeted known-down of genes of interest to examine their role in different behaviours, however the examination of neuronal activity using at the circuit level using optogenetic tools requires expression of exogenous genes.

In landmark experiments from the Westerfield laboratory, DNA from bacterial plasmids has been shown to be integrated into the zebrafish genome when injected between the 1- and 4-cell stage of development (Stuart et al., 1988; Stuart et al., 1990). Transmission of the integrated DNA was observed from roughly 5% of injected animals in these studies, allowing generation of stable transgenic lines. In order to improve the efficiency of this method, RNA from the Tol2 transposable element of the medaka fish, *Oryzias latipes*, (Koga et al., 1996) has been used to allow integration of exogenous DNA into the zebrafish genome through transposition from injected plasmid DNA (Kawakami et al., 2000). Germline transmission was found from 25% of injected animals in this instance, suggesting an improved efficiency of transgenesis. Since this time, Tol2 has been used extensively in zebrafish transgenesis, often in combination with bipartite genetic elements such as Cre-*loxP* to provide spatiotemporal flexibility and control.

Cre is a gene derived from the P1 bacteriophage that causes homologous recombination between *loxP* sites (Hoess et al., 1982). Often used in murine model systems, the Cre-*loxP* system has shown to be efficient in site-specific

recombination to genetically control insertion, deletion, inversion and translocation of target DNA sequences depending on the location and orientation of the *loxP* sites (Branda & Dymecki, 2004; García-Otín & Guillou, 2006; Sauer, 1998). When creating transgenic animals expressing proteins in pattern of a particular gene of interest, plasmids are often created in which two *loxP* sites are downstream of a given promoter region, with the coding sequence for an effector protein downstream of the second *loxP* site. Following Cre-dependent recombination, genetic elements downstream of the second loxP site are shifted in-frame and the protein is expressed in a targeted manner. In the zebrafish, Tol2-insertion of DNA into the genome has been used to generate *loxP* lines for Cre-dependent recombination either under control of a heat shock promoter (Thummel et al., 2005), or with the additional control of a tamoxifen-inducible Cre (Feil et al., 1996) for further temporal restriction (Hans et al., 2009; Hans et al., 2011). While the latter method can overcome the "leaky" expression of the heat shock promoter, different heat shock protocols have been shown to have various deleterious effects on zebrafish survival (Thummel et al., 2005). Therefore, more commonly used in the zebrafish for insertional mutagenesis is the bipartite Gal4/UAS system.

Originally identified in yeast, the bipartite Gal4/UAS system involves the Gal4 transcription factor driving expression of a gene downstream of an Upstream Activating Sequence (UAS) (Giniger et al., 1985). While first employed in *Drosophila* (Brand & Perrimon, 1993), this system has now been used extensively in zebrafish to generate libraries of novel expression patterns of the Gal4 transcription factor (Asakawa et al., 2008; Davison et al., 2007; Scott & Baier, 2009; Scott et al., 2007). By trapping endogenous promoters and enhancers with random Tol2-mediated insertion of the Gal4 gene, these studies have been able to generate transgenic animals with restricted expression patterns for any existing or future UAS-driven effector protein without prior knowledge of the precise genetic profiles underlying those patterns. By genetically restricting expression of the Gal4 transcription factor, specific expression profiles can therefore be generated within the zebrafish central nervous system of any UAS-linked transgene of interest, such as those encoding optogenetic proteins (Baier & Scott, 2009; Scott, 2009). As such, this provides the opportunity to both observe and manipulate activity in neural circuits and identify how information is encoded and processed in the brain.

It has recently been shown that homologous recombination using TALENs (Shin et al., 2014) and homology-independent double-stranded break repair mechanisms with a CRISPR-Cas9 system (Auer et al., 2014) can be used to insert long sequences of genetic cargo (> 500 base pairs) in a targeted manner. Germline transmission of in-frame insertions using these methods was observed from roughly 8 to 10% of injected fish, and between 0.3 and 61.3% from F1 animals carrying the insertion. While these rates are generally suitable, these techniques require extensive genetic screening for suitable integration and potential off-target effects (Cho et al., 2014; Frock et al., 2015; Koo et al., 2015; Veres et al., 2014). It is expected that these tools will play an important role in the development of future transgenic zebrafish lines for targeted expression of optogenetic proteins, however at the onset of this project these techniques were unpublished as a technique for insertional mutagenesis in zebrafish.

2.3.2 Generation of transgenic animals for measuring and manipulating neuronal activity

In order to describe the function of a neuronal circuit in the zebrafish brain, one of the first objectives is to record neural activity in an intact animal. As described in Chapter 1.2, the use of optogenetic indicators of activity such as GCaMP5 and VSFP2.3 (Akerboom et al., 2012; Perron et al., 2009) offer many advantages to achieve this goal. In addition, optogenetic tools have an impressive capacity to manipulate neuronal activity through the application of light (Fenno et al., 2011; Hausser, 2014; Yizhar et al., 2011a), a technique particularly amenable to zebrafish larvae (Baier & Scott, 2009; Del Bene & Wyart, 2012; Portugues et al., 2013; Wyart & Del Bene, 2011). In this study, several different transgenic lines have been generated in which different optogenetic indicators and manipulators of activity are expressed under control of a UAS element in order to analyse neural activity in larval zebrafish (Table 2.2). These lines were intended to cover a broad number of experimental approaches, not all of which are covered by the scope of this PhD. As such many lines have not been described in detail here. A transgenic line in which the Gal4 transcription factor was expressed under control of the *elavl3* (*HuC*) promoter was also created, such that animals would express Gal4 broadly across a large proportion of the neuronal cells of the central nervous system (Park et al.,

2000). By crossing lines for UAS-driven optogenetic indicators and manipulators to this Gal4 line, neuronal activity can be studied extensively across the nervous system in the resulting offspring expressing both transgenes.

In order to create the transgenic lines, the commercially available Gateway system (Life Technologies) was combined with the Tol2-kit developed by Kwan et al. (2007). In this system, Tol2 transposon elements allow the gene of interest to be inserted into the genome. The GCaMP5G construct was kindly provided by L. Looger (Howard Hughes Medical Institute, Janelia Farm Research Campus), the gene encoding Arch(D95N)-YFP (Kralj et al., 2011) was obtained from Addgene (Cambridge, USA), and the VSFP-Butterfly gene (Akemann et al., 2012) was obtained by special request from T. Knöpfel (RIKEN, Japan). Plasmids containing the genes encoding ArchT-YFP (Han et al., 2011) and eNpHR3.0-YFP (Gradinaru et al., 2010) were obtained from Addgene (Cambridge, USA), and ChR2(ET/TC)-mCherry (Berndt et al., 2011) was obtained by special request from K. Deisseroth (Stanford University). The promotor region for the gene encoding *elavl3* was kindly provided by B. Key (The University of Queensland).

pME-MCS (construct 237; Tol2kit v1.2, Kwan et al., 2007) was previously altered by Dr Rebecca Dunning of the Scott Laboratory (The University of Queensland) to insert additional multiple cloning sites and create pME-MCS_Linker using the forward primer CCCGGGACCGGTAGATCTTGATCAGGATCC, and the reverse primer GGATCCTGATCAAGATCTACCGGTCCCGGG.

Transgenes for all optogenetic proteins were similarly generated, and as such the construction of only one, GCaMP5G, is described in detail here. The middle-entry vector for GCaMP5G was generated by cloning the GCaMP5G gene into pME-MCS_Linker using AgeI and NotI sites, generating pME_GCaMP5G. This was then combined with a 10.5X UAS-containing 5’ entry vector (construct 327), polyA-containing 3’ entry vector (construct 302) and pDestTol2pA2 destination vector (construct 394) using LR Clonase II Plus (Life Technologies) in a multi-site Gateway reaction. This generated the injectable plasmid pDest_10.5X-UAS:GCaMP5G. Similarly, the 5’-entry vector for *elavl3* was generated by cloning the zebrafish *elavl3* promoter into p5E-MCS (construct 228) using ClaI and SacII sites, generating

p5E_*elavl3*. This was then combined with pME_Gal4VP16 (construct 387), p3E_polyA and pDestTol2pA2 using LR Clonase II Plus (Life Technologies) in a multi-site Gateway reaction generating the pDest_*elavl3*:Gal4VP16 plasmid.

After insertion into pME-MCS, the mCherry tag was cloned from pME-ChR2(ET/TC)-mCherry into pME-eNpHR3.0 in place of the YFP tag using the flanking NotI sites. Orientation was confirmed by Sanger sequencing (AGRF, The University of Queensland, Australia). The reverse experiment transferring the YFP tag from pME-eNpHR3.0 to pME-ChR2(ET/TC) in place of the mCherry tag was also performed.

Plasmids encoding an optogenetic protein were injected into single-cell zebrafish embryos within 40 minutes of fertilization using 100 ng/µL of plasmid DNA and 75 ng/µL Tol2 transposase RNA. Those proteins tagged with a red fluorescent marker were injected into embryos from an s1168t:Gal4;UAS:Kaede (Scott & Baier, 2009) animal crossed to a *nacre* mutant of the Tupfel long fin strain (TLN; Lister et al., 1999). The plasmid encoding *elavl3*:Gal4VP16 was also injected into s1168t:Gal4;UAS:Kaede x TLN embryos, as significantly different expression patterns were expected from these two Gal4 lines. In addition, the expression of Gal4 and UAS-driven proteins along the trunk muscles in the s1168t:Gal4 line could be used to clearly identify animals with dual expression patterns. Plasmids encoding a green or yellow fluorescent protein were injected into embryos from an s1168t:Gal4;UAS:mCherry (Heap et al., 2013) animal crossed to TLN. Injected embryos were screened for transient expression of the optogenetic proteins at 48 hours post fertilization and raised by the Australian Zebrafish Phenomics Facility (The University of Queensland) until breeding age.

Potential founders were crossed to screen for germline transmission to either a UAS:mCherry-expressing Gal4 line in the case of green or yellow fluorescent proteins a UAS:Kaede-expressing Gal4 line in the case of red fluorescent proteins, or a UAS:Kaede-expressing Gal4 line in the case of *elavl3*:Gal4VP16 injected animals. Founders with offspring containing the transgene were identified under fluorescence microscopy, then outcrossed to *nacre* mutants of the Tupfel long fin strain to generate stable lines. Table 2.2 shows a summary of the transgenic zebrafish lines developed during this thesis that express different optogenetic tools

under the control of the Gal4/UAS system. Prior to the development of these 10.5X UAS lines, several lines with the same optogenetic tools were created using a 4Xnr UAS (Akitake et al., 2011). In contrast to earlier reports (Akitake et al., 2011), these lines were found to have very low overall transgene expression and were not investigated further.

Table 2.2. Toolbox of Gal4/UAS-driven lines of optogenetic tools created for studies of neuronal circuit function.

Line	Description
10.5X-UAS:ChR2(ET/TC)-YFP	Cation channel - depolarises a cell in blue light
10.5X-UAS:ChR2(ET/TC)-mCherry	Cation channel - depolarises a cell in blue light
10.5X-UAS:eNpHR3.0-YFP	Chloride pump - hyperpolarises a cell in amber light
10.5X-UAS:eNpHR3.0-mCherry	Chloride pump - hyperpolarises a cell in amber light
10.5X-UAS:ArchT-YFP	Proton pump - hyperpolarises a cell in amber light
10.5X-UAS:GCaMP5G	Calcium indicator - fluorescence intensity changes in response to calcium influx
10.5X-UAS:Syn-GCaMP5G	Calcium indicator fused to syanptophysin - fluorescence intensity changes in response to calcium influx
10.5X-UAS:ClSensor	Chloride sensor - fluorescence intensity changes in response to chloride
10.5X-UAS:VSFP-Butterfly	Voltage indicator - Ratio of fluorescence intensities change in response to voltage changes
10.5X-UAS:Arch(D95N)-YFP	Voltage indicator - Fluorescence intensity changes in response to voltage changes
10.5X-UAS:Brainbow2.1	Fluorophore toolbox expressing random combinations of fluorophores following Cre-recombination
elavl3:Gal4	Promoter for pan-neuronal gene *elavl3* controlling Gal4 expression
elavl3:GCaMP5G	Promoter for pan-neuronal gene *elavl3* controlling GCaMP5G expression

2.3.3 Evaluation of transgenic animals for optical measurement and manipulation of neuronal activity

In order to investigate neuronal circuits, several transgenic lines for different optogenetic proteins were created that were designed to be used either alone or in combination with other optogenetic tools (Table 2.2). To validate the use of these animals, the expression of the target proteins for all transgenic lines was first confirmed by fluorescence microscopy. Transgenic lines for *elavl3*:Gal4VP16 and 10.5X-UAS:GCaMP5G were validated by first crossing these two lines and examining the offspring with the genotype *elavl3*:Gal4VP16;10.5X-UAS:GCaMP5G using spinning disk confocal microscopy (Yokogawa W1 Spinning Disk module attached to Zeiss Z1 Axio Observer; Zeiss, Germany). When exposed to 488 nm light, the circularly permutated GFP fragment of the GCaMP5G protein is excited and emits light with a peak wavelength of approximately 513 nm in 7 dpf larval zebrafish (Figure 2.5A-C). The pan-neuronal, cytoplasmic expression pattern observed was consistent with previous reports of GCaMP5G expression using the *elavl3* promoter (Ahrens et al., 2013; Akerboom et al., 2012; Portugues et al., 2014), and these fish were used specifically for the experiments described in Chapter 4. By crossing adult fish with the *elavl3*:Gal4VP16;10.5X-UAS:GCaMP5G genotype to fish carrying the 10.5X-UAS:ChR2(ET/TC)-mCherry insertion, the expression pattern for GCaMP5G versus ChR2(ET/TC)-mCherry was also compared. As before, GCaMP5G in 7 dpf larvae was imaged under 488 nm illumination while ChR2(ET/TC)-mCherry was imaged under 561 nm illumination. The expression patterns for the two proteins were found to be overlapping but distinct, with a higher number of fluorescent puncta in the red channel (Figure 2.5D-F). These are likely representing aggregations of the protein, suggesting sub-optimal trafficking to the cell membrane.

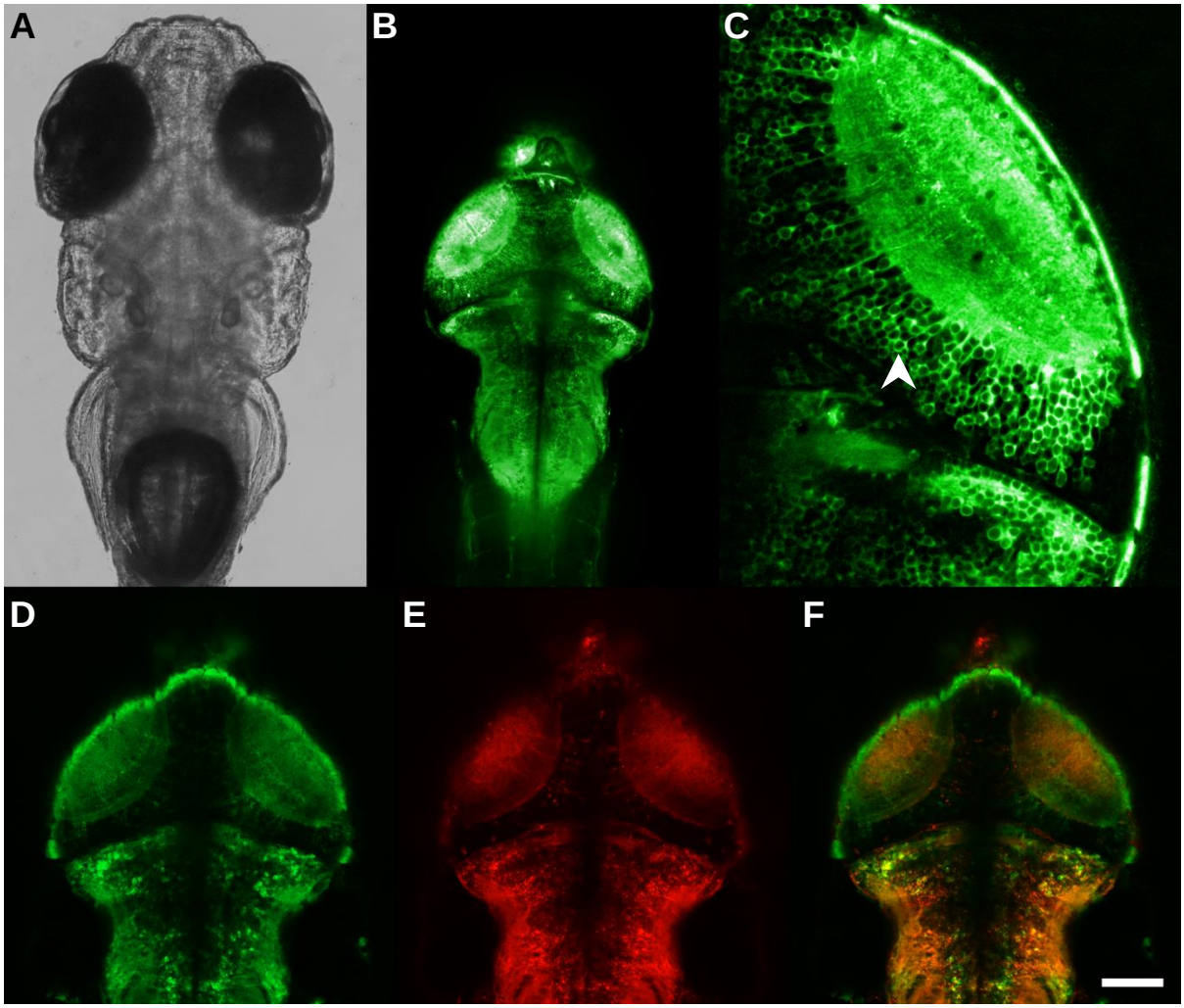

Figure 2.5. Expression of *elavl3*:Gal4;UAS:GCaMP5G in a larval zebrafish. (A) 7 dpf larva imaged dorsally at 10x using brightfield microscopy. (B) Same larva imaged with 488 nm illumination using spinning disk confocal microscopy. (C) Right tectal hemisphere of larva in panels A and B imaged at 40x using spinning disk confocal microscopy. Individual cell bodies are clearly identifiable in the periventricular region (arrowhead). (D-E) Expression of GCaMP5G (D) and ChR2(ET/TC)-mCherry (E) in a 7 dpf larva of the genotype *elavl3*:Gal4;UAS:GCaMP5G;UAS:ChR2(ET/TC)-mCherry. Many small puncta of high fluorescence intensity can be seen in the red (ChR2-mCherry) channel that are not observed in the green (GCaMP5G) channel. (F) Overlay of panels D and E, showing overlapping but distinct expression of the two proteins. Scale bar = 200 µm (A-B), 50 µm (C), 135 µm (D-F).

The ability to both activate and silence neural circuits is highly desired when examining the functional connections between networks of cells in the zebrafish brain. Of the lines generated above, only those for the channelrhodopsin variant ChR2(ET/TC) have the ability to stimulate cell firing. This variant has undergone Glu-123 to Thr and Thr-159 to Cys mutations from the wild-type ChR2 that improve the function of the protein, resulting in more rapid, sustained, and higher amplitude photocurrents than ChR2 (Berndt et al., 2011). Since Archearhodopsin3 (Arch) and eNpHR3.0 have previously been shown to have similar efficacy in suppressing activity in larval zebrafish (Kimura et al., 2013), the results of only one optogenetic silencer, eNpHR3.0, have been explored in detail here. For combined expression with the activity indicator GCaMP5G, the mCherry-tagged version of each of these proteins allows easier spectral separation of the respective fluorophores. Given that both of these optogenetic proteins are under control of a UAS element, they can theoretically be expressed in any specific cell-type or region of interest that can be targeted by Gal4 insertion for focused activation or inhibition of activity to assess neuronal function.

ChR2(ET/TC) is stimulated at approximately 75% of its peak activation using 475 nm (Berndt et al., 2011). Therefore, to test the efficacy of ChR2(ET/TC) in regulating activity in the larval zebrafish brain, larvae expressing either GCaMP5G alone (*elavl3*:Gal4VP16;UAS:GCaMP5G) or in combination with ChR2(ET/TC)-mCherry (*elavl3*:Gal4VP16;UAS:GCaMP5G;UAS:ChR2(ET/TC)-mCherry) were created. 7 dpf larvae were embedded dorsal-side up in low melt agarose and GCaMP5G fluorescence in the tectum was imaged from above to track changes in neuronal activity. These cells were exposed to broad illumination with 475 nm light (20 mW/mm^2; Lumencor Spectra light engine; Lumencor, USA) delivered through the imaging objective (XLUMPFLN 20XW) to both stimulate the optogenetic protein and image GCaMP5G fluorescence. While this was able to restrict illumination laterally to the field of view of this objective, a large distribution of cells in the dorso-ventral axis were illuminated simultaneously.

As expected, control fish expressing GCaMP5G without ChR2(ET/TC) showed a peak of fluorescence upon onset of the illumination that decreased slightly over time

due to photobleaching (Figure 2.6, blue curve). In animals expressing ChR2(ET/TC)-mCherry, activation of tectal cells under broad illumination caused an increase in GCaMP5G fluorescence that plateaued at a peak level roughly double that at illumination onset after approximately 5 seconds of stimulation (Figure 2.6, red curve). Therefore, blue light is able to drive ChR2(ET/TC) activation and trigger neuronal activity in these animals *in vivo*. Since GCaMP5G is typically imaged using the same wavelength as the peak ChR2(ET/TC) activation, 488 nm (Berndt et al., 2011), particular experimental considerations must be made to ensure that unwanted excitation of ChR2(ET/TC)-positive cells does not occur in studies designed to map functional connectivity in neural circuits using both of these proteins. This could be achieved by genetically restricting expression patterns of the different proteins, physical occlusion of the imaging light where ChR2(ET/TC) is expressed, or through the use of spectral variants of optogenetic activators such as C1V1 (Yizhar et al., 2011b) or Chrimson (Klapoetke et al., 2014).

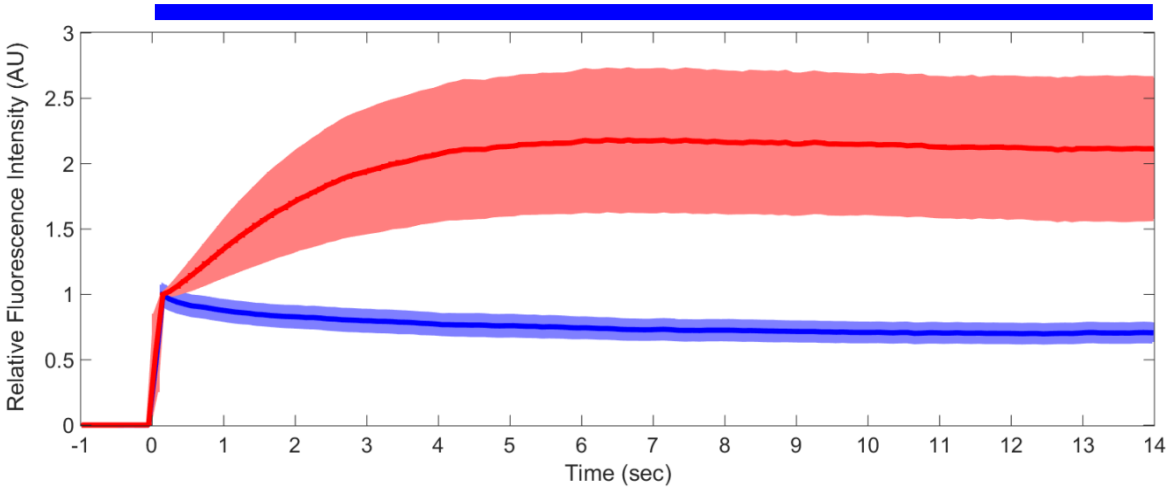

Figure 2.6. Effectiveness of channelrhodopsin in larval zebrafish. Onset of 475 nm illumination at time = 0 (solid blue bar) causes a sudden increase in fluorescence of GCaMP5G-expressing cells in the tectum. Fluorescence decays to a steady level in control siblings (blue trace) expressing only GCaMP5G. In larvae also expressing ChR2(ET/TC), fluorescence increases over approximately 5 seconds due to an increase in neuronal activity levels (red trace). Traces = mean +/- 1 standard deviation, relative to peak control fluorescence; n = 80 cells over 4 experiments.

Without genetic restriction or spectral variants of channelrhodopsin readily available in the timeframe of this PhD, an alternative method was employed to allow GCaMP5G imaging without ChR2(ET/TC) activation. Although 488 nm is the peak wavelength for both processes, if longer exposure times are used then low light intensities could potentially allow GCaMP5G to be imaged without significantly activating ChR2(ET/TC)-mCherry. GCaMP5G fluorescence was imaged in 7dpf larvae of the genotype *elavl3*:Gal4;UAS:GCaMP5G;UAS:ChR2(ET/TC)-mCherry in response to illumination with a 488 nm plane of light produced by a laser (OBIS 488-150 LX) in the SPIM configuration outlined in Chapter 2.2 (Figure 2.1). At 10 mW intensity at the sample, responses mimicked those of the broad 475 nm illumination generated by the Lumencor in Figure 2.6, gradually increasing over five seconds to nearly double the fluorescence intensity at onset of illumination. As previously, control animals expressing only GCaMP5G again elicited a peak fluorescence at illumination onset that decreased by almost 20% over five seconds.

The intensity of laser output was then decreased to determine if GCaMP5G could be imaged without significant ChR2(ET/TC) excitation. Illumination of the sample in the imaging plane was first reduced by 95% to 0.5 mW (measured by Digitech Luxmeter). Although this reduced the overall increase in fluorescence above levels at illumination onset, this intensity still exhibited characteristic ChR2(ET/TC) activation, producing gradual rise in fluorescence similar to that observed at higher intensities (Figure 2.7). When the intensity of the illumination plane was further reduced to 0.25 mW at the sample, GCaMP5G fluorescence fell below the level observed at onset of illumination, suggesting that ChR2(ET/TC) is not significantly activated at this intensity (Figure 2.7).

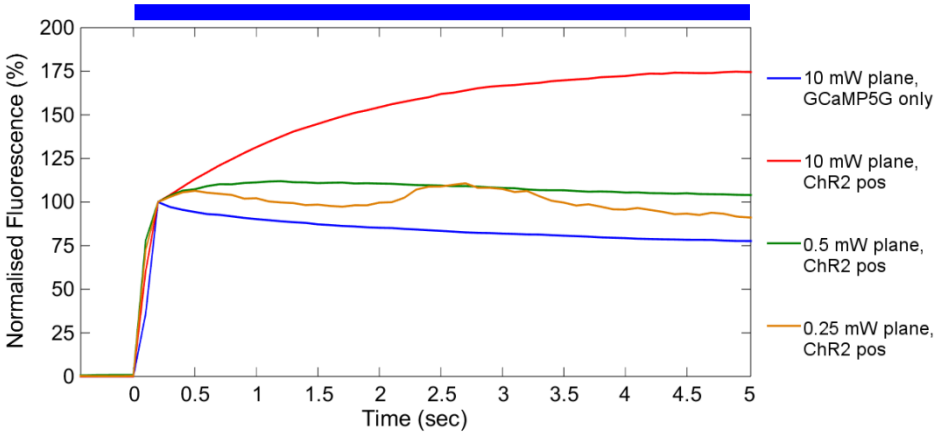

Figure 2.7. Light sheet intensity versus channelrhodopsin activation in larval zebrafish. Illumination of the tectum using a 10 mW plane of 488 nm light at time = 0 (solid blue bar) causes a sudden increase in fluorescence of GCaMP5G-expressing cells. Fluorescence decays to a steady level in control siblings (blue trace) expressing only GCaMP5G. In larvae also expressing ChR2(ET/TC), onset of the illumination plane causes fluorescence to increase gradually above initial levels over approximately 5 seconds due to an increase in neuronal activity (red trace). Lowering the intensity of the plane at the sample from 10 mW to 0.5 mW caused less activation of channelrhodopsin and a smaller increase above initial fluorescence intensity at plane onset. Similar to control fish at 10 mW, GCaMP5G fluorescence falls below the initial level at illumination onset after 5 seconds of constant illumination in ChR2(ET/TC)-positive larvae exposed to a light sheet with 0.25 mW intensity. This indicates that ChR2(ET/TC) is not being significantly activated at this intensity. Traces = mean +/- 1 standard deviation, relative to peak control fluorescence; n = 30-60 cells per condition, 3-6 experiments per condition.

For simplicity of imaging and stimulation, GCaMP5G activity in the tectum was also imaged to test the effectiveness of eNpHR3.0-mCherry. As above, the response of *elavl3*:Gal4VP16;UAS:GCaMP5G control larvae was compared to animals with the optogenetic protein of interest, *elavl3*:Gal4VP16;UAS:GCaMP5G;UAS:eNpHR3.0-mCherry. 7 dpf larvae were embedded dorsal-side up in low-melt agarose and presented with a visual stimulus consisting of a single bright, 7° wide vertical bar on a dark background, moving at 100°/s rostrally (from the tail to the head) over 1 second. This was projected onto a translucent screen positioned 10 cm from the larva by a PK320 miniature projector (Optoma), covering approximately 100° of the visual field of the eye contralateral to the tecta being imaged. Mean luminance of the moving vertical bar stimulus was approximately 34 cd/m^2. Neuronal activity in a single tectal hemisphere was measured by imaging changes in GCaMP5G fluorescence using the 488 nm excitation delivered through the light sheet microscope outlined in Chapter 2.2.

Since eNpHR3.0 is strongly photoactivated by wavelengths between 560 and 590 nm (Gradinaru et al., 2010), activity was compared in the presence or absence of broad 575 nm illumination delivered through the imaging objective (25 mW/mm^2; Lumencor). While under constant 575 nm illumination, control fish expressing only GCaMP5G had a rise in the average response to the moving bar stimulus of approximately 15% above baseline fluorescence. This was not statistically different to the average response in the same fish without 575 nm illumination (Figure 2.8A). Conversely, fish expressing both GCaMP5G and eNpHR3.0-mCherry had a consistently smaller rise in fluorescence above baseline in response to the moving vertical bar (Figure 2.8B). However, these eNpHR3.0-positive fish also had a significantly lower baseline response under control conditions without 575 nm illumination (Figure 2.8C). Despite the peak photocurrent being elicited by wavelengths close to 590 nm, this result is likely due to sub-optimal activation of the eNpHR3.0 protein by the 488 nm illumination for GCaMP5G imaging (Gradinaru et al., 2010). As such, this tool will be subject to the same experimental considerations as ChR2(ET/TC) with respect to separation of imaging and silencing light.

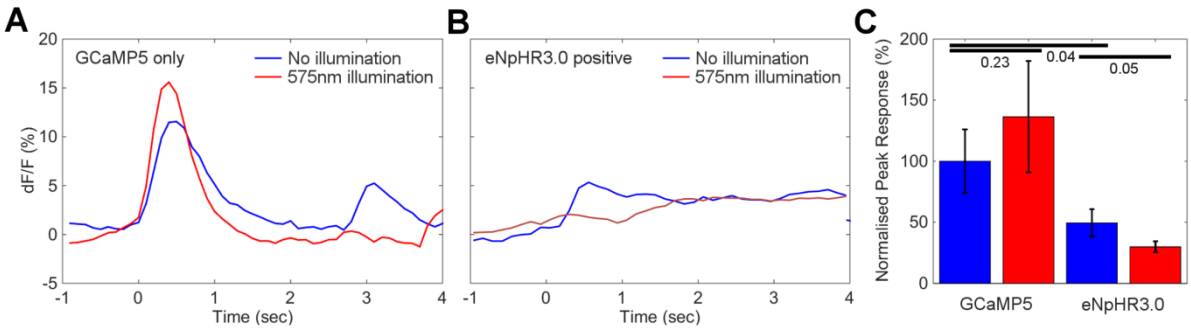

Figure 2.8. Effectiveness of halorhodopsin in larval zebrafish. (A-C) eNpHR3.0-expressing cells show a significantly lower response to visual stimuli than non-expressing siblings. Average response to onset visual stimulation (time = 0) is not significantly different under 575 nm illumination in control siblings (A, C), but is significantly lower in eNpHR3.0-expressing larvae (B, C). Second peak in GCaMP5 only control condition approximately 3 seconds after the stimulus is due to a broad wave of spontaneous activity in a single experiment that was not repeated across experiments. n = 60 cells per condition over 3 experiments; error bars = SEM; p-values = 1-tailed Student's t-test.

2.4 Combining optical and genetic technologies

2.4.1 Targeted optogenetic illumination

Advances in the fields of microscopy and genetics have become more frequent in recent times leading to a sudden expansion in the number of competing technologies available for functional neuroscience research, each with their own strengths and weaknesses. Various tools have been combined to great effect in the recording of activity from neuronal populations, however a number of improvements have also been developed in relation to optogenetic stimulation. Individual neurons have successfully been activated in mouse cortical slices by targeted excitation of the red-shifted channelrhodopsin variant, $C1V1_T$ (Packer et al., 2012). Here, a spatial light modulator (SLM) was used to target 1064 nm light to the somata of specific cells in which the resulting activity changes were recorded by patch-clamp electrodes. More recently, Hochbaum et al. (2014) described the targeted stimulation of Optopatch, a construct combining the QuasAr voltage indicator and CheRiff optogenetic actuator. In this study, the authors used a digital mirror device to selectively activate CheRiff in cultured hippocampal neurons while simultaneously imaging QuasAr activity in the broader population.

Optogenetic manipulations *in vivo* are often limited to fibre optic cannulas or widefield illumination, however targeting of individual cells in combination with network activity monitoring provides the greatest capacity for examining the role of individual cells in neuronal circuit function. This approach has rarely been demonstrated *in vivo*, however Warp et al. (2012) first used a digital mirror device to selectively silence single neurons using halorhodopsin in the zebrafish spinal cord while imaging calcium changes in nearby neurons using GCaMP3. Most recently, 2-photon imaging of GCaMP6s in the cortex of an awake, behaving mouse has been combined with excitation of C1V1 in groups of cells using a spatial light modulator (Packer et al., 2015). Conveniently, a spatial light modulator can be focused through the same objective that is used for imaging and therefore would also work well in combination with a light sheet microscope.

2.4.2 SLM with SPIM

The utility of combining SLM-targeted optogenetic activation with SPIM imaging to analyse neural circuits was investigated by examining the cerebello-tectal circuit previously identified by Heap and colleagues (2013). These foundation experiments were conducted in larval zebrafish by combining SLM-targeted excitation of ChR2(ET/TC) in the cerebellum with light sheet imaging of GCaMP5G in the tectum. To achieve this, larvae were created as per Chapter 2.3 that expressed both the calcium sensor and optogenetic activator broadly across a large proportion of the neuronal cells in the brain (*elavl3*:Gal4VP16;UAS:GCaMP5G;UAS:ChR2(ET/TC)-mCherry). 7 dpf larvae were embedded in 1.5% low melt agarose in chambers as described in Chapter 2.2.3 and transferred to the microscope. While imaging GCaMP5G activity using the SPIM, the SLM was used to target 488 nm illumination to small subset of cells in the cerebellum of the larvae.

In these experiments, a light path that incorporated a PLUTO Phase Only spatial light modulator (HOLOEYE Photonics, Germany) was added to the existing SPIM imaging system described in Chapter 2.2 by I. Favre-Bulle (School of Mathematics and Physics, The University of Queensland) (Favre-Bulle et al., 2015). Light from the 488 nm laser was split evenly between the SLM and the SPIM pathways using a 50:50 cable (FC488-50B-FC; Thorlabs). To prevent activation of ChR2(ET/TC) by the 488 nm light for GCaMPG imaging, the plane was used at 0.25 mW at the sample. In order to allow higher intensities of light through the SLM pathway than the SPIM pathway, a 97.5% neutral density filter was added to the SPIM light path prior to the beam expander. This reduced the amount of light to negligible ChR2(ET/TC) activation levels of 0.25 mW at the sample (see Figure 2.7).

GCaMP5G responses in a single plane of the tectum were imaged at 5 Hz while the SLM was used to selectively activate a 10 µm area of the ipsilateral cerebellum, midway along its medio-lateral axis and approximately 50 µm below the dorsal surface of the skin (Figure 2.9A). Imaging was repeated at 6 different depths, spaced evenly between 25 and 150 µm below the dorsal surface of the larva, while the focal plane of the SLM-generated spot was corrected by altering the image on the SLM. The stimulation site remained as consistent as possible across fish, and in all

experiments a significant rise in fluorescence was observed at the stimulation site upon cessation of the 488 nm stimulation light produced by the SLM.

The mean intensity projection of the tiff series was segmented into individual regions of interest (ROI) using a watershed function using MATLAB (MathWorks). Only regions with an area of between 10 and 200 μm^2, and with eccentricity of less than 0.8, were classified as cells. In order to measure the activity of each neuron identified above, the baseline fluorescence of each ROI was determined by finding the 25th percentile of its intensity over time (F_0). The raw intensity values at each time-point (F_i), minus this baseline, were then divided by the baseline fluorescence to yield a $\Delta F/F$ for each cell over time. Following 200 ms illumination, the peak change in fluorescence of tectal cells over the next 2 seconds was calculated.

To identify regions of the tectum preferentially innervated by the cerebellum, image registration was performed to align the responses of different animals. A template mask of the tectum at each depth imaged was produced from the average of ten hand-drawn binary masks of the PLV of each fish, to which the original images, with their segmented ROIs for each fish, were then geometrically morphed using affine transformation in MATLAB. By averaging the responses in each region across 10 different larvae, cerebellar activation was found to elicit the strongest activation of tectal cells along the ventricular edge of the periventricular layer in the deeper areas of the tectum (Figure 2.9B). While these experiments indicate that cerebello-tectal circuits can be mapped using optogenetic manipulation coupled with GCaMP5G, the appropriate experimental controls using ChR2(ET/TC)-negative siblings were not completed at the time of submission. In addition, due to the significantly reduced light levels used for imaging, the data presented were of a generally low quality. As outlined in Chapter 2.3.3, genetic restriction of optogenetic tools, as well as the use of spectral variants of these tools are expected to improve the quality of data obtained using this technique.

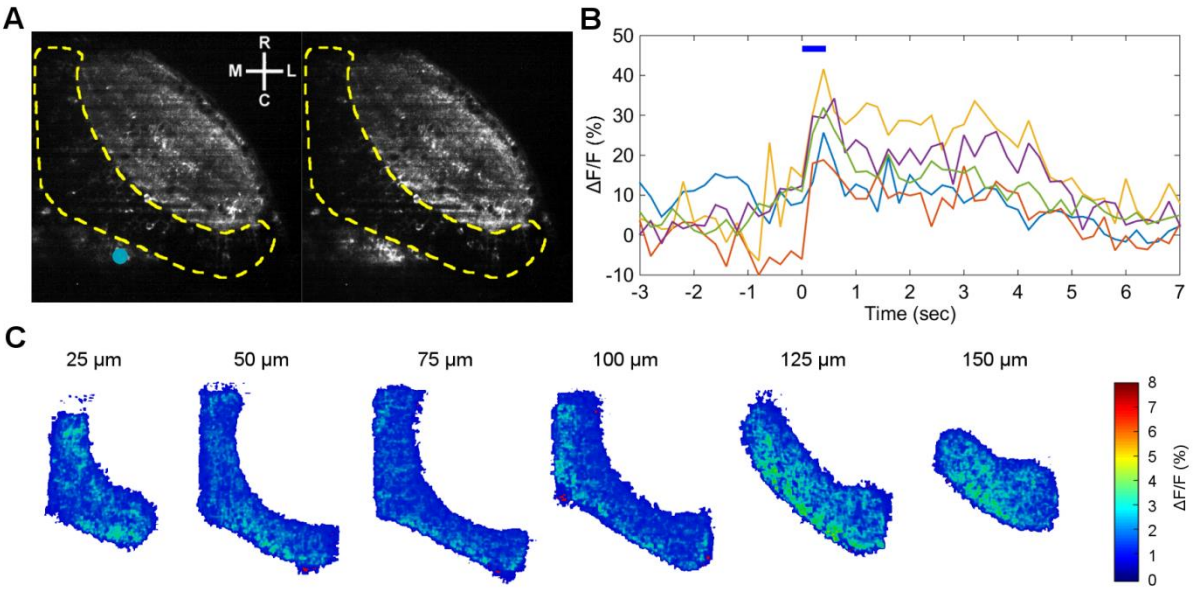

Figure 2.9. Light sheet imaging of GCaMP5G activity in channelrhodopsin-expressing larvae. (A) Example image of GCaMP5G in the right tectal periventricular layer (yellow outline) prior to (left) and immediately following (right) cerebellar excitation. A 10 µm SLM-generated spot of 488 nm light (cyan circle) was positioned in the middle of the ipsilateral cerebellum for optogenetic activation. Images taken 75 µm below the dorsal surface. R = rostral, C = caudal, M = medial, L = lateral. (B) GCaMP5G fluorescence traces for five example cells in the tectum responsive to the SLM-induced excitation of cerebellar ChR2(ET/TC) (blue bar). Large fluctuations in the fluorescence profiles show the reduced signal-to-noise ratio of GCaMP5G imaging when using a 0.25 mW plane to avoid ChR2(ET/TC) activation. (C) Average response profiles of tectal neurons at six different depths in response to cerebellar excitation. GCaMP5G was imaged using a 0.25 mW light sheet to prevent unwanted ChR2(ET/TC) activation. Cerebellar-induced responses in the tectum appear strongest in the more medial areas close to the ventricle. Each panel is the average of 5 trials across 10 animals.

2.5 Discussion

2.5.1 Future directions

Mapping neuronal circuit dynamics in response to optogenetic manipulation of individual or groups of cells can be achieved as shown here, however the utility of this process can be improved greatly by a number of experimental modifications. Firstly, circuit-specific targeting by genetic restriction of optogenetic activators such as ChR2 would benefit from the used of Gal4 enhancer trap lines (Asakawa et al., 2008; Davison et al., 2007; Scott & Baier, 2009; Scott et al., 2007). The latest generation of calcium indicators could then be separately expressed broadly across the neuronal cell population of the brain under direct control of the *elavl3* promoter (Vladimirov et al., 2014). This approach is currently being employed by members of the Scott laboratory to develop an improved understanding of the cerebello-tectal circuits described in Figure 2.9.

The analyses presented in Chapter 2.4.2 would be significantly improved by spectral separation of the imaging and activating wavelengths. This can be achieved either through the use of red-shifted optogenetic activators such as C1V1 (Yizhar et al., 2011b) or Chrimson (Klapoetke et al., 2014), or by the use of red-shifted calcium indicators such as RCaMP1 variants (Akerboom et al., 2013) or R-GECO1 (Zhao et al., 2011). While the first option can be used to circumvent some of the unintentional activation by illumination for calcium imaging, the activation curves for these proteins still overlap significantly with GCaMP5G excitation. Conversely, the red-shifted calcium indicator RCaMP1e paired with ChR2(TC) (Berndt et al., 2011) has been shown to elicit greater increases in fluorescence above baseline upon optogenetic stimulation than GCaMP3 paired with C1V1 (Akerboom et al., 2013). However, the stronger responses in the first of these pairs would be expected given that the Xenon lamp used in these would elicit stronger photocurrents in ChR2(TC) than C1V1, and also that the faster kinetics of GCaMP3 than RCaMP1e would reduce the observed responses in these cells at the very low sampling rate (0.3 Hz). Given that R-GECO1 undergoes photoactivation in both blue and green light (Akerboom et al., 2013), and the signal-to-noise ratio of the GCaMP5G variant has also been greatly improved over GCaMP3 (Akerboom et al., 2012), the benefits of red-shifted calcium indicators over red-shifted optogenetic activators remains questionable for optogenetic circuit mapping.

An alternative method that could be employed is the ‘stoplight’ technique, whereby excitation of an optogenetic activator under 488 nm light is prevented by a second wavelength of light, triggering excitation only when this light is switched off (Venkatachalam & Cohen, 2014). Use of the step-function opsin sdChR(C138S,E154A) in this assay with concurrent light sheet illumination by 488 nm and 594 nm light would allow capturing of GCaMP5 data with an improved signal-to-noise ratio, while preventing unwanted activation of the optogenetic protein. The only issue with this technique is that it would require very intense excitation of the opsin protein using through the SLM to overcome the inhibition of this opsin by the 594 nm light through the SPIM.

Technological advances in genetic targeting, optogenetic proteins and light microscopy have recently accelerated, and can be used to address a number of outstanding questions in functional neuroscience. This has increased the viability of achieving the ultimate goal to understand the role of individual cells in the brain networks that control behaviour. New techniques such as swept confocally-aligned planar excitation (SCAPE) may provide the next step in reaching this goal (Bouchard et al., 2015). Here, brains can be rapidly scanned across a 3D volume to record neuronal activity at rates exceeding the capacity of standard light sheet microscopy. However, differences in the point spread function across the imaging volume will likely need to be corrected during post-processing for accurate analysis of functional data. Other members of the Scott laboratory and I are currently exploring the practical applications of this technique for analysing zebrafish neural circuits.

Chapter 3

Investigation of cerebellar-dependent classical conditioning

3.1 Introduction

As outlined in Chapter 1, small, defined networks in the brain are an appealing model in which to analyse neural circuits. The cerebellum is one such brain region that is composed of a small, highly ordered and repeated circuit throughout to form a functional neuronal network. In vertebrates, the cerebellum is primarily responsible for motor learning and coordination, and is also believed to have roles in higher cognitive functions in humans such as attention, language and addiction (Strick et al., 2009). While a great deal is known about the anatomy, physiology and connectivity of the cerebellum, the intricate patterns of activity that are both necessary and sufficient to encode behaviours remain poorly defined. In this chapter, I aimed to develop a classical conditioning assay to allow optogenetic examination, as described in Chapter 2, of the cerebellar-dependent circuits responsible for learning in an immobilized larval zebrafish.

3.1.1 Cerebellar Architecture

The cerebellum is part of the hindbrain and consists of a highly ordered, repeating circuit of granule cells, Purkinje cells, climbing fibres, mossy fibres, and interneurons (Figure 3.1). It compares sensory information with predictions associated to motor commands, each of which enter the cerebellum via separate streams. The first pathway is thought to carry information about the prediction or 'context' of the learning to the cerebellum via the mossy fibres, which arise from the pontine nucleus and other sources including the spinal cord and lateral reticular nuclei (Steinmetz et al., 1986). The mossy fibres synapse abundantly among both granule cells and a class of interneurons known as Golgi cells, which provide feed-forward inhibition, also synapsing onto granule cells (D'Angelo & De Zeeuw, 2009). The granule cells transmit information via their parallel fibres to the distal dendrites of hundreds of inhibitory, GABAergic Purkinje cells.

The second pathway, thought to carry the sensory reinforcement or error signal, enters the cerebellum through the climbing fibres (Albus 1971; Gilbert 1974; McCormick et al., 1985). These originate in the inferior olive and usually synapse directly onto the body and proximal dendrites of individual Purkinje cells, where integration and processing of the two information streams occurs. In mammals, information about the success or failure of a response is carried by Purkinje cell

axons, which exit the cerebellar cortex and terminate in the deep cerebellar nuclei (DCN). The mammalian DCN are composed of a number of different types of output cell. The first class are generally large and excitatory, and project primarily to the thalamus and motor nuclei in the brainstem. The second class is mostly smaller and inhibitory, and forms a negative feedback loop in the climbing fibre pathway, projecting primarily to the inferior olive (Fredette et al., 1991).

Studies into the role of activity and plasticity in DCN cells during learning in alert, behaving animals has been limited given the heterogeneous and cloistered nature of the mammalian DCN. However, the use of a simple model organism such as zebrafish can allow for activity in these cells to be examined in a behaving animal in a previously unachievable manner. Zebrafish larvae develop externally and are transparent, and their cerebellum has a very similar circuit structure to that of mammals (Bae et al., 2009; Hashimoto & Hibi, 2012). The principal difference exists in the cerebellar output, with the zebrafish homologues of the DCN cells being the eurydendroid cells, situated in both the Purkinje and granule cell layers of the cerebellum. While mossy fibre and climbing fibre collaterals have not been observed explicitly in zebrafish, eurydendroid cells do receive inputs from parallel fibres as well as Purkinje cells, and have efferent projections analogous to those of the mammalian DCN (Ikenaga et al., 2005) (Figure 3.2). In summary, a number of useful aspects of the zebrafish model organism allow for the systematic investigation of the role of specific cell types and their patterns of activity in the cerebellum during motor learning that may not otherwise be achievable in mammalian systems.

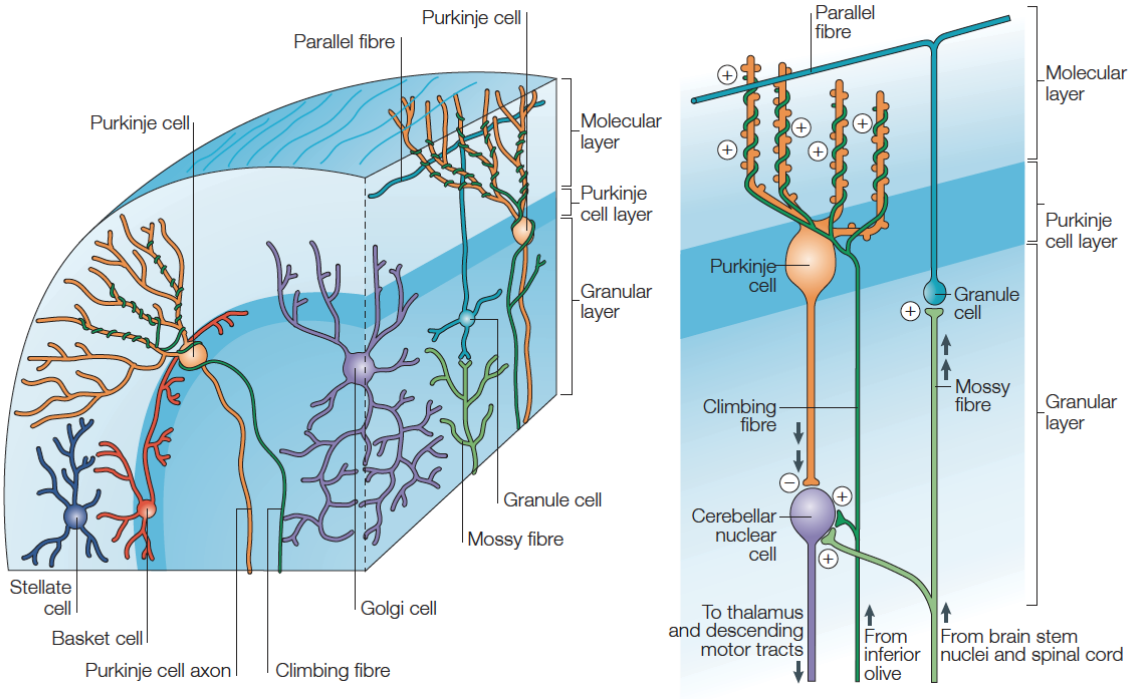

Figure 3.1. Illustration depicting the major cell types and connectivity of the mammalian cerebellum (reproduced from Apps & Garwicz, 2005). The afferent inputs to cerebellum are the climbing fibres and the mossy fibres. The climbing fibres make excitatory synapses onto Purkinje cells and the deep cerebellar nuclei, while mossy fibres make excitatory synapses onto granule cells, Golgi cells and the deep cerebellar nuclei. Granule cells make excitatory synapses onto Purkinje cells via parallel fibres and Golgi cells make inhibitory synapses onto granule cells and other Golgi cells. Other inhibitory interneurons receive input from parallel fibres and synapse onto Purkinje cells, which in turn make inhibitory synapses with the deep cerebellar nuclei, which are the output cells of the cerebellum. This circuit is highly ordered and repeated across the entire cerebellum.

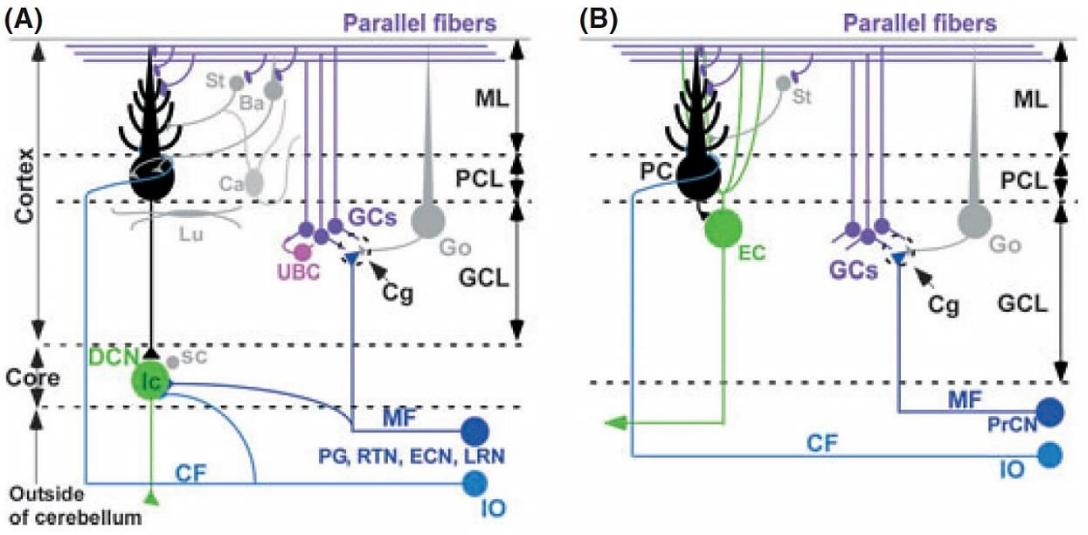

Figure 3.2. Comparative representation of the cell types and circuitry of the cerebellum of (A) mammals, and (B) zebrafish (reproduced from Hashimoto & Hibi, 2012). Note the difference in the output cells of the cerebellum. They are the deep cerebellar nuclei (DCN) in the mammalian system, located in the core of the cerebellum, and the eurydendroid cells (EC) in zebrafish, located superficially in the granule cell layer (GCL).

3.1.2 Classical conditioning

A simple form of motor learning known as classical conditioning has often been employed as a means to examine the circuitry of cerebellum. The most common assay testing this learning is eyeblink conditioning (reviewed by Mauk 1997; Thompson & Steinmetz, 2009; Freeman & Steinmetz, 2011). In this paradigm, a conditioning stimulus (CS), usually an auditory tone, is paired with an unconditioned stimulus (US), usually an air puff or electric shock near the eye. Through repetitive pairings, the animal learns to associate the natural eyeblink response to the US with the CS, and ultimately a conditioned eyeblink response is elicited by presentation of the CS alone. Lesion studies in mammals (reviewed by Freeman & Steinmetz, 2011) have shown that the cerebellum is necessary for this conditioning, but technical limitations of mammalian model systems have prevented the fine timing or cellular specificity of the necessary cerebellar activity from being identified.

It is important to note that conditioning can be induced using nonspecific stimulation of the mossy fibres as a CS (Hesslow et al., 1999), direct stimulation of the inferior olive as a US (Mauk et al., 1986), or even stimulation of both mossy fibres and the inferior olive acting as the CS and US respectively (Steinmetz et al., 1989). In this case the conditioned response is related to the specific reflex response elicited by the stimulation of the inferior olive, which varies depending on the location, current and frequency of the stimulation. This raises the question as to how changes to specific motor programs resulting in conditioned responses can be encoded in the cerebellum, and whether the common cerebellar circuitry may encode learning differently for different tasks, a question that is still hotly debated (Heck et al., 2013). The similar cerebellar architecture, combined with the fact that zebrafish larvae display motor coordination and learning by 6 days post fertilization (dpf), provides a rich opportunity for examining functional activity of the cerebellum during conditioning.

As in other vertebrates, the zebrafish cerebellum has been shown to play an important role in classical conditioning (Aizenberg & Schuman, 2011; Rodriguez et al., 2005; Salas et al., 2006). Robust classical conditioning was recently demonstrated in zebrafish greater than 3 weeks of age, however responses in younger animals were unreliable (Valente et al., 2012). This study paired a static

visual stimulus with a brief electric shock in immobilised or free-swimming 7 dpf larvae and failed to produce significant conditioning. This is in contrast to Aizenberg & Schuman (2011), who demonstrated that a moving visual stimulus paired with a tail touch was sufficient to induce conditioning in immobilised 6-8 dpf larvae. Ablation of the cerebellum was also shown to prevent acquisition but not recall of the learned responses in this assay, suggesting that eurydendroid cells may have different roles compared to the mammalian DCN. The conflicting results of Valente et al. (2012) and Aizenberg & Schuman (2011) may be a result of differences in the visual stimulus (static versus moving stimulus), or the inter-trial interval (10 seconds versus 6 minutes) used in the respective studies.

To address this conflict and investigate how cerebellar circuits in the larval zebrafish encode learning, optogenetics can be used to observe and manipulate cells in the cerebellum during a simple classical conditioning paradigm. Since it remains relatively simple to immobilize larval zebrafish younger than 10 dpf in agarose to analyse neural circuits, a classical conditioning assay is required that induces fast, reliable learning in fish at this age. In addition, while previous studies have used a visual conditioning stimulus to induce learning in larval (Aizenberg & Schuman, 2011) and juvenile (Lee et al., 2010; Valente et al., 2012) zebrafish, investigation of the underlying circuits responsible for learning using optogenetics requires the use of light to modulate neuronal activity. Therefore, a conditioning stimulus derived from a non-visual sensory modality is appropriate.

Auditory stimuli have been successfully used to induce conditioning in several model organisms, such as rat (Lindquist et al., 2009), rabbit (Steinmetz et al., 1987) and human (Steinmetz et al., 2009). Zebrafish have auditory responsiveness at 7 dpf to a wide range of frequencies, with a peak of around 400 Hz (Bang et al. 2002; Zeddies et al, 2005). Furthermore, larval zebrafish exhibit strong escape responses when presented with a brief electric shock stimulus (Lee et al., 2010; Tabor et al., 2014; Valente et al., 2012), which is a common unconditioned stimulus used in the literature. Until now however, no study has used a tone and shock to elicit a classical conditioning response in larval zebrafish. Therefore, the utility of these two stimuli to induce conditioning while allowing for optogenetic manipulations was examined.

3.2 Methods

3.2.1 Animals

Zebrafish of the strain Tupfel longfin were used for all experiments. Fish were maintained at 28.5 °C on a 14 hour ON/10 hour OFF light cycle, and were fed and mated in line with previously described protocols (Westerfield, 2000). Briefly, adult animals were housed in 3.5L tanks (ZebTec; Tecniplast, Italy) at an average of approximately 30 per tank, and fed a diet of equal parts O.range Wean-S (INVE Aquaculture, Thailand) and NRD 3/5 (INVE Aquaculture) at approximately 5% body mass (15 mg) of feed per adult fish per day, given an average weight of 300 mg for an adult fish. Once daily each tank was also presented with approximately 5000 live type-L marine rotifers (*Brachionus plicatilus*).

Adults were mated by placing a male and female in a polycarbonate breeding tank in the afternoon (Tecniplast), and collecting fertilized eggs from the bottom of the tank the following morning. Grated inserts were used to allow eggs to fall to the bottom of the tank and develop while preventing the adults from feeding on them. Embryos were raised in E3 embryo medium at 28.5 °C in 90 mm diameter vented petri dishes (Sarstedt, Germany) at approximately 50 per dish until 7 dpf. For experiments using juvenile animals, the population of larvae from a single petri dish were transferred to 80 x 120 mm containers at 7 dpf and maintained in approximately 100 mL E3, replaced daily. Juvenile animals were provided with an overabundance of rotifers twice daily to allow for *ad libitum* feeding.

3.2.2 Immobilized larval conditioning assay

7 dpf larvae were embedded in 1.5% low melt agarose with the tail positioned between two electrodes spaced approximately 2 mm apart (Figure 3.3A). The agarose from around the tail was carefully removed and the larva was allowed to acclimate in the experimental setup for 30 minutes prior to testing. During conditioning, larvae were presented with a 400 Hz tone for 2 seconds every 8 minutes (+/- 60 seconds), with a co-terminating shock for the last 100 ms of each presentation. Unpaired control animals were presented with a 400 Hz tone for 2 seconds every 8 minutes (+/- 60 seconds), with a 100 ms shock presented at randomly-generated time-points within each 8 minute inter-trial interval. The tone was played in isolation before and after training to assess the efficacy of the

conditioning protocol. Illuminated from below, the tail was recorded during every presentation of the tone at 100 Hz using a high-speed camera (HiSpec 1, Fastec Imaging) to manually identify the presence or absence of an attempted escape response. This was qualitatively characterized as tail movements with angular velocity significantly greater than that of spontaneous swim tail movements.

Electrodes were connected to a gated voltage supply provided from a 12V battery source that was triggered by a custom-written program in MATLAB (MathWorks). Resistance of the circuit was altered using a 1 kΩ trimming potentiometer (TSR-3296; Suntan Technology, Hong Kong) to tune the potential difference across the tail of the larva down from 12 V to the lowest voltage in which escape responses were reliably induced. Using 7 V across the electrodes, escape responses were observed in agarose-embedded larvae in more than 90% of trials using a 100 ms shock in this configuration. Below this value responses became less reliable and as such, 7 V across the electrodes was used for the experiments presented here.

Speakers were suspended approximately 10 cm from the larva so as to maximise volume but avoid vibrational artefacts to imaging or fish behaviour. In order to generate a low baseline of response that could be potentiated by training with a paired presentation of tone and shock, the volume of the tone presented was chosen carefully. Auditory stimuli were presented at approximately 81 dB in the assays outlined here, as this volume was found to elicit behavioural responses in less than 10% of presentations to zebrafish larvae.

3.2.3 Free-swimming juvenile conditioning assay

Experiments were performed using juvenile fish between the ages of 30 and 54 days post fertilization. Animals were fed rotifers (*Brachionus plicatilis*) twice per day from five dpf onwards until sacrificed after completion of conditioning experiment. Conditioning assays for juvenile fish were carried out in 80 x 120 mm containers with a clear bottom for illumination and darkened walls to reduce external visual input. Electrodes were positioned along the two longest walls and were connected to a 9 V battery for the brief shock stimulus. In most cases this was between 5 and 100 ms in duration (see Chapter 3.3.2). Eight animals were added to the experimental chamber in each experiment, and the response to the stimulus was recorded independently

for each animal. The mean response for all eight animals was used as a single data point for data analysis. Containers were filled to a depth of approximately 10 mm of media to maintain focus of all larvae as they swam freely.

At the start of each experiment, fish were presented with three tones without a co-terminating shock to assess the baseline level of startle response to the tone. Following training in the conditioning protocol, fish were again presented with three tones without co-terminating shock to determine the change in average response to the tone compared to the baseline. Startle responses were manually identified from high-speed recordings for all animals in each trial. All tones were presented at an interval equal to the inter-trial interval used during the training protocol (see Chapter 3.2.2).

3.2.4 Free-swimming juvenile conditioning assay with shock cancellation

Since juvenile conditioning responses were absent (see Results 3.3, below), juvenile fish were assayed for the ability to display a conditioned response when given the ability to cancel shock delivery during tone and shock pairings. This was intended to remove learned helplessness as a possible factor in the assay. Individual fish were moved to the conditioning chambers described above and were imaged using a high-speed camera. Instead of being recorded directly, images were processed in real-time during acquisition using custom-written MATLAB code to detect the presence or absence of startle responses during the delivery of the auditory tone (see Appendix 1). If the animal performed a startle response by moving more than one body-length (~ 9 mm) in any 200 msec period during the presentation of the tone, the delivery of the electric shock stimulus was prevented.

3.2.5 Data analysis

Linear regression was performed in MATLAB using the *fitlm()* function. P-values for the t-statistic were used to determine significance versus the null hypothesis that the slope is equal to that of the control larvae in Figure 3.3, or that the slope was equal to zero in Table 3.2 and Figures 3.5 and 3.7. Two-sample Kolmogorov-Smirnov tests were performed in MATLAB using the *kstest2()* function to compare the cumulative distribution functions of the non-normal distributions presented in Figure 3.4.

3.3 Results

3.3.1 Tone and shock conditioning of larval zebrafish

7 dpf larvae were embedded in low melt agarose with area around the tail removed to allow for visualisation of behavioural responses (Figure 3.3A). Each larva was presented with 15 pairings of a two-second auditory tone with a co-terminating 100 ms electric shock across the tail in order to induce a conditioned response to the tone. Larvae were found to experience a small but significant increase in the number of startle responses during presentation of the tone after the 15 pairings of the two stimuli (Figure 3.3B, blue curve) (see also Movie 2). However, an increase in the percentage of startle responses to the tone was also seen in control larvae that experienced 15 unpaired presentations of the tone and shock (Figure 3.3B, red curve). The reason for this increase in control animals was unclear, however as a result there was no significant difference between the change in startle responses between the experimental and control fish ($p = 0.22$, ANCOVA).

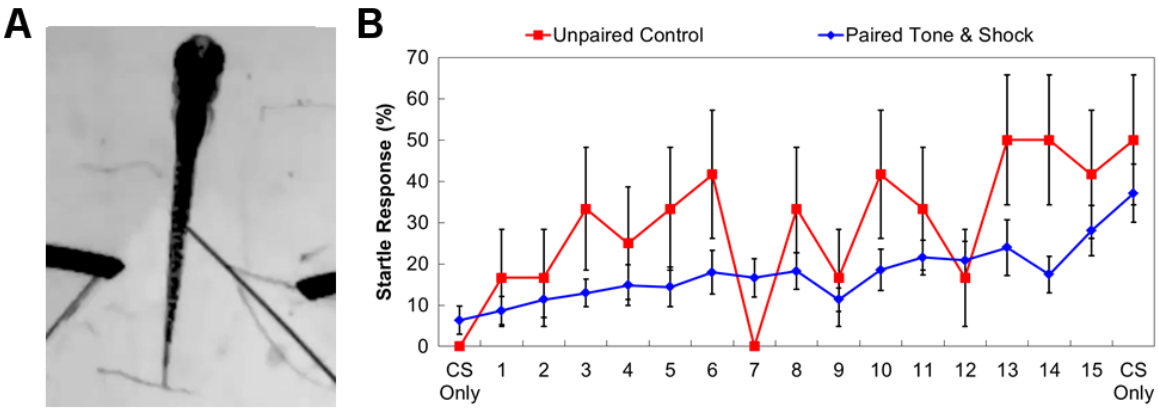

Figure 3.3. Larvae do not perform classical conditioning to tone and shock pairings. (A) Example larva with tail positioned between two electrodes for electric shock stimulus. (B) Larvae show a steady increase in likelihood of startle response to tone following increased number of pairings between tone and shock (blue curve; slope = 1.26% per pairing, r^2 = 0.12; p = 7.34×10^{-8}, linear least squares fit; n = 103 larvae, 13 experiments). This is not significantly different to the increase in responsiveness in larvae where tone and shock presentation is not paired (red curve; p = 0.22, ANCOVA). Significantly larger error bars in the unpaired controls are due to the use of only a single animal per data point in this condition (n = 12 larvae, 12 experiments) compared to the average of several animals in the paired condition.

3.3.2 Tone and shock conditioning of juvenile zebrafish

The conditions specified above were based on the protocol reported by Aizenberg & Schuman (2011). There are, however, a large number of parameters that can be varied in a conditioning paradigm to enhance learning, such as age, inter-stimulus interval and inter-trial interval. Recently, the ontogeny of learning in zebrafish has been examined from 7 dpf through to two months of age (Valente et al., 2012). In this study, larvae were unable to demonstrate learning in either classical or operant conditioning assays until beyond approximately 3 weeks of age. Given this strong dependence on age, conditioning assays were performed using juvenile animals in the tone and shock paradigm outlined above. Since larvae above 14 days of age require water flow across the gills to absorb enough oxygen (Rombough, 2002), fish were allowed to swim freely for subsequent experiments.

Juvenile zebrafish between 30 and 54 dpf were assayed in groups of eight animals per trial, allowed to swim and interact freely at all times. The responses of all eight animals were pooled per trial and the average rate of startle response during presentation of the tone was examined. Fish failed to elicit a change in the percentage of startle responses to the presentation of the tone in the new free-swimming preparation following 40 pairings of the tone and shock (Figure 3.4A; $p = 0.97$, Kolmogorov-Smirnov test; $n = 10$ experiments, 80 fish). Since zebrafish have also been observed to freeze rather than startle as a fear response to an aversive stimulus (Agetsuma et al., 2010), the number of fish that remained still in response to tone presentation was also observed. There was found to be no significant difference in the percentage of fish that remained still in response to the tone in these trials before and after training (Figure 3.4B; $p = 0.97$, Kolmogorov-Smirnov test; $n = 10$ experiments, 80 fish). Therefore, using the conditioning protocol presented here, learning was not demonstrated by juvenile zebrafish.

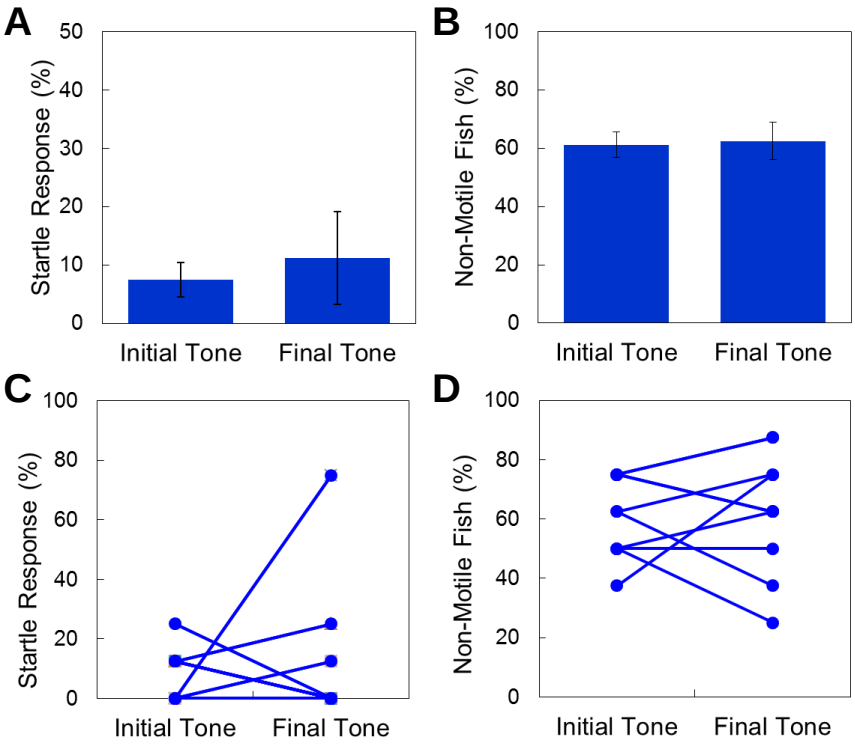

Figure 3.4. Juvenile zebrafish do not perform classical conditioning to tone and shock pairings. (A) The average rate of startle response to the tone at the beginning of the training period is not significantly different to the rate at the end of the training period under standard training conditions. n = 10 experiments, 8 fish per experiment; p =0.97, Kolmogorov-Smirnov test. (B) There is no difference in the rate of stationary fish during presentation of the tone, indicating fish do not learn to elicit a 'freezing' response to the tone by pairing it to a mild shock stimulus. p =0.97, Kolmogorov-Smirnov test. (C) Groups of larvae are as likely to decrease their rate of startle response to the tone after a conditioning training session as they are to increase. n = 10 experiments, 8 fish per experiment; p = 0.34, paired t-test. (D) Similarly, groups of larvae are as likely to decrease the number of stationary fish in response to the tone after a conditioning training session as they are to increase. p = 0.42, paired t-test.

In order to identify the optimal tone-and-shock conditioning protocol for juvenile zebrafish, several experiments were carried out whereby a range of parameters were systematically varied. Due to the remarkably large parameter space that could be explored to determine the optimal conditioning protocol, pseudorandom combinations of up to ten different parameters were varied within each experiment (Table 3.1). While this could lead to potential confounds in the identification of the main factors contributing to any observed improvements in conditioning, choosing to vary combinations of parameters in this way allowed for a greater potential exploration of the parameter space.

For each experiment, eight larvae were again pooled per trial and the average rate of startle response during presentation of the tone was examined. Following training, the change in the rate of startle responses during tone presentation was calculated for each combination of conditioning parameters and plotted as a function of each parameter tested (Figure 3.5). Linear regression was performed for each combination of change in response rate versus the tested variables to test for any underlying effects (Table 3.2). No significant relationships were found for any parameter tested, including age, tone frequency and duration, inter-trial interval or the number of training sessions provided. This is in contrast to published protocols for rabbit eyeblink conditioning in which conditioning improves significantly with the number of training sessions performed (Kim et al., 1995; McCormick & Thompson, 1984). To examine the combined effects of different variables, multiple linear regressions were performed. Coefficients were similar to those in Table 3.2, with no significant effects found (r^2 = 0.061, F-statistic = 0.284, p-value = 0.975 vs no combined linear relationship).

Age	Frequency	Tone duration	Shock duration	ISI	ITI	Inter-session interval	Total sessions	Pairings /session	Total pairings
38	250	350	20	330	35	30	6	5	30
50	400	400	50	350	180	5	2	10	20
37	250	350	10	340	30	30	13	6	78
45	200	3000	100	2900	60	0	1	20	20
32	300	400	50	350	300	0	1	60	60
41	250	350	20	330	45	70	5	5	25
35	300	400	50	350	300	1440	3	80	240
40	200	200	20	180	45	60	7	5	35
45	250	1000	70	930	10	0	1	15	15
45	250	1500	70	1430	15	0	1	5	5
45	200	250	50	200	30	0	1	20	20
49	200	1500	70	1430	30	0	1	15	15
50	350	400	70	330	60	0	1	10	10
49	400	400	70	330	20	5	3	10	30
33	300	400	50	350	300	1440	4	80	320
43	250	350	10	340	20	20	20	3	60
50	250	600	20	580	15	80	5	8	40
45	150	1500	30	1470	30	0	1	10	10
49	400	1500	70	1430	25	0	1	10	10
49	400	400	70	330	10	0	1	10	10
50	200	400	70	330	30	0	1	10	10
50	400	450	70	380	30	0	1	10	10
50	400	350	20	330	30	5	2	10	20
40	250	350	10	340	30	90	5	5	25
35	250	600	20	580	120	75	6	5	30
33	300	400	50	350	300	1440	5	80	400
49	200	500	70	430	10	0	1	10	10
50	400	450	70	380	180	0	1	10	10
49	400	400	70	330	90	5	3	10	30
50	400	400	50	350	10	5	2	10	20
51	650	400	50	350	30	5	2	10	20
33	300	400	50	350	300	1440	2	80	160
45	250	350	50	300	15	0	1	30	30
50	400	400	70	330	180	0	1	10	10
39	250	350	10	340	60	50	7	10	70
33	250	270	10	260	30	30	12	6	72
37	250	350	20	330	30	60	6	6	36
45	250	600	70	530	10	0	1	15	15
45	250	1500	70	1430	15	0	1	15	15
45	750	600	30	570	30	0	1	30	30
45	180	400	50	350	60	0	1	20	20
40	250	350	20	330	30	60	6	6	36
41	250	350	10	340	30	60	7	10	70
49	400	400	70	330	30	0	1	10	10
49	200	500	70	430	30	0	1	20	20
51	300	400	50	350	300	5	2	10	20
53	250	600	10	590	30	100	4	10	40
36	250	350	20	330	75	70	5	5	25
38	250	350	10	340	30	25	12	4	48

Table 3.1. Combinations of conditioning parameters varied pseudorandomly between experimental trials. Units for the different parameters are: age = days post fertilization; frequency = Hz; tone duration, shock duration, and inter-stimulus interval (ISI) = msec; inter-trial interval (ITI) = seconds; inter-session interval = minutes.

.

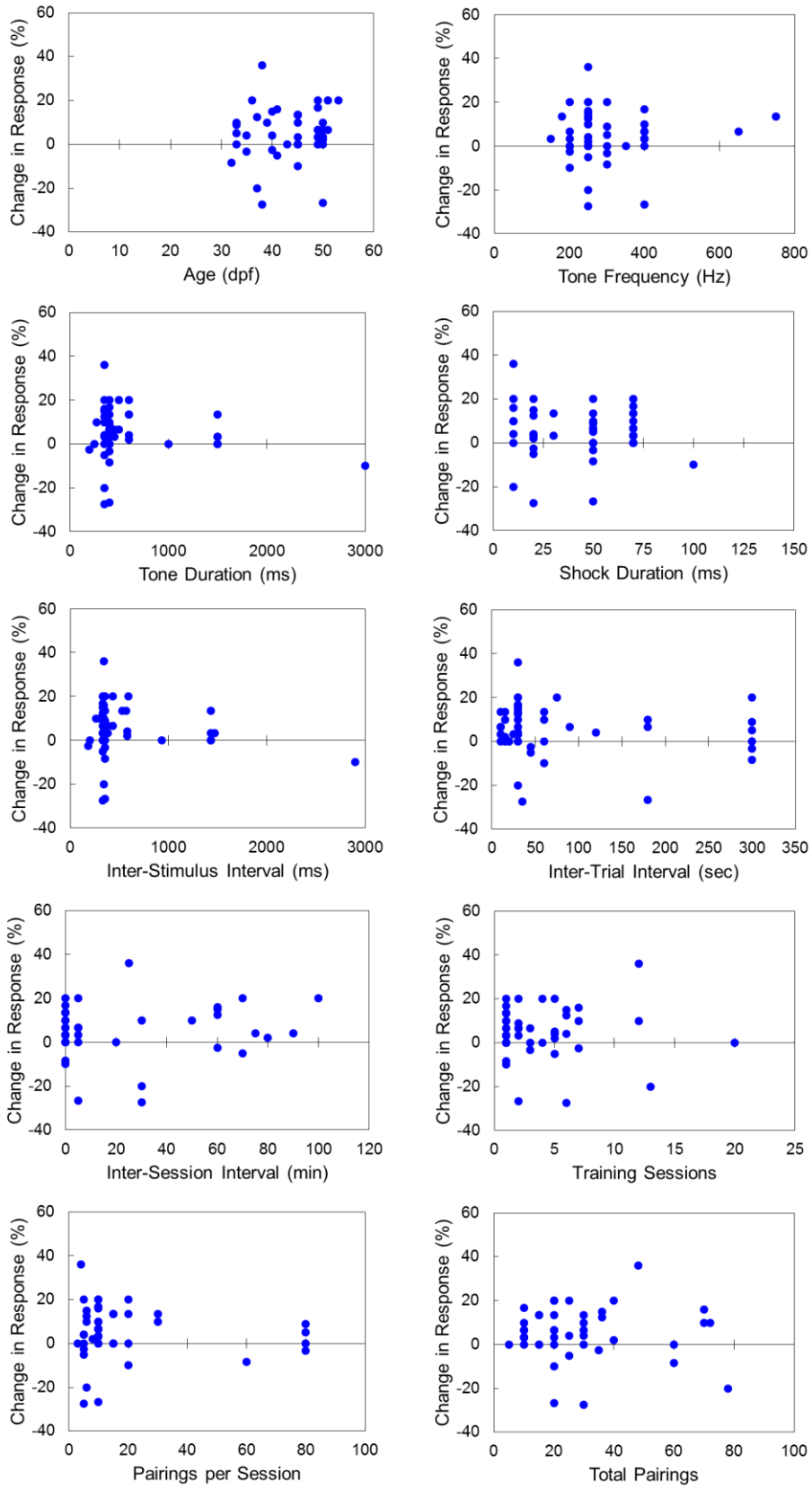

Figure 3.5. Adjustments to several key parameters do not elicit any significant change in the rate of startle response due to pairing of tone and shock stimuli in free-swimming juvenile zebrafish (n = 8 fish per data point).

	Coefficient	r-squared	t-statistic	p-value
Age	0.168	0.008	0.627	0.534
Frequency	0.002	4.11E-04	0.139	0.890
Tone duration	-0.003	0.020	-0.990	0.327
Shock duration	-0.040	0.008	-0.608	0.546
Inter-stimulus interval	-0.003	0.020	-0.980	0.332
Inter-trial interval	-0.014	0.013	-0.778	0.441
Inter-session interval	-0.002	0.003	-0.364	0.717
Number of sessions	-0.033	1.29E-04	-0.078	0.938
Pairings per session	-0.043	0.006	-0.546	0.588
Total pairings	-0.010	0.005	-0.465	0.644

Table 3.2. Statistical analysis of experimental parameters tested. Linear regression by ordinary least squares of parameters shows that no variable along has any significant effect on the change in startle response rate following pairing of tone and shock stimuli in free-swimming juvenile zebrafish.

3.3.3 Tone and preventable shock in conditioning of juvenile zebrafish

In assays that condition an eyeblink response, the reward for learning is that the eye is generally protected from the airpuff. In the free-swimming setup above however, there is no escape from the shock stimulus by eliciting a startle response. Since delivery of inescapable shocks prior to conditioning has been shown to prevent learned avoidance responses in juvenile zebrafish (Lee et al., 2010), the results above could be explained by helplessness in these animals. To address this concern an assay was developed in which fish could cancel the delivery of a shock stimulus by eliciting a startle response to the tone. The best parameters from the previous experiment were used for the tone frequency, duration and inter-stimulus interval (250 Hz, 350 msec and 330 msec respectively). Despite this fact, when animals had the ability to prevent shock delivery, they failed to show any significant increase in startle responses to the tone over 40 pairings (Figure 3.6; $p = 0.79$ vs slope = 0, linear least squares fit, $n = 10$).

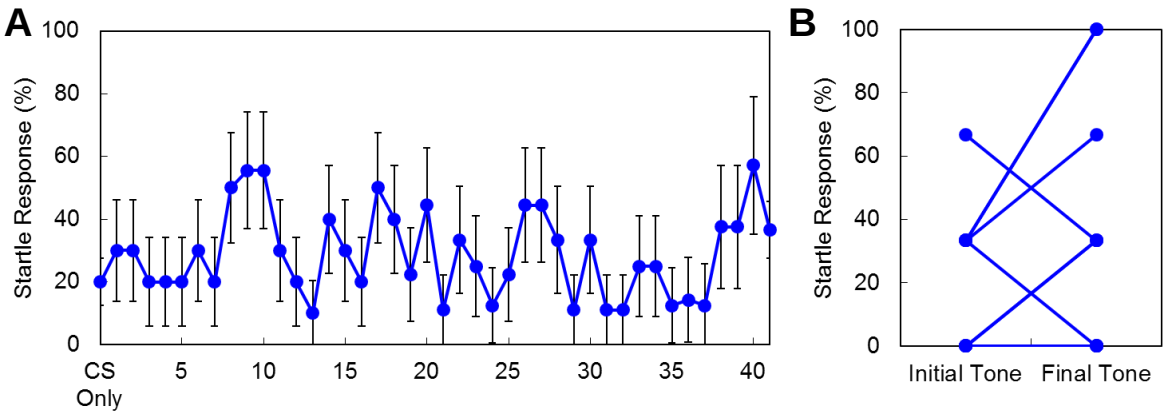

Figure 3.6. Classical conditioning with tone and shock pairings is not improved by the ability to cancel shock delivery. (A) When shock delivery was cancelled by expression of a startle response during tone delivery, juvenile zebrafish remained unable to increase the percentage of startle responses after 40 pairings. Learned helplessness is therefore unlikely to prevent the observation of conditioned responses. Slope = -4.74x10-4; p = 0.79 vs slope = 0, linear least squares fit, n = 10. (B) Individual fish displayed significant variability in the change of startle response rate following training with tone and shock pairings. p = 0.09, paired t-test.

3.4 Discussion

3.4.1 Classical conditioning of zebrafish larvae

The ability of an animal to learn to make associations between two different stimuli is critical to normal behaviour. Aizenman & Schuman (2011) report that larval zebrafish can undergo rapid learning by pairing a light and aversive tactile stimulus. As this conditioning was found to be cerebellar-dependant, the experiments presented in this chapter were devised such that the circuits responsible for learning could be analysed using optogenetics. The results presented here however, show that these associations are not always learnt quickly or easily, with zebrafish larvae up to approximately 6 weeks of age unable to be conditioned by any standard combination of tone and shock pairing. Valente and colleagues (2012) recently reported that a group of fish repeatedly trained on the same stimulus were unable to display significant learning until more than one month of age. This required the same population of fish to be trained six days per week until this late stage so cannot be directly compared to the results presented here, and such a lengthy training period does not lend itself to simple optogenetic dissection of the circuits responsible for cerebellar-dependent learning.

These results are also in stark contrast to the results presented by Aizenman & Schuman (2011). Here, conditioning was not observed as an increase in the rate of response as would normally be measured, but rather as an increase in the ratio of angular tail velocity of spontaneous tail movements during CS presentation versus those prior to CS presentation. This was further distorted by the exclusion of more than half of the fish tested from the final analysis that either did not have a high baseline of spontaneous activity or displayed a significant behavioural response to the CS during a pretest. Coupled with the very high variability in conditioned responses during later pairings of their assay, the reported conditioning may simply represent sensitization of a small number of animals with a low baseline to the stimulus leading to an artificially-inflated increase in angular tail velocity

Nevertheless, there are other notable examples of rapid learning in young zebrafish. Lee and colleagues (2010) were able to train 3-5 week old zebrafish to reliably show a conditioned place avoidance following pairings of a light and aversive shock stimulus. However, only a low percentage of fish were found to display a startle

response to the visual cue, and fear was able to reduce activity in the habenula and cause a reduction in avoidance behaviours. As such, startle responses may not be the most reliable outcome by which to examine conditioning. For example, Ahrens and colleagues, (2012) revealed that larval zebrafish could very rapidly change the strength of an optomotor response (OMR) to a moving visual grating. While not a typical learned behaviour, adaptation of the OMR may be more behaviourally relevant for the fish since, like classical conditioning, it was characterised by strong cerebellar and inferior olive activity. This may suggest that the circuitry required for learning is present in larval zebrafish, but the most relevant incentives for these animals should be explored in greater depth before the design of future training protocols.

In adult zebrafish, conditioning has been observed in a number of paradigms. With particular respect to aversive conditioning, visual cues have often been paired with a mild electric shock to elicit an avoidance response of a particular tank region (Aoki et al., 2013; Manuel et al., 2014; Xu et al., 2007). In these assays however, usually only 60 – 65% of animals are actually found to exhibit avoidance behaviours, suggesting a large discrepancy between the learning capacities of individual animals. The particular characteristics of the both the conditioning and unconditioned stimulus have also been shown to be important in zebrafish. For example, increasing the strength of the electric shock has led to higher rates of conditioning (Manuel et al., 2014), and olfactory cues produce better conditioning than visual cues when paired with an aversive water disturbance (Morin et al., 2013), however rates of conditioning here still peaked at only around 40%. As such, it is clear that range of confounding factors are able to hinder the acquisition of fast, reliable conditioning in larval zebrafish. Combined with the requirement for optogenetic analysis that conditioning be acquired in young, immobilised larvae, the conditioning paradigm that was sought in these experiments proved unattainable.

3.4.2 Limitations and future directions

In the experiments presented here, responsiveness to the tone during the experiment was found to increase in control animals where tone and shock presentations occur at random, unpaired intervals. This may be due to a number of reasons. First, larvae were given 30 minutes to acclimate to the experimental

apparatus prior to imaging. However, fish are social animals, and larvae as small as 7 mm in length have similar shoaling preferences to adult fish (Engeszer et al., 2007). Therefore the increased responsiveness may be due to isolated larvae requiring more than two hours to habituate to the testing environment, although this has not been seen in other studies (Aizenberg & Schuman, 2011; Lee et al., 2010). Secondly, repeated electric shock stimulation over a short period of time has been shown to cause a significantly increased heart rate in zebrafish larvae (Mann et al., 2010), which may result in a heightened state of arousal and responsiveness. Finally, increasing response rate to the auditory stimulus during the experiment may represent a genuine change in the preferences of the neurons that process auditory information. These cells may acquire this change similarly to cells in the *Xenopus* tectum, which increase their responsiveness to moving visual stimuli following repeated presentation of the same stimulus (Engert et al., 2002).

Other physiological factors may also influence the ability of larvae to exhibit conditioning in response to paired tone and shock stimuli. For example, hair cells of the zebrafish inner ear have recently been shown to only develop mature biophysical response profiles after about two months of age (Olt et al., 2014). As a result, it is possible that the animals fail to respond in many cases because they are unable to hear the tone reproducibly during all trials. However, the clear increase in responsiveness over time in control animals suggests that behavioural reasons rather than a lack of reliable audition across trials is the more likely cause. As in other animals, prepulse inhibition in zebrafish larvae from weak stimuli, like the auditory tone used in this chapter, can reduce the magnitude of response to subsequent startle-inducing stimuli (Burgess & Granato, 2007). This effect peaks at around 300 to 500 ms between the two stimuli (Bergeron et al., 2014), an identical period used to separate tone and shock in the majority of experiments on juvenile fish presented in this chapter. Therefore, there may be strong, competing effects of prepulse inhibition versus conditioning of the startle response in the assays presented. As a result, there are many important factors that determine whether fish are able to elicit reliably conditioned responses that will require further detailed investigation.

Chapter 4

Investigation of multisensory responses in the zebrafish tectum

4.1 Introduction

The analysis of functional neuronal circuits in the larval zebrafish has become a rapidly growing field in the last several years, in large part due to the technologies discussed in Chapter 2. The ability to examine whole brain circuits with single cell resolution has allowed a great many advances in the understanding of several basic behaviours with new discoveries emerging all the time. However, as discussed in Chapter 3, the number of behaviours capable of being robustly examined in the larval zebrafish remains quite low. As such, in this chapter I describe an application of the technologies previously discussed in order to examine functional circuits in the tectum of larval zebrafish in response to multiple different sensory stimuli.

4.1.1 The multisensory tectum

The mammalian superior colliculus and its homologous area in fish, the optic tectum (Ingle, 1973), are primarily thought of as visual processing centres. While there is a strong visual input into these structures, it has been linked to orientating behaviours in response to both visual and non-visual stimuli (Stein & Gaither, 1981), and excitatory feedback from the motor areas of the superior colliculus have been shown in the sensory areas of the rat cortex (Ghitani et al., 2014). An important function for the colliculus is the integration of multiple sources of sensory information including vision, audition, and somatosensation to regulate motor outputs (Dräger & Hubel, 1975; Meredith & Stein, 1986; Wallace et al., 1993). Different sensory modalities are partially segregated by different laminae, with non-visual inputs more prominent in the deeper laminae (Stein & Gaither, 1983). It has been observed in many cases that these modalities can then be integrated to regulate motor output by a simple overlap in their topographic organization (Dräger & Hubel, 1975; Finlay et al., 1978; Harris et al., 1980; King et al., 1996; Stein & Gaither 1983; Triplett et al., 2012).

Multisensory processing has also been observed in the tectum of many lower order vertebrates, including the barn owl (Knudsen 1982; Zahar et al., 2009), iguana (Stein & Gaither, 1981) and frog (Lowe, 1986 & 1987). Exclusively found in fish and aquatic vertebrates, and of particular interest in multisensory integration in these animals, is the lateral line system giving them the ability to sense water flow. Similarly to somatosensory stimulation mammalian systems, lateral line stimulation in the African claw frog (*Xenopus laevis*) appears to induce activity in the deep layers of the

contralateral tectum, as well as the torus semicircularis (Lowe, 1986). In keeping with the general trend, Hiramoto & Cline (2009) also suggest functional segregation of visual input to the superficial tectal layers and non-visual sensory input to the deeper layers. While many sensory modalities are separated by laminae in the adult frog tectum, integration can occur at the individual cell level as seen by the differential facilitation or suppression of visual responses by lateral line stimulation (Lowe, 1987). The larval *Xenopus* tectum has many similarities to larval zebrafish, but also has only a relatively simple circuit for potential multisensory processing (Hiramoto & Cline 2009).

4.1.2 The zebrafish tectum

Due to its small size, transparency, and conserved brain structure, the larval zebrafish has emerged as a model organism of choice for the functional investigation of neuronal circuits underlying perception and behaviour (Ahrens et al., 2012; Bianco & Engert, 2015; Muto et al., 2013; Portugues & Engert, 2009). In fish, the optic tectum has been extensively studied for its role in many visual behaviours including the optomotor response, optokinetic response, saccades and prey tracking (Bianco et al., 2011, Bianco & Engert, 2015; Gahtan et al., 2005; Muto et al., 2013; Portugues et al., 2009; Roeser et al., 2003). Visual information has been shown to differentially activate cells and circuits depending on the size (Del Bene et al., 2010; Niell & Smith, 2005; Preuss et al., 2015), orientation (Hunter et al., 2013; Nikolaou et al., 2012), direction (Gabriel et al., 2012; Gebhardt et al., 2013) and speed (Grama & Engert 2012), with different laminae and sublaminae in the neuropil targeted by cells with different anatomical and functional response properties.

Visual information passes from the retina to the contralateral tectum via retinal ganglion cell axons (RGCs) that terminate within the tectal neuropil (Figure 4.1A) to create a topographic map of the visual environment (Kita et al., 2015; Niell & Smith, 2005; Stuermer, 1988). Within the tectum, periventricular layer (PVL) neurons (Figure 4.1B-C) have dendrites usually in the middle layers of the neuropil (SFGS and SGC) and synaptic terminals usually slightly deeper than their dendrites (SGC and SAC) (Robles et al., 2011). Periventricular projection neurons (PVPNs) receive inputs in the deeper neuropil layers and send axons to premotor and motor areas of the brain, influencing numerous visual and orienting behaviours (Nevin et al., 2010).

Inhibitory neurons in the superficial neuropil (SO) preferentially inhibit deeper layers of the neuropil and are more active in response to larger visual stimuli (Preuss et al., 2015), and have a role in filtering visual perception for prey capture, but not optomotor responses (Del Bene et al., 2010) (Figure 4.1C). While these cells and circuits have been described thoroughly in terms of their visual responses, tectal responses to other modalities have remained unexplored in fish. As a result, little is known about how inputs from non-visual sensory modalities pass through the tectum or the mechanisms by which different modalities may be registered against one another during tectal processing.

With respect to non-visual sensory modalities, anatomical projections to the tectum have been observed in teleost in only a handful of studies. Water flow information received by the lateral line sensory organ is passed from primary ganglia to hindbrain nuclei such as the medullary nucleus medialis, with substantial second-order projections connecting to the contralateral torus semicircularis (Fame et al., 2006, McCormick & Hernandez, 1996). Contralateral projections from auditory midbrain nuclei have also been seen in the torus semicircularis (Echteler, 1984), although separated anatomically from lateral line areas (McCormick & Hernandez, 1996). Since large areas of the torus project to the deep layers of the ipsilateral optic tectum (Carr et al., 1981; Perez-Perez et al., 2003), it therefore has the potential to integrate the visual and non-visual sensory inputs from one half of the animal that converge on this brain region. However, the functional mechanisms by which different sensory modalities are processed in tectal networks remain unexplored in fish.

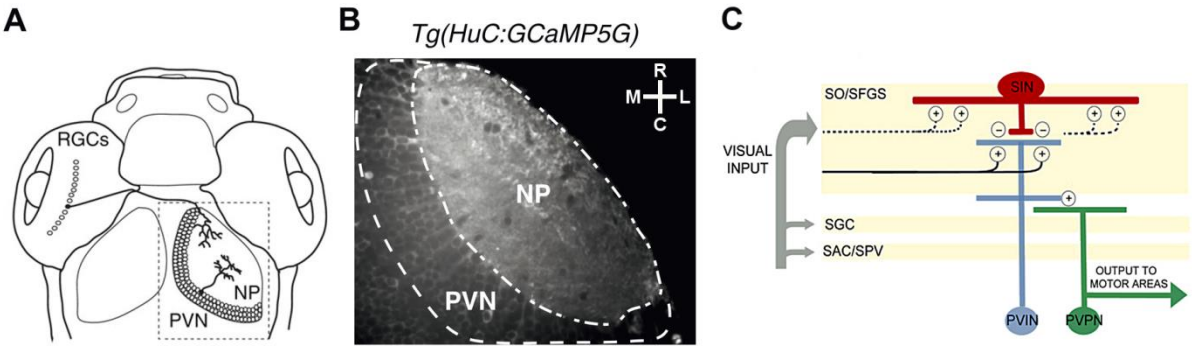

Figure 4.1. Organization of the larval zebrafish tectum. (A) Retinal ganglion cells (RGCs) project from the retina to the contralateral tectum and synapse within the neuropil (NP). RGCs located more towards the nasal region project more caudally in the neuropil and those located more temporally in the retina project more rostrally in the neuropil. Periventricular neurons (PVN) within the tectum project dendrites into the neuropil to receive and process visual information. (B) GCaMP5G expression in the tectum (dotted outline in panel A) shows the densely organized periventricular neurons (PVN) spatially separated from the axons and dendrites of the neuropil (NP). R = rostral, C = caudal, M = medial, L = lateral. (C) Visual information enters the tectum via RGC axons primarily in the outer neuropil layers (SO and SFGS). Inhibitory superficial interneurons (SINs; red) preferentially respond to large visual stimuli, with filtered information being received by periventricular interneurons (PVINs; blue). Periventricular projection neurons (PVPNs; green) receive processed information in the deeper neuropil layers and send axons to motor areas of the brain to direct orienting behaviours. SO, stratum opticum; SFGS, stratum fibrosum et griseum superficiale; SGC, stratum griseum centrale; SAC/SPV, stratum album centrale/stratum periventriculare. Panels A-B adapted from Auer et al. (2015); Panel C reproduced from Nevin et al. (2010).

4.1.3 Summary

Recent advances in imaging techniques and optogenetic activity indicators (described in Chapter 2) have allowed for whole-brain activity patterns to be mapped at a single-cell resolution (Vladimirov et al., 2015). With the unprecedented access provided by these techniques, the function of zebrafish neural circuits can be explored to uncover the principles governing neural processing in the vertebrate brain. In this chapter, I use selective plane illumination microscopy (SPIM) in combination with GCaMP5G to describe the response properties of cells in the larval zebrafish tectum to visual, water flow, and auditory stimuli. I reveal that different stimuli drive distinct spatial and temporal patterns of responses within the tectum that emerge as populations of concurrently activated cells, and improve understanding of the principles of by which tectal circuits encode multisensory information.

4.2 Methods

4.2.1 Animals

All procedures were performed with approval from The University of Queensland Animal Ethics Committee (in accordance with approval SBMS/305/13/ARC). Zebrafish (*Danio rerio*) larvae were maintained at 28.5 °C on a 14 hour ON/10 hour OFF light cycle. Adult fish were maintained, fed, and mated as previously described (Chapter 3.2.1). All functional experiments were performed using larvae of the *elavl3*:Gal4;UAS:GCaMP5G genotype (created in Chapter 2.3.2) in a *nacre* mutant background of the Tupfel long fin strain (TLN; Lister et al., 1999). Briefly, plasmids containing the genes of interest were created using the Gateway system (Life Technologies) and injected into single-cell embryos at 100 ng/µL. UAS:GCaMP5G and *elavl3*:Gal4VP16 founders were raised to adulthood and crossed to create *elavl3*:Gal4;UAS:GCaMP5G offspring. *Atoh7*:Gal4 fish (Del Bene et al., 2010) were crossed to UAS:Kaede fish (Scott et al., 2007) to determine the approximate layers of the tectal neuropil in *Atoh7*:Gal4;UAS:Kaede larvae.

4.2.2 Imaging tectal activity

6 day post-fertilization (dpf) larvae of the strain *elavl3*:Gal4;UAS:GCaMP5G were immobilised dorsal side up in 1.5% low melting point agarose (Progen Biosciences, Australia). The agarose surrounding the tail was gently freed by sequentially removing small segments of agarose perpendicular to the tail so as not to damage the neuromasts. A small cut was then made on the tail fin to allow the animal to be paralysed by bath application of 100 µM tubocurarine (tubocurarine hydrochloride pentahydrate, Sigma-Aldrich). Larvae were then transferred to custom-made, glass-walled imaging chambers and allowed to acclimate for 20 minutes prior to imaging on a custom-built selective plane illumination microscope (Figure 2.1, Table 2.1) on an sCMOS camera (PCO.Edge 5.5, PCO) through a 510 nm emission filter (FF03-510/20-25, Semrock). The light sheet intensity was delivered through a single illumination arm as described in Chapter 2.2 and measured to be approximately 4 mW at the sample during image acquisition (Digitech Luxmeter). This level was found to have negligible effects on calcium responses in the larva to a moving bar visual stimulus.

A single plane of one tectal hemisphere was imaged at 10 Hz for five consecutive trials. This was repeated at each of six different dorsal-to-ventral depths within each fish, spaced 25 μm apart beginning 25 μm below the first visible tectal cell body. The order of depths imaged was randomized on fish-by-fish basis. Each trial lasted 36 seconds and involved the presentation of 4 visual and 2 non-visual stimuli. In 8 of the animals presented here, the visual stimuli were presented first, followed by lateral line and auditory stimuli respectively. The remaining 3 animals received auditory stimulation first, followed by visual and then lateral line stimuli. There was found to be no difference in responsiveness to any stimulus depending on order of presentation.

A range of different visual stimuli have been used previously to examine the functional responses of tectal periventricular neurons. Strong responses have been elicited from stimuli such as small spots ranging between 1 and 13 degrees of visual angle (Bianco et al., 2011; Bianco & Engert, 2015; Muto et al., 2013; Niell & Smith, 2005; Preuss et al., 2014; Romano et al., 2015), and large spots up to 64 degrees of visual angle (Pruess et al., 2014), that were either stationary or moving horizontally at 15 (Bianco & Engert, 2015), 30 (Bianco et al., 2011; Bianco & Engert, 2015), 40 (Preuss et al., 2014) or 60 degrees per second (Bianco et al., 2011). In addition, strong responses have also been observed in response to moving bar stimuli coving 3 degrees of the visual field travelling at 60 degrees per second (Grama & Engert, 2012), 10 degrees of the visual field travelling at 20 degrees per second (Nikolaou et al., 2012), or between 2 and 50 degrees of the visual field travelling at 250 degrees per second (Del Bene et al., 2010). Given the extensive range of possible stimuli with which to assess neuronal responses in the larval tectum, a small subset of stimuli (four) that were observed to elicit qualitatively strong responses during preliminary experiments were chosen to address some generic features of visual processing.

The four visual stimuli were presented on a translucent screen positioned 10 cm from the larva by a PK320 miniature projector (Optoma). This screen was centred perpendicular to the eye contralateral to the tectal hemisphere being imaged and covered approximately 100° of the visual field of that eye. The first of these was a bright, 7° wide vertical bar on a dark background, moving at 50°/s rostrally then

caudally. The second stimulus was a bright, 7° wide horizontal bar on a dark background, moving at 50°/s ventrally then dorsally. Third was a simple full-field flash stimulus whereby the entire screen was bright for 1 second before returning to dark. Finally, a small spot of 6° was moved rostrally then caudally across the screen twice at 100°/s. Visual stimuli were restricted to blue wavelengths by a spare 472/30 bandpass filter (Semrock) to prevent any artefacts from the stimulus light entering the detection path of the microscope, with mean luminance from the moving bar stimuli of approximately 34 cd/m^2. Each visual stimulus was separated by 2 seconds of blank screen, as seen in Movie 3.

Lateral line stimulation was provided to the tail by means of a media-filled pipette positioned adjacent to the caudal-most part of the contralateral side of the tail. Media was ejected at approximately 50 µL/sec for 100 msec from a 20 µm bore pipette by triggering a linear solenoid (TP8X16-C-12D; Guardian Electronic) against an elastic rubber membrane. Auditory stimulation was provided by means of two speakers (Z200; Logitech) suspended 10 cm from the larva that played a 400 Hz tone for one second, followed immediately by an 800 Hz tone for one second, at 81 dB. This was intended to cover the likely range of frequencies to which larvae may respond (Bang et al. 2002; Zeddies et al, 2005).

4.2.3 Analysis of tectal responses

Small amounts of XY drift or motion artefacts from each tiff series were reduced by aligning each frame to its preceding frame using the 'Rigid Body' transformation in the ImageJ (NIH) plugin, StackReg (Thévenaz et al., 1998). Using a custom-written MATLAB code (Appendix 2), based on previous work by Panier et al. (2013), the tiff series was prepared for segmenting individual somata by first generating a mean intensity projection of the series, which was smoothed using a 2-D Laplacian of Gaussian filter. This image then underwent a morphological tophat transformation followed by Gaussian lowpass filter, each with a width of approximately half an average cell diameter (7 pixels). The resulting images were then segmented into individual regions of interest (ROI) using a watershed function based on the Meyer algorithm (Meyer, 1994). This algorithm finds local minima in image intensity and the continuous peak in intensity surrounding this region is marked as its border. Only

regions with an area of between 10 and 200 μm^2, and with eccentricity of less than 0.8, were classified as cells.

Neuropil regions were analysed in collaboration with G. Vanwalleghem (Scott Laboratory, The University of Queensland) where images were cropped to a hand-drawn mask in MATLAB followed by correlation to stimulus presentation in Thunder using a step-like function (Freeman et al., 2014). Average neuropil responses were generated by affine transformation of each neuropil to an average template in MATLAB. These were compared to confocal images of RGC axons of *Atoh7*:Gal4;UAS:Kaede larvae (performed by L. Heap, Scott Laboratory, The University of Queensland) to determine the approximate neuropil layer positions.

In order to measure the activity of each neuron identified above, the baseline fluorescence of each ROI was determined by finding the 25th percentile of its intensity over time (F_0). The raw intensity values at each time-point (F_i), minus this baseline, were then divided by the baseline fluorescence to yield a ΔF/F for each cell over time:

$$\Delta F/F = 100*(F_i - F_0)/F_0 \quad (\%)$$

It was observed in our recordings that shadows across the illumination plane could flicker due to minor movements of the animal or blood circulation. These flickers added to the noise of the fluorescence signal and as such, a knowledge-based detection method, similar to that proposed by Patel et al. (2015) was used to detect only significant neuronal firing. Specifically, the time-varying correlation coefficient between the fluorescence trace for each cell and an ‘example spike’ was calculated. The example spike was a 4 second trace created by averaging 50 user-defined calcium events (Figure 4.2). Calcium transients with a correlation coefficient greater than 0.7 to the example spike and a peak ΔF/F greater than 25% were classified as a neuronal response. To reduce the influence of spontaneous activity, only cells that initiated a neuronal response between the onset of a stimulus and 500 msec after the stimulus were deemed to be responsive to that stimulus. While this method may have reduced the absolute numbers of responsive cells detected, it prevented spurious signals from be included in the dataset. Despite the cytosolic expression of

GCaMP5G, the fluorescence changes in a given cell did not significantly influence the traces of surrounding ROIs (Figure 4.5D-E).

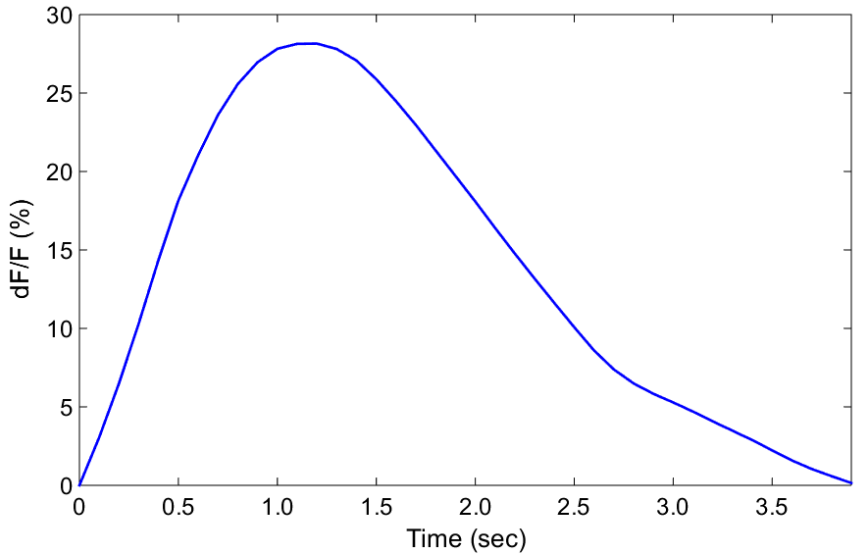

Figure 4.2. Example GCaMP5G spike trace. Average response profile of 50 GCaMP5G spike events in individual tectal neurons responding to a moving vertical bar stimulus with onset at time = 0 seconds.

To identify groups of similarly responsive neurons, a principal components analysis (PCA) followed by non-orthogonal promax factor rotation was performed on the data. This method has not only been shown to outperform other methods of clustering such as K-means or hierarchical clustering, it also allows a cell to be assigned to more than one ensemble (Romano et al., 2015). Unlike other common methods of clustering data, such as K-means (Panier et al., 2013), density peak-based clustering (Rodriguez & Laio, 2014), a dissimilarity matrix (Kiani et al., 2015), or clustering based on pairwise correlations (Bianco & Engert, 2015), PCA-promax allows cells to be incorporated into multiple different groups with overlapping responses to different stimuli across time. Thus, clusters are not exclusive and individual cells that are responsive to multiple stimuli can be shared across ensembles.

To avoid the most active neurons contributing the most variance to the PCA analysis, all ΔF/F traces were first z-scored to normalise the data. Following PCA, the components with eigenvalues above a theoretical lower bound, determined by the Tracy-Widom corrected Marcenko-Pastur distribution (Peyrache et al., 2010; Tracy & Widom, 1993), were retained and underwent non-orthogonal promax factor rotation. In this study, 29 components were retained for factor rotation. Each component was then designated as its own cluster, which was composed of cells having a coefficient of more than 1.5 standard deviations above the mean for that component. The average trace of the cells belonging to a given cluster was then compared to that of each other cluster to determine if clusters were too similar and should be joined. Clusters with correlation coefficients greater than 0.9 were merged and the process was repeated until no new clusters were created. Cells from all 19 of the clusters presented here were found in every fish, and 18 of these clusters were found to be composed of assemblies of at least 25 cells in one or more trials of at least 8 of the 11 fish examined.

In order to compare the medial-lateral and rostro-caudal position of cell assemblies belonging to different clusters between the tecta of different fish, the hand-drawn outline of the PVL of each fish was overlaid and averaged to create a template tectum at each depth. The original, segmented images for each fish were then geometrically morphed to this template image using affine transformation. A binary

mask of each morphed PVL was then skeletonised to find the midline of that PVL, the orientation of which was defined as the medial-lateral axis and the 90-degree rotation around the centroid being the rostro-caudal axis. The Euclidean distance from both axes was then calculated for each cell (Figure 4.8A-D). The ratio of cells responsive to each stimulus across the dorso-ventral axis was compared to a Poisson fit of the distribution of all responsive cells using a Chi-square goodness-of-fit test. All distributions were normalized by the number of cells segmented in each imaging plane.

The proportion of active cells that were common to two given assemblies, relative to the total number of active cells across both assemblies, was determined using the matching index (MI) described by Romano et al. (2015). This was used to determine the repeatability of neuronal assemblies of the same functional cluster between trials, and to determine the presence of cells shared between neuronal assemblies belonging to different clusters in the same trial. The MI between two groups of cells was defined as twice the number of cells shared between both assemblies (X) divided by the total number of active cells in both assemblies (K):

$$MI = 2*X/K$$

Assemblies were deemed to be significantly matching if the probability of their matching index was less than 0.01 according to the hypergeometric distribution.

The density of cells populating each assembly was calculated using the compactness index, as described by Romano et al. (2015). To achieve this, a circular border was created around the centroid of each assembly, with an area equal to the sum of the areas of each cell within the assembly. The compactness index was then calculated as the proportion of cells that from the assembly that had any part of the cell within this border.

The feature selectivity index was calculated by comparing the maximum rate of change of fluorescence (first derivative with respect to time) during presentation of feature 1 (R1) and feature 2 (R2) of the stimulus:

$$FSI = (R1-R2)/(abs(R1)-abs(R2))$$

Simulated control assemblies were generated by taking the distance of each cell in the assembly from the centroid, then creating a new dataset of distances with the same mean and standard deviation, and selecting cells that most closely matched these new distances from the centroid. These simulated assemblies had the same centroid, relative area and compactness compared to actual assemblies, while randomizing the actual cells included.

4.3 Results

4.3.1 The tectum receives multisensory information with cells responsive to vision, water flow and sound

To investigate the responses of tectal neurons to different sensory stimuli, 6 day post fertilization (dpf) zebrafish expressing pan-neuronal GCaMP5G were imaged using SPIM (Chapter 2.2; Table 2.1). Larvae were paralysed and embedded in agarose adjacent to a translucent projector screen and suspended speakers, with the tail freed to allow for water flow stimulation of the trunk lateral line neuromasts (Figure 4.3A). Four different visual stimuli were presented to the fish, including moving vertical and horizontal bars, a full-field flash, and a small moving spot, followed by two brief puffs of water directed along the tail, and finally an auditory tone (see Methods 4.2).

To allow for presentation of visual stimuli to the animal, a single rather than dual-plane illumination setup was utilized. In this configuration, a single plane of the tectal hemisphere contralateral to the screen was imaged dorsally for five consecutive trials during the presentation of the six different stimuli. This was repeated at each of six different depths, spaced 25μm apart, with the first plane imaged at 25μm below the first visible tectal cell body. From these movies, individual cells in the PVL were automatically segmented, and the fluorescence intensity for each neuron was recorded over time as a measure of activity (Figure 4.3B-C). Responsive cells were identified for each of the six stimuli presented across three sensory modalities. Approximately 29,000 cells across 11 fish (2626 +/– 607 cells per fish) were imaged for 5 presentations of each stimulus, yielding nearly 145,000 individual activity traces. 17.89% of these were responsive to at least one of the four visual stimuli, and 3.92% responded to at least one of the two non-visual stimuli (see Methods 4.2).

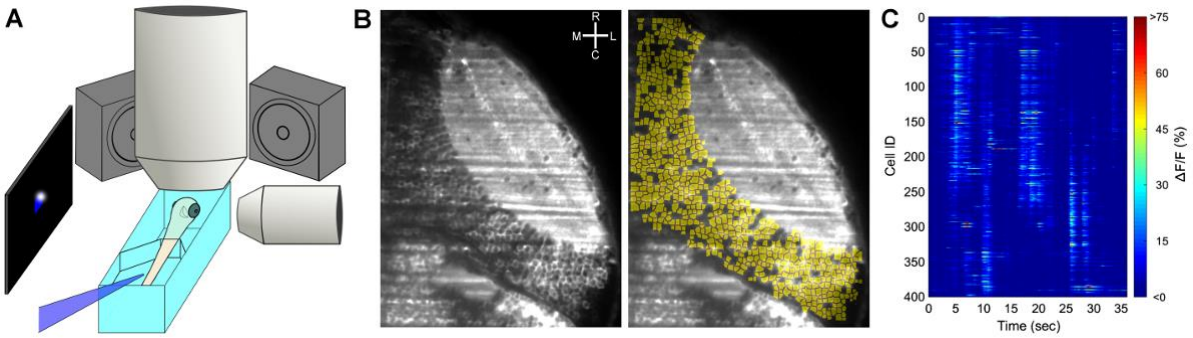

Figure 4.3. Imaging activity in tectal PVL cells. (A) Schematic of experimental protocol. Zebrafish larvae were exposed to four visual stimuli, lateral line and auditory stimulation while neuronal activity was simultaneously imaged using selective plane illumination microscopy. (B) Pan-neuronal GCaMP5G was imaged in the tectum contralateral to the visual stimulus and individual cells (yellow) were automatically segmented using custom-written MATLAB program. (C) Example raster plot of the change in fluorescence over time for each individual cell for a single experimental trial. Defined patterns of activity were observed in response to the presentation of the different sensory stimuli over time.

Since information processing is believed to rely on simultaneous patterns of activity across many co-active neurons (Averbeck et al., 2003; Sanger 2006; Singer 1999), we aimed to identify ensembles of cells with similar response characteristics. To do this, I applied principal components analysis followed by non-orthogonal factor rotation (PCA-promax) to z-scored traces of my data (Romano et al., 2015). Nineteen functional clusters of responsive neurons were generated from this approach, with more than 87% (26,072 out of 29,940) of stimulus-responsive traces represented in one or more of these clusters (Figure 4.4A). A number of clusters generated by PCA-promax were removed prior to these analyses as they were deemed to be artefacts corresponding to features such as a general decrease in fluorescence over the trial (Figure 4.5A), or stitching artefacts due to a different order of stimulus presentation (Figure 4.5B). For each remaining cluster, an average response profile was generated and clusters were ordered chronologically based on the times of their peak response during the stimulus train. The average correlation between the response profiles in each cluster and each of the six stimuli allowed us to match clusters to their preferred stimuli (Figure 4.4E). These revealed 15 clusters responsive preferentially to the visual stimuli, two to water flow, and two to the auditory tone (Figure 4.4E-F). In the 5 trials for each plane, responding cells were included in a cluster either once (Figure 4.6A), or in several trials (Figure 4.6B), or in multiple different clusters across trials (Figure 4.6C). While cells were often included in more than one cluster, it was rarely observed that cells were included in more than 3 different clusters (Figure 4.6D, see also Table 4.1). This suggests that cells may have a particular stimulus to which they respond preferentially.

Due to the cytosolic expression of GCaMP5G, signals could bleed through from neighbouring ROIs, especially if they have a higher baseline expression of protein (Figure 4.6E-F). As such, the extent of signal contamination from neighboring cells was determined from an example experiment by removing a two pixel border around the edge of each ROI. The traces of all ROIs for an example movie were compared before and after subtraction of the border pixels by linear correlation. Coefficients were found to range between 0.55 and 1.0 (mean 0.89, Pearson's correlation coefficient). In the example population of neighboring neurons shown in Figure 4.6E-F, the weakest correlation was found in a non-responsive cell with a low baseline fluorescence with noise contributing most to the fluorescence signal (Cell 4; r = 0.87,

Pearson’s correlation coefficient). Given these results, it is unlikely that neighboring cells considerably influence the fluorescence changes observed during the standard analysis protocol, or that responsive cells included in different functional clusters are included as an artefact of neighboring cells.

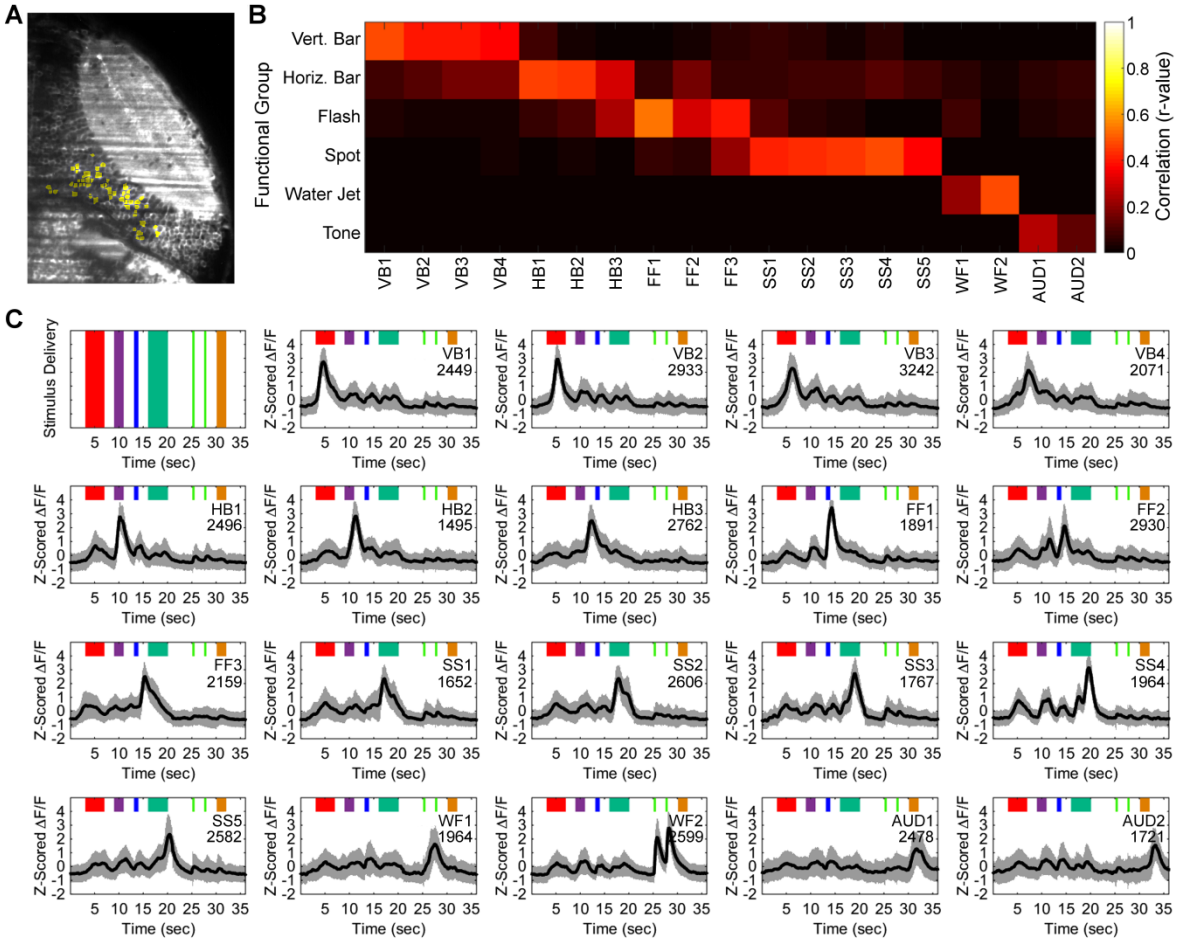

Figure 4.4. Groups of cells in the tectal PVL respond to both visual and non-visual input. (A) An example assembly of neurons (yellow) with functionally similar response profiles detected by PCA-promax, belonging to the second small spot-responsive cluster (SS2). (B) Functional classification of clusters by linear regression to the presentation of each of the six sensory stimuli. 4 vertical bar-responsive, 3 horizontal bar-responsive, 3 full-field flash-responsive, 5 small spot-responsive, 2 water jet responsive, and 2 auditory tone responsive clusters were identified. (C) The average (black) and standard deviation (grey) of the response of the 19 functional clusters of cells produced by PCA-promax, ordered sequentially by peak response showing clear correlation to stimulus presentation (vertical bar = red, horizontal bar = purple, full-field flash = blue, small spot = cyan, water jet = green, auditory tone = orange). Values indicate number of traces included in each cluster.

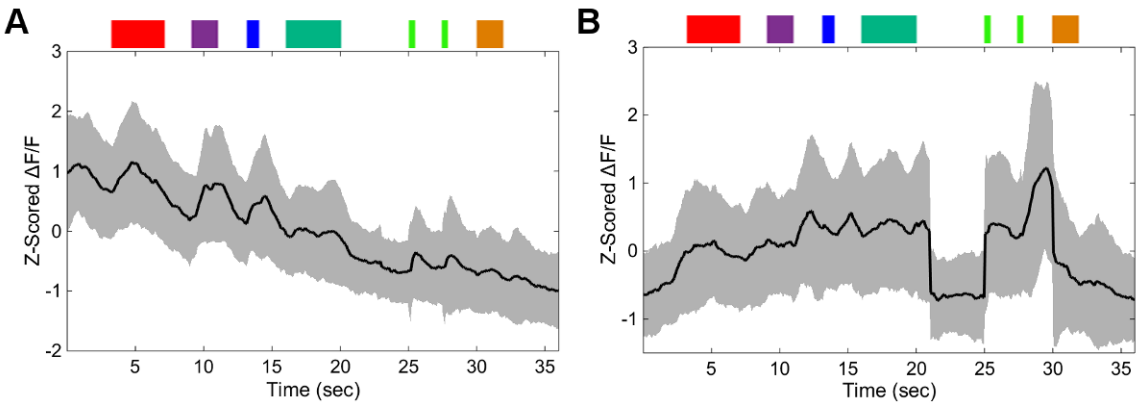

Figure 4.5. Artefactual clusters produced by PCA-promax method. (A) A cluster that is composed of cells with a gradual decrease in fluorescence over the course of the trial. (B) A cluster resulting from a stitching artefact, where results from trials with different stimulus orders are registered against each other. The salient features are seams that result from reordering the stimuli. Presentation of stimuli is shown above each trace with colours matching those in Figure 4.4C.

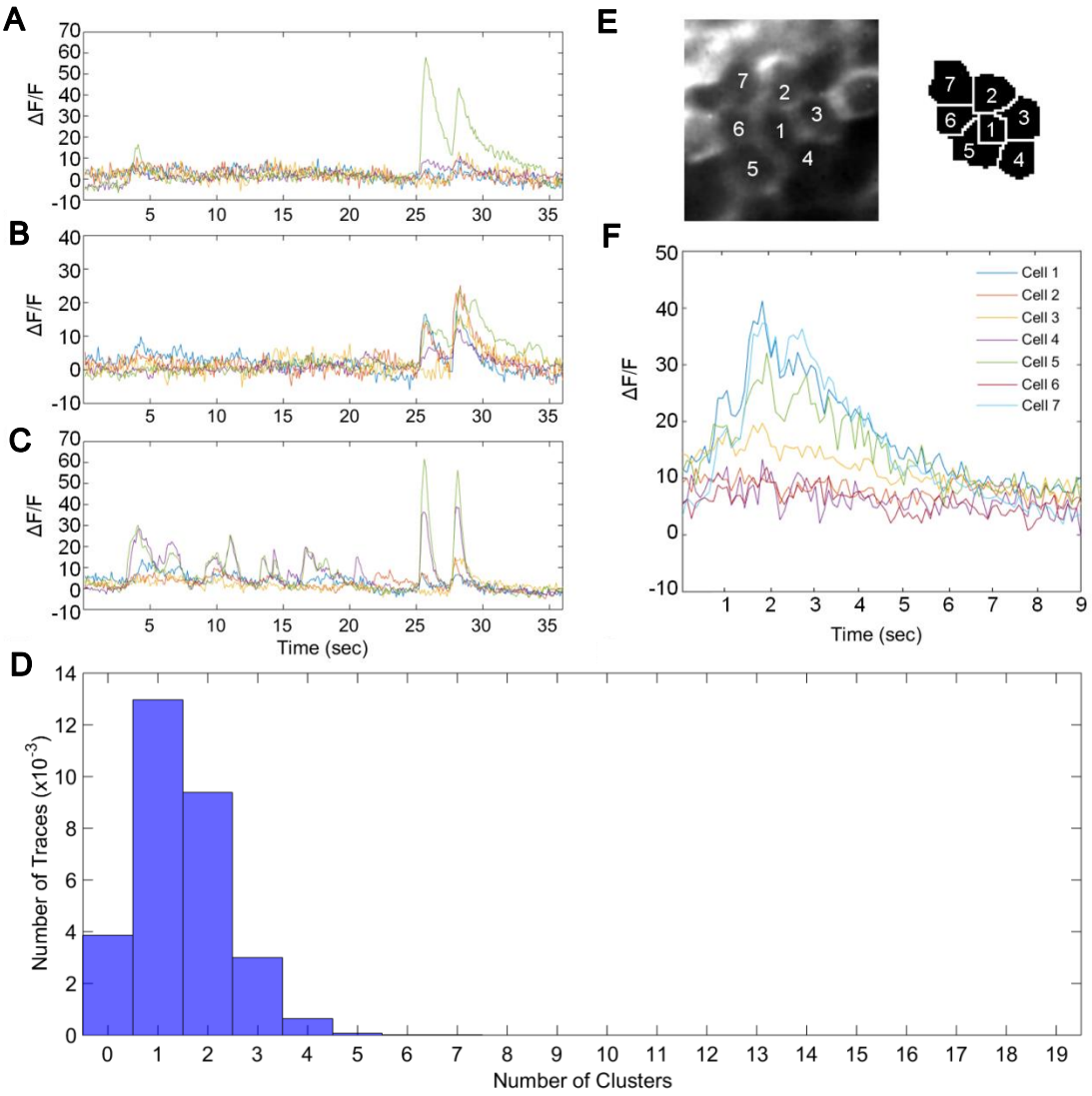

Figure 4.6. Response characteristics vary for individual cells. (A) Example traces of a cell in five different trials, responsive to water flow in WF2 cluster in only one out of the five trials. (B) Example traces of a cell responsive to water flow in WF2 cluster in five out of five trials. (C) Example traces of a cell responsive to multiple stimuli, including different combinations of VB1, VB3, HB1, SS1, SS5 and WF2 clusters across the five sequential trials. (D) Histogram showing the number of clusters, identified by PCA-promax, to which each trace (of 29940 responsive traces) belongs. (E-F) Cytosolic expression of GCaMP5 (E) has only a minor influence on the fluorescence traces of surrounding ROIs (F).

	VB1	VB2	VB3	VB4	HB1	HB2	HB3	FF1	FF2	FF3	SS1	SS2	SS3	SS4	SS5	WF1	WF2	AUD1	AUD2
VB1	2449	189	136	68	146	55	222	147	497	113	131	276	89	76	104	131	454	196	83
VB2	189	2933	96	145	378	150	134	205	155	130	72	188	97	209	298	135	174	203	119
VB3	136	96	3242	105	152	202	97	97	139	53	83	117	213	195	186	135	122	70	147
VB4	68	145	105	2071	89	208	189	68	93	57	45	68	66	149	132	61	96	96	84
HB1	146	378	152	89	2496	70	65	123	177	207	116	105	161	107	148	106	113	119	142
HB2	55	150	202	208	70	1495	136	153	57	69	41	51	100	62	123	34	68	77	171
HB3	222	134	97	189	65	136	2762	93	225	99	109	188	112	161	129	81	184	176	111
FF1	147	205	97	68	123	153	93	1891	62	127	99	176	117	91	166	174	121	109	247
FF2	497	155	139	93	177	57	225	62	2930	276	65	70	95	327	108	56	227	97	121
FF3	113	130	53	57	207	69	99	127	276	2159	100	99	135	217	188	108	156	150	104
SS1	131	72	83	45	116	41	109	99	65	100	1652	288	563	134	62	85	197	60	98
SS2	276	188	117	68	105	51	188	176	70	99	288	2606	110	146	114	150	508	97	96
SS3	89	97	213	66	161	100	112	117	95	135	563	110	1767	115	76	82	79	77	180
SS4	76	209	195	149	107	62	161	91	327	217	134	146	115	1964	55	38	66	112	111
SS5	104	298	186	132	148	123	129	166	108	188	62	114	76	55	2582	91	122	126	96
WF1	131	135	135	61	106	34	81	174	56	108	85	150	82	38	91	1964	173	129	56
WF2	454	174	122	96	113	68	184	121	227	156	197	508	79	66	122	173	2599	156	89
AUD1	196	203	70	96	119	77	176	109	97	150	60	97	77	112	126	129	156	2478	110
AUD2	83	119	147	84	142	171	111	247	121	104	98	96	180	111	96	56	89	110	1721

Table 4.1. Number of traces shared between different functional clusters. Each cell has a maximum of 5 traces, with a total of 29,490 responsive traces identified from the 28,886 total cells across 11 fish. The mean number of traces per cluster is 2303. For each cluster, an average of 136 traces will be shared with each other cluster, with a small number of these shared between more than two clusters (see Figure 4.6C). Red cells indicate total number of traces in each functional cluster.

4.3.2 Functional clusters respond to particular stimulus features

Given that multiple clusters were maximally responsive to each stimulus, I explored whether particular features of each stimulus could be responsible for individual clusters (Figure 4.7A-F). As seen in the inset panels in Figure 4.7, the peak response of each cluster occurred at a slightly different time during the relevant stimulus. The response for each trace in a given cluster was then compared to the discrete features of the stimuli (such as direction for moving visual stimuli, or on/off for the auditory stimuli), giving an average feature selectivity index for each cluster (Figure 4.7A'-F'). In each case, the highest spiking rates, corresponding to the fastest rise in GCaMP5G signal (Akerboom et al., 2012), were found to correspond to different salient features within the stimuli for different clusters.

Two clusters (VB1 & VB2) were preferentially responsive to movement of a vertical bar in the rostral direction, and two (VB3 & VB4) were selective for the caudal direction. In each pair of vertical bar-responsive clusters, there was an earlier responding (VB1 & VB3) and a later responding (VB2 & VB4) cluster. The horizontal bar, moving ventrally then dorsally, produced clusters for each direction (HB1 & HB2, respectively), as well as a third cluster (HB3) that appeared to respond to the disappearance of the bar at the end of the stimulus. The full-field flash stimulus produced two 'on' responsive clusters, one fast-onset (FF1) and one slower (FF2), as well as a clear 'off' responsive cluster (FF3). The small moving spot created a cluster for each of its two rostral movements (SS1 & SS3) and caudal movement (SS2 & SS5), as well as a fifth cluster that responded when the spot was in the rostral visual field (SS4). Water flow elicited a cluster that responded slow and moderately after the initial presentation (WF1), and another with rapid and strong responses to each of the two stimuli (WF2). Finally, the auditory stimulus elicited two specific clusters that preferentially responded to either the onset (AUD1) or cessation (AUD2) of the tone.

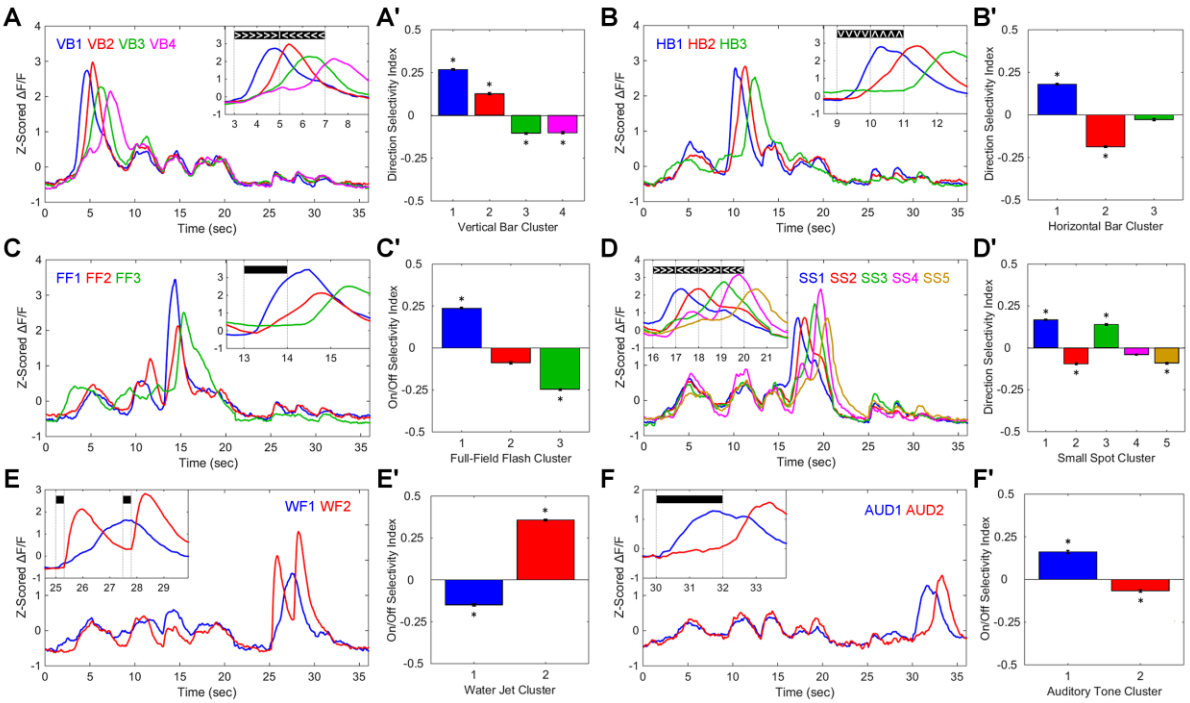

Figure 4.7. Stimulus features directing functional classification of different clusters. (A-F) Average overall trace of response of cells in clusters 1-19 separated by functional class. Cells responding to the moving vertical bar (A) respond either early (blue) or late (red) to the rostral-moving bar (>) or either early (green) or late (pink) to the caudal-moving bar (<). Each of the clusters had a significant preference for a particular direction of stimulus movement (A', $p<0.05$, Kolmogorov-Smirnov test, error bars = SEM). (B-B') Similar preferences were observed for direction selectivity to the moving horizontal bar (v = ventral, blue trace; ^ = dorsal, red trace). (C-C') Significant on/off selectivity was observed for the first (blue) and third (green) flash-responsive clusters (black bar = on, 1-second following flash = off). (D-D') Clusters with significant preference for one of the two rostral (>, blue & green) or caudal movements (<, red & orange) of the small spot. The fourth spot-responsive cluster (pink) had no significant direction selectivity, however it had a peak change in response when the spot was in the most rostral part of the visual field. (E-E') Water jet stimulation resulted in two clearly distinct responses that corresponded either to the onset of each water puff (black squares, red trace), or the termination of the first water puff (blue). (F-F') (C-C') Significant on/off selectivity was also observed for the first (blue) and second (red) auditory tone-responsive clusters (black bar = on, 1-second following flash = off).

4.3.3 Spatial profiles of visual, lateral line and auditory processing in the tectum

In both the tectal neuropil and PVL, the spatial location of a response plays an important role in the processing of visual stimuli. In particular, visual information is filtered along the apical-basal axis of the neuropil such that large stimuli more strongly activate superficial layers and smaller stimuli activate deeper layers (Del Bene et al., 2010; Preuss et al., 2015). In the present study, responses were registered against the approximate neuropil laminae previously described by Robles et al. (2013). Visual responses spanned from the superficial to intermediate layers of the neuropil, while water flow responses were strongest in the deeper layers, overlapping the SGC and SAC laminae (Figure 4.8A). Auditory responses were very rare in the neuropil. It should be noted that since we used a pan-neuronal calcium indicator, these responses represent a combination of activity from afferent axons and the dendrites of tectal neurons.

The functional characteristics of the tectum along the dorsal-ventral axis are largely unexplored in larval zebrafish. We found pronounced differences across stimuli and modalities in terms of the dorsal-ventral positions of their responsive PVL neurons (Figure 4.8B). Taking into account the increased population of cells in the intermediate depths of the tectum, cells in these layers were still more likely to respond to one of the stimuli used in this study than cells in the very dorsal or very ventral regions of the tectum. On average, vertical bar-responsive neurons were overrepresented in the 50µm depth ($p = 6.71x10^{-4}$), while neurons responding to full field flash were more ventral than the population as a whole ($p = 7.68x10^{-3}$; Chi square goodness-of-fit test). Water flow-responsive neurons in the WF2 cluster were significantly more represented in the dorsal PVL ($p = 2.90x10^{-5}$; Chi square goodness-of-fit test), while auditory neurons on average were significantly shifted toward the ventral PVL ($p = 1.27x10^{-10}$; Chi square goodness-of-fit test). These preferences were in line with the observed neuropil responses (Figure 4.8A). This reveals the importance of considering depth as an important axis over which to assess functional properties in the PVL.

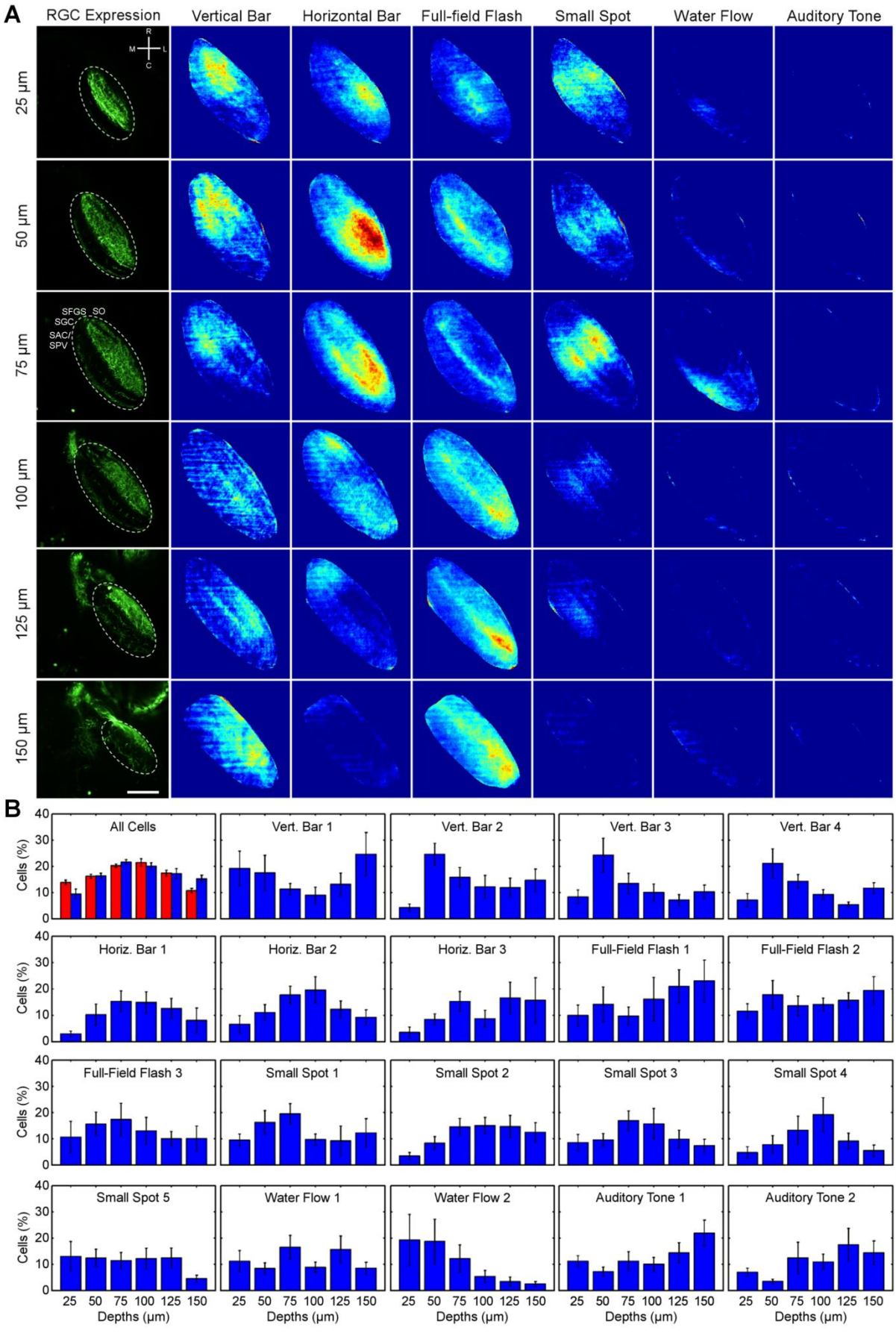
A
RGC Expression
Vertical Bar
Horizontal Bar
Full-field Flash
Small Spot
Water Flow
Auditory Tone
25 µm
50 µm
75 µm
100 µm
125 µm
150 µm
R
M
L
C
SFGS
SO
SGC
SAC/
SPV
B
All Cells
Vert. Bar 1
Vert. Bar 2
Vert. Bar 3
Vert. Bar 4
Horiz. Bar 1
Horiz. Bar 2
Horiz. Bar 3
Full-Field Flash 1
Full-Field Flash 2
Full-Field Flash 3
Small Spot 1
Small Spot 2
Small Spot 3
Small Spot 4
Small Spot 5
Water Flow 1
Water Flow 2
Auditory Tone 1
Auditory Tone 2
Cells (%)
0
10
20
30
40
25 50 75 100 125 150
Depths (µm)

Figure 4.8 (previous page). Different sensory stimuli are preferentially processed in different parts of the tectum. (A) Distribution of retinal ganglion cell axons within the tectal neuropil (dotted outlines) of a 6dpf Atho7:Gal4;UAS:Kaede larva at each imaging plane, as well as the average correlation between stimulus presentation and neuropil responses across all fish. SO = stratum opticum, SFGS = stratum fibrosum et griseum superficiale, SGC = stratum griseum centrale, SAC/SPV = stratum album centrale/stratum periventriculare. Scale bar = 50 µm. (B) The distribution of all segmented cells along the dorso-ventral axis of the PVL (red bars, first panel) compared to the total number responsive cells normalised by the number of cells per plane (blue bars, first panel). The distribution of cells belonging to each cluster, normalised by number of cells per plane are shown in the remaining panels (error bars = SEM).

The strongest and best described functional axis of the tectum results from the retinotectal map present along the rostro-caudal axis of the tectum (Gosse et al., 2008). As a consequence of this map, a moving bar or spot stimulus may be expected to elicit similar responses in cells across different locations as the stimulus moves along this axis, leading to artificial separation of responses during the clustering process. Thus we investigated whether cell assemblies belonging to sequential clusters were preferentially located along different parts of the rostro-caudal axis when responding to moving stimuli.

We first calculated the medio-lateral and rostro-caudal positions of the cells relative to the midline of the PVL by skeletonizing a hand-drawn mask and determining the distances from this line in MATLAB (Figure 4.9A-D). From this, we found that assemblies responding to all stimuli, including moving visual stimuli, occurred across the entire rostro-caudal extent of the PVL, with only minor variations in the distribution of cell assemblies (Figure 4.9E-J). Assemblies of cells responding sequentially to the moving stimuli were found to have no significant spatial separation within the PVL, indicating that these are not strongly determined by position in the visual field and are likely to represent true early and late responses (Figure 4.9E,H). Given that our moving stimuli were travelling quite fast relative to the position of tectal cells, and that individual retinal ganglion cell arbours can innervate hundreds of microns along the rostro-caudal extent of neuropil (Ben Fredj et al., 2010; Robles et al., 2013), the lack of a spatial separation in sequential clusters is not entirely surprising. Additionally, our results also conflict with the model proposed by Ramdya & Engert (2008), showing no observable preference in the direction selectivity of either bar or spot-responsive cells along the rostro-caudal axis of the tectum (Figure 4.10).

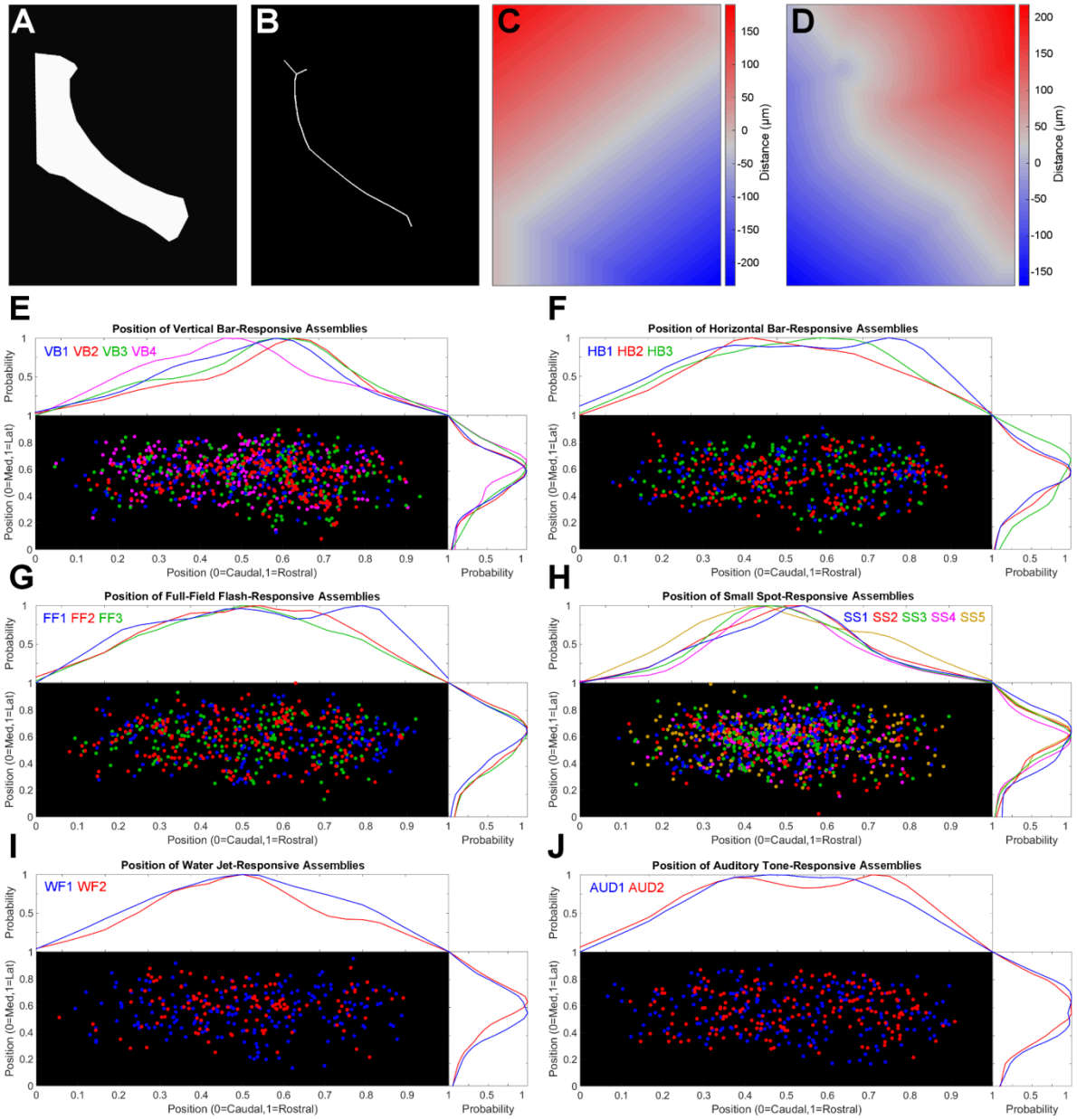

Figure 4.9. Determination of the medio-lateral and rostro-caudal position of cells within the tectal PVL. (A) Hand-drawn binary mask outline of the tectal periventricular layer (PVL). (B) Skeletonization of the binary PVL mask. (C) Distance from the centre of the PVL perpendicular to the skeletonised mask in panel B (rostral = red, caudal = blue). (D) Distance from the centre of the PVL parallel to the skeletonized mask in panel B (lateral = red, medial = blue). (E-J) Distribution of the positions of the centroid for each assembly of cells belonging to the 19 different functional clusters, separated by preferred stimulus. Vertical bar-responsive assemblies are slightly more frequent in the more rostral PVL and the small spot-responsive assemblies are more tightly restricted to the centre of the rostro-caudal axis, while the other assemblies are distributed extensively across the PVL. Colours correspond to the same clusters shown in Figure 4.7.

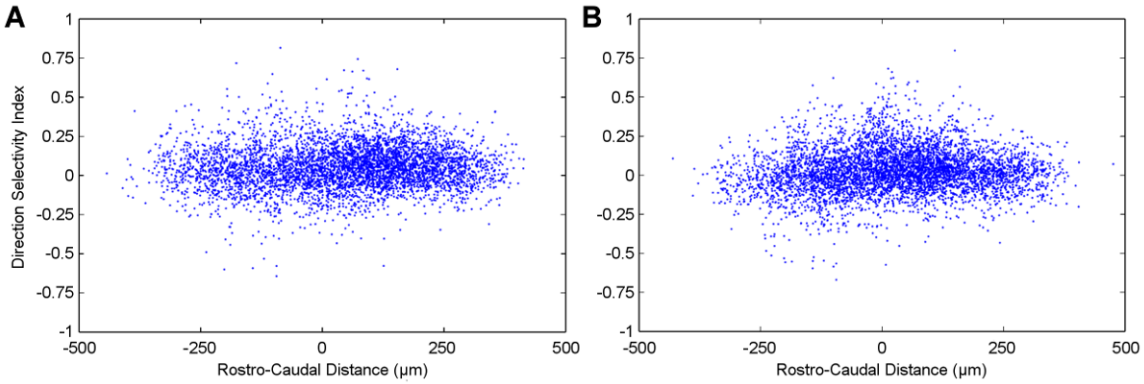

Figure 4.10. Comparison of the direction selectivity of (A) moving vertical bar-responsive, and (B) moving small spot-responsive cells versus position along the rostro-caudal axis of the tectal PVL. There is no obvious preference for direction selectivity along the rostro-caudal axis (slope = 5.28×10^{-5}, bar; slope = 7.56×10^{-5}, spot).

4.3.4 Assemblies are highly variable trial to trial, but contain reliably responsive cores

Assemblies of responsive neurons from different clusters were found to be generally quite small and compact in the PVL (Figure 4.11). Although it has been shown that tectal cells have preferences for particular stimuli features (Bianco & Engert, 2015; Hunter et al., 2013; Preuss et al., 2014), the cells responding as part of an assembly can vary across trials. To determine whether the cells in our trials were responding consistently, the matching index (MI) was calculated for each assembly across the five trials in each animal (Romano et al., 2015). The degree of matching was generally low across trials (Figure 4.12A), suggesting a high degree of variability in the cells responsive to a given stimulus presentation. Nevertheless, assemblies from all clusters except AUD2 had a significantly higher MI than predicted by random chance (Figure 4.12A). This result is consistent with highly variable assemblies anchored by a small core of consistently responsive cells.

Investigating this possibility, a “core” group of cells was identified in most assemblies that responded in at least four of the five trials (Figure 4.12B, red cells). In most cases, the number of these cells was significantly higher than predicted by chance (Figure 4.12C), although AUD2 contained no core. The cores were also generally more compact than simulated cores with the same number of cells (Figure 4.12D). The response profiles of the cores closely resembled the responses of the whole cluster, although there was a trend toward a stronger response to the preferred stimulus feature in core cells (Figure 4.12E). As a result, there was also a significant increase in the absolute value of the feature selectivity index for the cores of some, but not all clusters (Figure 4.13A). It was suspected that core cells may represent cells which integrate information from the variable population of cells in the assembly to fire consistently in response to a given stimulus. To test this hypothesis, the lag of the cross-correlation between core and non-core cells, as well as their medio-lateral positions within the PVL, were examined in each assembly responsive cells for each functional cluster. No clear trends were observed in either the lag (Figure 4.13B) or positions (Figure 4.13C) between core and non-core cells. Given the low acquisition frame rate compared to neuronal transmission though, these lag data may not represent a true reflection of the different temporal dynamics between core and non-core cells.

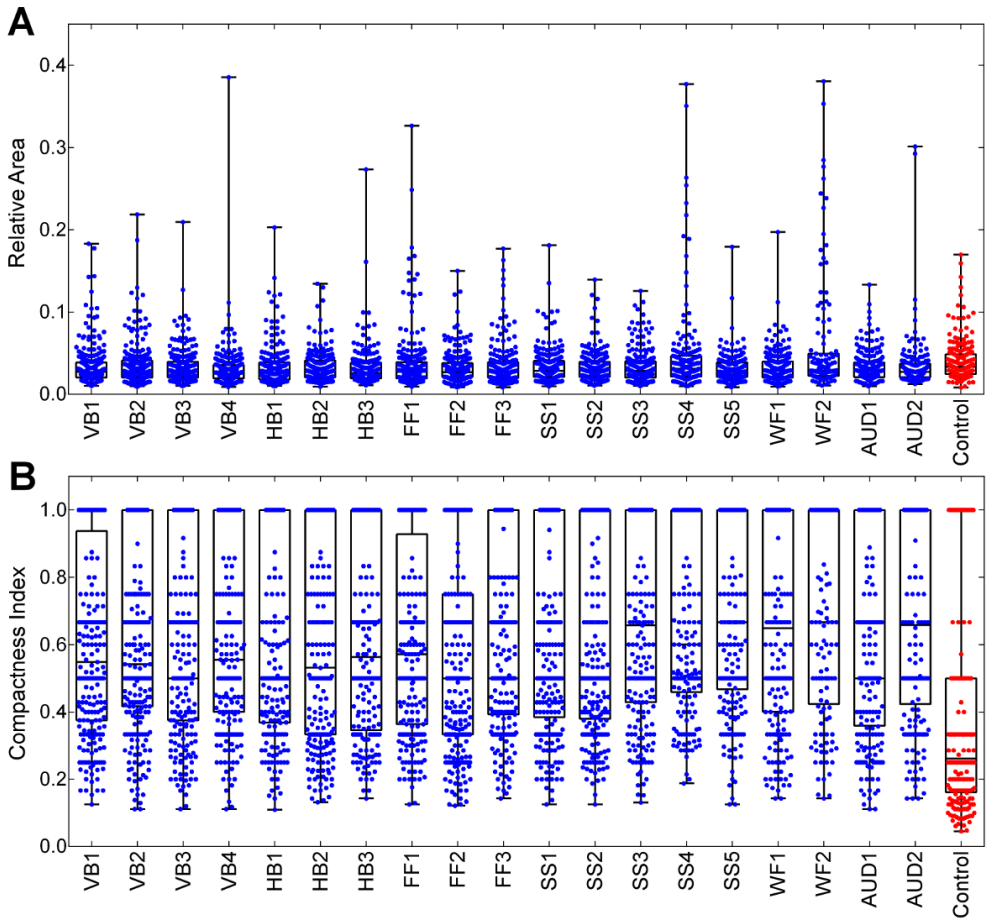

Figure 4.11. The size and density of cells across the PVL for each assembly in each cluster. (A) The proportion of the area occupied by cells in an assembly relative to the size of the PVL is quite low. Control assemblies (red) are simulated populations of cells chosen with the same average number of cells per assembly chosen at random from cells in random imaging planes. (B) The proportion of cells within a certain diameter of the assembly centroid relative to the number of cells in the assembly is generally high. All assemblies are more compact than predicted by a control assembly with cell positions distributed randomly across the PVL (red). Box and whiskers represent mean, interquartile range and extremes.

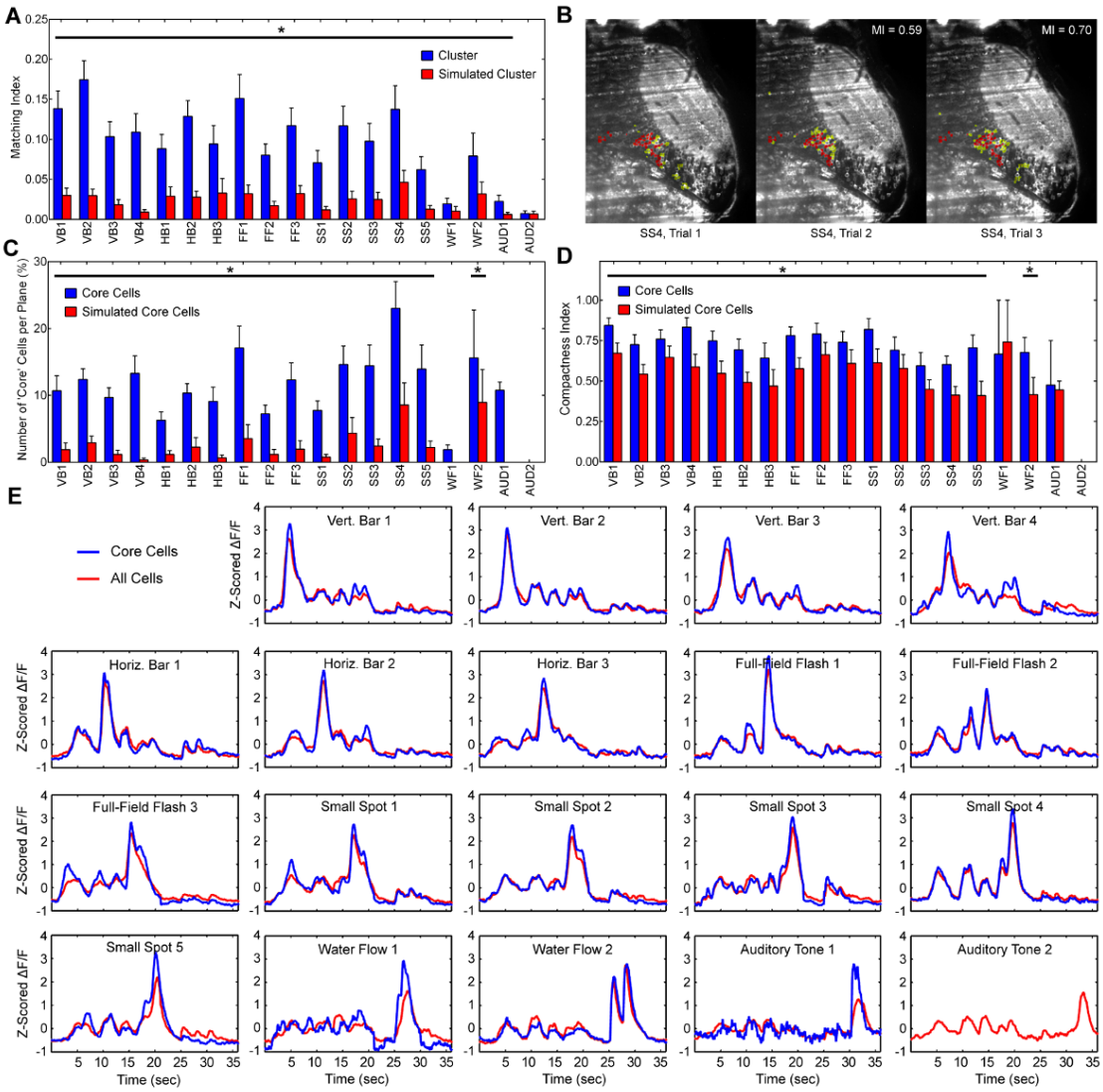

Figure 4.12. Assemblies of cells respond with both soft-wired and a hard-wired core of cells. (A) The average pairwise matching index across all trials for assemblies from each functional cluster of cells is low, but significantly greater than simulated assemblies with the same local distribution of cells for all but the last auditory cluster (* = p<0.01, Wilcoxon signed-rank test, error bars = SEM). (B) An example assembly of cells from SS4 cluster (small spot-responsive) in three repeated trials. The cellular composition of the assembly is more varied between trial 1 and 2 (matching index (MI) = 0.59) than between trial 2 and 3 (MI = 0.70). 'Core' cells that are present in the assembly in at least 80% of trials are highlighted in red, non-core cells are in yellow. (C) There are significantly more core cells in the assemblies for visual stimuli-responsive clusters and WF2 than expected by chance in simulated assemblies (* = p<0.01, Wilcoxon signed-rank test, error bars = SEM). No AUD2 cells (auditory off) were responsive in at least 4 of the 5 trials. (D) The core cells within an assembly are significantly more compact in all visual stimuli-responsive clusters and the second water flow-responsive cluster than a simulated core within each assembly (* = p<0.01, Wilcoxon signed-rank test, error bars = SEM). (E) The average response of core cells is broadly similar to that of the whole cluster.

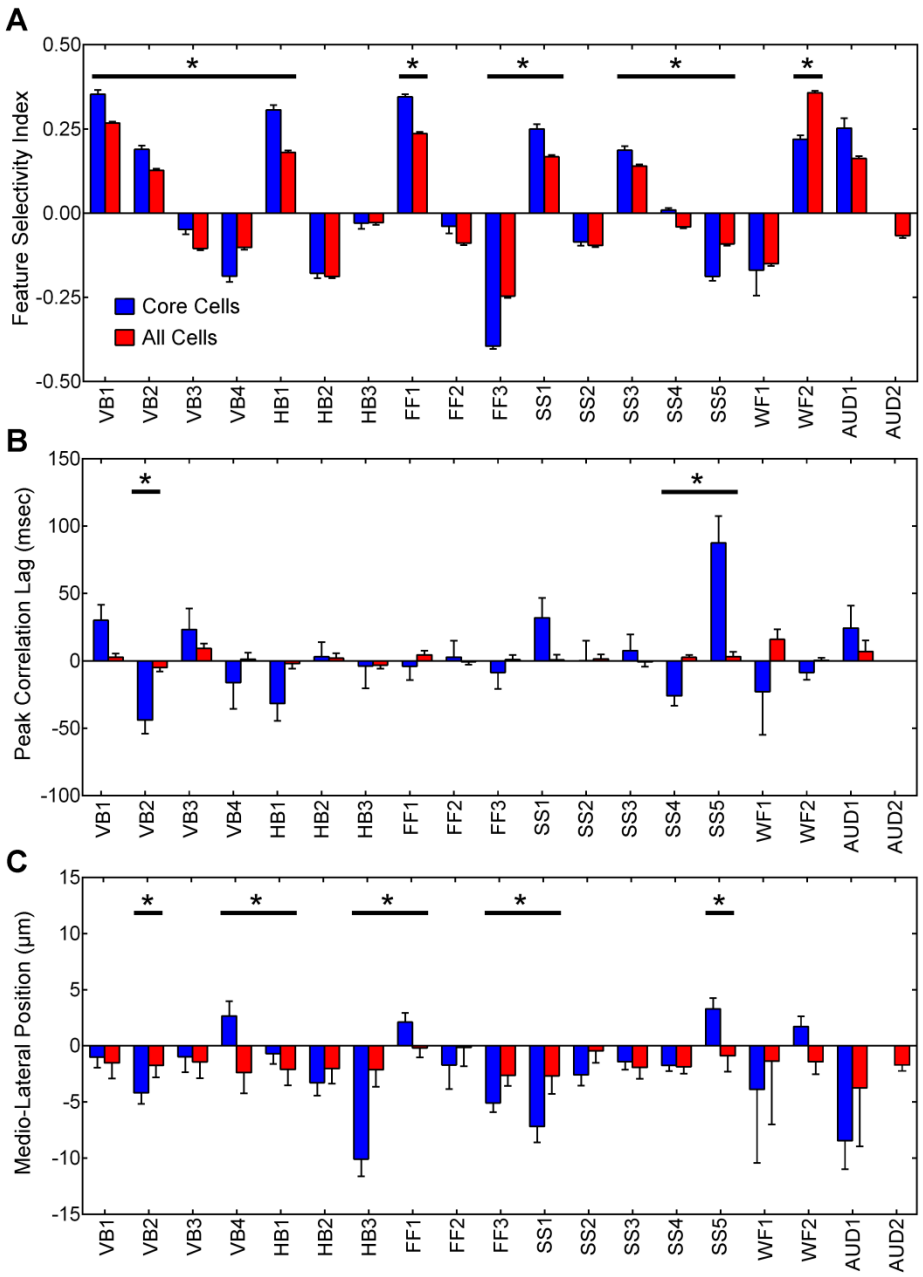

Figure 4.13. Properties of core cells compared to non-core cells. (A) Comparison of the selectivity of core (blue) versus all cells within a cluster (red) to particular features of the relevant stimulus. Direction selectivity indices are presented for VB, HB and SS clusters, while on/off selectivity indices are shown for FF, WF and AUD clusters. The absolute feature selectivity value of most core cells is often significantly higher than those of the cluster to which it belongs (* = $p<0.01$, Kolmogorov-Smirnov test, error bars = SEM). (B) Comparison of the average lag of the peak cross-correlations between core cells and all responsive cells of an assembly (blue), and between non-core cells and all cells of an assembly (red) (* = $p<0.05$, Wilcoxon signed-rank test, error bars = SEM). (C) Comparison of the average medio-lateral position of core cells (blue) and all cells of an assembly (red) relative to the midline of the PVL (* = $p<0.05$, Kolmogorov-Smirnov test, error bars = SEM).

To investigate whether cells responsive to a particular stimulus feature might occupy assemblies from multiple different clusters, we calculated the MI for each pairing across our 19 functional clusters (Figure 4.14A). Assemblies were found to have very few cells in common, though a higher proportion of cells were shared between assemblies that peaked at similar times during a given stimulus than at more disparate times or between different stimuli. This is likely an artefact resulting from some cells with broad responses that stretch into chronologically consecutive clusters during PCA-promax, in part due to GCaMP5G kinetics (Akerboom et al., 2012). When the analysis was restricted to core cells, MIs were lower again (Figure 4.14B). One exception to this was between VB4 and SS5, which have late responses to caudal-moving bars and spots respectively, suggesting a functionally unique type of responsive cell.

Cross-correlation provides another method for detecting groups of cells with common characteristics (Eggermont, 2006; Mukamel et al., 2008; Patel et al., 2015). We examined the correlation of responses between every cell within a given assembly and the responses of cells belonging to all other responsive assemblies within the same experimental trial. Again, chronologically consecutive clusters shared higher normalised cross-correlations due to the slow kinetics of GCaMP5G relative to the frame rate and peak response of sequential clusters (Figure 4.14C). Correlations between the core cells of different assemblies was generally increased compared to the responses of all cells within an assembly (Figure 4.14D), with strong correlations emerging for cells between VB1 and small spot-responsive clusters (SS1-4), and between water flow-responsive clusters (WF1-2) and the slow visual ‘on’ cluster (FF2).

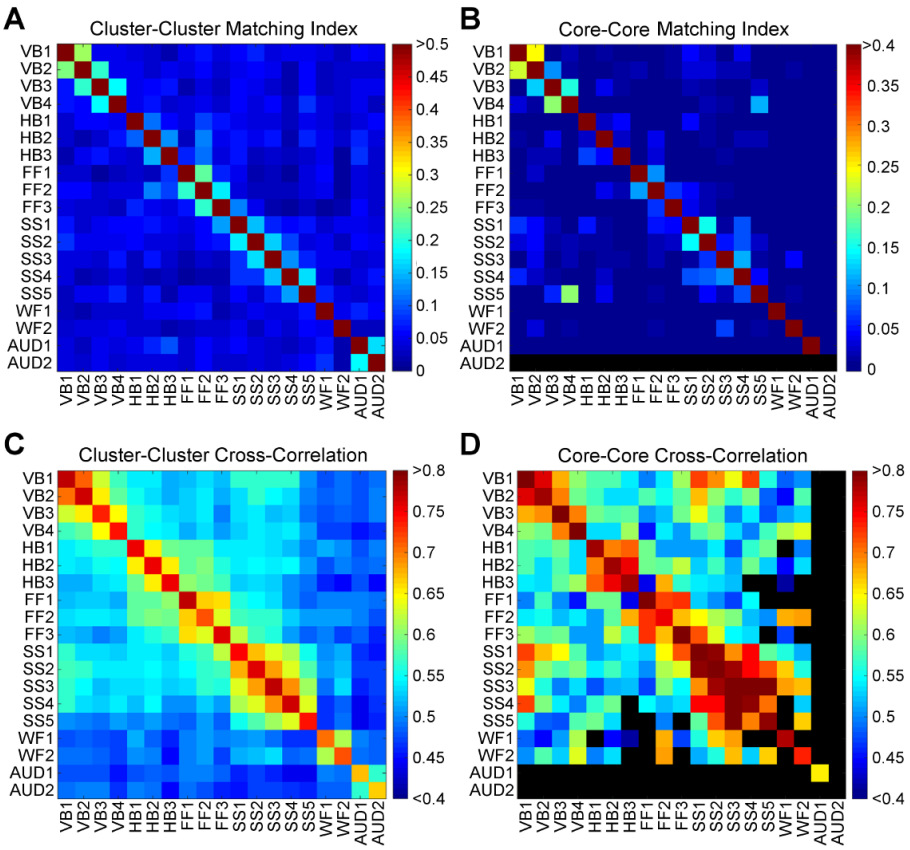

Figure 4.14. Overlap and interactions between separate assemblies of cells for functional clusters. (A) Matching indices between cells belonging to different assemblies in the same fish. There is no increase in matching between similar direction selective clusters for either the bar and spot or first and second movements of the spot. The slight increase in matching index in temporally-adjacent clusters is expected due to the PCA-promax clustering. (B) Matching indices between cells belonging to the assembly core across different assemblies in the same fish. Very few core cells are shared between different assemblies except those in VB4 and SS5 (late, caudal-moving bar and spot clusters). Black = no core cells for AUD1 cluster. (C) Average cross-correlation between assemblies of cells in different functional clusters. Cross-correlations are higher between temporally-adjacent clusters and lower between different sensory modalities. (D) Average cross-correlation between core cells of assemblies in different functional clusters. Cross-correlations are generally higher between core than non-core cells, especially between assemblies of the VB1 and the small spot-responsive clusters. Black = core cells not present in assemblies for both functional clusters within any imaging plane of any animal.

4.4 Discussion

4.4.1 Multisensory responses in the larval zebrafish tectum

These experiments have demonstrated for the first time the existence of tectal circuits in larval zebrafish involved in the processing of non-visual information. Water flow stimulation elicited responsive cells belonging to two different functional clusters, with the strong, rapid-responding cluster primarily in the dorsal PVL. This is in contrast to adult *Xenopus*, where lateral line stimulation showed electrophysiological activation in ventro-lateral areas of the tectum, merging into the torus semicircularis (Lowe 1986, Lowe 1987). This may represent a true difference in these species, or could result from the different stages of development and physiological technique. In zebrafish larvae, second-order projections from the posterior lateral line ganglion have been shown to innervate the torus semicircularis (Fame et al., 2006), with some branches also extending into the tectal neuropil. As such, water flow information may be passed to the dorsal tectum along the deep layers of the tectal neuropil, and may be involved in the correct orienting of larvae to flow stimuli (rheotaxis) (Suli et al., 2012). An analysis of PVL cells to simultaneous presentation of visual and water flow stimuli would be useful for examining this hypothesis.

Exploration of the different responses encoded along the dorso-ventral axis of the tectal PVL appears only sporadically in the literature (Gu et al., 2000; Lim et al., 2010), and never in larval zebrafish. In this study, auditory responses were relatively weak and sparsely distributed in ventral areas of the PVL. These findings are consistent with previous descriptions in the mammalian superior colliculus, where auditory responses are seen primarily in the deeper layers (Ingle, 1973; King et al., 1996). Despite the fact that circuits in this brain region are structured for integrating multiple sources of sensory information at very young ages, the synthesis of multimodal responses is believed to develop over an extended period (Stein, 1998; Stein et al., 2001).

The low proportion of cells responsive to multiple modalities in this study would suggest that information from different modalities is selectively processed in parallel rather than integrated by tectal circuits at this age. However, the localization of the sensory stimuli of different modalities could potentially explain the different trends

observed in the location of assemblies responsive to different sensory modalities. If these modalities were not representative of similar spatial areas in the external world, responses may not have overlapped to an extent that allowed significant detection of multimodal cells. Furthermore, integration was not explicitly examined in this study. Rather, stimuli from individual modalities were presented in isolation. Future experiments in which sub-optimal or sub-threshold stimuli from multiple modalities are presented simultaneously will be necessary to determine whether there may be integration among sensory modalities in the tectum.

4.4.2 Stimulus-specific assemblies in the tectum

Local groups of cells with synchronous responses to various stimuli (assemblies) have been described previously (Bianco & Engert, 2015; Friedrich & Laurent, 2001; Gray & Singer, 1989; Romano et al., 2015; Sumbre et al., 2008), and are thought to encode a population response that increases both the capacity and flexibility of information coding in neuronal circuits. In this study, we have identified assemblies of cells within the tectum belonging to one of 19 clusters with functionally unique response profiles. Of these, 15 are visually-responsive, two are water flow-responsive, and two are auditory-responsive. Most of the visual response types have been shown previously, including direction-selective responses (Niell & Smith, 2005; Gebhardt et al., 2013), small spot-selective responses (Niell & Smith, 2005; Preuss et al., 2015), and responses when a small spot enters a region of the visual field where it can be targeted for predation (Bianco & Engert, 2015).

We have shown one cluster with a slow response to the first, but not the second, presentation of a water flow stimulus. These cells could be involved in relaying sensory feedback or in tuning responsiveness of the lateral line system, although it is possible that the response is an off-target effect. While the fish was paralyzed, the tail may have moved passively as a result of the water flow stimulus, raising the possibility of proprioceptive or somatosensory signals. It is also possible that this cluster could be the result of reverberations from an escape response (although the response itself was blocked in the paralyzed animal), involving feedback to the tectum via other brain centers such as the cerebellum (Heap et al., 2013). If these responses are driven only by lateral line input, it is expected that ablation of the

lateral line hair cells using the antibiotic drug neomycin (Harris et al., 2003) should extinguish the presence of these responses. A second flow sensitive cluster responds prominently and rapidly to the onset of water flow. Auditory responses are observed in assemblies belonging to two clusters, which detect the beginning and end of the auditory stimulus, respectively.

There are several caveats inherent to clustering analyses that should be considered alongside these results. Given the dimensionality reduction methods used to analyze the data, the true spectrum of functionally-distinct response kinetics elicited by these stimuli may not be fully represented in the results presented here. Conversely, our clustering approach may somewhat over-represent the number of functionally unique response profiles present in the tectum. For example, two of clusters responding to the same stimulus feature, such as VB1 and VB2, may be populated by cells that fire equally across a temporal continuum that was artificially split by PCA-promax, with cells shared between clusters falling in the middle of that continuum. In the future, this could be addressed by the use of faster calcium probes such as GCaMP6f (Chen et al., 2013) to allow faster imaging of responses, and by changing the velocity and timing of the stimuli. Applying temporal deconvolution of the calcium signals could allow the underlying spike timing of the neurons to be estimated with reasonable accuracy (Yaksi & Friedrich, 2006; Vogelstein et al., 2010) and may also lead to inferences about the underlying functional connectivity among cells within or across the clusters presented here.

4.4.3 Assembly Cores

Several recent studies have reported assemblies of similarly-responding neurons in the zebrafish larval nervous system (Bianco & Engert, 2015; Hunter et al., 2013; Romano et al., 2015), although the trial-by-trial composition of these assemblies varies significantly (Hunter et al., 2013; Romano et al., 2015). In this study, core cells differentially combine with cells from a larger pool of inconsistently responding neurons to a given stimulus presentation. ‘Core’ cells of an assembly have only recently been described in the literature, but only in the context of cells most representative of, or having the highest correlation to, a particular responding cluster (Carrillo-Reid et al., 2015; Hung et al., 2015; Lin et al., 2014). To the best of our knowledge, this study provides the first description of a spatially localised population

of core cells in tectal assemblies that respond consistently and are more selective for their preferred stimulus features. These cells are not believed to be the same population as the ‘core’ cells described in earlier studies since unlike our core cells, a restricted analysis of the most representative neurons in the current dataset shows that they have a very low trial-to-trial repeatability (Figure 4.15).

As the number of technologies that allowing for simultaneous recording of vast networks of cells increase, the importance of core populations of neurons is able to be recognised. While the different roles of two classes of core cells described above remain unknown, they may represent activation of different populations of inhibitory interneurons versus excitatory, efferent cells. Inhibitory neurons have been shown to be critical in the zebrafish tectum to the filtering of large visual information (Del Bene et al., 2010, Preuss et al., 2014) and are also likely to influence direction selectivity (Grama & Engert, 2012). Likely to be an important direction for future research will be determining the role of these cells in deciding which networks of cells become activated in response to particular stimuli. Targeted manipulation of these cells with optogenetics can address this question but requires optical targeting of specific cells. New technologies, such as spatial light modulators, can aid in this endeavour by the production of complex patterns of light to activate optogenetic proteins, (Packer et al., 2012; Packer et al., 2015; Quirin et al., 2014). While difficult to target individual cells in the brain of a live, behaving animal, zebrafish offer a number of advantages with respect to circuit simplicity and penetration of light that may assist in dissecting out the roles of these cell types in modulating network responses.

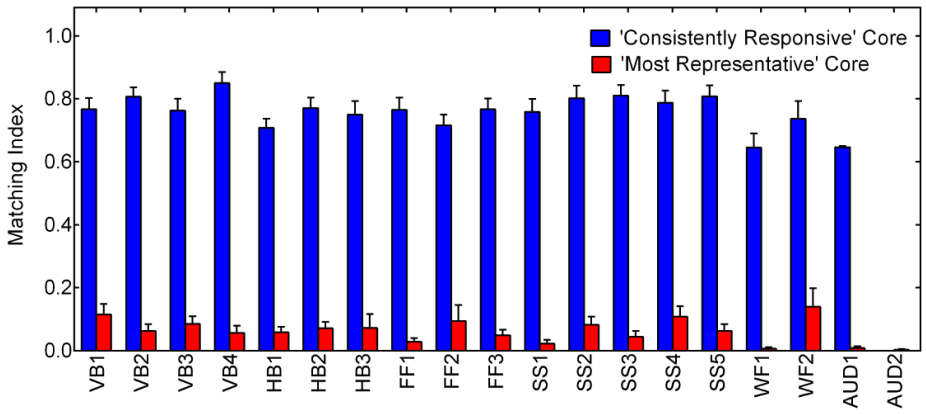

Figure 4.15. The average pairwise matching index across all trials for the core cells of each assembly of cells for all functional clusters defined by repeated presence in assembly across trials (blue) compared to that of the most representative cells of each cluster (coefficient scores > 3.5 SD above the mean) (red). All “representative core” cells (except AUD2) have significantly lower MIs than their corresponding “consistent core” cells ($p<0.01$, Wilcoxon signed-rank test, error bars = SEM).

While the core cells described in this study remain consistent across trials, the vast majority of cells responding synchronously in a given assembly can be quite varied. Circuits in the tectum must achieve a balance between reliable feature detection of expected stimuli, and the flexibility to respond appropriately to novel stimuli. This variability may play a role in encoding extra specificity or context in population responses to a given stimulus and permit the animal to respond to the same stimulus differently under different circumstances. If the low trial-to-trial matching indices result from a general lack of stimulus specificity, assemblies that respond to stimuli of increased specificity should become more distinct and reliable. Similarly, changes in ensemble firing patterns over time in mitral cells are believed to differentiate between broad and specific odour classification in zebrafish olfaction (Friedrich & Laurent, 2001). Future studies with higher temporal resolution and an increased number of analysed components may reveal similarly precise changes in activation patterns over time in the tectum. This highlights the need to examine the population coding of responses with respect to many variables including the tuning of individual cells, their weighting within population responses, and the response of the assembly as a whole.

It should be noted that the variability in cell responses in the present study may also be due to the tectal circuits in these fish being too immature to exhibit coherent activity. It has been shown that there is a critical period in *Xenopus* development during which the cells in the tectum undergo activity-dependent refinement, leading to more consistent signals from ensembles of cells (Pratt & Aizenman, 2007; Pratt et al., 2008; Xu et al., 2011). In particular, repeated exposure of a specific patterned visual stimulus during this period has also been seen to increase the strength and coherence of signals to that stimulus (Engert et al., 2002). This hypothesis would suggest an increase in the selectivity of cells between the first and last trials, however this is not seen across the five trials presented here and would require a much higher number or repeats to see this effect. The critical period in *Xenopus* also occurs at an earlier developmental period than the data presented here (Pratt & Aizenman, 2007), suggesting this may not be the major source of response variability.

4.4.4 Conclusion and future directions

While visual processing is one of the principal roles of the tectum, the results presented here make it clear that the tectum also has a role in processing other non-visual sensory stimuli. The three modalities that elicited a response from tectal neurons in this study (vision, water flow and audition) all have the potential to contain spatial information, suggesting that the tectum could play the role of a spatial integrator across those modalities. This idea is supported by different sensory modalities having overlapping topographical maps in the mammalian superior colliculus (Dräger & Hubel, 1975; Finlay et al., 1978; Harris et al., 1980; King et al., 1996; Stein et al., 1975; Triplett et al., 2012), however at this age the spatial refinement of these different maps has yet to be considered in zebrafish. No evidence for integration between modalities was observed in the larvae presented here, but future studies incorporating directional auditory stimuli and localized neuromast stimulations will be needed to determine whether these modalities are registered spatially in the tectum, as is the case for vision. For example, in our experiments the stronger activation of the caudal neuropil for from water flow (Figure 4.8) may be a result of stimulating neuromasts along the tail as opposed to those covering the head.

This study provides an important step in the analysis of the underlying principles of by which tectal circuits encode information, however it would also be worthwhile to vary the order of stimulus presentation, particularly visual, in order to determine any effects on recruitment of different assemblies. Another important question is whether information from different modalities is actually integrated by tectal circuits, or selectively processed in parallel. The low proportion of cells responsive to multiple modalities in this study would suggest that certain features of different stimuli are already specifically encoded in the zebrafish tectum at this age, however stimuli from individual modalities were presented in isolation. Future experiments, in which sub-optimal or sub-threshold stimuli from multiple modalities are presented simultaneously, will be necessary to determine whether there may be integration among sensory modalities in the tectum.

functional division

Chapter 5

General Discussion

5.1 Overview

The reduced size and complexity of the nervous system, coupled with the ease of transgenesis and optical transparency of larval zebrafish, has led to this model organism being established as a valuable system for the analysis of neural circuits. This thesis has aimed to better understand the neural mechanisms by which circuits in the brain regulate the processing of sensory information and generate behaviours. In order to do this, optogenetic proteins have been expressed in the zebrafish brain to observe and manipulate neural activity. While activity is observable in larval zebrafish using the genetically-encoded calcium indicator GCaMP5G, the wavelength of light used to image this protein makes it difficult to regulate optogenetic tools that modify activity. In the experiments described in Chapter 2, the activator ChR2(ET/TC), and inhibitor eNpHR3.0, are both stimulated by the 488 nm light used to image GCaMP5G activity. While there are intensities of light at which GCaMP5G can be imaged without significant activation of these other proteins, the low signal-to-noise ratio of GCaMP5G under these conditions demands that alternative methods such as occlusion of the light or genetic restriction of the proteins be employed.

This thesis aimed to use these optogenetic tools in order to uncover the neural mechanisms by which circuits in the cerebellum controlled the learning of a simple classical conditioning assay. Using a tone and shock paradigm described in Chapter 3, I was unable to consistently produce learning in either larval or juvenile zebrafish tested under a range of parameters. This was not attributable to learned helplessness in these animals, and the factors determining this result remain unknown. Arousal, prepulse inhibition, behavioural relevance of the stimuli, and the adaptation of response preferences may all have various contributions to the result. Consequently, the changes in cerebellar dynamics during the learning process could not be explored in this thesis.

The ability to rapidly image large volumes of the zebrafish brain with single-cell resolution using SPIM has been demonstrated recently (Panier et al., 2013; Vladimirov et al., 2014), and such a device has been constructed in parallel to these studies during this thesis. While current literature has focused primarily on the methodology of the imaging, the results presented in Chapter 4 of this thesis utilise

this technique to analyse the functional activity of a given neural circuit, namely that responsible for sensory perception in the zebrafish tectum. A large number of studies have examined the tectum of larval zebrafish in order to understand visual processing (Bianco & Engert, 2015; Del Bene et al., 2010; Hunter et al., 2013; Nikolaou et al., 2012; Preuss et al., 2014; Romano et al., 2015; Temizer et al., 2015), but this thesis aimed to extend this knowledge and study the response profiles of cells in the tectum to non-visual sensory modalities, a function known to be important in the homologous mammalian region. Until now this function of the tectum has been unexplored in larval zebrafish, and as such the results here provide a novel contribution to the field.

Water flow stimuli were found to elicit clear responses in cells of the larval tectum, predominantly in the dorsal regions, while auditory responses were observed to be relatively weak and ventrally located. Since the optic tectum receives the largest proportion of visual input from the retina (Burrill & Easter, 1994; Robles et al., 2014), it is unsurprising that visual stimuli generated the strongest and most selective responses in the cells of the tectum. Although the auditory stimulus presented to the larvae here was unlikely to contain any spatial information, the tectum is known to be topographically organised with respect to external world (Gosse et al., 2008; Kita et al., 2015; Niell & Smith, 2005; Stuermer, 1988). Therefore, it is possible that the locations of the visual and water flow responsive assemblies may reflect different spatial localization of the visual and lateral line receptive fields that were targeted during stimulus presentation. In order to fully explore this possibility, and identify the nature of any multimodal cells, sensory stimuli must be delivered at all possible spatial components at a variety of different strengths, speeds, frequencies and orientations for different stimuli.

Responses in the tectum were found to be selective for particular stimulus features such as the onset and cessation of the stimulus, as well as the direction of movement for visual stimuli. These responses were elicited as assemblies of simultaneously active cells with similar response profiles, a property also seen in other recent studies of the tectum (Bianco & Engert, 2015; Romano et al., 2015). In response to a given stimulus, these assemblies are likely to represent the

transiently-active state of a single network of tectal cells with various tuning profiles and connectivity from among a multitude of potential network activation patterns. As such they should not be considered exclusive functional units. Furthermore, the dimensionality reduction methods used to separate responses among these assemblies may be artificially clustering unrelated events in some instances. This limitation could be improved by the use of activity indicators with faster kinetics such as GCaMP6f (Chen et al., 2013), greater temporal separation between stimuli, and faster sampling rates during image acquisition.

5.2 Information processing by neural circuits

5.2.1 Assembly cores

Due to the combined use of optogenetic indicators and population imaging *in vivo*, this study has produced novel findings with relation to how information is received and processed by the brain. This thesis has identified core populations of cells with consistent and selective responses to particular features of different visual and non-visual stimuli. While the function of these core cells is not yet known, we speculate that these cells may encode broad stimulus features while cells not belonging to the core may represent the current network state or be involved in determining the stimulus context or fine feature discrimination. This will be tested in future experiments by the gradual variation of specific stimulus features such as speed and orientation of visual stimuli while examining the consistency of firing among these core cells. If an abrupt switch is seen in the composition of the core cell population when stimulus features pass a certain threshold, this would strongly support this hypothesis. This issue can also be addressed further by the specific manipulation of these cells during sensory processing using optogenetic proteins targeted by spatial light modulation, as described in Chapter 2. For example, the responses of small assemblies of tectal neurons appear to be linked to the initiation of convergent eye saccades and hunting behaviors (Bianco & Engert, 2015). If consistently-responsive core cells, rather than less-reliable cells in these assemblies are responsible for initiating movements, selectively activating optogenetic inhibitors in these cells with an SLM may prevent behavioural responses to prey-like stimuli. Conversely, inhibition of non-core cells in this way may have little or no effect on behavioural outcomes.

Advances in the field have allowed for the activity of broad populations of cells to be recorded simultaneously by various methods. Using eight-pin, multi-site electrodes, two recent studies have been able to describe the presence of 'core' cells in the macaque inferior temporal cortex (Hung et al., 2015; Lin et al., 2014). More recently, the presence of core cells in the mouse visual cortex have also been described from calcium dye recordings (Carrillo-Reid et al., 2015). In these studies, core cells are defined by the most representative responders within a given ensemble of cells. Using this criterion, the most representative cells in Chapter 4 of this thesis were observed to have a very low trial-to-trial repeatability and were therefore not the same as the spatially localized population of core cells that have been described. Furthermore, the synchrony of cells presented in the macaque may be exaggerated by the recording of multiple cells on the same pin within a single columnar unit of the inferior temporal cortex (Sato et al., 2013; Tanaka, 1997).

As it happens, the findings presented by Carrillo-Reid et al. (2015) were from a deeper analysis of the data presented in an earlier paper (Miller et al., 2014). While the latter paper describes these 'most representative' core cells, the original paper notes the presence of core cells that were consistently represented across repeatedly active neuronal ensembles. These core cells are highly analogous to the core cells revealed in Chapter 4 of this thesis and thus strengthen the data presented here. In further support of the data presented here, core cells that were shared between multiple ensembles were found to have no significant difference in their feature selectivity compared to that of either unshared core cells or all responsive cells in the visual cortex (Miller et al., 2014). This suggests that assemblies of neurons, rather than individual cells, may represent the functional units used during sensory processing and supports the idea of sparse coding as a means of representing information in the brain (Olshausen & Field, 2004; Rinberg et al., 2006; Spanne & Jörntell, 2015).

5.2.2 Population coding

Many important features determine the probability of a cell firing to any given stimulus, including the tuning preference of the cell, stimulus strength, local and long-range connections, as well as the intrinsic noise and recent activity of the

individual cell. Given the generally high intrinsic noise and broad tuning preferences of individual neurons, the information that can be encoded by single cells in the brain is thought to be insufficient to account for the fine discrimination of stimuli of which animals are behaviourally capable (Britten et al., 1996; Cohen & Newsome, 2009; Cook & Maunsell, 2002; Maynard et al., 1999; Shadlen et al., 1996). As such, integration of synchronous activity from populations of neurons is required provide enough breadth in encoding capacity. Just as individual neurons are unable to fully represent all possible stimulus feature combinations, core neurons within assemblies, such as those identified in this and other studies (Miller et al., 2014), are similarly unlikely to achieve such range and precision.

Theories of how the collective activity from populations of cells can encode information in the brain have been previously based on models that are experimentally untested (Averbeck et al., 2006; Pouget et al., 2000; Sanger, 2003), however several recent advances have allowed for the simultaneous recording of activity from broad networks of neurons within the brain. By imaging large populations of cells in this way, the correlated activity among neurons can be used to infer information about common inputs and the underlying connections between cells in the circuit. For example, the imaging of calcium dynamics from all cells within a small area of the mouse cortex, including those with low baseline activity, has revealed changes associated with learning that would otherwise remain undetected using traditional electrophysiological techniques (Clancy et al., 2014). There are however limitations to these current population imaging methods.

As outlined above, cells that fire together to form responsive assemblies can have a variety of preferred stimuli and tuning curves, ranging from very broad to very narrow selectivity. It has been suggested that the inclusion of many cells with broad tuning curves into responsive assemblies can in aid in information processing and fine discrimination (Series et al., 2004). It is also hypothesised that information processing and fine discrimination can be improved by increasing the weighting of the responses of neurons with narrow tuning curves (Jazayeri & Movshon, 2006; Seung & Sompolinsky, 1993; Vogels, 1990). While not examined explicitly, this theory is supported by experiments in the cat visual cortex in which both optimally and suboptimally activated neurons have been shown to engage in synchronous

discharges (König et al., 1995). Here, significantly more suboptimal cells than optimal were responsive to each visual stimulus due to the large tuning curves of most cells. Using electrophysiology, firing in optimally activated cells was found to precede firing in suboptimally activated cells by about two microseconds per degree from the optimal stimulus orientation. This is well below what is separable with GCaMP5G imaging and is therefore a limitation of these types of analyses when attempting to elucidate functional connections and information processing among networks of cells.

Since the composition of cells that fire synchronously to form assemblies, and the responses of those cells within the assembly, can vary significantly between trials, synchronous neuronal activity from neuronal assemblies is often determined from trial-averaged data (Panas et al., 2015; Prut et al., 1998). As such information about the underlying network structure can be lost. To better understand the effective connectivity between neurons and how information is carried through the network in a single trial, the patterns of activity in neural circuits can be analyzed using Granger causality (Barnett & Seth, 2014; Seth et al., 2015). This simple idea examines the covariance of cells and determines if the activity in a given cell can be used to improve the prediction of activity in another cell. Despite the low temporal resolution of GCaMP5G imaging presented in Chapter 4 of this thesis, Granger causality could be used effectively in these types of population imaging experiments to better understand how information is represented across zebrafish neural circuits (de Vico Fallani, et al., 2015).

5.3 Future directions

5.3.1 Multisensory integration in the zebrafish tectum

In addition to the experiments exploring the function of assembly cores outlined earlier, a number of further experiments could contribute to the understanding of sensory processing in the zebrafish tectum. Specifically, by presenting specific stimuli of different modalities to the animal simultaneously, information about the multisensory integration capacity of these circuits can be analysed. This would involve varying the saliency and timing of different stimuli to observe how signals are combined in tectal cells. Since sub-threshold activation would not be evident from GCaMP5G imaging, the presence of cells that are active only when sub-threshold

stimulation is integrated from two different stimuli would strongly suggest multisensory integration. In addition, firing rates can be approximated from calcium imaging data (Yaksi & Friedrich, 2006; Vogelstein et al., 2010), meaning that supralinear summation of activity between separate and simultaneous stimulus presentations would also be highly indicative of multisensory integration within tectal neurons. Once the cells responsible for integration have been identified in the tectum via calcium imaging, it would also be possible to identify the morphology and projection patterns of these cells by targeted conversion of a photoactivatable protein such as PATagRFP (Subach et al., 2010).

5.3.2 Cerebello-tectal circuit analysis

Responses induced by optogenetic stimulation of excitatory cells can be used easily to identify downstream synaptic partners (Wang et al., 2007). As outlined in Chapter 2, this can be achieved in larval zebrafish by the targeted excitation of ChR2 using a spatial light modulator while examining GCaMP5G signals in downstream circuits. This technique can be coupled to whole-brain imaging in order to undertake unbiased mapping of all regions downstream from signalling in a given circuit, or it can take a more targeted approach. For example, this thesis has described the activation of cerebellar cells while imaging tectal cell body responses. Analysis of this circuit can be extended further by imaging responses in a pan-neuronal GCaMP6 line such as *elavl3*:H2B-GCaMP6s (Vladimirov et al., 2014), the use of red-shifted activator Chrimson in a targeted Gal4 line such as s1168t:Gal4 (Heap et al., 2013; Scott & Baier, 2009), and occlusion of the imaging plane across the cerebellum. By making these improvements, optogenetic stimulation can be used to map cell-to-cell relationships in the cerebello-tectal circuit. Once again, the morphology of both the cerebellar and downstream tectal cells in this circuit can be traced following targeted photoconversion of a fluorescent marker such as PATagRFP. Mapping the axonal and dendritic processes of these cells would reveal whether the functional connections identified are likely to be direct, monosynaptic connections between cells or whether they are indirect, occurring via a more complex, polysynaptic pathway such as connections through other brain regions such as the pretectum, thalamus or torus semicircularis (Carr et al., 1981; Ito et al., 1986; Luiten, 1981; Northcutt, 1982; Wullimann & Northcutt, 1990).

The role of this circuit could also be examined during behaviours such as adaptation of OMR responses (Ahrens et al., 2012). It has been reported previously that the correct timing of saccades during OKR is affected by tectal ablation in larval zebrafish, but that they retain the ability to execute OMR and OKR behaviours (Roeser & Baier, 2003). Since deeper parts of the tectum were left intact in this study, and cerebellar projections are known to synapse in these deeper layers (Heap et al., 2013), these circuits should be investigated for their potential role in fine-tuning these behaviours. Specifically, during either sensory processing or motor adaptation tasks, cerebellar cells that project to the tectum can be activated or silenced optogenetically using targeted illumination from an SLM. The resulting changes in activity in tectal circuits, as well as the modification of behavioural responses, can all be measured to uncover the functional role of this cerebello-tectal circuit.

5.4 Conclusion

The ability to record activity from vast populations of neural circuits in the larval zebrafish brain makes it a powerful system in which to analyse the functional mechanisms responsible for sensory perception and behaviour. This thesis has outlined the generation of specific transgenic lines for optogenetic observation and control of neural circuits, as well as selective plane illumination microscopy in order to undertake analyses of a broad range of behavioural questions. The experiments described in Chapter 4 provide novel data related to the function of the zebrafish tectum in processing information from multiple sensory modalities, as well as the identification of consistently responsive cores of cells within assemblies with unique functional response profiles. Due to the development of these tools and initial findings in the tectum, further studies on the specific functional connectivity of these cells and their role in sensory processing can now be undertaken quickly and efficiently. In particular, multisensory integration will be examined by the simultaneous presentation of visual and non-visual sensory stimuli, and the role of cerebello-tectal circuits will be addressed by targeted optogenetic gain- and loss-of-function experiments. In summary I have brought together a comprehensive suite of techniques that I have used to examine important functional circuits in the larval zebrafish and lay the foundations for future studies.

References

Ablain, J., Durand, E.M., Yang, S., Zhou, Y., and Zon, L.I. (2015). A CRISPR/Cas9 vector system for tissue-specific gene disruption in zebrafish. Dev Cell 32, 756-764.

Adesnik, H., Bruns, W., Taniguchi, H., Huang, Z.J., and Scanziani, M. (2012). A neural circuit for spatial summation in visual cortex. Nature 490, 226-231.

Agetsuma, M., Aizawa, H., Aoki, T., Nakayama, R., Takahoko, M., Goto, M., Sassa, T., Amo, R., Shiraki, T., Kawakami, K., et al. (2010). The habenula is crucial for experience-dependent modification of fear responses in zebrafish. Nat Neurosci 13, 1354-1356.

Ahrens, M.B., Li, J.M., Orger, M.B., Robson, D.N., Schier, A.F., Engert, F., and Portugues, R. (2012). Brain-wide neuronal dynamics during motor adaptation in zebrafish. Nature 485, 471-U480.

Ahrens, M.B., Orger, M.B., Robson, D.N., Li, J.M., and Keller, P.J. (2013). Whole-brain functional imaging at cellular resolution using light-sheet microscopy. Nat Methods 10, 413-+.

Aizenberg, M., and Schuman, E.M. (2011). Cerebellar-Dependent Learning in Larval Zebrafish. J Neurosci 31, 8708-8712.

Akemann, W., Mutoh, H., Perron, A., Park, Y.K., Iwamoto, Y., and Knöpfel, T. (2012). Imaging neural circuit dynamics with a voltage-sensitive fluorescent protein. J Neurophysiol 108, 2323-2337.

Akerboom, J., Carreras Calderon, N., Tian, L., Wabnig, S., Prigge, M., Tolo, J., Gordus, A., Orger, M.B., Severi, K.E., Macklin, J.J., et al. (2013). Genetically encoded calcium indicators for multi-color neural activity imaging and combination with optogenetics. Front Mol Neurosci 6, 2.

Akerboom, J., Chen, T.W., Wardill, T.J., Tian, L., Marvin, J.S., Mutlu, S., Calderon, N.C., Esposti, F., Borghuis, B.G., Sun, X.R., et al. (2012). Optimization of a GCaMP Calcium Indicator for Neural Activity Imaging. J Neurosci 32, 13819-13840.

Akitake, C.M., Macurak, M., Halpern, M.E., and Goll, M.G. (2011). Transgenerational analysis of transcriptional silencing in zebrafish. Dev Biol 352, 191-201.

Albus, J.S. (1971). A theory of cerebellar function. Mathematical Biosciences 10, 25-61.

Al-Imari, L., and Gerlai, R. (2008). Sight of conspecifics as reward in associative learning in zebrafish (*Danio rerio*). Behav Brain Res 189, 216-219.

Al-Juboori, S.I., Dondzillo, A., Stubblefield, E.A., Felsen, G., Lei, T.C., and Klug, A. (2013). Light scattering properties vary across different regions of the adult mouse brain. PloS one 8, e67626.

Aoki, T., Kinoshita, M., Aoki, R., Agetsuma, M., Aizawa, H., Yamazaki, M., Takahoko, M., Amo, R., Arata, A., Higashijima, S., et al. (2013). Imaging of Neural Ensemble for the Retrieval of a Learned Behavioral Program. Neuron 78, 881-894.

Apps, R., and Garwicz, M. (2005). Anatomical and physiological foundations of cerebellar information processing. Nat Rev Neurosci 6, 297-311.

Arrenberg, A.B., Del Bene, F., and Baier, H. (2009). Optical control of zebrafish behavior with halorhodopsin. Proc Natl Acad Sci USA 106, 17968-17973.

Asakawa, K., Suster, M.L., Mizusawa, K., Nagayoshi, S., Kotani, T., Urasaki, A., Kishimoto, Y., Hibi, M., and Kawakami, K. (2008). Genetic dissection of neural circuits by Tol2 transposon-mediated Gal4 gene and enhancer trapping in zebrafish. Proc Natl Acad Sci USA 105, 1255-1260.

Auer, T.O., Duroure, K., De Cian, A., Concordet, J.P., and Del Bene, F. (2014). Highly efficient CRISPR/Cas9-mediated knock-in in zebrafish by homology-independent DNA repair. Genome Res 24, 142-153.

Auer, T.O., Xiao, T., Bercier, V., Gebhardt, C., Duroure, K., Concordet, J.P., Wyart, C., Suster, M., Kawakami, K., Wittbrodt, J., et al. (2015). Deletion of a kinesin I motor unmasks a mechanism of homeostatic branching control by neurotrophin-3. Elife 4.

Averbeck, B.B., Latham, P.E., and Pouget, A. (2006). Neural correlations, population coding and computation. Nat Rev Neurosci 7, 358-366.

Badura, A., Sun, X.R., Giovannucci, A., Lynch, L.A., and Wang, S.S. (2014). Fast calcium sensor proteins for monitoring neural activity. Neurophoton 1, 025008.

Bae, Y.K., Kani, S., Shimizu, T., Tanabe, K., Nojima, H., Kimura, Y., Higashijima, S., and Hibi, M. (2009). Anatomy of zebrafish cerebellum and screen for mutations affecting its development. Dev Biol 330, 406-426.

Baier, H., and Scott, E.K. (2009). Genetic and Optical Targeting of Neural Circuits and Behavior – Zebrafish in the Spotlight. Curr Opin Neurobiol 19, 553-560.

Bailey, C.H., Kandel, E.R., and Harris, K.M. (2015). Structural Components of Synaptic Plasticity and Memory Consolidation. Cold Spring Harb Perspect Biol 7.

Baker, P.F., Hodgkin, A.L., and Ridgway, E.B. (1971). Depolarization and calcium entry in squid giant axons. J Physiol 218, 709-755.

Bang, P.I., Yelick, P.C., Malicki, J.J., and Sewell, W.F. (2002). High-throughput behavioral screening method for detecting auditory response defects in zebrafish. J Neurosci Meth 118, 177-187.

Baraban, S.C., Dinday, M.T., Castro, P.A., Chege, S., Guyenet, S., and Taylor, M.R. (2007). A large-scale mutagenesis screen to identify seizure-resistant zebrafish. Epilepsia 48, 1151-1157.

Barnett, L., and Seth, A.K. (2014). The MVGC multivariate Granger causality toolbox: a new approach to Granger-causal inference. J Neurosci Methods 223, 50-68.

Barretto, R.P., Gillis-Smith, S., Chandrashekar, J., Yarmolinsky, D.A., Schnitzer, M.J., Ryba, N.J., and Zuker, C.S. (2015). The neural representation of taste quality at the periphery. Nature 517, 373-376.

Bedell, V.M., Wang, Y., Campbell, J.M., Poshusta, T.L., Starker, C.G., Krug, R.G., Tan, W.F., Penheiter, S.G., Ma, A.C., Leung, A.Y.H., et al. (2012). In vivo genome editing using a high-efficiency TALEN system. Nature 491, 114-U133.

Ben Fredj, N., Hammond, S., Otsuna, H., Chien, C.B., Burrone, J., and Meyer, M.P. (2010). Synaptic activity and activity-dependent competition regulates axon arbor

maturation, growth arrest, and territory in the retinotectal projection. J Neurosci 30, 10939-10951.

Bergeron, S.A., Carrier, N., Li, G.H., Ahn, S., and Burgess, H.A. (2014). Gsx1 expression defines neurons required for prepulse inhibition. Mol Psychiatry.

Berndt, A., Schoenenberger, P., Mattis, J., Tye, K.M., Deisseroth, K., Hegemann, P., and Oertner, T.G. (2011). High-efficiency channelrhodopsins for fast neuronal stimulation at low light levels. Proc Natl Acad Sci USA 108, 7595-7600.

Berridge, M.J., Lipp, P., and Bootman, M.D. (2000). The versatility and universality of calcium signalling. Nat Rev Mol Cell Biol 1, 11-21.

Bianco, I.H., and Engert, F. (2015). Visuomotor transformations underlying hunting behavior in zebrafish. Curr Biol 25, 831-846.

Bianco, I.H., Kampff, A.R., and Engert, F. (2011). Prey capture behavior evoked by simple visual stimuli in larval zebrafish. Front Syst Neurosci 5, 101.

Borla, M.A., Palecek, B., Budick, S., and O'Malley, D.M. (2002). Prey capture by larval zebrafish: Evidence for fine axial motor control. Brain Behav Evolut 60, 207-229.

Bouchard, M.B., Voleti, V., Mendes, C.S., Lacefield, C., Grueber, W.B., Mann, R.S., Bruno, R.M., and Hillman, E.M.C. (2015). Swept confocally-aligned planar excitation (SCAPE) microscopy for high-speed volumetric imaging of behaving organisms. Nat Photonics 9, 113-119.

Boyden, E.S., Zhang, F., Bamberg, E., Nagel, G., and Deisseroth, K. (2005). Millisecond-timescale, genetically targeted optical control of neural activity. Nat Neurosci 8, 1263-1268.

Bozza, T., McGann, J.P., Mombaerts, P., and Wachowiak, M. (2004). In Vivo Imaging of Neuronal Activity by Targeted Expression of a Genetically Encoded Probe in the Mouse. Neuron 42, 9-21.

Brand, A.H., and Perrimon, N. (1993). Targeted Gene-Expression as a Means of Altering Cell Fates and Generating Dominant Phenotypes. Development 118, 401-415.

Branda, C.S., and Dymecki, S.M. (2004). Talking about a Revolution: The Impact of Site-Specific Recombinases on Genetic Analyses in Mice. Dev Cell 6, 7-28.

Britt, J.P., McDevitt, R.A., and Bonci, A. (2001). Use of Channelrhodopsin for Activation of CNS Neurons. In Curr Protoc Neurosci (John Wiley & Sons, Inc.).

Britten, K.H., Newsome, W.T., Shadlen, M.N., Celebrini, S., and Movshon, J.A. (1996). A relationship between behavioral choice and the visual responses of neurons in macaque MT. Visual Neurosci 13, 87-100.

Budick, S.A., and O'Malley, D.M. (2000). Locomotor repertoire of the larval zebrafish: Swimming, turning and prey capture. J Exp Biol 203, 2565-2579.

Burgess, H.A., and Granato, M. (2007). Sensorimotor gating in larval zebrafish. J Neurosci 27, 4984-4994.

Burgess, H.A., Schoch, H., and Granato, M. (2010). Distinct Retinal Pathways Drive Spatial Orientation Behaviors in Zebrafish Navigation. Curr Biol 20, 381-386.

Burrill, J.D., and Easter, S.S., Jr. (1994). Development of the retinofugal projections in the embryonic and larval zebrafish (*Brachydanio rerio*). J Comp Neurol 346, 583-600.

Buzsáki, G., Anastassiou, C.A., and Koch, C. (2012). The origin of extracellular fields and currents--EEG, ECoG, LFP and spikes. Nature reviews Neuroscience 13, 407-420.

Carr, C.E., Maler, L., Heiligenberg, W., and Sas, E. (1981). Laminar Organization of the Afferent and Efferent Systems of the Torus Semicircularis of Gymnotiform Fish - Morphological Substrates for Parallel Processing in the Electrosensory System. J Comp Neurol 203, 649-670.

Carrillo-Reid, L., Miller, J.E., Hamm, J.P., Jackson, J., and Yuste, R. (2015). Endogenous Sequential Cortical Activity Evoked by Visual Stimuli. J Neurosci 35, 8813-8828.

Chen, T.W., Wardill, T.J., Sun, Y., Pulver, S.R., Renninger, S.L., Baohan, A., Schreiter, E.R., Kerr, R.A., Orger, M.B., Jayaraman, V., et al. (2013). Ultrasensitive fluorescent proteins for imaging neuronal activity. Nature 499, 295-300.

Cho, S.W., Kim, S., Kim, Y., Kweon, J., Kim, H.S., Bae, S., and Kim, J.S. (2014). Analysis of off-target effects of CRISPR/Cas-derived RNA-guided endonucleases and nickases. Genome Res 24, 132-141.

Chow, B.Y., Han, X., Dobry, A.S., Qian, X., Chuong, A.S., Li, M., Henninger, M.A., Belfort, G.M., Lin, Y., Monahan, P.E., et al. (2010). High-performance genetically targetable optical neural silencing by light-driven proton pumps. Nature 463, 98-102.

Chuong, A.S., Miri, M.L., Busskamp, V., Matthews, G.A., Acker, L.C., Sorensen, A.T., Young, A., Klapoetke, N.C., Henninger, M.A., Kodandaramaiah, S.B., et al. (2014). Noninvasive optical inhibition with a red-shifted microbial rhodopsin. Nat Neurosci 17, 1123-1129.

Clancy, K.B., Koralek, A.C., Costa, R.M., Feldman, D.E., and Carmena, J.M. (2014). Volitional modulation of optically recorded calcium signals during neuroprosthetic learning. Nat Neurosci 17, 807-809.

Cohen, L.B., Salzberg, B.M., Davila, H.V., Ross, W.N., Landowne, D., Waggoner, A.S., and Wang, C.H. (1974). Changes in axon fluorescence during activity: Molecular probes of membrane potential. J Membrain Biol 19, 1-36.

Cohen, L.B., Salzberg, B.M., and Grinvald, A. (1978). Optical Methods for Monitoring Neuron Activity. Annu Rev Neurosci 1, 171-182.

Cohen, M.R., and Newsome, W.T. (2009). Estimates of the contribution of single neurons to perception depend on timescale and noise correlation. J Neurosci 29, 6635-6648.

Cole, R.W., Jinadasa, T., and Brown, C.M. (2011). Measuring and interpreting point spread functions to determine confocal microscope resolution and ensure quality control. Nat Protoc 6, 1929-1941.

Cook, E.P., and Maunsell, J.H. (2002). Dynamics of neuronal responses in macaque MT and VIP during motion detection. Nat Neurosci 5, 985-994.

Cruz-Martin, A., El-Danaf, R.N., Osakada, F., Sriram, B., Dhande, O.S., Nguyen, P.L., Callaway, E.M., Ghosh, A., and Huberman, A.D. (2014). A dedicated circuit links direction-selective retinal ganglion cells to the primary visual cortex. Nature 507, 358-361.

D'Angelo, E., and De Zeeuw, C.I. (2009). Timing and plasticity in the cerebellum: focus on the granular layer. Trends Neurosci 32, 30-40.

Darrow, K.O., and Harris, W.A. (2004). Characterization and Development of Courtship in Zebrafish, *Danio rerio*. Zebrafish 1, 40-45.

Davie, J.T., Kole, M.H., Letzkus, J.J., Rancz, E.A., Spruston, N., Stuart, G.J., and Hausser, M. (2006). Dendritic patch-clamp recording. Nat Protoc 1, 1235-1247.

Davison, J.M., Akitake, C.M., Goll, M.G., Rhee, J.M., Gosse, N., Baier, H., Halpern, M.E., Leach, S.D., and Parsons, M.J. (2007). Transactivation from Gal4-VP16 transgenic insertions for tissue-specific cell labeling and ablation in zebrafish. Dev Biol 304, 811-824.

de Bono, M., and Maricq, A.V. (2005). Neuronal substrates of complex behaviors in *C. elegans*. Annu Rev Neurosci 28, 451-501.

de Bruijn, E., Cuppen, E., and Feitsma, H. (2009). Highly Efficient ENU Mutagenesis in Zebrafish. In Zebrafish, G.J. Lieschke, A.C. Oates, and K. Kawakami, eds. (Humana Press), pp. 3-12.

de Vico Fallani, F., Corazzol, M., Sternberg, J.R., Wyart, C., and Chavez, M. (2015). Hierarchy of Neural Organization in the Embryonic Spinal Cord: Granger-Causality Graph Analysis of In Vivo Calcium Imaging Data. IEEE Trans Neural Syst Rehabil Eng 23, 333-341.

Del Bene, F., and Wyart, C. (2012). Optogenetics: a new enlightenment age for zebrafish neurobiology. Dev Neurobiol 72, 404-414.

Del Bene, F., Wyart, C., Robles, E., Tran, A., Looger, L., Scott, E.K., Isacoff, E.Y., and Baier, H. (2010). Filtering of visual information in the tectum by an identified neural circuit. Science 330, 669-673.

Delgado Ruz, I., and Schultz, S.R. (2014). Localising and classifying neurons from high density MEA recordings. J Neurosci Meth 233, 115-128.

Denk, W., Strickler, J., and Webb, W. (1990). Two-photon laser scanning fluorescence microscopy. Science 248, 73-76.

Diez-Garcia, J., Akemann, W., and Knöpfel, T. (2007). In vivo calcium imaging from genetically specified target cells in mouse cerebellum. NeuroImage 34, 859-869.

Do-Monte, F.H., Quinones-Laracuente, K., and Quirk, G.J. (2015). A temporal shift in the circuits mediating retrieval of fear memory. Nature 519, 460-463.

Douglass, A.D., Kraves, S., Deisseroth, K., Schier, A.F., and Engert, F. (2008). Escape behavior elicited by single, channelrhodopsin-2-evoked spikes in zebrafish somatosensory neurons. Curr Biol 18, 1133-1137.

Dräger, U.C., and Hubel, D.H. (1975). Physiology of Visual Cells in Mouse Superior Colliculus and Correlation with Somatosensory and Auditory Input. Nature 253, 203-204.

Echteler, S.M. (1984). Connections of the Auditory Midbrain in a Teleost Fish, Cyprinus-Carpio. J Comp Neurol 230, 536-551.

Eggermont, J.J. (2006). Properties of correlated neural activity clusters in cat auditory cortex resemble those of neural assemblies. J Neurophysiol 96, 746-764.

Engert, F., Tao, H.Z.W., Zhang, L.I., and Poo, M.M. (2002). Moving visual stimuli rapidly induce direction sensitivity of developing tectal neurons. Nature 419, 470-475.

Engeszer, R.E., Alberici da Barbiano, L., Ryan, M.J., and Parichy, D.M. (2007). Timing and plasticity of shoaling behaviour in the zebrafish, *Danio rerio*. Anim Behav 74, 1269-1275.

Fajardo, O., Zhu, P., and Friedrich, R.W. (2013). Control of a specific motor program by a small brain area in zebrafish. Front Neural Circuit 7, 67.

Fame, R.M., Brajon, C., and Ghysen, A. (2006). Second-order projection from the posterior lateral line in the early zebrafish brain. Neural development 1, 4.

Favre-Bulle, I.A., Preece, D., Nieminen, T.A., Heap, L.A., Scott, E.K., and Rubinsztein-Dunlop, H. (2015). Scattering of Sculpted Light in Intact Brain Tissue, with implications for Optogenetics. Scientific reports 5, 11501.

Feil, R., Brocard, J., Mascrez, B., LeMeur, M., Metzger, D., and Chambon, P. (1996). Ligand-activated site-specific recombination in mice. Proc Natl Acad Sci USA 93, 10887-10890.

Fenno, L., Yizhar, O., and Deisseroth, K. (2011). The development and application of optogenetics. Annu Rev Neurosci 34, 389-412.

Finlay, B.L., Schneps, S.E., Wilson, K.G., and Schneider, G.E. (1978). Topography of visual and somatosensory projections to the superior colliculus of the golden hamster. Brain Res 142, 223-235.

Flusberg, B.A., Nimmerjahn, A., Cocker, E.D., Mukamel, E.A., Barretto, R.P., Ko, T.H., Burns, L.D., Jung, J.C., and Schnitzer, M.J. (2008). High-speed, miniaturized fluorescence microscopy in freely moving mice. Nat Methods 5, 935-938.

Fredette, B.J., and Mugnaini, E. (1991). The Gabaergic Cerebello-Olivary Projection in the Rat. Anat Embryol 184, 225-243.

Freeman, J., Vladimirov, N., Kawashima, T., Mu, Y., Sofroniew, N.J., Bennett, D.V., Rosen, J., Yang, C.T., Looger, L.L., and Ahrens, M.B. (2014). Mapping brain activity at scale with cluster computing. Nat Methods 11, 941-950.

Freeman, J.H., and Steinmetz, A.B. (2011). Neural circuitry and plasticity mechanisms underlying delay eyeblink conditioning. Learn Memory 18, 666-677.

Friedrich, R.W., and Laurent, G. (2001). Dynamic optimization of odor representations by slow temporal patterning of mitral cell activity. Science 291, 889-894.

Frock, R.L., Hu, J., Meyers, R.M., Ho, Y.J., Kii, E., and Alt, F.W. (2015). Genome-wide detection of DNA double-stranded breaks induced by engineered nucleases. Nat Biotechnol 33, 179-186.

Gabriel, J.P., Trivedi, C.A., Maurer, C.M., Ryu, S., and Bollmann, J.H. (2012). Layer-specific targeting of direction-selective neurons in the zebrafish optic tectum. Neuron 76, 1147-1160.

Gahtan, E., Tanger, P., and Baier, H. (2005). Visual prey capture in larval zebrafish is controlled by identified reticulospinal neurons downstream of the tectum. J Neurosci 25, 9294-9303.

García-Otín, A.L., and Guillou, F. (2006). Mammalian genome targeting using site-specific recombinases. Front Biosci 11, 1108-1136.

Gebhardt, C., Baier, H., and Del Bene, F. (2013). Direction selectivity in the visual system of the zebrafish larva. Front Neural Circuits 7, 111.

Ghitani, N., Bayguinov, P.O., Vokoun, C.R., McMahon, S., Jackson, M.B., and Basso, M.A. (2014). Excitatory Synaptic Feedback from the Motor Layer to the Sensory Layers of the Superior Colliculus. J Neurosci 34, 6822-6833.

Gilbert, P.F.C. (1974). Theory of Memory That Explains Function and Structure of Cerebellum. Brain Res 70, 1-18.

Giniger, E., Varnum, S.M., and Ptashne, M. (1985). Specific DNA-Binding of Gal4, a Positive Regulatory Protein of Yeast. Cell 40, 767-774.

Gonçalves, P.J., Arrenberg, A.B., Hablitzel, B., Baier, H., and Machens, C.K. (2014). Optogenetic perturbations reveal the dynamics of an oculomotor integrator. Front Neural Circuit 8, 10.

Gosse, N.J., Nevin, L.M., and Baier, H. (2008). Retinotopic order in the absence of axon competition. Nature 452, 892-895.

Gradinaru, V., Thompson, K.R., and Deisseroth, K. (2008). eNpHR: a Natronomonas halorhodopsin enhanced for optogenetic applications. Brain Cell Biol 36, 129-139.

Gradinaru, V., Zhang, F., Ramakrishnan, C., Mattis, J., Prakash, R., Diester, I., Goshen, I., Thompson, K.R., and Deisseroth, K. (2010). Molecular and Cellular Approaches for Diversifying and Extending Optogenetics. Cell 141, 154-165.

Grama, A., and Engert, F. (2012). Direction selectivity in the larval zebrafish tectum is mediated by asymmetric inhibition. Front Neural Circuits 6, 59.

Gray, C.M., and Singer, W. (1989). Stimulus-specific neuronal oscillations in orientation columns of cat visual cortex. Proc Natl Acad Sci USA 86, 1698-1702.

Greenberg, D.S., Houweling, A.R., and Kerr, J.N. (2008). Population imaging of ongoing neuronal activity in the visual cortex of awake rats. Nat Neurosci 11, 749-751.

Grewe, B.F., and Helmchen, F. (2009). Optical probing of neuronal ensemble activity. Curr Opin Neurobiol 19, 520-529.

Grienberger, C., and Konnerth, A. (2012). Imaging Calcium in Neurons. Neuron 73, 862-885.

Gu, Y., Wang, Y., and Wang, S.R. (2000). Regional variation in receptive field properties of tectal neurons in pigeons. Brain Behav Evolut 55, 221-228.

Han, X., Chow, B.Y., Zhou, H., Klapoetke, N.C., Chuong, A., Rajimehr, R., Yang, A., Baratta, M.V., Winkle, J., Desimone, R., et al. (2011). A high-light sensitivity optical neural silencer: development, and application to optogenetic control of nonhuman primate cortex. Front Syst Neurosci 5, 18.

Hans, S., Freudenreich, D., Geffarth, M., Kaslin, J., Machate, A., and Brand, M. (2011). Generation of a non-leaky heat shock-inducible Cre line for conditional Cre/lox strategies in zebrafish. Dev Dyn 240, 108-115.

Hans, S., Kaslin, J., Freudenreich, D., and Brand, M. (2009). Temporally-controlled site-specific recombination in zebrafish. PloS One 4, e4640.

Harris, L.R., Blakemore, C., and Donaghy, M. (1980). Integration of visual and auditory space in the mammalian superior colliculus. Nature 288, 56-59.

Harris, J.A., Cheng, A.G., Cunningham, L.L., MacDonald, G., Raible, D.W., and Rubel, E.W. (2003). Neomycin-induced hair cell death and rapid regeneration in the lateral line of zebrafish (*Danio rerio*). J Assoc Res Otolaryngol 4, 219-234.

Hashimoto, M., and Hibi, M. (2012). Development and evolution of cerebellar neural circuits. Dev Growth Differ 54, 373-389.

Hausser, M. (2014). Optogenetics: the age of light. Nat Methods 11, 1012-1014.

Heap, L.A., Goh, C.C., Kassahn, K.S., and Scott, E.K. (2013). Cerebellar output in zebrafish: an analysis of spatial patterns and topography in eurydendroid cell projections. Front Neural Circuit 7.

Heck, D.H., De Zeeuw, C.I., Jaeger, D., Khodakhah, K., and Person, A.L. (2013). The Neuronal Code(s) of the Cerebellum. J Neurosci 33, 17603-17609.

Heeger, D.J., Huk, A.C., Geisler, W.S., and Albrecht, D.G. (2000). Spikes versus BOLD: what does neuroimaging tell us about neuronal activity? Nature neuroscience 3, 631-633.

Heeger, D.J., and Ress, D. (2002). What does fMRI tell us about neuronal activity? Nat Rev Neurosci 3, 142-151.

Herculano-Houzel, S., Mota, B., and Lent, R. (2006). Cellular scaling rules for rodent brains. Proc Natl Acad Sci USA 103, 12138-12143.

Hesslow, G., Svensson, P., and Ivarsson, M. (1999). Learned movements elicited by direct stimulation of cerebellar mossy fiber afferents. Neuron 24, 179-185.

Hill, A., Howard, C.V., Strahle, U., and Cossins, A. (2003). Neurodevelopmental defects in zebrafish (*Danio rerio*) at environmentally relevant dioxin (TCDD) concentrations. Toxicol Sci 76, 392-399.

Hill, E.S., Bruno, A.M., and Frost, W.N. (2014). Recent developments in VSD imaging of small neuronal networks. Learn Memory 21, 499-505.

Hiramoto, M., and Cline, H.T. (2009). Convergence of Multisensory Inputs in Xenopus Tadpole Tectum. Dev Neurobiol 69, 959-971.

Hires, S.A., Zhu, Y., and Tsien, R.Y. (2008). Optical measurement of synaptic glutamate spillover and reuptake by linker optimized glutamate-sensitive fluorescent reporters. Proc Natl Acad Sci USA 105, 4411-4416.

Hochbaum, D.R., Zhao, Y., Farhi, S.L., Klapoetke, N., Werley, C.A., Kapoor, V., Zou, P., Kralj, J.M., Maclaurin, D., Smedemark-Margulies, N., et al. (2014). All-optical electrophysiology in mammalian neurons using engineered microbial rhodopsins. Nat Methods 11, 825-833.

Hoess, R.H., Ziese, M., and Sternberg, N. (1982). P1 site-specific recombination: nucleotide sequence of the recombining sites. Proc Natl Acad Sci USA 79, 3398-3402.

Huff, M.L., Miller, R.L., Deisseroth, K., Moorman, D.E., and LaLumiere, R.T. (2013). Posttraining optogenetic manipulations of basolateral amygdala activity modulate consolidation of inhibitory avoidance memory in rats. Proc Natl Acad Sci USA 110, 3597-3602.

Huisken, J., and Stainier, D.Y.R. (2007). Even fluorescence excitation by multidirectional selective plane illumination microscopy (mSPIM). Opt Lett 32, 2608-2610.

Huisken, J., Swoger, J., Del Bene, F., Wittbrodt, J., and Stelzer, E.H.K. (2004). Optical sectioning deep inside live embryos by selective plane illumination microscopy. Science 305, 1007-1009.

Hung, C.P., Cui, D., Chen, Y.P., Lin, C.P., and Levine, M.R. (2015). Correlated activity supports efficient cortical processing. Front Comput Neurosci 8, 16.

Hunter, P.R., Lowe, A.S., Thompson, I.D., and Meyer, M.P. (2013). Emergent properties of the optic tectum revealed by population analysis of direction and orientation selectivity. J Neurosci 33, 13940-13945.

Hwang, W.Y., Fu, Y.F., Reyon, D., Maeder, M.L., Tsai, S.Q., Sander, J.D., Peterson, R.T., Yeh, J.R.J., and Joung, J.K. (2013). Efficient genome editing in zebrafish using a CRISPR-Cas system. Nat Biotechnol 31, 227-229.

Ikenaga, T., Yoshida, M., and Uematsu, K. (2005). Morphology and immunohistochemistry of efferent neurons of the goldfish corpus cerebelli. J Comp Neurol 487, 300-311.

Ingle, D. (1973). Evolutionary perspectives on the function of the optic tectum. Brain, behavior and evolution 8, 211-237.

Ito, H., Murakami, T., Fukuoka, T., and Kishida, R. (1986). Thalamic fiber connections in a teleost (Sebastiscus marmoratus): visual somatosensory, octavolateral, and cerebellar relay region to the telencephalon. The Journal of comparative neurology 250, 215-227.

Jazayeri, M., and Movshon, J.A. (2006). Optimal representation of sensory information by neural populations. Nat Neurosci 9, 690-696.

Jefferis, G.S.X.E., and Livet, J. (2012). Sparse and combinatorial neuron labelling. Curr Opin Neurobiol 22, 101-110.

Jennings, J.H., Sparta, D.R., Stamatakis, A.M., Ung, R.L., Pleil, K.E., Kash, T.L., and Stuber, G.D. (2013). Distinct extended amygdala circuits for divergent motivational states. Nature 496, 224-228.

Jia, H., Rochefort, N.L., Chen, X., and Konnerth, A. (2010). Dendritic organization of sensory input to cortical neurons in vivo. Nature 464, 1307-1312.

Johansen, J.P., Diaz-Mataix, L., Hamanaka, H., Ozawa, T., Ycu, E., Koivumaa, J., Kumar, A., Hou, M., Deisseroth, K., Boyden, E.S., et al. (2014). Hebbian and neuromodulatory mechanisms interact to trigger associative memory formation. Proc Natl Acad Sci USA 111, E5584-5592.

Kaufmann, A., Mickoleit, M., Weber, M., and Huisken, J. (2012). Multilayer mounting enables long-term imaging of zebrafish development in a light sheet microscope. Development 139, 3242-3247.

Kawakami, K., Shima, A., and Kawakami, N. (2000). Identification of a functional transposase of the Tol2 element, an Ac-like element from the Japanese medaka fish, and its transposition in the zebrafish germ lineage. Proc Natl Acad Sci USA 97, 11403-11408.

Keller, P.J., Schmidt, A.D., Wittbrodt, J., and Stelzer, E.H.K. (2008). Reconstruction of Zebrafish Early Embryonic Development by Scanned Light Sheet Microscopy. Science 322, 1065-1069.

Kerr, J.N., de Kock, C.P., Greenberg, D.S., Bruno, R.M., Sakmann, B., and Helmchen, F. (2007). Spatial Organization of Neuronal Population Responses in Layer 2/3 of Rat Barrel Cortex. J Neurosci 27, 13316-13328.

Kiani, R., Cueva, C.J., Reppas, J.B., Peixoto, D., Ryu, S.I., and Newsome, W.T. (2015). Natural grouping of neural responses reveals spatially segregated clusters in prearcuate cortex. Neuron 85, 1359-1373.

Kim, J.J., Clark, R.E., and Thompson, R.F. (1995). Hippocampectomy Impairs the Memory of Recently, but Not Remotely, Acquired Trace Eyeblink Conditioned-Responses. Behav Neurosci 109, 195-203.

Kimura, Y., Satou, C., Fujioka, S., Shoji, W., Umeda, K., Ishizuka, T., Yawo, H., and Higashijima, S. (2013). Hindbrain V2a neurons in the excitation of spinal locomotor circuits during zebrafish swimming. Curr Biol 23, 843-849.

King, A.J., Schnupp, J.W.H., Carlile, S., Smith, A.L., and Thompson, I.D. (1996). The development of topographically-aligned maps of visual and auditory space in the superior colliculus. Prog Brain Res 112, 335-350.

Kita, E.M., Scott, E.K., and Goodhill, G.J. (2015). Topographic wiring of the retinotectal connection in zebrafish. Dev Neurobiol 75, 542-556.

Klapoetke, N.C., Murata, Y., Kim, S.S., Pulver, S.R., Birdsey-Benson, A., Cho, Y.K., Morimoto, T.K., Chuong, A.S., Carpenter, E.J., Tian, Z.J., et al. (2014). Independent optical excitation of distinct neural populations. Nat Methods 11, 338-U333.

Kleinlogel, S., Terpitz, U., Legrum, B., Gokbuget, D., Boyden, E.S., Bamann, C., Wood, P.G., and Bamberg, E. (2011). A gene-fusion strategy for stoichiometric and co-localized expression of light-gated membrane proteins. Nat Methods 8, 1083-1088.

Knöpfel, T., Diez-Garcia, J., and Akemann, W. (2006). Optical probing of neuronal circuit dynamics: genetically encoded versus classical fluorescent sensors. Trends Neurosci 29, 160-166.

Knöpfel, T., Gallero-Salas, Y., and Song, C. (2015). Genetically encoded voltage indicators for large scale cortical imaging come of age. Curr Opin Chem Biol 27, 75-83.

Knudsen, E.I. (1982). Auditory and Visual Maps of Space in the Optic Tectum of the Owl. J Neurosci 2, 1177-1194.

Koga, A., Suzuki, M., Inagaki, H., Bessho, Y., and Hori, H. (1996). Transposable element in fish. Nature 383, 30-30.

Komiyama, T., Sato, T.R., O'Connor, D.H., Zhang, Y.X., Huber, D., Hooks, B.M., Gabitto, M., and Svoboda, K. (2010). Learning-related fine-scale specificity imaged in motor cortex circuits of behaving mice. Nature 464, 1182-1186.

König, P., Engel, A.K., Roelfsema, P.R., and Singer, W. (1995). How Precise is Neuronal Synchronization? Neural Comput 7, 469-485.

Koo, T., Lee, J., and Kim, J.S. (2015). Measuring and Reducing Off-Target Activities of Programmable Nucleases Including CRISPR-Cas9. Mol Cells 38, 475-481.

Kralj, J.M., Douglass, A.D., Hochbaum, D.R., Maclaurin, D., and Cohen, A.E. (2012). Optical recording of action potentials in mammalian neurons using a microbial rhodopsin. Nat Methods 9, 90-95.

Kuhlman, S.J., Olivas, N.D., Tring, E., Ikrar, T., Xu, X., and Trachtenberg, J.T. (2013). A disinhibitory microcircuit initiates critical-period plasticity in the visual cortex. Nature 501, 543-546.

Kwan, K.M., Fujimoto, E., Grabher, C., Mangum, B.D., Hardy, M.E., Campbell, D.S., Parant, J.M., Yost, H.J., Kanki, J.P., and Chien, C.B. (2007). The Tol2kit: A multisite Gateway-based construction kit for Tol2 transposon transgenesis constructs. Dev Dynam 236, 3088-3099.

Lee, A., Mathuru, A.S., Teh, C., Kibat, C., Korzh, V., Penney, T.B., and Jesuthasan, S. (2010). The Habenula Prevents Helpless Behavior in Larval Zebrafish. Curr Biol 20, 2211-2216.

Lee, H., Kim, D.W., Remedios, R., Anthony, T.E., Chang, A., Madisen, L., Zeng, H., and Anderson, D.J. (2014). Scalable control of mounting and attack by Esr1+ neurons in the ventromedial hypothalamus. Nature 509, 627-632.

Levoy, M., Ng, R., Adams, A., Footer, M., and Horowitz, M. (2006). Light field microscopy. Acm T Graphic 25, 924-934.

Lewis, C.M., Bosman, C.A., and Fries, P. (2015). Recording of brain activity across spatial scales. Curr Opin Neurobiol 32, 68-77.

Li, C.L., and Jasper, H. (1953). Microelectrode studies of the electrical activity of the cerebral cortex in the cat. J Physiol 121, 117-140.

Lim, B.K., Cho, S.J., Sumbre, G., and Poo, M.M. (2010). Region-Specific Contribution of Ephrin-B and Wnt Signaling to Receptive Field Plasticity in Developing Optic Tectum. Neuron 65, 899-911.

Lin, C.P., Chen, Y.P., and Hung, C.P. (2014). Tuning and spontaneous spike time synchrony share a common structure in macaque inferior temporal cortex. J Neurophysiol 112, 856-869.

Lin, J.Y., Lin, M.Z., Steinbach, P., and Tsien, R.Y. (2009). Characterization of Engineered Channelrhodopsin Variants with Improved Properties and Kinetics. Biophys J 96, 1803-1814.

Lindquist, D.H., Vogel, R.W., and Steinmetz, J.E. (2009). Associative and non-associative blinking in classically conditioned adult rats. Physiol Behav 96, 399-411.

Lister, J.A., Robertson, C.P., Lepage, T., Johnson, S.L., and Raible, D.W. (1999). nacre encodes a zebrafish microphthalmia-related protein that regulates neural-crest-derived pigment cell fate. Development 126, 3757-3767.

Ljunggren, E.E., Haupt, S., Ausborn, J., Ampatzis, K., and El Manira, A. (2014). Optogenetic Activation of Excitatory Premotor Interneurons Is Sufficient to Generate Coordinated Locomotor Activity in Larval Zebrafish. J Neurosci 34, 134-139.

Lo, S.Q., Koh, D.X., Sng, J.C., and Augustine, G.J. (2015). All-optical mapping of barrel cortex circuits based on simultaneous voltage-sensitive dye imaging and channelrhodopsin-mediated photostimulation. Neurophoton 2, 021013-021013.

Looger, L.L., and Griesbeck, O. (2012). Genetically encoded neural activity indicators. Curr Opin Neurobiol 22, 18-23.

Lovett-Barron, M., Kaifosh, P., Kheirbek, M.A., Danielson, N., Zaremba, J.D., Reardon, T.R., Turi, G.F., Hen, R., Zemelman, B.V., and Losonczy, A. (2014). Dendritic inhibition in the hippocampus supports fear learning. Science 343, 857-863.

Lowe, D.A. (1986). Organisation of lateral line and auditory areas in the midbrain of *Xenopus laevis*. J Comp Neurol 245, 498-513.

Lowe, D.A. (1987). Single-unit study of lateral line cells in the optic tectum of *Xenopus laevis*: evidence for bimodal lateral line/optic units. J Comp Neurol 257, 396-404.

Luiten, P.G.M. (1981). Afferent and efferent connections of the optic tectum in the carp (Cyprinus carpio L.). Brain Res 220, 51-65.

Lundby, A., Akemann, W., and Knopfel, T. (2010). Biophysical characterization of the fluorescent protein voltage probe VSFP2.3 based on the voltage-sensing domain of Ci-VSP. Eur Biophys J 39, 1625-1635.

Mann, K.D., Hoyt, C., Feldman, S., Blunt, L., Raymond, A., and Page-McCaw, P.S. (2010). Cardiac response to startle stimuli in larval zebrafish: sympathetic and parasympathetic components. Am J Physiol-Reg I 298, R1288-R1297.

Manuel, R., Gorissen, M., Roca, C.P., Zethof, J., van de Vis, H., Flik, G., and van den Bos, R. (2014). Inhibitory Avoidance Learning in Zebrafish (*Danio Rerio*): Effects of Shock Intensity and Unraveling Differences in Task Performance. Zebrafish 11, 341-352.

Markova, O., Mukhtarov, M., Real, E., Jacob, Y., and Bregestovski, P. (2008). Genetically encoded chloride indicator with improved sensitivity. J Neurosci Meth 170, 67-76.

Martin, S.J., Grimwood, P.D., and Morris, R.G.M. (2000). Synaptic plasticity and memory: an evaluation of the hypothesis. Annu Rev Neurosci 23, 649-711.

Matsui, H., Namikawa, K., Babaryka, A., and Koster, R.W. (2014). Functional regionalization of the teleost cerebellum analyzed in vivo. Proc Natl Acad Sci USA 111, 11846-11851.

Mauk, M.D. (1997). Roles of cerebellar cortex and nuclei in motor learning: Contradictions or clues? Neuron 18, 343-346.

Mauk, M.D., Steinmetz, J.E., and Thompson, R.F. (1986). Classical-Conditioning Using Stimulation of the Inferior Olive as the Unconditioned Stimulus. Proc Natl Acad Sci USA 83, 5349-5353.

Maynard, E.M., Hatsopoulos, N.G., Ojakangas, C.L., Acuna, B.D., Sanes, J.N., Normann, R.A., and Donoghue, J.P. (1999). Neuronal interactions improve cortical population coding of movement direction. J Neurosci 19, 8083-8093.

McCormick, C.A., and Hernandez, D.V. (1996). Connections of octaval and lateral line nuclei of the medulla in the goldfish, including the cytoarchitecture of the secondary octaval population in goldfish and catfish. Brain Behav Evolut 47, 113-137.

McCormick, D.A., Steinmetz, J.E., and Thompson, R.F. (1985). Lesions of the inferior olivary complex cause extinction of the classically conditioned eyeblink response. Brain Res 359, 120-130.

Mccormick, D.A., and Thompson, R.F. (1984). Neuronal Responses of the Rabbit Cerebellum during Acquisition and Performance of a Classically-Conditioned Nictitating Membrane-Eyelid Response. J Neurosci 4, 2811-2822.

McElligott, M.B., and O'Malley, D.M. (2005). Prey Tracking by Larval Zebrafish: Axial Kinematics and Visual Control. Brain Behav Evol 66, 177-196.

Meredith, M.A., and Stein, B.E. (1986). Visual, auditory, and somatosensory convergence on cells in superior colliculus results in multisensory integration. J Neurophysiol 56, 640-662.

Meyer, F. (1994). Topographic Distance and Watershed Lines. Signal Process 38, 113-125.

Miller, N., and Gerlai, R. (2012). From schooling to shoaling: patterns of collective motion in zebrafish (*Danio rerio*). PloS one 7, e48865.

Miller, E.W., Lin, J.Y., Frady, E.P., Steinbach, P.A., Kristan, W.B., Jr., and Tsien, R.Y. (2012). Optically monitoring voltage in neurons by photo-induced electron transfer through molecular wires. Proc Natl Acad Sci USA 109, 2114-2119.

Miri, A., Daie, K., Arrenberg, A.B., Baier, H., Aksay, E., and Tank, D.W. (2011). Spatial gradients and multidimensional dynamics in a neural integrator circuit. Nat Neurosci 14, 1150-1159.

Momosaki, S., Hatano, K., Kawasumi, Y., Kato, T., Hosoi, R., Kobayashi, K., Inoue, O., and Ito, K. (2004). Rat-PET study without anesthesia: Anesthetics modify the dopamine D1 receptor binding in rat brain. Synapse 54, 207-213.

Morin, C., Silva, M.A.D., Muller, C.P., Hardigan, P., and Spieler, R.E. (2013). Active avoidance learning in zebrafish (*Danio rerio*)-The role of sensory modality and inter-stimulus interval. Behav Brain Res 248, 141-143.

Mostany, R., Miquelajauregui, A., Shtrahman, M., and Portera-Cailliau, C. (2015). Two-Photon Excitation Microscopy and Its Applications in Neuroscience. In Advanced Fluorescence Microscopy, P.J. Verveer, ed. (Springer New York), pp. 25-42.

Movshon, J.A., Albright, T.D., Stoner, G.R., Majaj, N.J., and Smith, M.A. (2003). Cortical responses to visual motion in alert and anesthetized monkeys. Nat Neurosci 6, 3-3.

Mueller, T., Dong, Z., Berberoglu, M.A., and Guo, S. (2011). The Dorsal Pallium in Zebrafish, *Danio rerio* (Cyprinidae, Teleostei). Brain Res 1381, 95-105.

Mueller, T., and Wullimann, M.F. (2005). Atlas of Early Zebrafish Brain Development: A Tool for Molecular Neurogenetics (Amsterdam: Elsevier Science).

Mukamel, E.A., Nimmerjahn, A., and Schnitzer, M.J. (2009). Automated analysis of cellular signals from large-scale calcium imaging data. Neuron 63, 747-760.

Muto, A., Ohkura, M., Abe, G., Nakai, J., and Kawakami, K. (2013). Real-time visualization of neuronal activity during perception. Curr Biol 23, 307-311.

Nagel, G., Szellas, T., Huhn, W., Kateriya, S., Adeishvili, N., Berthold, P., Ollig, D., Hegemann, P., and Bamberg, E. (2003). Channelrhodopsin-2, a directly light-gated cation-selective membrane channel. Proc Natl Acad Sci USA 100, 13940-13945.

Nakai, J., Ohkura, M., and Imoto, K. (2001). A high signal-to-noise Ca(2+) probe composed of a single green fluorescent protein. Nat Biotechnol 19, 137-141.

Nevin, L.M., Robles, E., Baier, H., and Scott, E.K. (2010). Focusing on optic tectum circuitry through the lens of genetics. BMC biology 8, 126.

Niell, C.M., and Smith, S.J. (2005). Functional imaging reveals rapid development of visual response properties in the zebrafish tectum. Neuron 45, 941-951.

Nikolaou, N., Lowe, A.S., Walker, A.S., Abbas, F., Hunter, P.R., Thompson, I.D., and Meyer, M.P. (2012). Parametric functional maps of visual inputs to the tectum. Neuron 76, 317-324.

Northcutt, R.G. (1982). Localization of neurons afferent to the optic tectum in longnose gars. The Journal of comparative neurology 204, 325-335.

Obien, M.E., Deligkaris, K., Bullmann, T., Bakkum, D.J., and Frey, U. (2015). Revealing neuronal function through microelectrode array recordings. Front Neurosci 8, 423.

Oliveira, R.F., Silva, J.F., and Simoes, J.M. (2011). Fighting zebrafish: characterization of aggressive behavior and winner-loser effects. Zebrafish 8, 73-81.

Olsen, S.R., Bortone, D.S., Adesnik, H., and Scanziani, M. (2012). Gain control by layer six in cortical circuits of vision. Nature 483, 47-52.

Olshausen, B.A., and Field, D.J. (2004). Sparse coding of sensory inputs. Curr Opin Neurobiol 14, 481-487.

Olt, J., Johnson, S.L., and Marcotti, W. (2014). In vivo and in vitro biophysical properties of hair cells from the lateral line and inner ear of developing and adult zebrafish. J Physiol-London 592, 2041-2058.

Orger, M.B., Kampff, A.R., Severi, K.E., Bollmann, J.H., and Engert, F. (2008). Control of visually guided behavior by distinct populations of spinal projection neurons. Nat Neurosci 11, 327-333.

Owald, D., Lin, S., and Waddell, S. (2015). Light, heat, action: neural control of fruit fly behaviour. Philos Trans R Soc Lond B Biol Sci 370, 20140211.

Ozden, I., Lee, H.M., Sullivan, M.R., and Wang, S.S. (2008). Identification and Clustering of Event Patterns From In Vivo Multiphoton Optical Recordings of Neuronal Ensembles. J Neurophysiol 100, 495-503.

Pack, C.C., Berezovskii, V.K., and Born, R.T. (2001). Dynamic properties of neurons in cortical area MT in alert and anaesthetized macaque monkeys. Nature 414, 905-908.

Packer, A.M., Peterka, D.S., Hirtz, J.J., Prakash, R., Deisseroth, K., and Yuste, R. (2012). Two-photon optogenetics of dendritic spines and neural circuits. Nat Methods 9, 1202-U1103.

Packer, A.M., Roska, B., and Hausser, M. (2013). Targeting neurons and photons for optogenetics. Nat Neurosci 16, 805-815.

Packer, A.M., Russell, L.E., Dalgleish, H.W.P., and Hausser, M. (2015). Simultaneous all-optical manipulation and recording of neural circuit activity with cellular resolution in vivo. Nat Methods 12, 140-U186.

Panas, D., Amin, H., Maccione, A., Muthmann, O., van Rossum, M., Berdondini, L., and Hennig, M.H. (2015). Sloppiness in spontaneously active neuronal networks. J Neurosci 35, 8480-8492.

Panier, T., Romano, S.A., Olive, R., Pietri, T., Sumbre, G., Candelier, R., and Debregeas, G. (2013). Fast functional imaging of multiple brain regions in intact zebrafish larvae using Selective Plane Illumination Microscopy. Front Neural Circuit 7.

Papagiakoumou, E. (2013). Optical developments for optogenetics. Biol Cell 105, 443-464.

Park, H.C., Kim, C.H., Bae, Y.K., Yeo, S.Y., Kim, S.H., Hong, S.K., Shin, J., Yoo, K.W., Hibi, M., Hirano, T., et al. (2000). Analysis of upstream elements in the HuC promoter leads to the establishment of transgenic zebrafish with fluorescent neurons. Dev Biol 227, 279-293.

Patel, T.P., Man, K., Firestein, B.L., and Meaney, D.F. (2015). Automated quantification of neuronal networks and single-cell calcium dynamics using calcium imaging. J Neurosci Methods 243, 26-38.

Perez-Perez, M.P., Luque, M.A., Herrero, L., Nunez-Abades, P.A., and Torres, B. (2003). Afferent connectivity to different functional zones of the optic tectum in goldfish. Visual Neurosci 20, 397-410.

Perron, A., Mutoh, H., Launey, T., and Knöpfel, T. (2009). Red-Shifted Voltage-Sensitive Fluorescent Proteins. Chem Biol 16, 1268-1277.

Peterka, D.S., Takahashi, H., and Yuste, R. (2011). Imaging voltage in neurons. Neuron 69, 9-21.

Peyrache, A., Benchenane, K., Khamassi, M., Wiener, S.I., and Battaglia, F.P. (2010). Principal component analysis of ensemble recordings reveals cell assemblies at high temporal resolution. J Comput Neurosci 29, 309-325.

Pitrone, P.G., Schindelin, J., Stuyvenberg, L., Preibisch, S., Weber, M., Eliceiri, K.W., Huisken, J., and Tomancak, P. (2013). OpenSPIM: an open-access light-sheet microscopy platform. Nat Methods 10, 598-599.

Portugues, R., and Engert, F. (2009). The neural basis of visual behaviors in the larval zebrafish. Curr Opin Neurobiol 19, 644-647.

Portugues, R., Severi, K.E., Wyart, C., and Ahrens, M.B. (2013). Optogenetics in a transparent animal: circuit function in the larval zebrafish. Curr Opin Neurobiol 23, 119-126.

Pouget, A., Dayan, P., and Zemel, R. (2000). Information processing with population codes. Nat Rev Neurosci 1, 125-132.

Prakash, R., Yizhar, O., Grewe, B., Ramakrishnan, C., Wang, N., Goshen, I., Packer, A.M., Peterka, D.S., Yuste, R., Schnitzer, M.J., et al. (2012). Two-photon optogenetic toolbox for fast inhibition, excitation and bistable modulation. Nat Methods 9, 1171-1179.

Pratt, K.G., and Aizenman, C.D. (2007). Homeostatic regulation of intrinsic excitability and synaptic transmission in a developing visual circuit. J Neurosci 27, 8268-8277.

Pratt, K.G., Dong, W., and Aizenman, C.D. (2008). Development and spike timing-dependent plasticity of recurrent excitation in the Xenopus optic tectum. Nat Neurosci 11, 467-475.

Preuss, S.J., Trivedi, C.A., vom Berg-Maurer, C.M., Ryu, S., and Bollmann, J.H. (2014). Classification of object size in retinotectal microcircuits. Curr Biol 24, 2376-2385.

Prevedel, R., Yoon, Y.G., Hoffmann, M., Pak, N., Wetzstein, G., Kato, S., Schrodel, T., Raskar, R., Zimmer, M., Boyden, E.S., et al. (2014). Simultaneous whole-animal

3D imaging of neuronal activity using light-field microscopy. Nat Methods 11, 727-U161.

Prut, Y., Vaadia, E., Bergman, H., Haalman, I., Slovin, H., and Abeles, M. (1998). Spatiotemporal structure of cortical activity: properties and behavioral relevance. J Neurophysiol 79, 2857-2874.

Quirin, S., Jackson, J., Peterka, D.S., and Yuste, R. (2014). Simultaneous imaging of neural activity in three dimensions. Front Neural Circuit 8.

Ramdya, P., and Engert, F. (2008). Emergence of binocular functional properties in a monocular neural circuit. Nat Neurosci 11, 1083-1090.

Rinberg, D., Koulakov, A., and Gelperin, A. (2006). Sparse odor coding in awake behaving mice. J Neurosci 26, 8857-8865.

Roberts, A.C., Bill, B.R., and Glanzman, D.L. (2013). Learning and Memory in Zebrafish Larvae. Front Neural Circuit 7, 126.

Robles, E., Filosa, A., and Baier, H. (2013). Precise lamination of retinal axons generates multiple parallel input pathways in the tectum. J Neurosci 33, 5027-5039.

Robles, E., Laurell, E., and Baier, H. (2014). The retinal projectome reveals brain-area-specific visual representations generated by ganglion cell diversity. Curr Biol 24, 2085-2096.

Robles, E., Smith, S.J., and Baier, H. (2011). Characterization of genetically targeted neuron types in the zebrafish optic tectum. Front Neural Circuits 5, 1.

Rochefort, N.L., Garaschuk, O., Milos, R.I., Narushima, M., Marandi, N., Pichler, B., Kovalchuk, Y., and Konnerth, A. (2009). Sparsification of neuronal activity in the visual cortex at eye-opening. Proc Natl Acad Sci USA 106, 15049-15054.

Rodriguez, A., and Laio, A. (2014). Machine learning. Clustering by fast search and find of density peaks. Science 344, 1492-1496.

Rodriguez, F., Duran, E., Gomez, A., Ocana, F.M., Alvarez, E., Jimenez-Moya, F., Broglio, C., and Salas, C. (2005). Cognitive and emotional functions of the teleost fish cerebellum. Brain Res Bull 66, 365-370.

Roeser, T., and Baier, H. (2003). Visuomotor behaviors in larval zebrafish after GFP-guided laser ablation of the optic tectum. J Neurosci 23, 3726-3734.

Romano, S.A., Pietri, T., Perez-Schuster, V., Jouary, A., Haudrechy, M., and Sumbre, G. (2015). Spontaneous neuronal network dynamics reveal circuit's functional adaptations for behavior. Neuron 85, 1070-1085.

Rombough, P. (2002). Gills are needed for ionoregulation before they are needed for O(2) uptake in developing zebrafish, *Danio rerio*. J Exp Biol 205, 1787-1794.

Ross, W.N. (1989). Changes in Intracellular Calcium During Neuron Activity. Annu Rev Physiol 51, 491-506.

Sachse, S., and Galizia, C.G. (2002). Role of Inhibition for Temporal and Spatial Odor Representation in Olfactory Output Neurons: A Calcium Imaging Study. Journal of neurophysiology 87, 1106-1117.

Sakai, R., Repunte-Canonigo, V., Raj, C.D., and Knopfel, T. (2001). Design and characterization of a DNA-encoded, voltage-sensitive fluorescent protein. Eur J Neurosci 13, 2314-2318.

Salas, C., Broglio, C., Duran, E., Gomez, A., Ocana, F.M., Jimenez-Moya, F., and Rodriguez, F. (2006). Neuropsychology of Learning and Memory in Teleost Fish. Zebrafish 3, 157-171.

Sanger, T.D. (2003). Neural population codes. Curr Opin Neurobiol 13, 238-249.

Sankaranarayanan, S., De Angelis, D., Rothman, J.E., and Ryan, T.A. (2000). The use of pHluorins for optical measurements of presynaptic activity. Biophys J 79, 2199-2208.

Sato, T., Uchida, G., Lescroart, M.D., Kitazono, J., Okada, M., and Tanifuji, M. (2013). Object representation in inferior temporal cortex is organized hierarchically in a mosaic-like structure. J Neurosci 33, 16642-16656.

Sauer, B. (1998). Inducible gene targeting in mice using the Cre/lox system. Methods 14, 381-392.

Scanziani, M., and Hausser, M. (2009). Electrophysiology in the age of light. Nature 461, 930-939.

Scheibler, P., Kronfeld, A., Illes, P., and Allgaier, C. (1999). Trichloroethanol impairs NMDA receptor function in rat mesencephalic and cortical neurones. Eur J Pharmacol 366, R1-R2.

Schneider, D.M., Nelson, A., and Mooney, R. (2014). A synaptic and circuit basis for corollary discharge in the auditory cortex. Nature 513, 189-194.

Schoonheim, P.J., Arrenberg, A.B., Del Bene, F., and Baier, H. (2010). Optogenetic localization and genetic perturbation of saccade-generating neurons in zebrafish. J Neurosci 30, 7111-7120.

Schuetze, S.M. (1983). The Discovery of the Action-Potential. Trends Neurosci 6, 164-168.

Scott, E.K. (2009). The Gal4/UAS toolbox in zebrafish: new approaches for defining behavioral circuits. J Neurochem 110, 441-456.

Scott, E.K., and Baier, H. (2009). The cellular architecture of the larval zebrafish tectum, as revealed by Gal4 enhancer trap lines. Front Neural Circuit 3.

Scott, E.K., Mason, L., Arrenberg, A.B., Ziv, L., Gosse, N.J., Xiao, T., Chi, N.C., Asakawa, K., Kawakami, K., and Baier, H. (2007). Targeting neural circuitry in zebrafish using GAL4 enhancer trapping. Nat Methods 4, 323-326.

Sejnowski, T.J., Churchland, P.S., and Movshon, J.A. (2014). Putting big data to good use in neuroscience. Nat Neurosci 17, 1440-1441.

Series, P., Latham, P.E., and Pouget, A. (2004). Tuning curve sharpening for orientation selectivity: coding efficiency and the impact of correlations. Nat Neurosci 7, 1129-1135.

Seth, A.K., Barrett, A.B., and Barnett, L. (2015). Granger causality analysis in neuroscience and neuroimaging. J Neurosci 35, 3293-3297.

Seung, H.S., and Sompolinsky, H. (1993). Simple models for reading neuronal population codes. Proc Natl Acad Sci USA 90, 10749-10753.

Shadlen, M.N., Britten, K.H., Newsome, W.T., and Movshon, J.A. (1996). A computational analysis of the relationship between neuronal and behavioral responses to visual motion. J Neurosci 16, 1486-1510.

Shin, J., Chen, J., and Solnica-Krezel, L. (2014). Efficient homologous recombination-mediated genome engineering in zebrafish using TALE nucleases. Development 141, 3807-3818.

Siegelbaum, S.A., and Kandel, E.R. (1991). Learning-related synaptic plasticity: LTP and LTD. Curr Opin Neurobiol 1, 113-120.

Siegman, A.E. (1986). Lasers (Mill Valley, Calif.: University Science Books).

Simms, B.A., and Zamponi, G.W. (2014). Neuronal voltage-gated calcium channels: structure, function, and dysfunction. Neuron 82, 24-45.

Singer, W. (1999). Neuronal synchrony: a versatile code for the definition of relations? Neuron 24, 49-65, 111-125.

Spanne, A., and Jörntell, H. (2015). Questioning the role of sparse coding in the brain. Trends Neurosci 38, 417-427.

Spira, M.E., and Hai, A. (2013). Multi-electrode array technologies for neuroscience and cardiology. Nat Nanotech 8, 83-94.

Stein, B.E. (1998). Neural mechanisms for synthesizing sensory information and producing adaptive behaviors. Experimental brain research 123, 124-135.

Stein, B.E., and Gaither, N.S. (1981). Sensory Representation in Reptilian Optic Tectum - Some Comparisons with Mammals. J Comp Neurol 202, 69-87.

Stein, B.E., and Gaither, N.S. (1983). Receptive-field properties in reptilian optic tectum: some comparisons with mammals. J Neurophysiol 50, 102-124.

Stein, B.E., Jiang, W., Wallace, M.T., and Stanford, T.R. (2001). Nonvisual influences on visual-information processing in the superior colliculus. Prog Brain Res 134, 143-156.

Stein, B.E., Magalhaes-Castro, B., and Kruger, L. (1975). Superior colliculus: visuotopic-somatotopic overlap. Science 189, 224-226.

Steinmetz, A.B., Edwards, C.R., Steinmetz, J.E., and Hetrick, W.P. (2009). Comparison of auditory and visual conditioning stimuli in delay eyeblink conditioning in healthy young adults. Learn Behav 37, 349-356.

Steinmetz, J.E., Lavond, D.G., and Thompson, R.F. (1989). Classical-Conditioning in Rabbits Using Pontine Nucleus Stimulation as a Conditioned-Stimulus and Inferior Olive Stimulation as an Unconditioned Stimulus. Synapse 3, 225-233.

Steinmetz, J.E., Logan, C.G., Rosen, D.J., Thompson, J.K., Lavond, D.G., and Thompson, R.F. (1987). Initial Localization of the Acoustic Conditioned-Stimulus Projection System to the Cerebellum Essential for Classical Eyelid Conditioning. Proc Natl Acad Sci USA 84, 3531-3535.

Steinmetz, J.E., Rosen, D.J., Chapman, P.F., Lavond, D.G., and Thompson, R.F. (1986). Classical-Conditioning of the Rabbit Eyelid Response with a Mossy-Fiber Stimulation Cs .1. Pontine Nuclei and Middle Cerebellar Peduncle Stimulation. Behav Neurosci 100, 878-887.

Strick, P.L., Dum, R.P., and Fiez, J.A. (2009). Cerebellum and Nonmotor Function. Annu Rev Neurosci 32, 413-434.

Stuart, G.W., McMurray, J.V., and Westerfield, M. (1988). Replication, integration and stable germ-line transmission of foreign sequences injected into early zebrafish embryos. Development 103, 403-412.

Stuart, G.W., Vielkind, J.R., McMurray, J.V., and Westerfield, M. (1990). Stable lines of transgenic zebrafish exhibit reproducible patterns of transgene expression. Development 109, 577-584.

Stuermer, C.A.O. (1988). Retinotopic Organization of the Developing Retinotectal Projection in the Zebrafish Embryo. J Neurosci 8, 4513-4530.

Subach, F.V., Patterson, G.H., Renz, M., Lippincott-Schwartz, J., and Verkhusha, V.V. (2010). Bright monomeric photoactivatable red fluorescent protein for two-color super-resolution sptPALM of live cells. J Am Chem Soc 132, 6481-6491.

Suli, A., Watson, G.M., Rubel, E.W., and Raible, D.W. (2012). Rheotaxis in larval zebrafish is mediated by lateral line mechanosensory hair cells. PloS one 7, e29727.

Sumbre, G., Muto, A., Baier, H., and Poo, M.M. (2008). Entrained rhythmic activities of neuronal ensembles as perceptual memory of time interval. Nature 456, 102-106.

Szobota, S., Gorostiza, P., Del Bene, F., Wyart, C., Fortin, D.L., Kolstad, K.D., Tulyathan, O., Volgraf, M., Numano, R., Aaron, H.L., et al. (2007). Remote control of neuronal activity with a light-gated glutamate receptor. Neuron 54, 535-545.

Tabor, K.M., Bergeron, S.A., Horstick, E.J., Jordan, D.C., Aho, V., Porkka-Heiskanen, T., Haspel, G., and Burgess, H.A. (2014). Direct activation of the Mauthner cell by electric field pulses drives ultrarapid escape responses. J Neurophysiol 112, 834-844.

Tanaka, K. (1997). Columnar Organization in the Inferotemporal Cortex. In Extrastriate Cortex in Primates, K.S. Rockland, J.H. Kaas, and A. Peters, eds. (Springer US), pp. 469-498.

Tantama, M., Hung, Y.P., and Yellen, G. (2012). Optogenetic reporters: Fluorescent protein-based genetically encoded indicators of signaling and metabolism in the brain. Prog Brain Res 196, 235-263.

Temizer, I., Donovan, J.C., Baier, H., and Semmelhack, J.L. (2015). A Visual Pathway for Looming-Evoked Escape in Larval Zebrafish. Curr Biol 25, 1823-1834.

Thevenaz, P., Ruttimann, U.E., and Unser, M. (1998). A pyramid approach to subpixel registration based on intensity. IEEE transactions on image processing : a publication of the IEEE Signal Processing Society 7, 27-41.

Thiele, T.R., Donovan, J.C., and Baier, H. (2014). Descending control of swim posture by a midbrain nucleus in zebrafish. Neuron 83, 679-691.

Thompson, R.F., and Steinmetz, J.E. (2009). The Role of the Cerebellum in Classical Conditioning of Discrete Behavioral Responses. Neuroscience 162, 732-755.

Thummel, R., Burket, C.T., Brewer, J.L., Sarras, M.P., Jr., Li, L., Perry, M., McDermott, J.P., Sauer, B., Hyde, D.R., and Godwin, A.R. (2005). Cre-mediated site-specific recombination in zebrafish embryos. Dev Dyn 233, 1366-1377.

Tian, L., Akerboom, J., Schreiter, E.R., and Looger, L.L. (2012). Neural activity imaging with genetically encoded calcium indicators. In Prog Brain Res, T. Knöpfel, and E.S. Boyden, eds. (Elsevier), pp. 79-94.

Tian, L., Hires, S.A., Mao, T., Huber, D., Chiappe, M.E., Chalasani, S.H., Petreanu, L., Akerboom, J., McKinney, S.A., Schreiter, E.R., et al. (2009). Imaging neural activity in worms, flies and mice with improved GCaMP calcium indicators. Nat Methods 6, 875-881.

Tracy, C.A., and Widom, H. (1993). Level-Spacing Distributions and the Airy Kernel. Phys Lett B 305, 115-118.

Triplett, J.W., Phan, A., Yamada, J., and Feldheim, D.A. (2012). Alignment of multimodal sensory input in the superior colliculus through a gradient-matching mechanism. J Neurosci 32, 5264-5271.

Tsien, R.Y. (1980). New calcium indicators and buffers with high selectivity against magnesium and protons: design, synthesis, and properties of prototype structures. Biochemistry 19, 2396-2404.

Tsien, R.Y., Pozzan, T., and Rink, T.J. (1982). Calcium homeostasis in intact lymphocytes: cytoplasmic free calcium monitored with a new, intracellularly trapped fluorescent indicator. J Cell Biol 94, 325-334.

Tsuchiya, R., Yoshiki, F., Kudo, Y., and Morita, M. (2002). Cell type-selective expression of green fluorescent protein and the calcium indicating protein, yellow cameleon, in rat cortical primary cultures. Brain Res 956, 221-229.

Tsytsarev, V., Liao, L.D., Kong, K.V., Liu, Y.H., Erzurumlu, R.S., Olivo, M., and Thakor, N.V. (2014). Recent Progress in Voltage-Sensitive Dye Imaging for Neuroscience. J Nanosci Nanotechnol 14, 4733-4744.

Tye, K.M., Prakash, R., Kim, S.Y., Fenno, L.E., Grosenick, L., Zarabi, H., Thompson, K.R., Gradinaru, V., Ramakrishnan, C., and Deisseroth, K. (2011). Amygdala circuitry mediating reversible and bidirectional control of anxiety. Nature 471, 358-362.

Valente, A., Huang, K.H., Portugues, R., and Engert, F. (2012). Ontogeny of classical and operant learning behaviors in zebrafish. Learn Memory 19, 170-177.

Vaziri, A., and Emiliani, V. (2012). Reshaping the optical dimension in optogenetics. Curr Opin Neurobiol 22, 128-137.

Venkatachalam, V., and Cohen, A.E. (2014). Imaging GFP-Based Reporters in Neurons with Multiwavelength Optogenetic Control. Biophys J 107, 1554-1563.

Veres, A., Gosis, B.S., Ding, Q., Collins, R., Ragavendran, A., Brand, H., Erdin, S., Cowan, C.A., Talkowski, M.E., and Musunuru, K. (2014). Low incidence of off-target mutations in individual CRISPR-Cas9 and TALEN targeted human stem cell clones detected by whole-genome sequencing. Cell Stem Cell 15, 27-30.

Vladimirov, N., Mu, Y., Kawashima, T., Bennett, D.V., Yang, C.T., Looger, L.L., Keller, P.J., Freeman, J., and Ahrens, M.B. (2014). Light-sheet functional imaging in fictively behaving zebrafish. Nat Methods, 883-884.

Vogels, R. (1990). Population coding of stimulus orientation by striate cortical cells. Biol Cybern 64, 25-31.

Vogelstein, J.T., Packer, A.M., Machado, T.A., Sippy, T., Babadi, B., Yuste, R., and Paninski, L. (2010). Fast nonnegative deconvolution for spike train inference from population calcium imaging. J Neurophysiol 104, 3691-3704.

Wallace, M.T., Meredith, M.A., and Stein, B.E. (1993). Converging influences from visual, auditory, and somatosensory cortices onto output neurons of the superior colliculus. J Neurophysiol 69, 1797-1809.

Wang, H., Peca, J., Matsuzaki, M., Matsuzaki, K., Noguchi, J., Qiu, L., Wang, D., Zhang, F., Boyden, E., Deisseroth, K., et al. (2007). High-speed mapping of synaptic connectivity using photostimulation in Channelrhodopsin-2 transgenic mice. Proc Natl Acad Sci USA 104, 8143-8148.

Warp, E., Agarwal, G., Wyart, C., Friedmann, D., Oldfield, C.S., Conner, A., Del Bene, F., Arrenberg, A.B., Baier, H., and Isacoff, E.Y. (2012). Emergence of Patterned Activity in the Developing Zebrafish Spinal Cord. Curr Biol 22, 93-102.

Westerfield, M. (2000). The zebrafish book: A guide for the laboratory use of zebrafish *Danio* (*Brachydanio*) *rerio*, 4 edn (Eugene: Univ. of Oregon Press).

Williams, R.W. (2000). Mapping Genes that Modulate Mouse Brain Development: A Quantitative Genetic Approach. In Mouse Brain Development, A.M. Goffinet, and P. Rakic, eds. (Springer Berlin Heidelberg), pp. 21-49.

Wilson, T., and Sheppard, C. (1984). Theory and practice of scanning optical microscopy (London: Academic Press).

Winship, I.R., and Murphy, T.H. (2008). In Vivo Calcium Imaging Reveals Functional Rewiring of Single Somatosensory Neurons after Stroke. J Neurosci 28, 6592-6606.

Witten, I.B., Lin, S.C., Brodsky, M., Prakash, R., Diester, I., Anikeeva, P., Gradinaru, V., Ramakrishnan, C., and Deisseroth, K. (2010). Cholinergic interneurons control local circuit activity and cocaine conditioning. Science 330, 1677-1681.

Wullimann, M.F., and Northcutt, R.G. (1990). Visual and electrosensory circuits of the diencephalon in mormyrids: an evolutionary perspective. The Journal of comparative neurology 297, 537-552.

Wyart, C., and Del Bene, F. (2011). Let there be light: zebrafish neurobiology and the optogenetic revolution. Rev Neurosci 22, 121-130.

Xu, H., Khakhalin, A.S., Nurmikko, A.V., and Aizenman, C.D. (2011). Visual Experience-Dependent Maturation of Correlated Neuronal Activity Patterns in a Developing Visual System. J Neurosci 31, 8025-8036.

Xu, X.J., Scott-Scheiern, T., Kempker, L., and Simons, K. (2007). Active avoidance conditioning in zebrafish (*Danio rerio*). Neurobiol Learn Mem 87, 72-77.

Yaksi, E., and Friedrich, R.W. (2006). Reconstruction of firing rate changes across neuronal populations by temporally deconvolved Ca2+ imaging. Nat Methods 3, 377-383.

Yizhar, O., Fenno, L.E., Davidson, T.J., Mogri, M., and Deisseroth, K. (2011). Optogenetics in Neural Systems. Neuron 71, 9-34.

Yizhar, O., Fenno, L.E., Prigge, M., Schneider, F., Davidson, T.J., O'Shea, D.J., Sohal, V.S., Goshen, I., Finkelstein, J., Paz, J.T., et al. (2011). Neocortical excitation/inhibition balance in information processing and social dysfunction. Nature 477, 171-178.

Zahar, Y., Reches, A., and Gutfreund, Y. (2009). Multisensory Enhancement in the Optic Tectum of the Barn Owl: Spike Count and Spike Timing. J Neurophysiol 101, 2380-2394.

Zeddies, D.G., and Fay, R.R. (2005). Development of the acoustically evoked behavioral response in zebrafish to pure tones. J Exp Biol 208, 1363-1372.

Zhang, F., Cong, L., Stuber, G.D., Adamantidis, A., and Deisseroth, K. (2012). Analysis of Neuronal Circuits with Optogenetics. In Controlled Genetic Manipulations, A. Morozov, ed. (Humana Press), pp. 207-223.

Zhang, F., Prigge, M., Beyriere, F., Tsunoda, S.P., Mattis, J., Yizhar, O., Hegemann, P., and Deisseroth, K. (2008). Red-shifted optogenetic excitation: a tool for fast neural control derived from Volvox carteri. Nat Neurosci 11, 631-633.

Zhao, Y., Araki, S., Wu, J., Teramoto, T., Chang, Y.F., Nakano, M., Abdelfattah, A.S., Fujiwara, M., Ishihara, T., Nagai, T., et al. (2011). An expanded palette of genetically encoded Ca(2)(+) indicators. Science 333, 1888-1891.

Zhou, W.L., Yan, P., Wuskell, J.P., Loew, L.M., and Antic, S.D. (2007). Intracellular long-wavelength voltage-sensitive dyes for studying the dynamics of action potentials in axons and thin dendrites. J Neurosci Meth 164, 225-239.

Appendices

Movie 1. *elavl3*:Gal4;UAS:GCaMP5G expression between 25 and 125 µm below the skin in the tectum of a 7 dpf larval zebrafish. Images acquired at 40 Hz with 2 µm intervals using the selective plane illumination microscope described in Chapter 2.

Movie 2. Comparison between responses of 7 dpf larval zebrafish at the beginning and end of training during the classical conditioning assay outlined in Chapter 3. Tail flick responses are seen during presentation of the tone at the end of the assay (right) that are not seen during the early trials (left). Onset of the tone and shock are indicated in the top right of each panel.

Movie 3. Example of GCaMP5G responses 75 µm below the skin in the right tectum of a 6 dpf zebrafish (left) to the presentation of four different visual stimuli, as well as water flow and auditory stimuli (right). Representations of non-visual stimuli are for interpretation only and were not shown to fish. Movie is shown at 2x normal speed.

Appendix 1: Shock cancellation code

```
function image_Fish_noshock()
global C;
global vid;
global shockGate;
global toneonset;
global shockonset;
global pahandle;
global currdate;

pause(1.0);
flushdata(vid,'all');
pause(1.0);

H = fspecial('gaussian',3,10);
toneonset = 100;
shockonset = 108;
circBuffer = 200;
Frame = cell(double(circBuffer),1);
C = [];
dist = 1;

shockGate = false;


i = 1;

for i = 1:circBuffer

    if i < toneonset

        trigger(vid);
        x = getdata(vid);
        Frame{i} = deal(x);
        I1 = imcrop(x, [30 30 365 565]);
        maxx = max(I1(:));
        m1 = double(maxx)/255;
        m3 = double(m1)*0.5;
        I1 = imadjust(I1, [0;double(m1)],[]);
        minn = (min(I1(:))+0.5);
        m2 = (double(minn)*(130*(double(minn)^(-0.94))))/255;
        I1 = imadjust(I1, [0;double(m2)],[]);
        I1 = imadjust(I1, [], [],0.7);
        I1 = imadjust(I1, [double(m3);double(m1)],[]);
        I1 = imfilter(I1,H);
        I1 = imcrop(I1,[6 6 353 553]);
        minn2 = min(min(I1));
        m4 = double(minn2)/255;
        if m4 < 0.9
            I1 = imadjust(I1, [double(m4);0.9],[]);
        else
            I1 = imadjust(I1, [0.9;0.99],[]);
        end
        I1 = im2bw(I1,0.5);
        I1 = ~I1;
        a = regionprops(I1,'centroid');
        if isempty(a) == false
```

```
            b = a(1,1).Centroid;
            C = [C;b];
        else
            b = [1 1];
            C = [C;b];
        end

        if i > 5
            D1 = [C(i-3,:);C(i-2,:)];
            D2 = [C(i-2,:);C(i-1,:)];
            D3 = [C(i-1,:);C(i,:)];
            dist =
pdist(D1,'euclidean')+pdist(D2,'euclidean')+pdist(D3,'euclidean');
        end


    elseif i == toneonset
        PsychPortAudio('Start', pahandle);
        trigger(vid);
        x = getdata(vid);
        Frame{i} = deal(x);
        I1 = imcrop(x, [30 30 365 565]);
        maxx = max(I1(:));
        m1 = double(maxx)/255;
        m3 = double(m1)*0.5;
        I1 = imadjust(I1, [0;double(m1)],[]);
        minn = (min(I1(:))+0.5);
        m2 = (double(minn)*(130*(double(minn)^(-0.94))))/255;
        I1 = imadjust(I1, [0;double(m2)],[]);
        I1 = imadjust(I1, [], [],0.7);
        I1 = imadjust(I1, [double(m3);double(m1)],[]);
        I1 = imfilter(I1,H);
        I1 = imcrop(I1,[6 6 359 559]);
        minn2 = min(min(I1));
        m4 = double(minn2)/255;
        if m4 < 0.9
            I1 = imadjust(I1, [double(m4);0.9],[]);
        else
            I1 = imadjust(I1, [0.9;0.99],[]);
        end
        I1 = im2bw(I1,0.5);
        I1 = ~I1;
        a = regionprops(I1,'centroid');
        if isempty(a) == false
            b = a(1,1).Centroid;
            C = [C;b];
        else
            b = [1 1];
            C = [C;b];
        end

        D1 = [C(i-3,:);C(i-2,:)];
        D2 = [C(i-2,:);C(i-1,:)];
        D3 = [C(i-1,:);C(i,:)];
        dist =
pdist(D1,'euclidean')+pdist(D2,'euclidean')+pdist(D3,'euclidean');

    elseif i == shockonset
```

```
        trigger(vid);
        x = getdata(vid);
        Frame{i} = deal(x);
        I1 = imcrop(x, [30 30 365 565]);
        maxx = max(I1(:));
        m1 = double(maxx)/255;
        m3 = double(m1)*0.5;
        I1 = imadjust(I1, [0;double(m1)],[]);
        minn = (min(I1(:))+0.5);
        m2 = (double(minn)*(130*(double(minn)^(-0.94))))/255;
        I1 = imadjust(I1, [0;double(m2)],[]);
        I1 = imadjust(I1, [], [],0.7);
        I1 = imadjust(I1, [double(m3);double(m1)],[]);
        I1 = imfilter(I1,H);
        I1 = imcrop(I1,[6 6 359 559]);
        minn2 = min(min(I1));
        m4 = double(minn2)/255;
        if m4 < 0.9
            I1 = imadjust(I1, [double(m4);0.9],[]);
        else
            I1 = imadjust(I1, [0.9;0.99],[]);
        end
        I1 = im2bw(I1,0.5);
        I1 = ~I1;
        a = regionprops(I1,'centroid');
        if isempty(a) == false
            b = a(1,1).Centroid;
            C = [C;b];
        else
            b = [1 1];
            C = [C;b];
        end

        D1 = [C(i-3,:);C(i-2,:)];
        D2 = [C(i-2,:);C(i-1,:)];
        D3 = [C(i-1,:);C(i,:)];
        dist =
pdist(D1,'euclidean')+pdist(D2,'euclidean')+pdist(D3,'euclidean');


    elseif i <= circBuffer
        trigger(vid);
        x = getdata(vid);
        Frame{i} = deal(x);
        I1 = imcrop(x, [30 30 365 565]);
        maxx = max(I1(:));
        m1 = double(maxx)/255;
        m3 = double(m1)*0.5;
        I1 = imadjust(I1, [0;double(m1)],[]);
        minn = (min(I1(:))+0.5);
        m2 = (double(minn)*(130*(double(minn)^(-0.94))))/255;
        I1 = imadjust(I1, [0;double(m2)],[]);
        I1 = imadjust(I1, [], [],0.7);
        I1 = imadjust(I1, [double(m3);double(m1)],[]);
        I1 = imfilter(I1,H);
        I1 = imcrop(I1,[6 6 359 559]);
        minn2 = min(min(I1));
        m4 = double(minn2)/255;
        if m4 < 0.9
            I1 = imadjust(I1, [double(m4);0.9],[]);
        else
```

```
            I1 = imadjust(I1, [0.9;0.99],[]);
        end
        I1 = im2bw(I1,0.5);
        I1 = ~I1;
        a = regionprops(I1,'centroid');
        if isempty(a) == false
            b = a(1,1).Centroid;
            C = [C;b];
        else
            b = [1 1];
            C = [C;b];
        end

        D1 = [C(i-3,:);C(i-2,:)];
        D2 = [C(i-2,:);C(i-1,:)];
        D3 = [C(i-1,:);C(i,:)];
        dist =
pdist(D1,'euclidean')+pdist(D2,'euclidean')+pdist(D3,'euclidean');


    end

    flushdata(vid,'triggers');
    imshow(x);

end

currTime = datestr(now,'ddmmyy_HHMMSS');
Mov = VideoWriter(['C:\Users\scott lab\Documents\Andrews Folder\1month old
free swimming conditioning tests\' currdate '\Mov_' currTime '_ns.avi']);
open(Mov);
j = 1;
while j <= circBuffer
    if isempty(Frame{j,1}) ~= 1
        writeVideo(Mov, Frame{j});
    end
    j = j+1;
end

shockGate = false;

close(Mov);

flushdata(vid, 'all');
close
```

```
function image_Fish()
global C;
global vid;
global shockGate;
global toneonset;
global shockonset;
global pahandle;
global s;
global currdate;

pause(1.0);
flushdata(vid,'all');
pause(1.0);

H = fspecial('gaussian',3,10);
toneonset = 100;
shockonset = 108;
circBuffer = 200;
Frame = cell(double(circBuffer),1);
C = [];

shockGate = false;


i = 1;

for i = 1:circBuffer

    if i < toneonset

        trigger(vid);
        x = getdata(vid);
        Frame{i} = deal(x);
        I1 = imcrop(x, [30 30 365 565]);
        maxx = max(I1(:));
        m1 = double(maxx)/255;
        m3 = double(m1)*0.5;
        I1 = imadjust(I1, [0;double(m1)],[]);
        minn = (min(I1(:))+0.5);
        m2 = (double(minn)*(130*(double(minn)^(-0.94))))/255;
        I1 = imadjust(I1, [0;double(m2)],[]);
        I1 = imadjust(I1, [], [],0.7);
        I1 = imadjust(I1, [double(m3);double(m1)],[]);
        I1 = imfilter(I1,H);
        I1 = imcrop(I1,[6 6 353 553]);
        minn2 = min(min(I1));
        m4 = double(minn2)/255;
        if m4 < 0.9
            I1 = imadjust(I1, [double(m4);0.9],[]);
        else
            I1 = imadjust(I1, [0.9;0.99],[]);
        end
        I1 = im2bw(I1,0.5);
        I1 = ~I1;
        a = regionprops(I1,'centroid');
        if isempty(a) == false
            b = a(1,1).Centroid;
            C = [C;b];
        else
            b = [1 1];
```

```
            C = [C;b];
        end



    elseif i == toneonset
        PsychPortAudio('Start', pahandle);
        trigger(vid);
        x = getdata(vid);
        Frame{i} = deal(x);
        I1 = imcrop(x, [30 30 365 565]);
        maxx = max(I1(:));
        m1 = double(maxx)/255;
        m3 = double(m1)*0.5;
        I1 = imadjust(I1, [0;double(m1)],[]);
        minn = (min(I1(:))+0.5);
        m2 = (double(minn)*(130*(double(minn)^(-0.94))))/255;
        I1 = imadjust(I1, [0;double(m2)],[]);
        I1 = imadjust(I1, [], [],0.7);
        I1 = imadjust(I1, [double(m3);double(m1)],[]);
        I1 = imfilter(I1,H);
        I1 = imcrop(I1,[6 6 359 559]);
        minn2 = min(min(I1));
        m4 = double(minn2)/255;
        if m4 < 0.9
            I1 = imadjust(I1, [double(m4);0.9],[]);
        else
            I1 = imadjust(I1, [0.9;0.99],[]);
        end
        I1 = im2bw(I1,0.5);
        I1 = ~I1;
        a = regionprops(I1,'centroid');
        if isempty(a) == false
            b = a(1,1).Centroid;
            C = [C;b];
        else
            b = [1 1];
            C = [C;b];
        end

        D0 = [C(i-4,:);C(i-3,:)];
        D1 = [C(i-3,:);C(i-2,:)];
        D2 = [C(i-2,:);C(i-1,:)];
        D3 = [C(i-1,:);C(i,:)];
        dist =
pdist(D0,'euclidean')+pdist(D1,'euclidean')+pdist(D2,'euclidean')+pdist(D3,
'euclidean');

        if (300 > dist) && (dist > 50)
            shockGate = true;
        end

    elseif (i > toneonset) && (i < shockonset)
        trigger(vid);
        x = getdata(vid);
        Frame{i} = deal(x);
        I1 = imcrop(x, [30 30 365 565]);
        maxx = max(I1(:));
        m1 = double(maxx)/255;
        m3 = double(m1)*0.5;
```

```
        I1 = imadjust(I1, [0;double(m1)],[]);
        minn = (min(I1(:))+0.5);
        m2 = (double(minn)*(130*(double(minn)^(-0.94))))/255;
        I1 = imadjust(I1, [0;double(m2)],[]);
        I1 = imadjust(I1, [], [],0.7);
        I1 = imadjust(I1, [double(m3);double(m1)],[]);
        I1 = imfilter(I1,H);
        I1 = imcrop(I1,[6 6 359 559]);
        minn2 = min(min(I1));
        m4 = double(minn2)/255;
        if m4 < 0.9
            I1 = imadjust(I1, [double(m4);0.9],[]);
        else
            I1 = imadjust(I1, [0.9;0.99],[]);
        end
        I1 = im2bw(I1,0.5);
        I1 = ~I1;
        a = regionprops(I1,'centroid');
        if isempty(a) == false
            b = a(1,1).Centroid;
            C = [C;b];
        else
            b = [1 1];
            C = [C;b];
        end

        D0 = [C(i-4,:);C(i-3,:)];
        D1 = [C(i-3,:);C(i-2,:)];
        D2 = [C(i-2,:);C(i-1,:)];
        D3 = [C(i-1,:);C(i,:)];
        dist =
pdist(D0,'euclidean')+pdist(D1,'euclidean')+pdist(D2,'euclidean')+pdist(D3,
'euclidean');

        if (300 > dist) && (dist > 50)
            shockGate = true;
        end

    elseif i == shockonset
        if shockGate == false
            set(s,'DataTerminalReady', 'off');
            WaitSecs(0.01);
            set(s,'DataTerminalReady', 'on');
        end
        trigger(vid);
        x = getdata(vid);
        Frame{i} = deal(x);
        I1 = imcrop(x, [30 30 365 565]);
        maxx = max(I1(:));
        m1 = double(maxx)/255;
        m3 = double(m1)*0.5;
        I1 = imadjust(I1, [0;double(m1)],[]);
        minn = (min(I1(:))+0.5);
        m2 = (double(minn)*(130*(double(minn)^(-0.94))))/255;
        I1 = imadjust(I1, [0;double(m2)],[]);
        I1 = imadjust(I1, [], [],0.7);
        I1 = imadjust(I1, [double(m3);double(m1)],[]);
        I1 = imfilter(I1,H);
        I1 = imcrop(I1,[6 6 359 559]);
        minn2 = min(min(I1));
        m4 = double(minn2)/255;
```

```
        if m4 < 0.9
            I1 = imadjust(I1, [double(m4);0.9],[]);
        else
            I1 = imadjust(I1, [0.9;0.99],[]);
        end
        I1 = im2bw(I1,0.5);
        I1 = ~I1;
        a = regionprops(I1,'centroid');
        if isempty(a) == false
            b = a(1,1).Centroid;
            C = [C;b];
        else
            b = [1 1];
            C = [C;b];
        end

        D0 = [C(i-4,:);C(i-3,:)];
        D1 = [C(i-3,:);C(i-2,:)];
        D2 = [C(i-2,:);C(i-1,:)];
        D3 = [C(i-1,:);C(i,:)];
        dist =
pdist(D0,'euclidean')+pdist(D1,'euclidean')+pdist(D2,'euclidean')+pdist(D3,
'euclidean');

        if (300 > dist) && (dist > 50)
            shockGate = true;
        end

    elseif i <= circBuffer
        trigger(vid);
        x = getdata(vid);
        Frame{i} = deal(x);
        I1 = imcrop(x, [30 30 365 565]);
        maxx = max(I1(:));
        m1 = double(maxx)/255;
        m3 = double(m1)*0.5;
        I1 = imadjust(I1, [0;double(m1)],[]);
        minn = (min(I1(:))+0.5);
        m2 = (double(minn)*(130*(double(minn)^(-0.94))))/255;
        I1 = imadjust(I1, [0;double(m2)],[]);
        I1 = imadjust(I1, [], [],0.7);
        I1 = imadjust(I1, [double(m3);double(m1)],[]);
        I1 = imfilter(I1,H);
        I1 = imcrop(I1,[6 6 359 559]);
        minn2 = min(min(I1));
        m4 = double(minn2)/255;
        if m4 < 0.9
            I1 = imadjust(I1, [double(m4);0.9],[]);
        else
            I1 = imadjust(I1, [0.9;0.99],[]);
        end
        I1 = im2bw(I1,0.5);
        I1 = ~I1;
        a = regionprops(I1,'centroid');
        if isempty(a) == false
            b = a(1,1).Centroid;
            C = [C;b];
        else
            b = [1 1];
            C = [C;b];
        end
```

```
        D0 = [C(i-4,:);C(i-3,:)];
        D1 = [C(i-3,:);C(i-2,:)];
        D2 = [C(i-2,:);C(i-1,:)];
        D3 = [C(i-1,:);C(i,:)];
        dist =
pdist(D0,'euclidean')+pdist(D1,'euclidean')+pdist(D2,'euclidean')+pdist(D3,
'euclidean');

    end

    flushdata(vid,'triggers');
    imshow(x);

end

currTime = datestr(now,'ddmmyy_HHMMSS');
Mov = VideoWriter(['C:\Users\scott lab\Documents\Andrews Folder\1month old
free swimming conditioning tests\' currdate '\Mov_' currTime '.avi']);
open(Mov);
j = 1;
while j <= circBuffer
    if isempty(Frame{j,1}) ~= 1
        writeVideo(Mov, Frame{j});
    end
    j = j+1;
end

shockGate = false;

close(Mov);

flushdata(vid, 'all');
close
```

```
global vid;
global src;
global wavedata;
global repetitions;
global freq;
global nrchannels;
global pahandle;
global s;
global currdate;

currdate = datestr(now, 'ddmmyy');
mkdir(['C:\Users\scott lab\Documents\Andrews Folder\1month old free
swimming conditioning tests\' currdate]);

[tonename,tonepath,filtindex] = uigetfile('.wav');
[y, Fs]=wavread([tonepath,tonename]);
nrchannels = 2; % Number of channels (1 = Mono sound, 2 = stereo, etc)
freq = Fs;      % Fs is the correct playback frequency for handel.
wavedata = y';  % Need sound vector as row vector, one row per channel.
repetitions=1;

numberSets = 5; %usually 6
numberReps = 9; %usually 9
betweenReps = 30; % number of seconds between reps, usually 30
variation = 5; %thse value of between reps will vary up or down by this

% Perform basic initialization of the sound driver:
InitializePsychSound;

% Initialization the USB/serial port (on this PC = 'com4') for controlling
!mode com4:19200,n,8,1
!mode com2:19200,n,8,1

% define and open the port to send shock data
    s = serial('COM4');
    fopen(s);
    set(s,'DataTerminalReady', 'on');

% Open the default audio device [], with default mode [] (==Only playback),
% and a required latencyclass of zero 0 == no low-latency mode, as well as
% a frequency of freq and nrchannels sound channels.
% This returns a handle to the audio device:
pahandle = PsychPortAudio('Open', [], [], 0, freq, nrchannels);

% Fill the audio playback buffer with the audio data 'wavedata':
PsychPortAudio('FillBuffer', pahandle, wavedata);



% initialise the camera
[vid,src] = startCamera();
disp('Camera ready');


KbName('UnifyKeyNames'); %collects names of the keys on the keyboard
escapeKey = KbName('ESCAPE'); %define the escape key
eKey = KbName('e'); %define the e key
sKey = KbName('s'); %define the s key

% This is a loop that flips around doing anything as long as KbCheck
```

```
% reports back that a key is pressed on the keyboard. Means that the
% program doesn't continue until all keys have been released.
disp('Press S to start, E to exit');
while 1
    % while 1 is always true, so this loop will continue indefinitely
    % unless the break command is given when the e key is pressed.

    % Check the state of the keyboard.
    % See if a key is currently pressed on the keyboard. If not, we skip
    % the next for loop from lines 20-38, and basically check again almost
    % immediately.


    [ keyIsDown, seconds, keyCode ] = KbCheck;

    % If the user is pressing a key,
    % then display its code number and name.
    if keyIsDown
        if keyCode(sKey)
            %plays the sound once when the S key is pressed, then starts
            %the conditioning routine

            disp('Starting...');
            pause(1.0);

            WaitSecs(1800);

            image_Fish_noshock;
            pause(2.0);
            flushdata(vid,'all');
            pause(1.0);
            close;
            pause(1.0);

            WaitSecs(240.00);

            image_Fish_noshock;
            pause(2.0);
            flushdata(vid,'all');
            pause(1.0);
            close;
            pause(1.0);

            WaitSecs(240.00);

            image_Fish_noshock;
            pause(2.0);
            close;

            WaitSecs(1200.00);

            m = numberSets;
            n = numberReps;
            for i=1:m

                WaitSecs(10.00);

                for j=1:n
```

```
                    randomness = 2 * rand * variation;
                    %this will be a pseudorandom number between 0 and 2 x
'variation', so
                    %subtracting 'randomness' from 'variation' should give
a pseudorandom
                    %number from -variation to +variation

                    states2 = 1:(betweenReps + variation - randomness);
                    %creates an array from 1 to the randomised value of
betweenReps

                    sortedstates2 = sort(states2, 'descend');
                    %creates a new array that's sorted in descending order

                    states3 =
cellfun(@num2str,num2cell(sortedstates2),'uniformoutput',0);
                    %creates a cell array where the numbers are converted
to strings

                    % Example Code for Printing Progress to the Command
Window
% %                     fprintf(1,'Seconds until next sound:  ');
% %                     for h=1:length(states3)
% %                         chalk(states3{h})
% %                     pause(1)
% %                     end
% %                     fprintf('\n')
% %                     chalk('',1)
                    WaitSecs(str2double(states3(1)));

                    image_Fish;
                    pause(1.0);
                    flushdata(vid,'all');
                    pause(1.0);
                    close;
                    pause(1.0);


                    fprintf(1,'Played sound %d time(s). %#d sounds
remain.\n',j,n-j);

                end


            randomness = 2 * rand * variation;
            %this will be a pseudorandom number between 0 and 2 x
'variation', so
            %subtracting 'randomness' from 'variation' should give a
pseudorandom
            %number from -variation to +variation

            states2 = 1:(betweenReps + variation - randomness);
            %creates an array from 1 to the randomised value of betweenReps

            sortedstates2 = sort(states2, 'descend');
            %creates a new array that's sorted in descending order
```

```
            states3 =
cellfun(@num2str,num2cell(sortedstates2),'uniformoutput',0);
            %creates a cell array where the numbers are converted to
strings

            % Example Code for Printing Progress to the Command Window
% %             fprintf(1,'Seconds until next sound:  ');
% %             for h=1:length(states3)
% %                 chalk(states3{h})
% %                 pause(1)
% %             end
% %             fprintf('\n')
% %             chalk('',1)
            WaitSecs(str2double(states3(1)));


            image_Fish;
            pause(1.0);
            flushdata(vid,'all');
            pause(1.0);
            close;
            pause(1.0);
            disp('played last tone of session');
            pause(2.0);


            WaitSecs(3600);


            end


                image_Fish_noshock;
                pause(2.0);
                close;
                fprintf(1,'Played CS alone 1 time(s). %#d sounds
remain.\n',i,m-i);


                WaitSecs(240.00);

                image_Fish_noshock;
                pause(2.0);
                close;
                fprintf(1,'Played CS alone 2 time(s). %#d sounds
remain.\n',i,m-i);


                WaitSecs(240.00);

                image_Fish_noshock;
                pause(2.0);
                close;
                fprintf(1,'Played CS alone 3 time(s). %#d sounds
remain.\n',i,m-i);
```

```
            fprintf('Done!\n');
            % Start audio playback for 'repetitions' repetitions of the
sound data,
            % start it immediately (0) and wait for the playback to start,
return onset
            % timestamp.

        end

        if keyCode(eKey)
            break;
        end

    end
    WaitSecs(0.2);
end


flushdata(vid,'all');
stop(vid);
delete(vid);


% Wait for release of all keys on keyboard:
while KbCheck; end;

% Stop playback:
PsychPortAudio('Stop', pahandle);

% Close the audio device:
PsychPortAudio('Close', pahandle);

% Done.
disp('Completed all sounds');
```

Appendix 2: GCaMP5G analysis code

```
function Img = dsimage(Img,dsize)
% --- downsamples an image by the factor, dsize --- %

Img = downsample(downsample(Img,dsize)',dsize)';
% downsamples the image


function a = field2num(s, f)
%FIELD2NUM put the values of a field into an array.
%*  A = FIELD2NUM(S, F) extract all the values of the field F of struct S
%   and put them in the numerical array A.
%
%*  See also: field2cell.

N = numel(s);
if N==0
    a = NaN;
    return
end
n = numel(s(1).(f));

a = NaN(N, n);
for i = 1:numel(s)
    a(i,:) = s(i).(f)(:);
end


function [ L ] = segmentgd2( im )
%UNTITLED Summary of this function goes here
%   Detailed explanation goes here


Fxy=double(im);
smwindow1=7;
smwindow2=7;
SE = strel('octagon', 12);
filter1=fspecial('log', [smwindow1 smwindow1], smwindow1/2+1);
filter2=fspecial('gaussian', [smwindow2 smwindow2], smwindow1/+2);

SmFxy=imfilter(Fxy,filter1);
SmFxyInv = SmFxy*(-1);
SmFxyInvFilt = imfilter(SmFxyInv,filter2);
SmFxyTHInv = imtophat(SmFxyInvFilt, SE);
SmFresc1 = imfilter(SmFxyTHInv,filter2);

L = watershed(SmFresc1);

end
```

```
[fName,fDir,fIndex] = uigetfile(...
{'*.tif','TIFF Image Stack (*.tif)';'*.mat','Matlab Data File (*.mat)'},...
'Select A Data File','F:\Data\RawMovies');
fFile = fullfile(fDir,fName);

ds = 1;
areamax = 600;
areamin = 30;
excentmax = 0.80;

visual = 20;
visual_length = 190;
jet = 253;
jet_length = 45;
jet_exl = [276,277];
tone = 300;
tone_length = 40;
slm = 354;
slm_length = 5;

A = imfinfo(fFile);
I = cell(length(A),1);

for i = 1:length(A)
Inw = imread(fFile,i);
if (size(Inw,3) == 3)
else
I{i} = dsimage(double(Inw),ds);
end

if (i == 1)
[Imx,Imn,Isum] = deal(I{i});
else
[Imx,Imn,Isum] = deal(max(Imx,I{i}),...
min(Imn,I{i}),Isum+I{i});
end
end

Imean = Isum/length(I);
im = Imean;
imMean = mean(mean(im));

clims(1) = prctile(reshape(im,1,[]),0.25);
clims(2) = prctile(reshape(im,1,[]),99.5);
figure; imagesc(im,clims); colormap(gray);

wpoly=roipoly;
[xpoly, ypoly]=find(wpoly==1);
xmin=min(xpoly);
xmax=max(xpoly);
ymin=min(ypoly);
ymax=max(ypoly);
x=[xmin xmin xmax xmax xmin];
y=[ymin ymax ymax ymin ymin];
wpoly=double(wpoly);
mask=wpoly(xmin:xmax,ymin:ymax);
im2 = im(xmin:xmax,ymin:ymax);
imagesc(im2,clims); colormap(gray);
```

```
J = cell(size(I));
for i = 1:numel(I)
    J{i,1} = I{i}(xmin:xmax,ymin:ymax);
end

m = matfile([fName 'mask.mat']);
m.Properties.Writable = true;
m.mask = mask;
m.xmin = xmin;
m.ymin = ymin;
m.xmax = xmax;
m.ymax = ymax;


% CELL SEGMENTATION CODE


L=segmentgd2(im(xmin:xmax,ymin:ymax));
STATS = regionprops(double(L).*mask,
'Area','PixelIdxList','Eccentricity','Centroid','Extrema');
a=field2num(STATS,'Area');
ex=field2num(STATS,'Eccentricity');
wneuron=ones(size(a,1),1);
w=find(a>areamax | a<areamin | ex>excentmax);
wneuron(w)=0;
Nneurons=squeeze(sum(wneuron));
neuronlist = find(wneuron);

m.L = L;
m.STATS = STATS;

[Lia, Locb] = ismember(L, neuronlist);
Locb2 = Locb;
dLia = double(Lia);
figure; imagesc(dLia); colormap(gray);

im2 = im(xmin:xmax,ymin:ymax);
im2 = double(im2);
gtmax = gt(im2,clims(2));
ltmin = lt(im2,clims(1));
im_sc = im2;
im_sc(gtmax) = clims(2);
im_sc(ltmin) = clims(1);
im3 = im2.*dLia;
im4 = im_sc-(im3*0.08);
clear rgb;
rgb(:,:,3) = im2*0.8;
rgb(:,:,1) = im4*0.4;
rgb(:,:,2) = im4*0.9;
rgb = uint16(rgb);
imwrite(rgb,[fName 'segment.tif'],'tif');
RGB64 = double(rgb)/65535;
rgblims(1) = prctile(reshape(RGB64,1,[]),0.25);
rgblims(2) = prctile(reshape(RGB64,1,[]),99.0);
JJJ = imadjust(RGB64,rgblims);
figure; imagesc(JJJ);
```

```
% dF/F ANALYSIS CODE

cells = cell(1,numel(STATS));
for i = 1:numel(STATS)
    if sum(ismember(neuronlist,i)) == 1
        cells{i} = STATS(i,1).PixelIdxList;
    end
end

data = zeros(numel(J),numel(cells));
for j = 1:numel(J)
    for i = 1:numel(cells)
        data(j,i) = nanmean(J{j,1}(cells{i}));
    end
end

headers = transpose(neuronlist);
data = data(:,all(~isnan(data),1));
rawdata = [headers;data];
xlswrite([fName 'rawdata'],rawdata);
Fbackground = prctile(reshape(im,1,[]),10);
Fbackground = repmat(Fbackground,numel(I),size(data,2));
data2 = data - Fbackground;
Fnaught = prctile(data2,25);
Fnaught = repmat(Fnaught,numel(I),1);
deltaFonF = 100.*((data2-Fnaught)./Fnaught);
xlswrite([fName 'deltaFonF'],deltaFonF);

m = matfile([fName 'results.mat']);
m.Properties.Writable = true;
m.headers = headers;
m.deltaFonF = deltaFonF;
m.Locb = Locb;


% % % % % % % %

clear A; clear I; clear J; clear data; clear m;

fName = strrep(fName,'_1_','_2_');
fFile = fullfile(fDir,fName);

A = imfinfo(fFile);
I = cell(length(A),1);

for i = 1:length(A)
Inw = imread(fFile,i);
if (size(Inw,3) == 3)
else
I{i} = dsimage(double(Inw),ds);
end

if (i == 1)
[Imx,Imn,Isum] = deal(I{i});
else
[Imx,Imn,Isum] = deal(max(Imx,I{i}),...
min(Imn,I{i}),Isum+I{i});
end
end
```

```
Imean = Isum/length(I);
im = Imean;
imMean = mean(mean(im));

clims(1) = prctile(reshape(im,1,[]),0.25);
clims(2) = prctile(reshape(im,1,[]),99.5);
imagesc(im,clims); colormap(gray);

J = cell(size(I));
for i = 1:numel(I)
    J{i,1} = I{i}(xmin:xmax,ymin:ymax);
end

cells = cell(1,numel(STATS));
for i = 1:numel(STATS)
    if sum(ismember(neuronlist,i)) == 1
        cells{i} = STATS(i,1).PixelIdxList;
    end
end

data = zeros(numel(J),numel(cells));
for j = 1:numel(J)
    for i = 1:numel(cells)
        data(j,i) = nanmean(J{j,1}(cells{i}));
    end
end

headers = transpose(neuronlist);
data = data(:,all(~isnan(data),1));
rawdata = [headers;data];
xlswrite([fName 'rawdata'],rawdata);
Fbackground = prctile(reshape(im,1,[]),10);
Fbackground = repmat(Fbackground,numel(I),size(data,2));
data2 = data - Fbackground;
Fnaught = prctile(data2,25);
Fnaught = repmat(Fnaught,numel(I),1);
deltaFonF = 100.*((data2-Fnaught)./Fnaught);
xlswrite([fName 'deltaFonF'],deltaFonF);


m = matfile([fName 'results.mat']);
m.Properties.Writable = true;
m.headers = headers;
m.deltaFonF = deltaFonF;
m.Locb = Locb;


% % % % % % % %

clear A; clear I; clear J; clear data; clear m;

fName = strrep(fName,'_2_','_3_');
fFile = fullfile(fDir,fName);

A = imfinfo(fFile);
I = cell(length(A),1);
```

```
for i = 1:length(A)
Inw = imread(fFile,i);
if (size(Inw,3) == 3)
else
I{i} = dsimage(double(Inw),ds);
end

if (i == 1)
[Imx,Imn,Isum] = deal(I{i});
else
[Imx,Imn,Isum] = deal(max(Imx,I{i}),...
min(Imn,I{i}),Isum+I{i});
end
end

Imean = Isum/length(I);
im = Imean;
imMean = mean(mean(im));

clims(1) = prctile(reshape(im,1,[]),0.25);
clims(2) = prctile(reshape(im,1,[]),99.5);
imagesc(im,clims); colormap(gray);

J = cell(size(I));
for i = 1:numel(I)
    J{i,1} = I{i}(xmin:xmax,ymin:ymax);
end

cells = cell(1,numel(STATS));
for i = 1:numel(STATS)
    if sum(ismember(neuronlist,i)) == 1
        cells{i} = STATS(i,1).PixelIdxList;
    end
end

data = zeros(numel(J),numel(cells));
for j = 1:numel(J)
    for i = 1:numel(cells)
        data(j,i) = nanmean(J{j,1}(cells{i}));
    end
end

headers = transpose(neuronlist);
data = data(:,all(~isnan(data),1));
rawdata = [headers;data];
xlswrite([fName 'rawdata'],rawdata);
Fbackground = prctile(reshape(im,1,[]),10);
Fbackground = repmat(Fbackground,numel(I),size(data,2));
data2 = data - Fbackground;
Fnaught = prctile(data2,25);
Fnaught = repmat(Fnaught,numel(I),1);
deltaFonF = 100.*((data2-Fnaught)./Fnaught);
xlswrite([fName 'deltaFonF'],deltaFonF);


m = matfile([fName 'results.mat']);
m.Properties.Writable = true;
m.headers = headers;
m.deltaFonF = deltaFonF;
```

```
m.Locb = Locb;

% % % % % % % %

clear A; clear I; clear J; clear data; clear m;

fName = strrep(fName,'_3_','_4_');
fFile = fullfile(fDir,fName);

A = imfinfo(fFile);
I = cell(length(A),1);

for i = 1:length(A)
Inw = imread(fFile,i);
if (size(Inw,3) == 3)
else
I{i} = dsimage(double(Inw),ds);
end

if (i == 1)
[Imx,Imn,Isum] = deal(I{i});
else
[Imx,Imn,Isum] = deal(max(Imx,I{i}),...
min(Imn,I{i}),Isum+I{i});
end
end

Imean = Isum/length(I);
im = Imean;
imMean = mean(mean(im));

clims(1) = prctile(reshape(im,1,[]),0.25);
clims(2) = prctile(reshape(im,1,[]),99.5);
imagesc(im,clims); colormap(gray);

J = cell(size(I));
for i = 1:numel(I)
    J{i,1} = I{i}(xmin:xmax,ymin:ymax);
end

cells = cell(1,numel(STATS));
for i = 1:numel(STATS)
    if sum(ismember(neuronlist,i)) == 1
        cells{i} = STATS(i,1).PixelIdxList;
    end
end

data = zeros(numel(J),numel(cells));
for j = 1:numel(J)
    for i = 1:numel(cells)
        data(j,i) = nanmean(J{j,1}(cells{i}));
    end
end

headers = transpose(neuronlist);
data = data(:,all(~isnan(data),1));
rawdata = [headers;data];
xlswrite([fName 'rawdata'],rawdata);
Fbackground = prctile(reshape(im,1,[]),10);
```

```
Fbackground = repmat(Fbackground,numel(I),size(data,2));
data2 = data - Fbackground;
Fnaught = prctile(data2,25);
Fnaught = repmat(Fnaught,numel(I),1);
deltaFonF = 100.*((data2-Fnaught)./Fnaught);
xlswrite([fName 'deltaFonF'],deltaFonF);


m = matfile([fName 'results.mat']);
m.Properties.Writable = true;
m.headers = headers;
m.deltaFonF = deltaFonF;
m.Locb = Locb;

% % % % % % % %

clear A; clear I; clear J; clear data; clear m;

fName = strrep(fName,'_4_','_5_');
fFile = fullfile(fDir,fName);

A = imfinfo(fFile);
I = cell(length(A),1);

for i = 1:length(A)
Inw = imread(fFile,i);
if (size(Inw,3) == 3)
else
I{i} = dsimage(double(Inw),ds);
end

if (i == 1)
[Imx,Imn,Isum] = deal(I{i});
else
[Imx,Imn,Isum] = deal(max(Imx,I{i}),...
min(Imn,I{i}),Isum+I{i});
end
end

Imean = Isum/length(I);
im = Imean;
imMean = mean(mean(im));

clims(1) = prctile(reshape(im,1,[]),0.25);
clims(2) = prctile(reshape(im,1,[]),99.5);
imagesc(im,clims); colormap(gray);

J = cell(size(I));
for i = 1:numel(I)
    J{i,1} = I{i}(xmin:xmax,ymin:ymax);
end

cells = cell(1,numel(STATS));
for i = 1:numel(STATS)
    if sum(ismember(neuronlist,i)) == 1
        cells{i} = STATS(i,1).PixelIdxList;
    end
end
```

```
data = zeros(numel(J),numel(cells));
for j = 1:numel(J)
    for i = 1:numel(cells)
        data(j,i) = nanmean(J{j,1}(cells{i}));
    end
end

headers = transpose(neuronlist);
data = data(:,all(~isnan(data),1));
rawdata = [headers;data];
xlswrite([fName 'rawdata'],rawdata);
Fbackground = prctile(reshape(im,1,[]),10);
Fbackground = repmat(Fbackground,numel(I),size(data,2));
data2 = data - Fbackground;
Fnaught = prctile(data2,25);
Fnaught = repmat(Fnaught,numel(I),1);
deltaFonF = 100.*((data2-Fnaught)./Fnaught);
xlswrite([fName 'deltaFonF'],deltaFonF);


m = matfile([fName 'results.mat']);
m.Properties.Writable = true;
m.headers = headers;
m.deltaFonF = deltaFonF;
m.Locb = Locb;
```

```
% Pooling Data Across All Fish for a Single Imaging Plane (75µm)

clear all;
cd('D:\Data\Andrew\SEGMENTATION_PROGR\');

s = what('D:\Data\Andrew\SEGMENTATION_PROGR\');

for i = 1:numel(s.mat)
    if strfind(s.mat{i,1},'_1_crop.tifmask') >=1 &
strfind(s.mat{i,1},'_75um') >=1 & isempty(strfind(s.mat{i,1},'ChR2')) == 1
& ...
            isempty(strfind(s.mat{i,1},'Chr2')) == 1 &
isempty(strfind(s.mat{i,1},'Goodhill')) == 1 &
isempty(strfind(s.mat{i,1},'ovie')) == 1
        maskname{i,1} = s.mat{i,1};
    end
    if strfind(s.mat{i,1},'_1_crop.tifresults') >=1 &
strfind(s.mat{i,1},'_75um') >=1 & isempty(strfind(s.mat{i,1},'ChR2')) == 1
& ...
            isempty(strfind(s.mat{i,1},'Chr2')) == 1 &
isempty(strfind(s.mat{i,1},'Goodhill')) == 1 &
isempty(strfind(s.mat{i,1},'ovie')) == 1
        resultsname{i,1} = s.mat{i,1};
    end
end
maskname = maskname(~cellfun('isempty',maskname));
resultsname = resultsname(~cellfun('isempty',resultsname));


i = 1;
for i = 1:numel(maskname)
    fName = maskname{i,1};
    load(fName);
    maskname = ['F' num2str(i) '_mask_75'];
    statsname = ['F' num2str(i) '_STATS_75'];
    datas{i,1} = mask;
    datas{i,2} = STATS;
    fName = resultsname{i,1};
    load(fName);
    datas{i,3} = Locb;
    load(fName,'deltaFonF');
    avg_traces_1 = deltaFonF;
    fName = strrep(fName,'_1_','_2_');
    load(fName,'deltaFonF');
    avg_traces_2 = deltaFonF;
    fName = strrep(fName,'_2_','_3_');
    load(fName,'deltaFonF');
    avg_traces_3 = deltaFonF;
    fName = strrep(fName,'_3_','_4_');
    load(fName,'deltaFonF');
    avg_traces_4 = deltaFonF;
    fName = strrep(fName,'_4_','_5_');
    load(fName,'deltaFonF');
    avg_traces_5 = deltaFonF;
    while size(avg_traces_5,1) < 360
        avg_traces_5(size(avg_traces_5,1)+1,:) =
avg_traces_5(size(avg_traces_5,1),:);
    end
    avg_traces_75um = (avg_traces_1 + avg_traces_2 + avg_traces_3 +
avg_traces_4 + avg_traces_5)/5;
```

```
    all_traces_75um =
[avg_traces_1;avg_traces_2;avg_traces_3;avg_traces_4;avg_traces_5];
    traces{i,1} = all_traces_75um;
    traces{i,2} = avg_traces_75um;
end

clear masknames;
clear resultsnames;

cd('D:\Data\Andrew\GCaMP5_Vis_Jet_Tone\Masks\');

s = what('D:\Data\Andrew\GCaMP5_Vis_Jet_Tone\Masks\');

for i = 1:numel(s.mat)
    if strfind(s.mat{i,1},'_1_crop.tifmask') >=1 &
strfind(s.mat{i,1},'_75um') >=1 & isempty(strfind(s.mat{i,1},'ChR2')) == 1
& ...
            isempty(strfind(s.mat{i,1},'Chr2')) == 1 &
isempty(strfind(s.mat{i,1},'Goodhill')) == 1 &
isempty(strfind(s.mat{i,1},'ovie')) == 1
        masknames{i,1} = s.mat{i,1};
    end
    if strfind(s.mat{i,1},'_1_crop.tifresults') >=1 &
strfind(s.mat{i,1},'_75um') >=1 & isempty(strfind(s.mat{i,1},'ChR2')) == 1
& ...
            isempty(strfind(s.mat{i,1},'Chr2')) == 1 &
isempty(strfind(s.mat{i,1},'Goodhill')) == 1 &
isempty(strfind(s.mat{i,1},'ovie')) == 1
        resultsnames{i,1} = s.mat{i,1};
    end
end
masknames = masknames(~cellfun('isempty',masknames));
resultsnames = resultsnames(~cellfun('isempty',resultsnames));

sizedata1 = size(datas,1);

for i = 1:numel(masknames)
    fName = masknames{i,1};
    load(fName);
    maskname = ['F' num2str(i) '_mask_75'];
    statsname = ['F' num2str(i) '_STATS_75'];
    datas{(sizedata1+i),1} = mask;
    datas{(sizedata1+i),2} = STATS;
    fName = resultsnames{i,1};
    load(fName);
    datas{(sizedata1+i),3} = Locb;
    load(fName,'deltaFonF');
    avg_traces_1 = deltaFonF;
    fName = strrep(fName,'_1_','_2_');
    load(fName,'deltaFonF');
    avg_traces_2 = deltaFonF;
    fName = strrep(fName,'_2_','_3_');
    load(fName,'deltaFonF');
    avg_traces_3 = deltaFonF;
    fName = strrep(fName,'_3_','_4_');
    load(fName,'deltaFonF');
    avg_traces_4 = deltaFonF;
    fName = strrep(fName,'_4_','_5_');
    load(fName,'deltaFonF');
    avg_traces_5 = deltaFonF;
```

```
    while size(avg_traces_5,1) < 360
        avg_traces_5(size(avg_traces_5,1)+1,:) =
avg_traces_5(size(avg_traces_5,1),:);
    end
    avg_traces_75um = (avg_traces_1 + avg_traces_2 + avg_traces_3 +
avg_traces_4 + avg_traces_5)/5;
    all_traces_75um =
[avg_traces_1;avg_traces_2;avg_traces_3;avg_traces_4;avg_traces_5];
    traces{(sizedata1+i),1} = all_traces_75um;
    traces{(sizedata1+i),2} = avg_traces_75um;
end


for i = 1:size(traces,1)
    ind_traces{i,1} = traces{i,1}(1:360);
    ind_traces{i,2} = traces{i,1}(361:720);
    ind_traces{i,3} = traces{i,1}(721:1080);
    ind_traces{i,4} = traces{i,1}(1081:1440);
    ind_traces{i,5} = traces{i,1}(1441:1800);
end


for i = 1:size(datas,1)
    for j = 1:max(max(datas{i,3}))
        datas{i,4}(j,1) = numel(find(datas{i,3}==j));
    end
end

i = 1;
maxLength = max(size(datas{i,1},1),size(datas{i+1,1},1));
for i = 2:(size(datas,1)-1)
    maxLength = max(maxLength,size(datas{i+1,1},1));
end

i = 1;
maxWidth = max(size(datas{i,1},2),size(datas{i+1,1},2));
for i = 2:(size(datas,1)-1)
    maxWidth = max(maxWidth,size(datas{i+1,1},2));
end

maxMask = [maxLength,maxWidth];

for i = 1:size(datas,1)
    datas{i,5} = padarray(datas{i,1}, [floor((maxMask(1)-
size(datas{i,1},1))/2), floor((maxMask(2)-size(datas{i,1},2))/2)]);
datas{i,5} = imresize(datas{i,5},maxMask);
end

avg_mask_75 = datas{1,5}+datas{2,5};
for i = 3:(size(datas,1)-2)
    avg_mask_75 = avg_mask_75+datas{i,5};
end
avg_mask_75 = round(avg_mask_75/size(datas,1));

[optimizer,metric] = imregconfig('multimodal'); optimizer.InitialRadius =
0.005; optimizer.MaximumIterations = 200; optimizer.InitialRadius = 0.001;

for i = 1:size(datas,1)
```

```
    datas{i,6} =
imregtform(datas{i,5},avg_mask_75,'affine',optimizer,metric);
end

for i = 1:size(datas,1)
    datas{i,7} =
imwarp(datas{i,5},datas{i,6},'OutputView',imref2d(size(avg_mask_75)));
end

for i = 1:size(datas,1)
    datas{i,8} = padarray(datas{i,3}, [floor((maxMask(1)-
size(datas{i,3},1))/2), floor((maxMask(2)-size(datas{i,3},2))/2)]);
datas{i,8} = imresize(datas{i,8},maxMask); datas{i,8}(datas{i,8}<0)=0;
datas{i,8} = round(datas{i,8});
end

for i = 1:size(datas,1)
    datas{i,9} =
imwarp(datas{i,8},datas{i,6},'OutputView',imref2d(size(avg_mask_75)));
datas{i,9} = round(datas{i,9});
end


for i = 1:size(datas,1)
    for j = 1:max(max(datas{i,3}))
        [aaaaa,bbbbb] = find(datas{i,9}==j);
        datas{i,10}(j) = mean(aaaaa);
        datas{i,11}(j) = mean(bbbbb);
    end
end


m = matfile('Responses_at_75um.mat','Writable',true);
m.datas = datas;
m.traces = traces;
m.ind_traces = ind_traces;
clear m;
pln = 75;
for m = 1:size(datas,1)
    fish{m}.plane{pln}.datas = datas{m,:};
    fish{m}.plane{pln}.ind_traces = ind_traces(m,:);
end
```

```
% Find All Cells Responsive to Different Stimuli

for m = 1:size(fish,2)
    pln = 25;
    for k = 1:6
        for n = 1:size(fish{m}.plane{pln}.ind_traces,2)
            fish{m}.plane{pln}.ztraces{n} =
zscore(fish{m}.plane{pln}.ind_traces{n});
            for i = 1:(size(fish{m}.plane{pln}.ind_traces{n},1)-
size(exampleSpike,1))
                for j = 1:size(fish{m}.plane{pln}.ind_traces{n},2)
                    a =
corrcoef(fish{m}.plane{pln}.ind_traces{n}(i:(i+(size(exampleSpike,1)-
1)),j),exampleSpike);
                    spikeCorr(i,j) = a(2,1);
                    if spikeCorr(i,j) > 0.7 &&
(ismember(1,fish{m}.plane{pln}.ztraces{n}([(i+5):(i+20)],j)>4)==1 ...
                            ||
ismember(1,fish{m}.plane{pln}.ind_traces{n}([(i+5):(i+20)],j)>20)==1)
                        fish{m}.plane{pln}.spikeYN{n}(i,j) = 1;
                    else
                        fish{m}.plane{pln}.spikeYN{n}(i,j) = 0;
                    end
                    clear a;
                end
            end
        end
        clear spikeCorr;
        for n = 1:size(fish{m}.plane{pln}.ind_traces,2)
            for i = 1:size(fish{m}.plane{pln}.spikeYN{n},2)
                fish{m}.plane{pln}.V1Cells{n}(i,1) =
max(fish{m}.plane{pln}.spikeYN{n}(31:75,i));
fish{m}.plane{pln}.V1CellsInd{n} = find(fish{m}.plane{pln}.V1Cells{n});
                fish{m}.plane{pln}.V2Cells{n}(i,1) =
max(fish{m}.plane{pln}.spikeYN{n}(91:115,i));
fish{m}.plane{pln}.V2CellsInd{n} = find(fish{m}.plane{pln}.V2Cells{n});
                fish{m}.plane{pln}.V3Cells{n}(i,1) =
max(fish{m}.plane{pln}.spikeYN{n}(131:150,i));
fish{m}.plane{pln}.V3CellsInd{n} = find(fish{m}.plane{pln}.V3Cells{n});
                fish{m}.plane{pln}.V4Cells{n}(i,1) =
max(fish{m}.plane{pln}.spikeYN{n}(161:200,i));
fish{m}.plane{pln}.V4CellsInd{n} = find(fish{m}.plane{pln}.V4Cells{n});
                fish{m}.plane{pln}.WFCells{n}(i,1) =
max(fish{m}.plane{pln}.spikeYN{n}([254:274,279:299],i));
fish{m}.plane{pln}.WFCellsInd{n} = find(fish{m}.plane{pln}.WFCells{n});
                fish{m}.plane{pln}.ToneCells{n}(i,1) =
max(fish{m}.plane{pln}.spikeYN{n}(301:320,i));
fish{m}.plane{pln}.ToneCellsInd{n} = find(fish{m}.plane{pln}.ToneCells{n});
            end
        end
        pln = pln + 25;
    end
end



for m = 1:size(fish,2)
    pln = 25;
    for k = 1:6
        for n = 1:size(fish{m}.plane{pln}.ind_traces,2)
```

```
            for i = 1:size(fish{m}.plane{pln}.spikeYN{n},2)
                fish{m}.plane{pln}.V1Cells{n}(i,1) =
max(fish{m}.plane{pln}.spikeYN{n}(31:75,i));
fish{m}.plane{pln}.V1CellsInd{n} = find(fish{m}.plane{pln}.V1Cells{n});
                fish{m}.plane{pln}.V2Cells{n}(i,1) =
max(fish{m}.plane{pln}.spikeYN{n}(91:115,i));
fish{m}.plane{pln}.V2CellsInd{n} = find(fish{m}.plane{pln}.V2Cells{n});
                fish{m}.plane{pln}.V3Cells{n}(i,1) =
max(fish{m}.plane{pln}.spikeYN{n}(131:150,i));
fish{m}.plane{pln}.V3CellsInd{n} = find(fish{m}.plane{pln}.V3Cells{n});
                fish{m}.plane{pln}.V4Cells{n}(i,1) =
max(fish{m}.plane{pln}.spikeYN{n}(161:200,i));
fish{m}.plane{pln}.V4CellsInd{n} = find(fish{m}.plane{pln}.V4Cells{n});
                fish{m}.plane{pln}.WFCells{n}(i,1) =
max(fish{m}.plane{pln}.spikeYN{n}([254:274,279:299],i));
fish{m}.plane{pln}.WFCellsInd{n} = find(fish{m}.plane{pln}.WFCells{n});
                fish{m}.plane{pln}.ToneCells{n}(i,1) =
max(fish{m}.plane{pln}.spikeYN{n}(301:320,i));
fish{m}.plane{pln}.ToneCellsInd{n} = find(fish{m}.plane{pln}.ToneCells{n});
            end
        end
        pln = pln + 25;
    end
end


totalcells=0;
for m = 1:size(fish,2)
    pln = 25;
    for k = 1:6
        totalcells = totalcells+size(fish{m}.plane{pln}.ztraces{1,1},2);
        pln = pln+25;
    end
end
totalcells=totalcells*5;


AllV1Responses = [];
AllV2Responses = [];
AllV3Responses = [];
AllV4Responses = [];
AllWFResponses = [];
AllToneResponses = [];
AnyResponse = [];
i = 1;
for m = 1:size(fish,2)
    pln = 25;
    for k = 1:6
        for n = 1:size(fish{m}.plane{pln}.ztraces,2)
            NewV1Responses =
fish{m}.plane{pln}.ztraces{n}(:,fish{m}.plane{pln}.V1CellsInd{n});
            NewV2Responses =
fish{m}.plane{pln}.ztraces{n}(:,fish{m}.plane{pln}.V2CellsInd{n});
            NewV3Responses =
fish{m}.plane{pln}.ztraces{n}(:,fish{m}.plane{pln}.V3CellsInd{n});
            NewV4Responses =
fish{m}.plane{pln}.ztraces{n}(:,fish{m}.plane{pln}.V4CellsInd{n});
            NewWFResponses =
fish{m}.plane{pln}.ztraces{n}(:,fish{m}.plane{pln}.WFCellsInd{n});
```

```
            NewToneResponses =
fish{m}.plane{pln}.ztraces{n}(:,fish{m}.plane{pln}.ToneCellsInd{n});
            fish{m}.plane{pln}.AnyResponsiveCell{n} =
unique([fish{m}.plane{pln}.V1CellsInd{n};fish{m}.plane{pln}.V2CellsInd{n};.
..

fish{m}.plane{pln}.V3CellsInd{n};fish{m}.plane{pln}.V4CellsInd{n};fish{m}.p
lane{pln}.WFCellsInd{n};...
                fish{m}.plane{pln}.ToneCellsInd{n}]);
            AnyNewResponse{i} =
fish{m}.plane{pln}.ztraces{n}(:,fish{m}.plane{pln}.AnyResponsiveCell{n});

            AllV1Responses = [AllV1Responses,NewV1Responses];
            AllV2Responses = [AllV2Responses,NewV2Responses];
            AllV3Responses = [AllV3Responses,NewV3Responses];
            AllV4Responses = [AllV4Responses,NewV4Responses];
            AllWFResponses = [AllWFResponses,NewWFResponses];
            AllToneResponses = [AllToneResponses,NewToneResponses];
            AnyResponse = [AnyResponse,AnyNewResponse{i}];
            i = i+1;
        end
        pln = pln+25;
    end
end
```

```
% Clustering by PCA-promax

AnyResponse = transpose(AnyResponse);
[coeff,score,latent,~,explained,mu] = pca(AnyResponse);
i = 1;

maxEigenValPastur=(1+sqrt(size(AnyResponse,2)/size(AnyResponse,1)))^2;
minEigenValPastur=(1-sqrt(size(AnyResponse,2)/size(AnyResponse,1)))^2;
correctionTracyWidom=size(AnyResponse,2)^(-2/3);

smaller = latent < maxEigenValPastur + correctionTracyWidom;
cutOffPC = find(smaller,1)-1; % The significant PCs go up to cutOffPC


PCs = coeff;
if cutOffPC > 1
    [PCsRot,
Rot]=rotatefactors(PCs(:,1:cutOffPC),'Method','promax','Maxit',500000);
else
    PCsRot = PCs(:,1);
end
for i=1:size(PCsRot,2)
    PCsRot(:,i)=PCsRot(:,i)/norm(PCsRot(:,i));
    if max(PCsRot(:,i))<=abs(min(PCsRot(:,i)))
        PCsRot(:,i)=-PCsRot(:,i);
    end

end

% define clusters based on zscore of the PC score along rotated Principal
components
for i=1:cutOffPC
    [values, inds]= sort(PCsRot(:,i),'descend');
    normCutOff = 1.5*std(values);
    AllResponseClusters{i} = inds(values>=normCutOff)';
end


% Merge Similar Clusters

loop = 2;
for i = 1:size(AllResponseClusters,2)
    MergedEnsemble{i,loop} = transpose(AllResponseClusters{1,i});
end
for s = 1:size(MergedEnsemble,1)
    sizes(s,loop) = size(MergedEnsemble{s,loop},1);
end
while isequal(sizes(:,loop-1),sizes(:,loop))==0
    loop = loop+1;
    MergedEnsemble(:,loop) = MergedEnsemble(:,loop-1);
    for i = 1:size(MergedEnsemble,1)
        for j = 1:size(MergedEnsemble,1)
            [cc,cp] =
corrcoef(mean(AnyResponse(:,MergedEnsemble{i,loop}),2),...
                mean(AnyResponse(:,MergedEnsemble{j,loop}),2));
            if cp(2)<0.01
                clCor(i,j) = cc(2);
            else
                clCor(i,j) = 0;
            end
```

```
        end
    end
    for i = 1:size(clCor,1)
        for j = 1:size(clCor,2)
            if clCor(i,j) >= 0.9
                MergedEnsemble{i,loop} =
union(MergedEnsemble{i,loop},MergedEnsemble{j,loop},'stable');
            else
                MergedEnsemble{i,loop} = MergedEnsemble{i,loop};
            end
        end
    end
    for s = 1:size(MergedEnsemble,1)
        sizes(s,loop) = size(MergedEnsemble{s,loop},1);
    end
end
clear clCor sizes;
for i = 1:size(MergedEnsemble,1)
    MergedEnsemble{i,loop+1} = sort(MergedEnsemble{i,loop});
end
loop = loop+1;


i = 1;
while i <= size(MergedEnsemble,1)
    j = i+1;
    while j <= size(MergedEnsemble,1)
        if isequal(MergedEnsemble{i,loop},MergedEnsemble{j,loop})==1
            MergedEnsemble(j,:) = [];
            j = j;
        else
            j = j+1;
        end
    end
    i = i+1;
end
AllMergedClusters = MergedEnsemble(:,loop);
AllMergedClustersStable = MergedEnsemble(:,loop-1);
clear loop MergedEnsemble;
AllMergedEnsembles = AllMergedClusters;


for i=1:size(AllMergedEnsembles,1)
    AllMergedEnsemblesMean{i,1} =
mean(AnyResponse(:,AllMergedEnsembles{i,1}),2);
    [~,AllMergedEnsemblesMean{i,2}] = max(AllMergedEnsemblesMean{i,1});
end
for i=1:size(AllMergedEnsembles,1)
    AllMergedEnsemblesMean{1,3}(i,1) = AllMergedEnsemblesMean{i,2}(:,:);
end
[AllMergedEnsemblesMean{2,3},AllMergedEnsemblesMean{3,3}] =
sort(AllMergedEnsemblesMean{1,3});

for i = 1:size(AllMergedClusters,1)
    AllMergedClusters{i,2} =
AllMergedClusters{AllMergedEnsemblesMean{3,3}(i,1),1};
end

AllMergedClusters(:,1) = AllMergedClusters(:,2);
```

```
for i=1:size(AllMergedClusters,1)
    for m = 1:size(fish,2)
        pln = 25;
        for k = 1:6
            for n = 1:size(fish{m}.plane{pln}.ind_traces,2)
                    fish{m}.plane{pln}.trial{n}.AllResponseEnsemble{i,1} =
[];
                    fish{m}.plane{pln}.trial{n}.AllResponseEnsemble{i,1} =
fish{m}.plane{pln}.AnyResponsiveCell{n}(AllMergedClusters{i,1}(AllMergedClu
sters{i,1}<=size(fish{m}.plane{pln}.AnyResponsiveCell{n},1)));
                    AllMergedClusters{i,1} =
AllMergedClusters{i,1}(AllMergedClusters{i,1}>size(fish{m}.plane{pln}.AnyRe
sponsiveCell{n},1));
                    AllMergedClusters{i,1} = AllMergedClusters{i,1}-
size(fish{m}.plane{pln}.AnyResponsiveCell{n},1);
            end
        pln = pln+25;
        end
    end
end



% Calculate number of cells in each cluster represented in each fish

ClusterFishCounts = [];

for i=1:size(AllMergedClusters,1)
    for m = 1:size(fish,2)
        pln = 25;
        for k = 1:6
            xyz = [];
            for n = 1:size(fish{m}.plane{pln}.ind_traces,2)
                xyz =
[xyz;fish{m}.plane{pln}.trial{n}.AllResponseEnsemble{i,1}(:,:)];
            end
            xyz = unique(xyz);
            ClusterFishCounts{i,1}(m,k) = size(xyz,1);
            pln = pln+25;
        end
    end
end
for i = 1:size(ClusterFishCounts,1)
    for m = 1:size(ClusterFishCounts{i,1},1)
        FishClusterNumbers(i,m) = max(ClusterFishCounts{i,1}(m,:));
        FishClusterNumbers3(i,m) = sum(ClusterFishCounts{i,1}(m,:));
    end
end
for i = 1:size(FishClusterNumbers,1)
    FishClusterNumbers2(i,1) = numel(find(FishClusterNumbers(i,:)>=25));
end
for i = 1:size(FishClusterNumbers,1)
    FishClusterNumbers4(i,1) =
100*max(FishClusterNumbers3(i,:))/sum(FishClusterNumbers3(i,:));
end
for i = 1:size(FishClusterNumbers,1)
    FishClusterNumbers5(i,1) = sum(FishClusterNumbers3(i,:));
end
```

```
% Calculate Trial-to-Trial Matching Index
for m = 1:size(fish,2)
    pln = 25;
    for k = 1:6
        for i = 1:size(AllMergedClusters,1)
            fish{m}.plane{pln}.WholeSeriesCl{i} = [];
            for n = 1:size(fish{m}.plane{pln}.ztraces,2)
                for p = 1:size(fish{m}.plane{pln}.ztraces,2)
                    if
isempty(fish{m}.plane{pln}.trial{n}.AllResponseEnsemble{i,1})==0
                        X =
numel(intersect(fish{m}.plane{pln}.trial{n}.AllResponseEnsemble{i,1},fish{m
}.plane{pln}.trial{p}.AllResponseEnsemble{i,1}));
                        M =
size(fish{m}.plane{pln}.ind_traces{n},2)+size(fish{m}.plane{pln}.ind_traces
{p},2);
                        K =
numel(fish{m}.plane{pln}.trial{n}.AllResponseEnsemble{i,1})+numel(fish{m}.p
lane{pln}.trial{p}.AllResponseEnsemble{i,1});
                        N =
numel(fish{m}.plane{pln}.trial{n}.AllResponseEnsemble{i,1});
                        P_MI = hygepdf(X,M,K,N);
                        if P_MI <0.01
                            fish{m}.plane{pln}.WholeSeriesCl{i}(n,p) =
(2*X)/K;
                        else
                            fish{m}.plane{pln}.WholeSeriesCl{i}(n,p) = 0;
                        end
                        clear X M K N P_MI;
                    else
                        fish{m}.plane{pln}.WholeSeriesCl{i}(n,p) = NaN;
                    end
                end
            end
            abc = [];
            for k = 1:size(fish{m}.plane{pln}.WholeSeriesCl{i},2)
                abc = [abc;diag(fish{m}.plane{pln}.WholeSeriesCl{i},k)];
            end
            fish{m}.plane{pln}.WholeSeriesCl{i} = [];
            fish{m}.plane{pln}.WholeSeriesCl{i} = abc; clear abc;
        end
        pln = pln + 25;
    end
end

TrialTrialMI = cell(size(AllMergedClusters,1),1);
for i = 1:size(AllMergedClusters,1)
    for m = 1:size(fish,2)
        pln = 25;
        for k= 1:6
            TrialTrialMI{i,1} =
[TrialTrialMI{i,1},nanmean(fish{m}.plane{pln}.WholeSeriesCl{i})];
            pln = pln + 25;
        end
    end
end
```

```
% Calculate Cross-Cluster Matching Indices

for i = 1:size(AllMergedClusters,1)
    for m = 1:size(fish,2)
        pln = 25;
        for k = 1:6
            fish{m}.plane{pln}.AnyTrialEnsembleCells{i,1} = [];
            for n = 1:size(fish{m}.plane{pln}.ztraces,2)
                fish{m}.plane{pln}.AnyTrialEnsembleCells{i,1} =
[fish{m}.plane{pln}.AnyTrialEnsembleCells{i,1};fish{m}.plane{pln}.trial{n}.
AllResponseEnsemble{i,1}];
            end
            fish{m}.plane{pln}.AnyTrialEnsembleCells{i,1} =
unique(fish{m}.plane{pln}.AnyTrialEnsembleCells{i,1});
            pln = pln + 25;
        end
    end
end



for m = 1:size(fish,2)
    pln = 25;
    for k = 1:6
        for i = 1:size(AllMergedClusters,1)
            for p = 1:size(AllMergedClusters,1)
                if
isempty(fish{m}.plane{pln}.AnyTrialEnsembleCells{i,1})==0
                    X =
numel(intersect(fish{m}.plane{pln}.AnyTrialEnsembleCells{i,1},fish{m}.plane
{pln}.AnyTrialEnsembleCells{p,1}));
                    M =
size(fish{m}.plane{pln}.ind_traces{1},2)+size(fish{m}.plane{pln}.ind_traces
{1},2);
                    K =
numel(fish{m}.plane{pln}.AnyTrialEnsembleCells{i,1})+numel(fish{m}.plane{pl
n}.AnyTrialEnsembleCells{p,1});
                    N =
numel(fish{m}.plane{pln}.AnyTrialEnsembleCells{i,1});
                    P_MI = hygepdf(X,M,K,N);
                    if P_MI <0.01
                        fish{m}.plane{pln}.CrossStimEnsembleMI(i,p) =
(2*X)/K;
                    else
                        fish{m}.plane{pln}.CrossStimEnsembleMI(i,p) = 0;
                    end
                    clear X M K N P_MI;
                else
                    fish{m}.plane{pln}.CrossStimEnsembleMI(i,p) = NaN;
                end
            end
        end
        pln = pln + 25;
    end
end



i = 1;
```

```
for m = 1:size(fish,2)
    pln = 25;
    for k = 1:6
        AllCrossStimMIs(:,:,i) = fish{m}.plane{pln}.CrossStimEnsembleMI;
        i = i+1;
        pln = pln + 25;
    end
end

AllCrossStimMIsMean = nanmean(AllCrossStimMIs,3);


relevantClusters = [3,5,6,7,9:19,22,24,27,28];



% What is the correlation coefficent or linear regression of cells within
% a cluster to a boolean trace of each stimulus?


V1Bool = zeros(360,1);
V2Bool = zeros(360,1);
V3Bool = zeros(360,1);
V4Bool = zeros(360,1);
WFBool = zeros(360,1);
ToneBool = zeros(360,1);
V1Bool(31:85,1) = 1;
V2Bool(91:125,1) = 1;
V3Bool(131:165,1) = 1;
V4Bool(161:215,1) = 1;
WFBool(251:300,1) = 1;
ToneBool(301:334,1) = 1;


for i = 1:size(AllMergedClusters,1)
    ClTraces{i,1} = AnyResponse(:,AllMergedClusters{i,2});
end


for i = 1:size(ClTraces,1)
    for j = 1:size(ClTraces{i,1},2)
        a = corrcoef(V1Bool,ClTraces{i,1}(:,j));
        V1Corr{i,1}(j,1) = a(1,2);
        a = corrcoef(V2Bool,ClTraces{i,1}(:,j));
        V2Corr{i,1}(j,1) = a(1,2);
        a = corrcoef(V3Bool,ClTraces{i,1}(:,j));
        V3Corr{i,1}(j,1) = a(1,2);
        a = corrcoef(V4Bool,ClTraces{i,1}(:,j));
        V4Corr{i,1}(j,1) = a(1,2);
        a = corrcoef(WFBool,ClTraces{i,1}(:,j));
        WFCorr{i,1}(j,1) = a(1,2);
        a = corrcoef(ToneBool,ClTraces{i,1}(:,j));
        ToneCorr{i,1}(j,1) = a(1,2);
    end
end

for i = 1:size(V1Corr,1)
    V1CorrMean(i,1) = mean(V1Corr{i,1});
    V2CorrMean(i,1) = mean(V2Corr{i,1});
```

```
    V3CorrMean(i,1) = mean(V3Corr{i,1});
    V4CorrMean(i,1) = mean(V4Corr{i,1});
    WFCorrMean(i,1) = mean(WFCorr{i,1});
    ToneCorrMean(i,1) = mean(ToneCorr{i,1});
end




%  Direction Selectivity Indexes

 for i = 1:size(ClTraces,1)
     for j = 1:size(ClTraces{i,1},2)
         ClTraceDiffs{i,1}(:,j) = diff(ClTraces{i,1}(:,j));
     end
 end

for i = [3,5,6,7];
    ClDSIs{i,1} = [];
    r1 = [];
    r2 = [];
    % DirectionSelectivityIndex
    r1 = max(ClTraceDiffs{i,1}(30:49,:));
    r2 = max(ClTraceDiffs{i,1}(50:69,:));
    for cc = 1:size(r1,2)
        ClDSIs{i,1}(1,cc) = (r1(1,cc)-
r2(1,cc))/(abs(r1(1,cc))+abs(r2(1,cc)));
    end
end

for i = [9,10,11];
    ClDSIs{i,1} = [];
    r1 = [];
    r2 = [];
    % DirectionSelectivityIndex
    r1 = max(ClTraceDiffs{i,1}(90:99,:));
    r2 = max(ClTraceDiffs{i,1}(100:109,:));
    for cc = 1:size(r1,2)
        ClDSIs{i,1}(1,cc) = (r1(1,cc)-
r2(1,cc))/(abs(r1(1,cc))+abs(r2(1,cc)));
    end
end
for i = [12,13,14];
    ClDSIs{i,1} = [];
    r1 = [];
    r2 = [];
    % DirectionSelectivityIndex
    r1 = max(ClTraceDiffs{i,1}(130:139,:));
    r2 = max(ClTraceDiffs{i,1}(140:149,:));
    for cc = 1:size(r1,2)
        ClDSIs{i,1}(1,cc) = (r1(1,cc)-
r2(1,cc))/(abs(r1(1,cc))+abs(r2(1,cc)));
    end
end
for i = 15:19;
    ClDSIs{i,1} = [];
    r1 = [];
    r2 = [];
    % DirectionSelectivityIndex
    r1 = max(ClTraceDiffs{i,1}([160:169,180:189],:));
```

```
    r2 = max(ClTraceDiffs{i,1}([170:179,190:199],:));
    for cc = 1:size(r1,2)
        ClDSIs{i,1}(1,cc) = (r1(1,cc)-
r2(1,cc))/(abs(r1(1,cc))+abs(r2(1,cc)));
    end
end
for i = [22,24];
    ClDSIs{i,1} = [];
    r1 = [];
    r2 = [];
    % DirectionSelectivityIndex
    r1 = max(ClTraceDiffs{i,1}([253:259,278:284],:));
    r2 = max(ClTraceDiffs{i,1}([260:274,285:299],:));
    for cc = 1:size(r1,2)
        if (r1(1,cc))<0
            r1(1,cc) = 0;
        end
        if (r2(1,cc))<0
            r2(1,cc) = 0;
        end
        ClDSIs{i,1}(1,cc) = (r1(1,cc)-
r2(1,cc))/(abs(r1(1,cc))+abs(r2(1,cc)));
    end
end
for i = [27,28];
    ClDSIs{i,1} = [];
    r1 = [];
    r2 = [];
    % DirectionSelectivityIndex
    r1 = max(ClTraceDiffs{i,1}(300:319,:));
    r2 = max(ClTraceDiffs{i,1}(320:339,:));
    for cc = 1:size(r1,2)
        if (r1(1,cc))<0
            r1(1,cc) = 0;
        end
        if (r2(1,cc))<0
            r2(1,cc) = 0;
        end
        ClDSIs{i,1}(1,cc) = (r1(1,cc)-
r2(1,cc))/(abs(r1(1,cc))+abs(r2(1,cc)));
    end
end

for i = 1:size(ClDSIs,1)
    if isempty(ClDSIs{i,1})==0
        ClusterDSIMean(i,1) = nanmean(ClDSIs{i,1},2);
    else
        ClusterDSIMean(i,1) = NaN;
    end
end
i = 29;
ClusterDSIMean(i,1) = NaN;




% What is the Cross correlation of cells within a given cluster to cells
% within a different cluster?

for m = 1:size(fish,2)
```

```
    pln = 25;
    for k = 1:6
        for n = 1:size(fish{m}.plane{pln}.ind_traces,2)
            fish{m}.plane{pln}.trial{n}.CrossCorr = [];
            fish{m}.plane{pln}.trial{n}.CrossCorrLg = [];
            for i = 1:size(AllMergedClusters,1)
                for p = 1:size(AllMergedClusters,1)
                    if
isempty(fish{m}.plane{pln}.trial{n}.AllResponseEnsemble{i,1})==0
                        if
isempty(fish{m}.plane{pln}.trial{n}.AllResponseEnsemble{p,1})==0
                            xcor_co = [];
                            xcor_lg = [];
                            for mnm =
1:size(fish{m}.plane{pln}.trial{n}.AllResponseEnsemble{i,1},1)
                                xcor2 = [];
                                for pnp =
1:size(fish{m}.plane{pln}.trial{n}.AllResponseEnsemble{p,1},1)
                                    xcor1 = [];
                                    if
fish{m}.plane{pln}.trial{n}.AllResponseEnsemble{i,1}(mnm,1) ==
fish{m}.plane{pln}.trial{n}.AllResponseEnsemble{p,1}(pnp,1)
                                        xcor1(1:11,pnp) = NaN;
                                    else
                                        xcor1(:,pnp) =
xcorr(fish{m}.plane{pln}.ind_traces{n}(:,fish{m}.plane{pln}.trial{n}.AllRes
ponseEnsemble{i,1}(mnm,1)),...

fish{m}.plane{pln}.ind_traces{n}(:,fish{m}.plane{pln}.trial{n}.AllResponseE
nsemble{p,1}(pnp,1)),5,'coeff');
                                    end
                                    [xcor2(1,pnp),xcor2(2,pnp)] =
nanmax(xcor1(:,pnp));
                                end
                                for g = 1:size(xcor2,2)
                                    if isnan(xcor2(1,g))==1
                                        xcor2(2,g) = NaN;
                                    end
                                end
                                xcor_co(mnm,1) = nanmean(xcor2(1,:),2);
                                xcor_lg(mnm,1) = nanmean(xcor2(2,:),2);
                            end
                            xcor_lg = xcor_lg-5;
                            fish{m}.plane{pln}.trial{n}.CrossCorr(i,p) =
nanmean(xcor_co);
                            fish{m}.plane{pln}.trial{n}.CrossCorrLg(i,p) =
nanmean(xcor_lg);
                        else
                            fish{m}.plane{pln}.trial{n}.CrossCorr(i,p) =
NaN;
                            fish{m}.plane{pln}.trial{n}.CrossCorrLg(i,p) =
NaN;
                        end
                    else
                        fish{m}.plane{pln}.trial{n}.CrossCorr(i,p) = NaN;
                        fish{m}.plane{pln}.trial{n}.CrossCorrLg(i,p) = NaN;
                    end
                end
            end
        end
        pln = pln + 25;
```

```
    end
end


i = 1;
for m = 1:size(fish,2)
    pln = 25;
    for k = 1:6
        for n = 1:5
            AllCrossCorrs(:,:,i) = fish{m}.plane{pln}.trial{n}.CrossCorr;
            AllCrossCorrLgs(:,:,i) =
fish{m}.plane{pln}.trial{n}.CrossCorrLg;
            i = i+1;
        end
        pln = pln + 25;
    end
end

AllCrossCorrLgs = AllCrossCorrLgs-1;
AllCrossCorrLgs = AllCrossCorrLgs*0.1;

AllCrossCorrsMean = nanmean(AllCrossCorrs,3);
AllCrossCorrsLgMean = nanmean(AllCrossCorrLgs,3);



% Are there 'Core Cells'

for m = 1:size(fish,2)
    pln = 25;
    for k = 1:6
        for i = 1:29
            cores = [];
            for n = 1:5
                cores(:,n) =
zeros(size(fish{m}.plane{pln}.ztraces{1,1},2),1);

cores(fish{m}.plane{pln}.trial{n}.AllResponseEnsemble{i,1},n) = 1;
            end
            fish{m}.plane{pln}.CoreCells{i,1} = find(sum(cores,2)>=4);
        end
        pln = pln + 25;
    end
end



for i = 1:size(AllMergedClusters,1)
    CoreCellsCount{i,1} = [];
    for m = 1:size(fish,2)
        pln = 25;
        for k = 1:6
            CoreCellsCount{i,1} =
[CoreCellsCount{i,1}(:,:);fish{m}.plane{pln}.CoreCells{i,1}(:,:)];
            pln = pln + 25;
        end
    end
    CoreCellsCount{i,1} = numel(CoreCellsCount{i,1});
end
CoreCellsCount = cell2mat(CoreCellsCount);
```

```
% Calculate Relative Area, Compactness and Position


SE = strel('diamond',1);
for m = 1:size(fish,2)
    pln = 25;
    for k = 1:6

        %Skel&Euclid
        h2 = fspecial('gaussian',100,10);
        br = imfilter(fish{m}.plane{pln}.datas{1,7}, h2); br = br>0.25;
        bw1 = bwmorph(br,'thin', Inf);
        t = regionprops(bw1, 'Centroid','Orientation',
'Extrema','PixelIdxList');
        for stx = 1:size(t,1)
            trex(stx,1) = size(t(stx).PixelIdxList,1);
        end
        [~,strex] = max(trex);
        t = t(strex); clear trex strex;
        t1 = t.Extrema(1,:);
        t2 = t.Extrema(5,:);
        xd = cosd(t.Orientation(1,1));
        yd = sind(t.Orientation(1,1));
        t1 = ceil(t1);
        t2 = floor(t2);
        bw3 = bw1;
        mIx = t1/abs(xd);
        mIy = t1/abs(yd);
        maxIter = round(max(max(mIx,mIy)));

        for r = 1:maxIter
            if round(t1(1))<1 && round(t1(2))<1
                bw3(1,1) = 1;
            elseif round(t1(1))<1
                bw3(round(t1(2)),1) = 1;
            elseif round(t1(2))<1
                bw3(1,round(t1(1))) = 1;
            else
                bw3(round(t1(2)),round(t1(1))) = 1;
            end
            t1 = t1 + [-xd,yd];
        end

        mIx = (max(size(bw1))-t2)/abs(xd);
        mIy = (max(size(bw1))-t2)/abs(yd);
        maxIter = round(max(max(mIx,mIy)));
        for r = 1:maxIter
            if round(t2(1))>max(size(bw1,2)) &&
round(t2(2))>max(size(bw1,1))
                bw3(max(size(bw1,1)),max(size(bw1,2))) = 1;
            elseif round(t2(1))>max(size(bw1,2))
                bw3(round(t2(2)),max(size(bw1,2))) = 1;
            elseif round(t2(2))>max(size(bw1,1))
                bw3(max(size(bw1,1)),round(t2(1))) = 1;
            else
                bw3(round(t2(2)),round(t2(1))) = 1;
            end
            t2 = t2 + [+xd,-yd];
        end
```

```
bw3 = imdilate(bw3,SE);
mldist = bwdist(bw3);
for r = 1:size(mldist,1)
    dx = find(bw3(r,:));
    if isempty(dx)
    else
        mldist(r,1:dx(1,1)) = mldist(r,1:dx(1,1))*-1;
    end
end

bw4 = zeros(size(bw1));
xd1 = yd*-1;
yd1 = xd*-1;
z1 = round(t.Centroid);
mIx = (size(bw4,2)-z1(1))/abs(xd);
mIy = z1(2)/abs(yd);
mIxx = z1(1)/abs(xd);
mIyy = (size(bw4,1)-z1(2))/abs(yd);
maxIter = round(max(max(mIx,mIy)));
maxIter = round(max(maxIter,mIxx));
maxIter = round(max(maxIter,mIyy));
bw4(z1(2),z1(1)) = 1;
for r = 1:maxIter
    if round(z1(2))<1 && round(z1(1))>size(bw4,2)
        bw4(size(bw4,2),1) = 1;
    elseif round(z1(2))<1
        bw4(1,round(z1(1))) = 1;
    elseif round(z1(1))>size(bw4,2)
        bw4(round(z1(2)),size(bw4,2)) = 1;
    else
        bw4(round(z1(2)),round(z1(1))) = 1;
    end
    z1 = z1 + [xd1,yd1];
end
z1 = round(t.Centroid);

for r = 1:maxIter
    if round(z1(2))>size(bw4,1) && round(z1(1))<1
        bw4(size(bw4,1),1) = 1;
    elseif round(z1(1))<1
        bw4(round(z1(2)),1) = 1;
    elseif round(z1(2))>size(bw4,1)
        bw4(size(bw4,1),round(z1(1))) = 1;
    else
        bw4(round(z1(2)),round(z1(1))) = 1;
    end
    z1 = z1 - [xd1,yd1];
end

bw4 = imdilate(bw4,SE);
rcdist = bwdist(bw4);
for r = 1:size(rcdist,1)
    dx = find(bw4(r,:));
    if isempty(dx)
    else
        rcdist(r,1:dx(1,1)) = rcdist(r,1:dx(1,1))*-1;
    end
end
rcdist = rcdist*-1;
fish{m}.plane{pln}.mldist = mldist;
fish{m}.plane{pln}.rcdist = rcdist;
```

```
        for n = 1:size(fish{m}.plane{pln}.ztraces,2)
            fish{m}.plane{pln}.ClusterStats = [];

            for i = 1:size(AllMergedClusters,1)
                fish{m}.plane{pln}.trial{n}.ClusterCompactInd{i,1} = [];
                fish{m}.plane{pln}.trial{n}.ClusterRelArea{i,1} = [];
                fish{m}.plane{pln}.trial{n}.ClusterXYZ{i,1} = [];
                if
isempty(fish{m}.plane{pln}.trial{n}.AllResponseEnsemble{i,1})==0

                    % Relative area
                    maxMask = size(fish{m}.plane{pln}.datas{8});
                    blabla =
padarray(ismember(fish{m}.plane{pln}.datas{3},fish{m}.plane{pln}.trial{n}.A
llResponseEnsemble{i,1}),...
                        [floor((maxMask(1)-
size(fish{m}.plane{pln}.datas{3},1))/2),...
                        floor((maxMask(2)-
size(fish{m}.plane{pln}.datas{3},2))/2)]);
                    blabla = logical(imresize(blabla,maxMask));
                    blabla =
imwarp(double(blabla),fish{m}.plane{pln}.datas{6},'OutputView',imref2d(maxM
ask)); clear maxMask;
                    ras = ismember(blabla,1);
                    ar = regionprops(ras,'Area','PixelIdxList');
                    h =
fspecial('gaussian',(50+20*size(fish{m}.plane{pln}.trial{n}.AllResponseEnse
mble{i,1},1)),...

(15+(15*0.7^size(fish{m}.plane{pln}.trial{n}.AllResponseEnsemble{i,1},1))))
;
                    aar = imfilter(double(ras),h);abr =
aar>(max(max(aar))/2);
                    fish{m}.plane{pln}.trial{n}.ClusterRelArea{i,1} =
numel(find(abr))/numel(find(fish{m}.plane{pln}.datas{1,7}));

                    % Compactness index
                    ax = regionprops(abr,'Area','Centroid');
                    for arsi = 1:size(ax,1)
                        arsz(arsi,1) = ax(arsi).Area;
                    end
                    [~,mea] = max(arsz);
                    abx = zeros(size(abr));
abx(round(ax(mea).Centroid(2)),round(ax(mea).Centroid(1))) = 1; abx =
bwdist(abx);
                    abx = abx<sqrt(ax(mea).Area/pi); ax =
regionprops(abx,'Area','PixelIdxList','Centroid');
                    acx = [];
                    for j = 1:size(ar,1)
                        if
max(ismember(ar(j,1).PixelIdxList,ax.PixelIdxList))==1
                            acx(j,1) = 1;
                        else
                            acx(j,1) = 0;
                        end
                    end
```

```
                    fish{m}.plane{pln}.trial{n}.ClusterCompactInd{i,1} =
numel(find(acx))/size(fish{m}.plane{pln}.trial{n}.AllResponseEnsemble{i,1},
1);

                    %ML, RC and Z Position
                    fish{m}.plane{pln}.trial{n}.ClusterXYZ{i,1}(1,1) =
mldist(round(ax.Centroid(1,2)),round(ax.Centroid(1,1)));
                    fish{m}.plane{pln}.trial{n}.ClusterXYZ{i,1}(1,2) =
rcdist(round(ax.Centroid(1,2)),round(ax.Centroid(1,1)));
                    fish{m}.plane{pln}.trial{n}.ClusterXYZ{i,1}(1,3) = pln;

                    clear arsz acx;
                else
                    fish{m}.plane{pln}.trial{n}.ClusterCompactInd{i,1} =
[];
                    fish{m}.plane{pln}.trial{n}.ClusterRelArea{i,1} = [];
                    fish{m}.plane{pln}.trial{n}.ClusterXYZ{i,1} = [];
                end
            end

            fish{m}.plane{pln}.ClusterStats{1,n} =
[fish{m}.plane{pln}.trial{n}.ClusterRelArea];
            fish{m}.plane{pln}.ClusterStats{2,n} =
[fish{m}.plane{pln}.trial{n}.ClusterCompactInd];
            fish{m}.plane{pln}.ClusterStats{3,n} =
[fish{m}.plane{pln}.trial{n}.ClusterXYZ];
        end
        pln = pln + 25;
    end
end


AllFishClusterStatistics{5,1} = [];

for m = 1:size(fish,2)
    pln = 25;
    for k = 1:6
        for n = 1:5
            AllFishClusterStatistics{1,1} =
[AllFishClusterStatistics{1,1}(:,:),fish{m}.plane{pln}.trial{n}.ClusterComp
actInd];
            AllFishClusterStatistics{2,1} =
[AllFishClusterStatistics{2,1}(:,:),fish{m}.plane{pln}.trial{n}.ClusterRelA
rea];

            abcd = [];
            for i = 1:size(AllMergedClusters,1)
                if isempty(fish{m}.plane{pln}.trial{n}.ClusterXYZ{i,1})==1
                    abcd(i,1) = NaN;
                else
                    abcd(i,1) =
fish{m}.plane{pln}.trial{n}.ClusterXYZ{i,1}(1,1);
                end
            end
            AllFishClusterStatistics{3,1} =
[AllFishClusterStatistics{3,1}(:,:),abcd];

            abcd = [];
            for i = 1:size(AllMergedClusters,1)
                if isempty(fish{m}.plane{pln}.trial{n}.ClusterXYZ{i,1})==1
```

```
                    abcd(i,1) = NaN;
                else
                    abcd(i,1) =
fish{m}.plane{pln}.trial{n}.ClusterXYZ{i,1}(1,2);
                end
            end
            AllFishClusterStatistics{4,1} =
[AllFishClusterStatistics{4,1}(:,:),abcd];

            abcd = [];
            for i = 1:size(AllMergedClusters,1)
                if isempty(fish{m}.plane{pln}.trial{n}.ClusterXYZ{i,1})==1
                    abcd(i,1) = NaN;
                else
                    abcd(i,1) =
fish{m}.plane{pln}.trial{n}.ClusterXYZ{i,1}(1,3);
                end
            end
            AllFishClusterStatistics{5,1} =
[AllFishClusterStatistics{5,1}(:,:),abcd];
        end
        pln = pln + 25;
    end
end

for i = 1:size(AllFishClusterStatistics{1,1},1)
    for j = 1:size(AllFishClusterStatistics{1,1},2)
        if isempty(AllFishClusterStatistics{1,1}{i,j})==1
            AllFishClusterStatistics{1,1}{i,j} = NaN;
        end
    end
end
AllFishClusterStatistics{1,1} = cell2mat(AllFishClusterStatistics{1,1});

for i = 1:size(AllFishClusterStatistics{2,1},1)
    for j = 1:size(AllFishClusterStatistics{2,1},2)
        if isempty(AllFishClusterStatistics{2,1}{i,j})==1
            AllFishClusterStatistics{2,1}{i,j} = NaN;
        end
    end
end
AllFishClusterStatistics{2,1} = cell2mat(AllFishClusterStatistics{2,1});
```